Physiologically Based Pharmacokinetic Modeling of Monoclonal Antibodies in Children

by

Paul Ravi Vijh Malik

A thesis
presented to the University of Waterloo
in fulfillment of the
thesis requirement for the degree of
Doctor of Philosophy
in
Pharmacy

Waterloo, Ontario, Canada, 2021

©Paul Ravi Vijh Malik 2021

Author's Declaration

This thesis consists of material all of which I authored or co-authored: see Statement of Contributions included in the thesis. This is a true copy of the thesis, including any required final revisions, as accepted by my examiners.

I understand that my thesis may be made electronically available to the public.

Statement of Contributions

Chapter 1 (Open access)

Malik PRV, Temrikar Z, Chelle P, Edginton AN, Meibohm B. Pediatric dose selection for therapeutic proteins. *J Clin Pharmacol*. 2021;[epub ahead of print]

Chapter 2 (Letter of copyright permission included)

Malik PRV, Phipps C, Edginton AN, Blay J. Pharmacokinetic considerations for antibody-drug conjugates against cancer. *Pharm Res*. 2017;34(12):2579-2595

Chapter 3 (Letter of copyright permission included)

Malik PRV, Hamadeh A, Phipps C, Edginton AN. Population PBPK modelling of trastuzumab: A framework for quantifying and predicting inter-individual variability. *J Pharmacokinet Pharmacodyn.* 2017;44(3):277-290

Chapter 4 (Open access)

Malik PRV, Edginton AN. Physiologically-based pharmacokinetic modeling vs. allometric scaling for the prediction of infliximab pharmacokinetics in pediatric patients. *CPT Pharmacometrics Sys Pharmacol.* 2019;8(11):835-844

Chapter 5 (Letter of copyright permission included)

Malik PRV, Edginton AN. Pediatric physiology in relation to the pharmacokinetics of monoclonal antibodies. *Expert Opin Drug Metab Toxicol.* 2018;14(6):585-599

Chapter 6 (Letter of copyright permission included)

Malik PRV, Edginton AN. Integration of ontogeny into a physiologically based pharmacokinetic model for monoclonal antibodies in premature infants. *J Clin Pharmacol*. 2020;60(4):466-476

Chapter 7 (No previous copyright)

Unpublished. Abdullah Hamadeh and Andrea Edginton assisted with scientific content.

Abstract

The following thesis chapters chronicle evolving efforts throughout 2016 – 2021 to support research toward improving the pediatric clinical pharmacology of monoclonal antibodies (mAbs). Translating the benefits of successful mAbs from adults to children (and even infants) has proved challenging since the first attempts in the early 2000s. Children tend to achieve low pharmacokinetic exposures and poor efficacy when the adult dose is scaled to children by body weight alone (mg/kg), with infliximab as the main example of this case. Physiologically-based pharmacokinetic (PBPK) models were selected as the tool of choice to explore this discrepancy based on their established success with pediatric extrapolation for small molecule drugs. PBPK models enable mechanistic representations of drug disposition in virtual individuals and can be used to identify the drivers of altered pharmacokinetics in anatomically or physiologically distinct special populations, such as children.

The early chapters review the state of the field and the mechanistic underpinnings of mAb pharmacokinetics, and an example of an adult PBPK model for trastuzumab is provided. An open-source model for large molecule drugs was launched in 2018 inside the Open Systems Pharmacology software package, and shortly thereafter we trialed the use of this model to predict infliximab pharmacokinetics in children 4 – 17 years of age. Scaling pharmacokinetics to children by size alone failed to correctly predict the pharmacokinetics in this population, suggesting that other factors were at play. Therefore, a comprehensive review was conducted to generate physiological hypotheses to explain the observation with particular attention to infants (< 2 years of age), where the pharmacokinetic differences are most drastic. The following hypotheses were proposed:

1. The fraction of extracellular fluid volume in the body decreases with age and provides large weight-normalized volumes of distribution in infants.

2. Extravasation of antibodies into tissues occurs quickly in infants as they have a large capillary surface area per unit volume available for plasma protein exchange and a large proportion of “leaky” tissues, where capillary permeability is highest.

3. A fast rate of lymph flow in infants drives a fast rate of absorption after extravascular administration.

4. Infants have higher concentrations of circulating hematopoietic cells, which may contribute to extensive cellular uptake and fast elimination.

5. Intracellular metabolism and elimination may be increased due to low expression of FcRn – the neonatal salvage receptor – and the relatively high concentration of endogenous IgG competing for FcRn binding after birth.

In 2019, the first four hypotheses were integrated into a PBPK model for mAbs in premature infants that was successful for characterizing pharmacokinetics in infants even 1 day old at 28 weeks gestational age. However, this parameterization was based on the mechanistic understanding of mAb disposition at that time, and it was destined for change.

The results of the latest experiments in mice with site-specific FcRn deletion and macrophage knockdown prompted a reinvestigation of the contribution of hematopoietic cells – in particular monocytes and macrophages – to mAb pharmacokinetics. In this work, the role of the macrophage is redefined to a highly efficient protector of IgG, rather than an eliminating cell. A model-based analysis of the data revealed that it is very unlikely that a high concentration of circulating monocytes can contribute to explaining the fast weight-based clearance of mAbs in very young children.

In the end, four of the five hypotheses remain, and the investigations continue. Pediatric extrapolation for mAbs is a modestly more achievable task because of the efforts herein, hopefully improving outcomes for this vulnerable population in the future. Other contributions of the thesis include highlighting the influence of cancer and inflammatory disease states on mAb pharmacokinetics, proposing an empirical exponent for scaling volume of distribution to children and formalizing a foundation of pediatric literature on which this field can continue to grow.

Acknowledgements

Andrea Edginton
David Edwards
Brian Ingalls
Pierre Chelle
Colin Phipps
Abdullah Hamadeh
Anil Maharaj
Alanna McEneny-King
Jacky Yu
Cindy Yeung
Yannick Traore
Jessica Nicastro
Lokesh Narsineni
Roger Chen
Deep Patel
Mohamed Aborig
Satish Mistry
Sarah Delaney
Bernd Meibohm
Hyunjin Park
Christoph Niederalt

This work was funded in large part by the Canadian Institutes of Health Research through the Frederick Banting and Charles Best Canada Graduate Scholarship (CGS-D)

The most important acknowledgement is to my wife, Rachel Malik.

Table of Contents

List of Figures

List of Tables

Chapter 1
Pediatric Dose Selection for Therapeutic Proteins

1.1 Abstract

Selecting optimal dosing regimens in support of the clinical use of monoclonal antibodies and other therapeutic proteins in pediatric indications needs to appreciate the unique pharmacokinetic properties of this class of biologicals as well as the underlying physiologic and pathophysiologic processes and their modulation by childhood growth and development. During drug development, first-in-pediatric dose selection is a capstone event in the pediatric investigation plan that relies heavily on extrapolation of pharmacokinetic and pharmacodynamic data from adult to pediatric populations. It is facilitated by combinations of pharmacometric approaches, including allometry, physiologically-based pharmacokinetic modeling and population pharmacokinetic analyses, although data on reliability and qualification of some of these tools in the context of therapeutic proteins are still limited but emerging. Presented data suggest nonlinear relationships between body weight and both clearance and volume of distribution for therapeutic proteins in pediatric populations, with allometric exponents of 0.75 and 0.8, respectively. For newborns and infants (<1 year), even higher nonlinearity seems to occur. Translation of the quantitative characterization of the pediatric pharmacokinetics of therapeutic proteins into dosing regimens for the drug label requires compromising between precision dosing and clinical practicability, with tiered dosing algorithms based on size or age strata being the currently most frequently applied methodology.

1.2 Introduction

Harnessing the advances in biotechnology and genetic engineering to develop proteins for therapeutic applications is one of the greatest feats of modern medicine. The first successes for therapeutic proteins (TPs) were in protein replacement therapy, oncology, endocrinology, and immunology, with the latter largely spurred on by the popularity of monoclonal antibodies (mAbs). Twenty-five years later, TPs are offered as treatments in almost every clinical domain, from cardiology to neurology. In contrast to traditional small molecule drugs, TPs often possess favorable safety profiles, high specificity, and long circulating half-lives, making them preferred therapeutic interventions in many indications.[1,2]

Children deserve equal access to these interventions. Both the US Food and Drug Administration (FDA) and the European Medicines Agency (EMA) have enacted regulations to advance drug

development for pediatric indications. FDA regulations were mandated by the Best Pharmaceuticals for Children Act (BPCA) in 2002 and the Pediatric Research Equity Act (PREA) in 2003. The EMA followed close behind with pediatric regulations in 2007. For all new drug applications, including biologic license applications, clinical studies must now be conducted in children to inform labelling unless a waiver, partial waiver or deferral is granted.[3,4]

Based on this legislative framework, a pediatric investigation plan (PIP) is formulated during early clinical development for most drug development projects that lays out the design for the first trial or sequence of trials in pediatric patients, and the rationale for the first-in-pediatric dose. Fewer children are required for the trial when efficacy can be extrapolated from adults, as guided by the FDA Pediatric Study Decision Tree.[4] To extrapolate, the foundational assumptions are that the disease progression and the exposure-response relationship are sufficiently similar between the two populations.[5] In this case, studies seek to evaluate pediatric dosing regimens to produce exposure levels that match the adult exposure levels. Among TPs, and even among TPs with similar structure and mechanism of action, different exposure metrics have been used to guide dosing in children. Most commonly, the trough concentration at steady state ($C_{min,ss}$) or the area-under-the-curve over the dosing interval ($AUC_{0-\tau,ss}$) is used as the exposure target.[6-8]

Selecting the first-in-pediatric dose is frequently done when little or no pediatric data are available. Pharmacokinetic (PK) data from adults is usually leveraged heavily to create mathematical models of drug disposition in the body, either empirical or mechanistic in nature. When the mechanisms of drug disposition and/or their age-dependency are not well understood, the principle of allometry is often used to scale PK from adults to different age groups of children based on the power relationship between basal metabolic rate and body weight across multiple species.[9-11] On the other hand, a physiologically based pharmacokinetic (PBPK) modeling approach can be used when the mechanisms of disposition have been deeply explored, and when there is a solid understanding of how young age, developmental stage and disease processes may modulate them in pediatric patients.[12] In this framework, virtual adults are created with quantitative knowledge of anatomy and physiology, and drug disposition is modeled with rate-based equations representing the underlying mechanisms responsible.[13,14] The adults are then replaced with virtual children for simulating PK while holding all other parameters constant. PBPK modeling may be particularly advantageous relative to allometry for predicting PK in children less than 2 years of age since the impact of immature physiology can be more readily considered if their mechanistic basis is well understood and

characterized.[15] While these approaches have been qualified and applied for many small molecule drugs, the same is not yet true for TPs.

After first experiences with the first-in-pediatric dose studies have been obtained, the applied PK models can be further optimized by refining uncertain model parameters with the newly available data to better understand drug disposition in children. A population pharmacokinetic (PopPK) analysis using non-linear mixed effects modeling can be performed to identify demographic or disease covariates that affect and are predictive of exposure in patient subgroups. If a suitable biomarker for pharmacodynamic (PD) effects is measurable, a combined PK/PD model can be created to test alternative dosing regimens for therapeutic response. Full exposure-response analyses are often impractical to conduct in children since multiple dose levels are required to derive the relationship, but the data collected on pediatric outcomes can be used to confirm or deny the assumption that the exposure-response relationship is similar between adults and children.[16] With the results of these advanced analyses, the final dose recommended in the drug label can be different from the first-in-pediatric dose rationalized in the PIP.[4]

From beginning to end, pediatric dose selection for TPs is complicated by several factors. Inter-individual variability in PK is substantial (but within the same magnitude of many small molecule drugs), and often remains unexplained.[17,18] So far, body size is the only consistent covariate found to explain some of this variability between individuals.

TPs binding to abundant in vivo targets may display non-linear PK as a result of target-mediated drug disposition (TMDD).[19] Drugs subject to TMDD are often dosed to saturate the in vivo target, or at least achieve a high receptor occupancy.[20] When extrapolating the pharmacokinetic behavior of TPs to pediatric patients, knowledge about potential differences in abundance, turnover kinetics, and binding affinity to these targets in pediatric populations are usually lacking. Consequently, the pragmatic assumption is often made that the in vivo target levels are equivalent between adults and children if they are not measurable. Clearance, however, can be dramatically increased if the concentrations of target or its turnover kinetics are higher in the pediatric disease state. For example, IL-6 levels and other inflammatory cytokines are significantly elevated in systemic juvenile idiopathic arthritis (sJIA) as compared to the standard form of juvenile idiopathic arthritis and adult rheumatoid arthritis.[21] As a consequence, the anti-IL6 mAb tocilizumab requires a two-fold higher weight-based dose given twice as frequently in children and adolescents with sJIA relative to adult indications.[22]

Finally, patients can experience sudden loss of response to TPs after therapy that was initially successful. Development of anti-drug antibodies is a common cause.[23] There is currently very limited, if any evidence of different immunogenic potential between adults and children.[24,25] However, there may be differences in the incidence of immunogenicity over time if children are significantly under-dosed relative to adults, as subtherapeutic TP concentrations have been associated with an increased propensity of anti-drug antibody formation.[26]

The story of the pediatric use of infliximab highlights these concepts. Infliximab was among the first TPs approved for adults and later approved for children. It is an intravenously administered IgG1 mAb directed against tumor necrosis factor alpha and is used to treat autoimmune conditions. The approved weight-based induction and maintenance dose algorithm for children is the same as for adults (e.g., 5 mg/kg for inflammatory bowel disease). The first and largest evaluation of infliximab PK in pediatric patients over 6 years of age was conducted by Fasanmade et al. and noted comparable clearance (in mL/kg/day), but higher peripheral volume of distribution (in L/kg) in children.[27] Applying the same principles as for small molecules, the consensus was that no dose adjustment was necessary. In the landmark REACH trial, over 60% of pediatric patients with Crohn's disease achieved clinical response or remission after one year of therapy.[28] However, half of the patients required an increased dose or a shortened dosing interval to maintain a clinical response.[29] While the dose adjustments in the REACH trial were based on clinical evaluation and response, a target trough concentration of 3 – 5 µg/mL was soon identified for therapeutic drug monitoring in practice.[30-32] Re-visiting the original analyses by Fasanmade et al. revealed that 60% of children would achieve subtherapeutic trough concentrations with the labelled dose.[33] The European Society for Paediatric Gastroenterology Hepatology and Nutrition subsequently revised their recommendations and advocates for upfront intensification of the induction regimen for children less than 10 years of age.[31] Results of a systematic review further suggest that dose increases are necessary for all pediatric inflammatory bowel disease patients with low serum albumin or with no concurrent immunomodulator therapy.[32] In retrospect, it can be concluded that the adult weight-based dosing was not appropriate for the pediatric label.[32]

Considering these complexities of the pediatric use of TPs, this manuscript summarizes what is known about the disposition of TPs in children and offers a commentary about the utility of different methods for pediatric PK extrapolation and dose selection. There are two pivotal events in the process of pediatric dose selection that are presented – determining the first-in-pediatric dose for the PIP and

preparing the final pediatric dosing regimen for the drug label. To address foundational concepts, the discussion is primarily focused on the case where a TP is administered intravenously and exhibits linear pharmacokinetics. For a more detailed discussion on the current knowledge regarding age-associated differences in the mechanisms underlying disposition of TPs, the reader is referred to other recent reviews by our groups.[25,34]

1.3 Observations on Pediatric Exposure

Deriving dosing regimens for TPs in children requires a consensus for the typical PK in children as compared to adults. Until recently, the statement that children have a larger weight-normalized volume of distribution and faster weight-normalized clearance than adults has been based on the pediatric experience with mAbs, with some conflicting reports.[35,36] More recently, additional PopPK models have been published for mAb and non-mAb-based TPs that provided the opportunity to further clarify the body weight effect on PK parameters for TPs.

A literature search was performed to collect PopPK models for TPs and explore trends in exposure from very young children to adults. Models were included if they described the PK of an intravenous TP from adults down to children less than 1 year of age with dose-independent clearance. By focusing on intravenous TPs with linear PK, we limited possible confounding factors on distribution and elimination parameters, such as the effect of TMDD or incomplete absorption from an extravascular administration site. In the reviewed pediatric PopPK models, trends in exposure are described by quantitative relationships between body size measures (weight, lean body weight, fat-free mass, body surface area) and PK parameters (clearance, volume of distribution). For small molecules, the principle of allometry suggests that there is a nonlinear power relationship between body weight and clearance with an exponent of 0.75, and a linear relationship between body weight and volume of distribution (an exponent of 1.0). In other words, conventional allometry suggests that the weight-normalized clearance should be higher in young children (in mL/h/kg), but that weight-normalized volume of distribution should be consistent with adults (in L/kg). We investigated whether this relationship also holds true for TPs.

Table 1. Select population pharmacokinetic models for intravenous therapeutic proteins across adults and young children

Study	Drug INN *(Trade name)*	Class	Age Range (years)	Covariate Relationships for PK Parameters[a] (CL, Q2, Q3 in mL/h; V1, V2, V3 in L)
Abrantes et al., 2017[37]	Moroctocog Alfa *(Xyntha/ReFacto)*	Clotting factor *(Factor VIII)*	0 – 73 *correction for age ≤1	$CL = 276 \times \left(\frac{BW}{70}\right)^{0.75} \times [1 - 0.0068 \times (Age - 20)]$ $V1 = 2.45 \times \left(\frac{BW}{70}\right)^{0.812}$ $Q2 = 2510 \times \left(\frac{BW}{70}\right)^{0.75}$ $V2 = 0.923 \times \left(\frac{BW}{70}\right)^{0.812}$
Bjorkman et al., 2012[38]	Octocog Alfa *(Advate)*	Clotting factor *(Factor VIII)*	1.1 – 66	$CL = 193 \times \left(\frac{BW}{56}\right)^{0.80} \times [1 - 0.0045 \times (Age - 22)]$ $V1 = 2.22 \times \left(\frac{BW}{56}\right)^{0.95}$ $Q2 = 147$ $V2 = 0.73 \times \left(\frac{BW}{56}\right)^{0.76}$
Chelle et al., 2019[39]	Plasma derived Factor VIII and VWF complex *(Fanhdi/Alphanate)*	Clotting factor *(Factor VIII)*	1 – 72	$CL = 195 \times \left(\frac{FFM}{50.5}\right)^{0.701} \times [1 - 0.0121 \times (Age - 25)]^{Age>25}$ $V1 = 2.30 \times \left(\frac{FFM}{50.5}\right)^{0.726}$ $Q2 = 78$ $V2 = 0.449 \times \left(\frac{FFM}{50.5}\right)^{0.842}$
Clements et al., 2020[40]	Blinatumomab *(Blincyto)*	Bispecific antibody derivative	0.6 – 80	$CL = 2220 \times \left(\frac{BSA}{1.876}\right)^{0.620}$ $V1 = 5.98$
Garmann et al., 2017[41]	Octocog Alfa *(Kovaltry)*	Clotting factor *(Factor VIII)*	1 – 61	$CL = 188 \times \left(\frac{LBW}{51.1}\right)^{0.610}$ $V1 = 3.00 \times \left(\frac{LBW}{51.1}\right)^{0.95}$ $Q2 = 190$ $V2 = 0.637$

Han et al., 2016[42]	Bevacizumab *(Avastin)*	Monoclonal antibody	0.5 – 21	$CL = 9.9 \times \left(\frac{BW}{70}\right)^{0.75} \times 1.11$ $V1 = 2.85 \times \left(\frac{BW}{70}\right)^{0.701} \times 1.14$ $Q2 = 28 \times \left(\frac{BW}{70}\right)^{0.75}$ $V2 = 2.564 \times \left(\frac{BW}{70}\right)^{0.766}$
Jodele et al., 2016[43]	Eculizumab *(Soliris)*	Monoclonal antibody	NR	$CL = 98.6 \times \left(\frac{BW}{70}\right)^{0.75}$ $V1 = 5.72 \times \left(\frac{BW}{70}\right)^{1.0}$
Preijers et al., 2018[44]	Assorted Factor IX Products	Clotting factor *(Factor IX)*	0.2 – 90	$CL = 284 \times \left(\frac{BW}{70}\right)^{0.75} \times [1 - 0.0089 \times (Age - 34)]^{Age<34}$ $V1 = 5.45 \times \left(\frac{BW}{70}\right)^{1.0} \times [1 - 0.0115 \times (Age - 34)]^{Age<34}$ $Q2 = 110 \times \left(\frac{BW}{70}\right)^{0.75}$ $V2 = 4.8 \times \left(\frac{BW}{70}\right)^{1.0}$ $Q3 = 1610 \times \left(\frac{BW}{70}\right)^{0.75}$ $V3 = 2.04 \times \left(\frac{BW}{70}\right)^{1.0}$
Shemesh et al., 2019[45]	Atezolizumab *(Tecentriq)*	Monoclonal antibody	0.6 – 29	$CL = 9.04 \times \left(\frac{BW}{77}\right)^{0.795}$ $V1 = 3.01 \times \left(\frac{BW}{77}\right)^{0.766}$ $Q2 = 7.625$ $V2 = 1.36$
Suzuki et al., 2016[46]	Nonacog Alfa *(BeneFIX)*	Clotting factor *(Factor IX)*	0 – 69	$CL = 551 \times \left(\frac{BW}{70}\right)^{0.799}$ $V1 = 9.77 \times \left(\frac{BW}{70}\right)^{0.881}$ $Q2 = 577 \times \left(\frac{BW}{70}\right)^{0.741}$

				$V2 = 4.62 \times \left(\frac{BW}{70}\right)^{1.02}$
Zhang et al., 2017[47]	Lonoctocog Alfa *(Afstyla)*	Clotting factor *(Factor VIII)*	1 – 60	$CL = 212 \times \left(\frac{BW}{68}\right)^{0.756} \times \left(\frac{VWF}{113}\right)^{-0.633}$ $V1 = 3.36 \times \left(\frac{BW}{68}\right)^{0.903}$ $Q2 = 134$ $V2 = 0.265$

BW = body weight, LBW = lean body weight, FFM = fat-free mass, BSA = body surface area, VWF = von Willebrand factor
[a] Covariates not related to body size or age are excluded

Eleven PopPK models were available in the literature for a variety of TPs with molecular weights ranging from 50 to 267 kDa (Table 1). Most of the PK models used a two-compartment structure (n=8), though one-compartment (n=2) and three-compartment (n=1) models were also used. Four of the models used at least one fixed allometric exponent (0.75 or 1) to describe the relationship between body weight and PK parameters according to conventional allometry.[37,42-44] Consistent with the allometry hypothesis, the median exponent for the effect of body weight on clearance was 0.80 (range 0.76 – 0.80) among the models where body weight effects were estimated from the available data.[38,45-47] Two of the models with data-informed body weight effects on clearance also found mild effects of age-related covariates, but excluding these studies does not change the median result.[38,47] For volume of distribution parameters, the median exponent derived for the covariate effect of body weight was 0.81 (range 0.70 – 1.02), in contrast to the conventional linear relationship (with an exponent of 1.0) from small molecule PK.[37,38,42,45-47]

This result supports the notion that – in contrast to conventional allometry – both clearance and volume of distribution for TPs are expected to be higher in children than in adults on a per kg body weight basis. The consequence is that terminal elimination half-life can be the similar between adults and children, but overall concentrations are lower for an intravenously administered TP with weight-normalized dosing. These observations are in agreement with similar results reported specifically for mAbs.[48] A consistent pattern of exposure was observed for all TPs in this study, regardless of size or affinity for the neonatal Fc receptor (FcRn). Consequently, children will require higher weight-based doses of TPs to match the exposures in adults.

To determine the degree of underdosing that may occur when children are given the same weight-based doses as adults, we performed simulations with a generic two compartment PK model with parameters of a typical mAb:[49]

$$V1 = 3 \times \left(\frac{BW}{70\ kg}\right)^{0.8} L$$

$$V2 = 1.5 \times \left(\frac{BW}{70\ kg}\right)^{0.8} L$$

$$CL = 10 \times \left(\frac{BW}{70\ kg}\right)^{0.75} mL/h$$

$$Q2 = 10 \times \left(\frac{BW}{70\ kg}\right)^{0.75} mL/h$$

where V1 and V2 are the volumes of distribution of the two compartments, CL is the elimination clearance, Q2 is the intercompartmental clearance, and BW is the body weight in kg.

The model was simulated with body weights for one mean individual at each year of age from 1 to 18 years together with a 25-year-old adult (n = 19). Typical body weights were taken from the ICRP database.[50] The area-under-the-curve (AUC) and 28-day trough concentration for each individual were then compared against the simulated adult values (Figure 1). With the same weight-based dose, the generic model predicts that typical children who are 1, 5, 10 and 15 years old would achieve plasma AUC measurements that are only 64%, 74%, 83% and 95% of the AUC of a 25-year-old adult, respectively. The deficits in trough concentrations are even slightly larger, with typical children who are 1, 5, 10 and 15 years old achieving trough concentrations of 59%, 70%, 81% and 94% of the trough concentration of a 25-year-old adult, respectively.

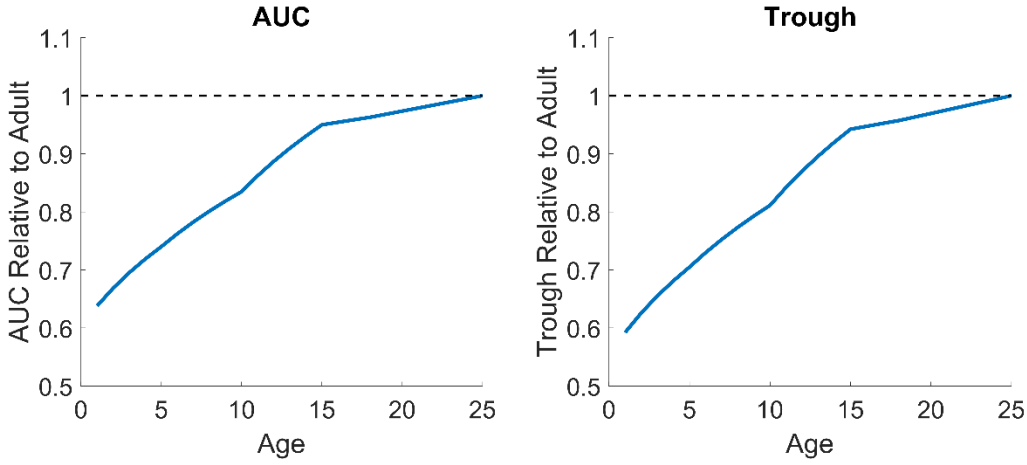

Figure 1. Projected AUC and trough concentrations for a typical mAb in typical individuals aged 1 to 25 years relative to adults if a constant weight-based dose were given across all ages.

These findings are supported by real-world data from the Web-Accessible Population Pharmacokinetic Service - Hemophilia program (www.WAPPS-Hemo.org).[51] This program provides a PK-based dose tailoring for clotting factor replacement therapy in hemophilia-A patients that produce minimal or no endogenous clotting factor VIII (molecular weight: ~240 kDa). WAPPS-Hemo uses Bayesian techniques to calculate individual PK parameters for clotting factor VIII concentrates in hemophilia patients using underlying PopPK models, with only small numbers of factor VIII activity measurements. Figure 2 presents the dose-normalized AUC for factor VIII derived by WAPPS-Hemo based on dosing and demographic information for 2,453 infusions of factor VIII

concentrate in 1,897 patients between 1 and 35 years of age, including a trendline fitted by locally estimated scatterplot smoothing (Loess). With the same weight-based dose, typical children who are 1, 5, 10 and 15 years old achieve plasma AUC measurements that are only 58%, 70%, 82% and 91% relative to the AUC in a 25-year-old adult (100%), respectively. An allometric function for clearance with an exponent of 0.75 was tested against the data and was able to characterize the trend well.

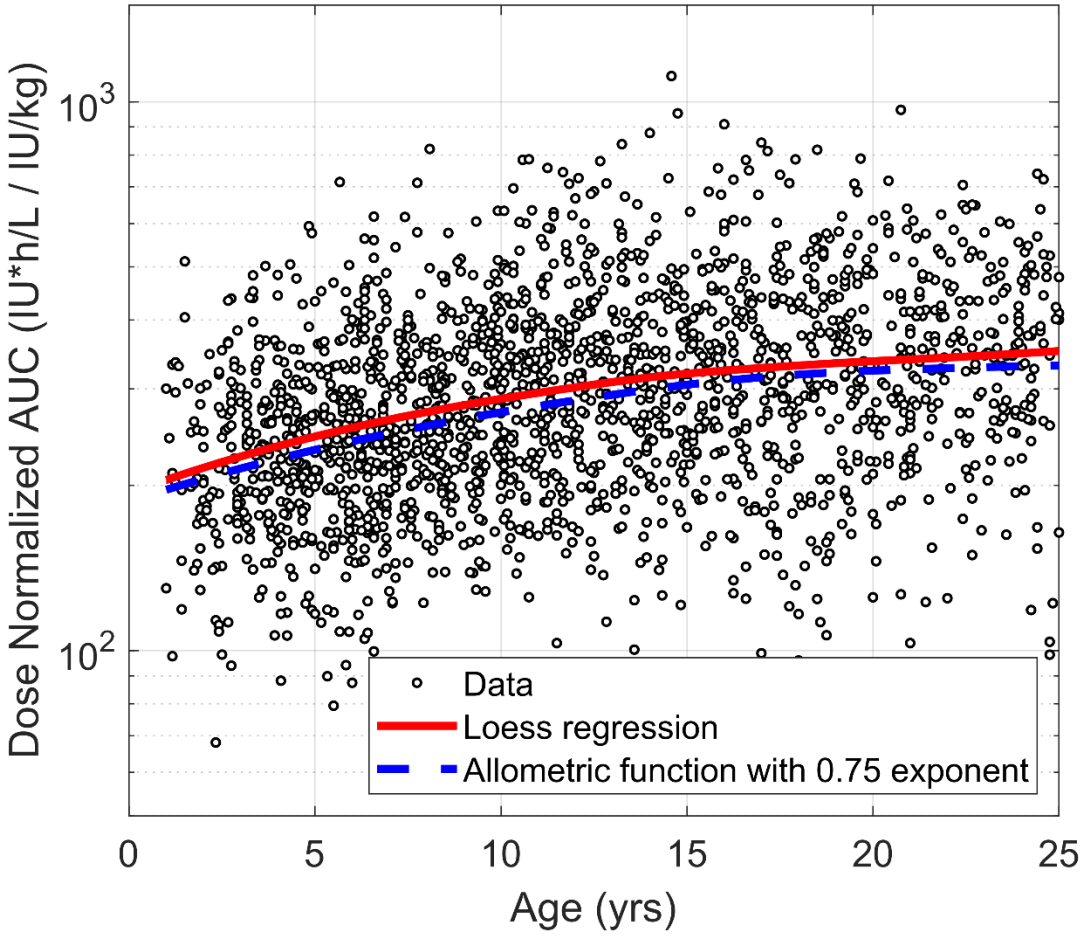

Figure 2. Dose-normalized AUC for factor VIII concentrates in pediatric and adult patients with hemophilia, derived from real-world data of the WAPPS-Hemo program. The circles denote individual patient data, the red solid line was created with locally estimated scatterplot smoothing (Loess) and the blue dashed line was projected with allometry ($\boldsymbol{CL} \sim \left(\frac{\boldsymbol{BW}}{\boldsymbol{70\ kg}}\right)^{\boldsymbol{0.75}}$).

Limited available data suggest that the observed nonlinearity between TP clearance and volume of distribution versus body weight may be even more pronounced in neonates and infants. Figure 3 presents PK data for intravenous TPs in preterm and term neonates relative to adults. In both cases, volume distribution and clearance are higher in infants than adults on a per kg basis, and the infant plasma concentrations are markedly lower. Pagibaximab is a chimeric monoclonal antibody (MW 150 kDa) against lipoteichoic acid (LTA) for the prevention of staphylococcal sepsis. The presented concentration-time profiles were digitized from publications of studies in healthy adults and very-low-birth-weight preterm infants less than 7 days old.[52,53] Since the assay measured total anti-LTA, the baseline measurement was subtracted from each subsequent concentration to approximate the exogenous pagibaximab concentration. For epoetin alfa (MW 30.4 kDa), the data originated from studies in healthy adults and neonates with hypoxic-ischemic encephalopathy receiving an intravenous infusion on the first day of life.[54,55] The neonates had induced hypothermia as part of the treatment protocol for encephalopathy, and half of the subjects had renal dysfunction – two conditions that theoretically slow the clearance of epoetin. Nevertheless, the same trend of lower exposures and faster clearance (in mL/h/kg) was also observed for these infants.

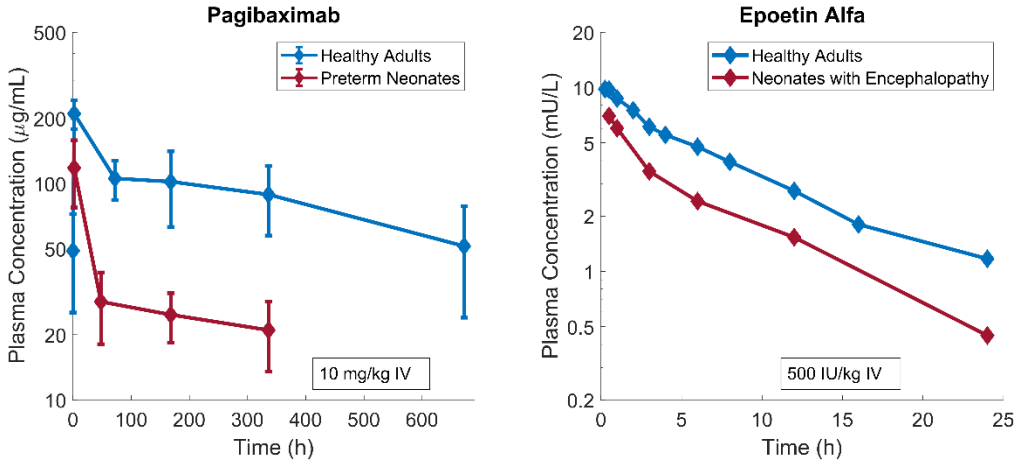

Figure 3. Pharmacokinetic profiles for preterm and term neonates for intravenous therapeutic proteins as contrasted with adults: Left panel: Pagibaximab[52,53]; Right panel: Epoetin Alfa[54,55]

To summarize, neonates, infants and children receiving weight-based doses of TPs are expected to achieve lower AUC and trough concentrations than their adult counterparts. This trend seems consistent across multiple types and sizes of TPs including mAbs, growth factors and clotting factors. At 2 years of age, children are projected to require weight-based doses that are ~60% higher than adults for equivalent exposure. Real-world data from the WAPPS-Hemo program support the

projected pediatric exposures and showed that an allometric exponent of 0.75 is appropriate for characterizing the unspecific clearance of TPs in children down to 1 year of age. Furthermore, our review of PopPK models describing the pediatric PK of intravenous TPs with linear kinetics did not find sufficient evidence to support a linear relationship between volume of distribution parameters and body weight (i.e. an allometric exponent of 1). Instead, a median exponent of 0.8 was noted to describe the effect of body weight on volume of distribution among existing models.

1.4 First-in-Pediatric Dose Selection

The first-in-pediatric dose is selected as part of the PIP with usually little or no pediatric data available to inform the decision. Thus, drug developers have to rely heavily on mathematical methods to scale PK and PD from adults to children. Allometry is preferred for scaling PK when the drug exhibits linear kinetics without time-dependent clearance or TMDD. PBPK modeling can be used when disposition processes for the TP and their age-associated differences are reasonably well understood and a mechanistic framework for characterizing drug disposition would be beneficial. The rationale for the first-in-pediatric dose selection is rarely published, but the underlying reasoning was explained for abatacept and tocilizumab.[25] In the primary literature, one combination of allometry and PK/PD strategy is described for domagrozumab, but its success is unknown since the development program was terminated in 2018.[6] Similarly there is one PBPK strategy published for asunercept.[56]

The exposure target for the first-in-pediatric study depends on the exposure-response relationship derived in adults and the confidence with which investigators can anticipate PD effects in children. Steady state AUC, steady state trough concentrations or post-induction trough concentrations are the parameters commonly linked to response. If a full or partial extrapolation exercise indicates that the exposure-response relationship can be assumed similar between adults and children, the plasma exposure target will be the same as for adults. If the exposure-response relationship is different, a new exposure target must be derived. Measurable biomarkers of disease in children (e.g., circulating antigen concentrations) can be incorporated into a PK/PD or PBPK/PD framework for extrapolation of an exposure target.[6,57-59]

Since children require higher weight-based doses of TPs than adults in cases where the exposure-response relationship is similar as discussed in the preceding section, it is arguably ethically questionable to initiate a trial with the adult dose and perform a subsequent dose escalation. Ethical recruitment of children for clinical studies mandates that the pharmacotherapy is for a therapeutic

purpose. For a dose escalation study, more children would be required for the trial, and some of them would be knowingly exposed to doses that are likely subtherapeutic. Thus, this strategy should only be entertained if very little is known about the PD and exposure-response of the drug in children and the risks of unintended over-exposure are high (e.g., in the case of cytotoxic protein-drug conjugates).

The commonly used approaches for first-in-pediatric dose selection include conventional allometric approaches, modified allometric approaches, hybrid approaches and PBPK modeling. As already mentioned, conventional allometric approaches scale PK parameters in proportion to body weight with empirical power relationships, with allometric exponents of 1 for volume and 0.75 for clearance terms. This approach has, in many instances, acceptable accuracy for predicting the PK of small molecules in children down to 2 years of age.[15] However, the allometric approach has not been fully qualified for use with TPs, with ongoing debate about the proper exponents, and limitations with respect to very young age groups. Published examples are largely limited to older children where the effects of maturation and ontogeny on PK are expected to be mild. One case study, for example, describes how allometry was used to guide the first-in-pediatric dose for domagrozumab in children 6-10 years of age.[6] Similarly, several objective evaluations of conventional allometry for children older than 4 years suggest that predictions for TP concentrations fell within a 1.5 to 2-fold error in the majority of the model extrapolations.[48,60] However, there was considerable variability in accuracy when multiple adult PopPK models were scaled for one drug (infliximab), with the poorest model making predictions within 2-fold error for only 47% of the observed concentrations.[60] This result stresses the importance of a strong understanding of TP disposition in adults prior to scaling to children and provides some idea of the worst case prediction scenario.

Deviating from conventional allometry, our review finds that exponents between 0.7 and 1.0 are most frequently applied for describing the effect of body weight on volume of distribution for TPs in children (median = 0.81). Similarly, but specific to mAbs, a recent review also noted allometric exponents between 0.7 and 0.9 in 20 PopPK models for children, although the authors cautioned that their results may have been confounded by poor sampling schemes.[48] The allometric exponent of 0.8 for volume of distribution has physiological relevance, as it reflects that young children have higher extracellular water fractions than adults.[61,62] Convincingly, Figure 4 shows a good fit between the allometric function with an exponent of 0.8 and the observed data for extracellular water fraction in children (as estimated by iohexol distribution volume).[61] This allometric approach only misses to capture the very high extracellular water fractions for infants under 1 year of age or 10 kg in body

weight (values up to 60% in newborns). Considering the totality of evidence, we anticipate that the allometric exponents of 0.75 for clearance and 0.8 for volume of distribution will be best when empirically scaling the PK of a TP for children from >1 – 18 years of age.

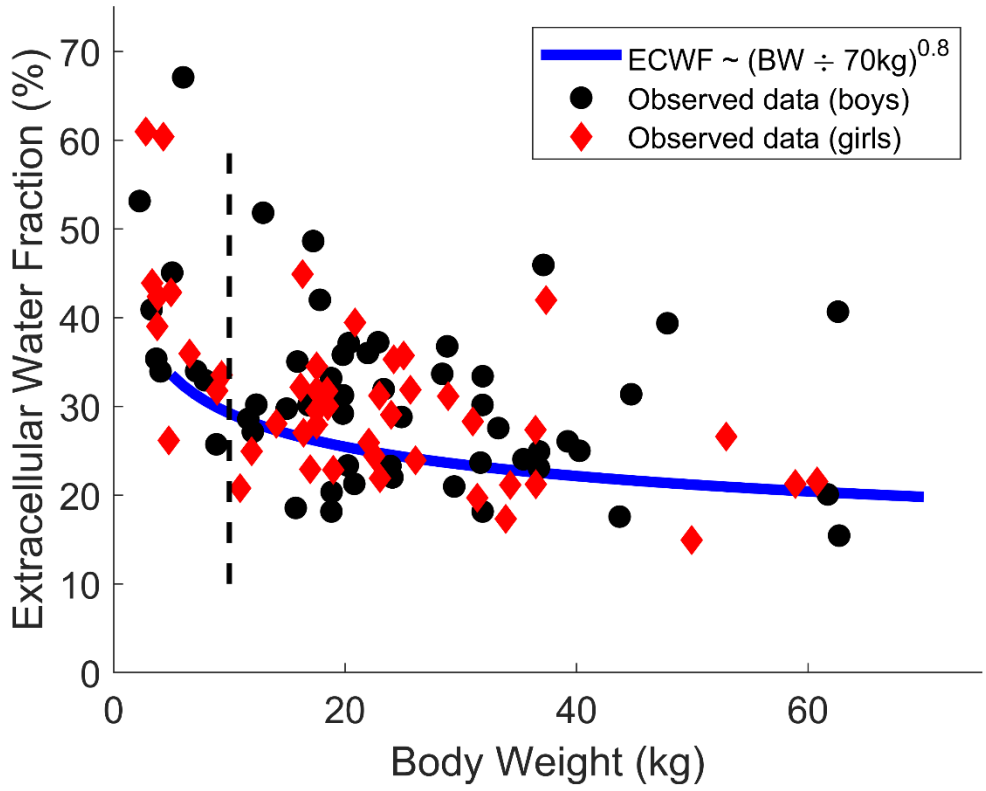

Figure 4. Observed data for extracellular water fraction (ECWF) in children as approximated by the iohexol distribution volume.[61] The circles denote individual data for boys, the diamonds denote individual data for girls, and the blue solid line was projected with allometry ($\boldsymbol{ECWV_{child} = ECWV_{adult} \times \left(\frac{BW_{child}}{70\ kg}\right)^{0.8}}$). The reference value for the ECWF of a 70 kg adult is 19% of body weight. The black dashed line marks the threshold of 10 kg body weight, below which the use of the allometric function to describe ontogeny in ECWF does not seem warranted.

In theory, a modified allometric approach could be used when age-dependent effects on PK parameters are known. For instance, age-dependent effects on PK can be captured by a maturation function with post-menstrual or post-natal age as an input to clearance. However, maturation functions with any predictive value would need to be derived from dense PK data in very young

children for multiple TPs. As these functions are generally not rooted in well understood age-associated molecular or physiological processes, their current use is often merely a fudge factor in pediatric PopPK modeling that compensates for the error associated with assumptions in the model development process (e.g., using fixed allometric exponents for newborns and infants, or assuming consistent extravascular bioavailability across age for subcutaneously administered TPs).[35,36]

A hybrid approach of allometry and PBPK modeling is offered for TPs in the commercially available software SimCyp (Certara, Princeton, NJ).[63] In this package, virtual individuals are represented by physiological organ volumes and blood flows. Distribution of TPs is modeled by a combination of convection, diffusion, and transcytosis within the two-pore framework, with lymph recirculation from the interstitial fluid. Non-specific catabolism of TPs is modeled as a plasma clearance and optimized using the adult data. Pan et al. made excellent predictions for pediatric PK by replacing the virtual adults with virtual children (with modifications for lymph flow) and scaling the non-specific catabolism by conventional allometry.[63] Evaluated protein products for the hybrid approach include recombinant erythropoietin and anakinra, which support the use of the model to predict plasma PK for non-mAb based proteins down to neonates. For mAbs and Fc fusion proteins, the software package pragmatically attributes the effect of ontogeny on elimination to a lower FcRn concentration in children that was optimized to the circulating IgG levels at each age, although there are currently no convincing mechanistic data available to suggest reduced abundance or function of FcRn in young pediatric patients. The lower circulating IgG subclass concentrations can also be explained by other plausible mechanisms, for example the well-described increased generalized protein metabolism in young pediatric patients, and/or a potentially reduced IgG synthesis rate,[25] and further understanding of the ontogeny of the underlying physiological processes will be needed to fully support this approach for the typical uses of full PBPK models (e.g. approximating target organ exposure, modeling disease effects on PK, etc.) in pediatric patients younger than 2 years of age.

PBPK modeling is considerably more complex than allometry and can be used to scale PK from adults to children when the mechanisms of drug disposition are well-understood. The processes governing the absorption, distribution, and elimination of TPs are very different from the processes driving the PK of small molecules, and have been reviewed previously.[2] Despite this complexity, the PK of a wide range of TPs (10 kDa to 300 kDa) can be described within one common paradigm. As mentioned, the distribution of a TP is confined to the extracellular water volume. Extravasation from the plasma to the interstitial fluid occurs by a combination of convection and diffusion through

vascular pores and is limited by the hydrodynamic radius. Lymph flow returns the drug from the interstitial fluid to the venous blood. Elimination occurs when TPs are taken up into cells by phagocytosis, pinocytosis, or in specific cases, receptor-mediated endocytosis. Certain TPs related to immunoglobulins or albumin escape intracellular degradation by interacting with the salvage receptor FcRn. Renal metabolism can be prominent for TPs less than 70 kDa.[64]

The workflow to build a pediatric PBPK model is well-established.[12,13] Virtual adults are first created with quantitative knowledge of anatomy and physiology, and drug disposition is modeled with rate-based equations representing the actual mechanisms responsible. Uncertain or unknown parameters are optimized to the observed data in adults, and the final model is externally verified by predicting PK in heterogeneous scenarios. The virtual adults are then replaced with virtual children that are parameterized to account for immaturity in physiological processes relevant to drug disposition. PBPK modeling may be advantageous over allometry for predicting PK in children less than 2 years of age since the impact of immature physiology can be mechanistically considered.

The physiological drivers of faster absorption, distribution, and clearance of endogenous and exogenous (i.e, therapeutic) proteins in children have been reviewed and applied to a PBPK model for mAbs in premature infants.[34,65] Fast absorption is driven by a lymph flow that is up to three times faster in infants than in adults. High extracellular water volumes increase the extent of distribution on a per kg body weight basis. Relatively large central organs with leaky vasculature and dense capillary networks enable fast extravasation into interstitial fluid. High concentrations of circulating leukocytes increase cellular uptake and subsequent degradation. FcRn function has sometimes been postulated to be lower in children, but this argument is not supported by clear in vitro or in vivo evidence. The strongest argument against the hypothesis is that the pattern of pediatric exposure is identical for proteins that bind to FcRn, and those that do not (Table 1).[63] Two PBPK models for TPs are available [PK-Sim (Open Systems Pharmacology)[66]; SimCyp[63]], but have not been mechanistically translated to pediatrics for these purposes.

The inherent strength of a PBPK model is that drug concentrations or receptor occupancy at the target site (e.g., the brain, a tumor, or an inflamed bowel) can be feasibly extrapolated from animals through adults to pediatric patients with sufficient in vivo evidence.[67] The burden of an active disease state and its impact on PK can be mechanistically represented, as it has for example been done for the impact of inflammation on the PK of TPs in animals and humans.[60,68,69] In addition, PBPK modeling allows us to concurrently explore more multiple competing mechanisms relevant for TP disposition

and their changes in children, such as the interaction of endogenous IgG and exogenous Fc-containing TPs with FcRn and the interdependencies of the resulting effects. As this application is in its infancy, there have been no PBPK models used to inform a pediatric drug label for a TP to date.[70] The growing PK data available for TPs and the foundational similarities in disposition throughout the drug class will likely enable more broad pediatric PBPK applications for first-in-pediatric dose selection in the near future, especially if more mechanistic understanding on the ontogeny of underlying drug disposition processes is emerging.

For a substantial number of TPs, extrapolation of PK to pediatric patients is further complicated by TMDD.[71] TMDD is the phenomenon where the binding of the TP to its target, either soluble or membrane-bound, triggers an additional elimination pathway for the TP. Since this TMDD elimination pathway is usually saturable at therapeutic concentrations, clearance decreases with increasing doses until the target is overwhelmingly saturated, resulting in dose-dependent, nonlinear PK behavior. As nonlinear clearance parameters are rarely correlated with body weight, scaling non-linear clearance depends on what is known about differences in target abundance, turnover, binding kinetics and TP-target complex degradation between the adult and pediatric populations.[71] A Michaelis-Menten approximation is often used to model nonlinear clearance, particularly when there is limited information available on the target kinetics. Among adults and young children with the same disease state, constant values for the Michaelis-Menten constant (K_M) and the maximum elimination rate (V_{MAX}) for all ages have achieved acceptable PopPK model fits for thymoglobulin, alemtuzumab and nab-paclitaxel.[72-74] While there is usually consensus to use the same K_M parameter in both populations, weight based scaling has at least been suggested for V_{MAX} when scaled for first-in-human studies.[75] If sufficiently characterized at least in adults, the full TMDD model allows for more flexibility in pediatric scaling as physiologic and mechanistic information about age-specific or population-specific differences in target concentration or production can be integrated.[6,58] This was recently exemplified in a PBPK model for epoetin alfa with a quasi-equilibrium approximation of the TMDD model where the nonlinear PK in adults and children was characterized with a constant parameter set.[63] In one combined TMDD and PK/PD model for canakinumab, the turnover of the target (IL-1β) was noted to be modestly increased in young children vs. older children.[57]

Similar to TMDD, extrapolating the processes related to subcutaneous or intramuscular administration from adult to pediatric patients remains challenging. Currently first-in-pediatric dosing of mAbs administered via the extravascular route is done through allometric extrapolation from adult

extravascular dosing.[70] Development programs typically seek approval for an intravenous route of administration first and later add the subcutaneous route approval based on exposure matching and non-inferiority trials. Examples include secukinumab, pertuzumab, abatacept, tocilizumab, and daratumumab. For pediatrics, doses are then extrapolated from adult subcutaneous doses, as for example done for abatacept, tocilizumab, and etanercept. Due to the limited understanding of the determinants of rate and extent of absorption after subcutaneous administration of TPs, the ability for mechanism-based extrapolation to pediatric patients remains limited.[76] Based on the increased extracellular water content and a higher perfusion rate (both blood and lymph) relative to adults, one might expect a faster rate of absorption in young pediatric patients relative to adults.[34] For the extent of absorption, the situation seems to be less clear, having potentially counteracting increased protein turnover and decreased lymphatic residence time and degradation.[34] These mechanistic differences seem to translate into quantifiable differences in the PK of TPs: For example, the absorption rate was three times faster in infants and young children compared to adults on IM administration of palivizumab, but the extent of absorption remained unchanged.[35] Some of these aspects have been incorporated into semi-mechanistic and PBPK models used to predict absorption pharmacokinetics in pediatric patients by borrowing animal and human physiological data from the literature, but published success of these approaches remains scarce.[77-79]

Considering the available tools and anticipated challenges, we have formulated general recommendations for first-in-pediatric dose selection for TPs (Figure 5). Presented data suggest nonlinear relationships between body weight and both clearance and volume of distribution for TPs in pediatric populations, with allometric exponents of 0.75 and 0.8, respectively. The ease of use for allometry and relative confidence as compared to PBPK modeling make allometry or hybrid allometry the preferred approaches to scaling PK down to children 1 year of age, or ≥10 kg body weight. For newborns and infants (i.e. <1 year of age or <10 kg body weight), even higher nonlinearity seems to occur. PBPK models are under development to support extrapolation to these vulnerable populations. Previous clinical trial experience with older children increases the confidence with which an extrapolation can be made. When administering by an extravascular route or when the drug is subject to significant TMDD, the same allometric principles can be used to scale foundational PK parameters with the modifications outlined in the previous paragraphs, but more uncertainty in the dose predictions can be expected. An uncertainty analysis should be conducted to assess the risk of potential under- and especially overexposure.

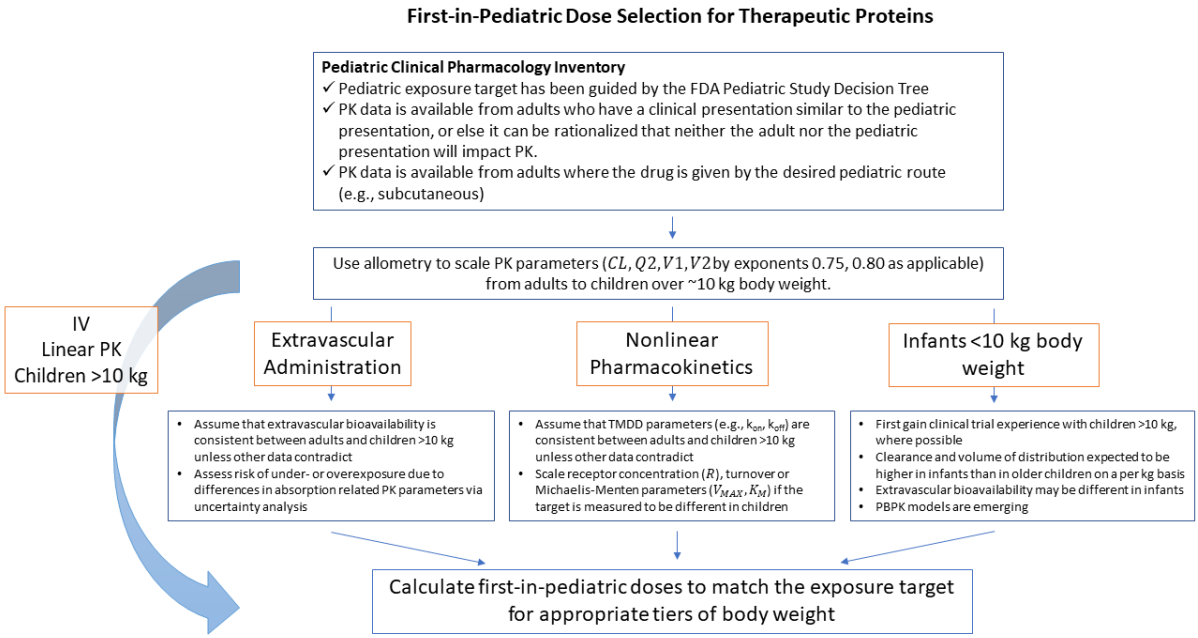

Figure 5. Rationalized approach to first-in-pediatric dose selection for therapeutic proteins. PK = pharmacokinetics, FDA = US Food and Drug Administration, CL = clearance, Q2 = intercompartmental clearance, V1 = volume of distribution in the central compartment, V2 = volume of distribution in the peripheral compartment, TMDD = target-mediated drug disposition, VMAX = maximal rate of nonlinear elimination, KM = Michaelis-Menten constant, PBPK model = physiologically based pharmacokinetic model

The way forward for improving first-in-pediatric dose selection will be paved by more detailed access to pediatric PK data for TPs from which we can learn, more detailed physiological data on ontogeny of processes relevant for TP disposition, and in general more pediatric drug development experience for TPs. Inevitably, the ontogeny of the extravascular absorption rate and processes, for example, will be able to be quantified with enough PK data for a variety of molecules. More detailed physiological data can be directed toward refining ontogeny profiles in infant PBPK models for parameters such as leukocyte content, capillary density, lymph flow rate and FcRn concentration. Finally, there is a need to standardize an approach to variability and virtual pediatric populations. While adult parameters from a PopPK model can be scaled to children by allometry, it is not known whether the interindividual variability in these parameters will be consistent between adults and children.

1.5 Pediatric Dose Selection for Labelling

When pediatric data has been collected in the first-in-pediatric trial and subsequent studies, the disposition of a TP drug in pediatric patients can often be characterized with high granularity using the aforementioned PopPK or PBPK tools.[16] However, translating the mathematical relationships established in these models back into clinically useful dosing recommendations is far from trivial. After all, healthcare providers cannot be expected to use complex mathematical relationships to derive a dose, especially if they involve patient-specific covariates that may be difficult to measure (e.g., body surface area).

The first-in-pediatric dose selection as outlined in the previous section and the underlying understanding of the influence of body size, age and disease on PK, PD and the exposure-response relationship for the TP of interest can either be confirmed or further refined during the pediatric clinical development program. Independent of the exact course of this pathway, however, in the end usually carefully characterized PK and/or PKPD relationships and their modulation by physiologic, pathophysiologic and ontogenic processes need to be converted into pediatric dosing recommendations that are part of the drug product labeling. As such, pediatric dose selection for labeling can be viewed as a compromise between precision medicine and practicability: The relatively precisely defined mathematical relationship between demographic, physiologic and pathophysiologic covariates and dose requirements in individual patients has to be balanced with the clinical requirements of limited complexity to avoid overburdening healthcare providers and prevent medication dosing errors. The acceptable degree of simplification is dependent on the individual TP in a specific indication, particularly the steepness of the exposure-response relationship, the narrowness of the therapeutic index of the TP, and the degree of between-patient variability in PK and PD.

While TPs, and most specifically mAbs, have been reported to exhibit 20-59% between-subject variabilities in PK parameters (similar to those of small molecule drugs), many TPs have high tolerability and very limited off target toxicity, leading to relatively wide therapeutic indices for many indications.[16,18,49] In these instances, wider ranges of exposure may be equally safe and efficacious as compared to more narrowly defined exposure metrics. Consequently, pediatric dosing recommendations for TPs are frequently defined by relatively broad patient strata that can easily be implemented in healthcare settings but provide sufficient granularity for age-appropriate dosing.[4,80]

Tiered dosing is the most frequently used approach to implement this concept in pediatric pharmacotherapy, and has been explored in detail for use with TPs.[3] With this dosing approach, one of several body weight- or age-defined patient strata receive either a flat or a body size-adjusted dose. For example, adalimumab pediatric dosing in juvenile idiopathic arthritis is based on body weight where patients above 2 years of age receive a subcutaneous dose of either 10, 20 or 40 mg every other week, dependent on whether their body weight falls within the strata of 10 to <15 kg, 15 to <30 kg, or ≥30 kg.[81] Similarly, patients above 2 years of age also receive different doses of tocilizumab if their body weight is lower or higher than 30 kg. But in contrast to adalimumab, tocilizumab dosing is further weight normalized (12 mg/kg and 8 mg/kg IV every 4 weeks for <30 kg and ≥30 kg, respectively) to allow for more granular dose adjustments.[82] If available, dose selection may be further guided by clinically accessible biomarkers if these have a major impact on the PK and PD of the TP. Omalizumab is a prime example for this application, where the pediatric dosing recommendations are based on age and weight strata that are further modified by pretreatment serum IgE levels, the molecular target of omalizumab in the treatment of allergic asthma.[83]

The translation of a pediatric PK model into clinical dosing recommendations for regulatory approval is exemplified by the approval of adalimumab for adolescents 12 years and older with hidradenitis suppurativa.[84] While the underlying population pharmacokinetic modeling framework described the clearance of adalimumab with a nonlinear weight-based relationship, the resulting approved dosing recommendation is a tiered dosing with flat dosing in two body weight strata, 30 to <60 kg and ≥60 kg. The translation was facilitated through extensive model-based exposure simulations in the target population supported by extrapolation exercises for efficacy and safety of adalimumab from adults to adolescents, particularly the assumptions of similar disease progression and response to adalimumab in hidradenitis suppurativa, and a similar exposure-efficacy relationship in adults and adolescents.[84]

While dose individualization based on therapeutic drug monitoring is performed for clotting factors with their relatively short half-lives as shown earlier in this manuscript, we do feel that such dosing approaches are neither practical nor warranted for most TPs with long elimination half-lives, except in situations where between-patient exposure is highly variable, difficult to predict and may lead to treatment failure, such as infliximab dosing in pediatric patients with inflammatory bowel disease.[85]

1.6 Conclusion

In summary, pediatric dose selection for TPs is an evolutionary process from allometric and model-based approaches over first-in-pediatric dosing to clinical dosing recommendation that is grounded in a strong scientific framework of understanding the PK and PD of these compounds and their dependency on ontogeny and differences in body size, composition, and functioning between children and adults. Thus, TPs require approaches distinctively different compared to small molecule drugs based on their disposition properties and the molecular and physiological processes determining them. While some understanding of these processes is emerging, substantial gaps and uncertainties are remaining that hamper a more widespread and reliable application of especially model-based approaches to support pediatric dose selection. We are hopeful that filling these gaps with an improved understanding of the ontogeny of clinically relevant drug disposition processes for TPs, pediatric dose selection for this class of medications will become a more reliable and precise process in the near future.

1.7 Study Highlights

This manuscript describes the current state of knowledge on the pediatric pharmacokinetics of monoclonal antibodies and therapeutic proteins. The scope of the problem when extrapolating doses from adults to children is presented. Relevant methods for extrapolation are reviewed, and best-practice recommendations are synthesized for use by drug developers and regulators.

Chapter 2
Pharmacokinetic Considerations for Antibody-Drug Conjugates against Cancer

2.1 Abstract

Antibody-drug conjugates (ADCs) are ushering in the next era of targeted therapy against cancer. An ADC for cancer therapy consists of a potent cytotoxic payload that is attached to a tumour-targeted antibody by a chemical linker, usually with an average drug-to-antibody ratio (DAR) of 3.5 – 4. The theory is to deliver potent cytotoxic payloads directly to tumour cells while sparing healthy cells. However, practical application has proven to be more difficult. At present (September 18, 2017) there are only two ADCs approved for clinical use. Nevertheless, in the last decade there has been an explosion of options for ADC engineering to optimize target selection, Fc receptor interactions, linker, payload and more. Evaluation of these strategies requires an understanding of the mechanistic underpinnings of ADC pharmacokinetics. Development of ADCs for use in cancer further requires an understanding of tumour properties and kinetics within the tumour environment, and how the presence of cancer as a disease will impact distribution and elimination. Key pharmacokinetic considerations for the successful design and clinical application of ADCs in oncology are explored in this review, with a focus on the mechanistic determinants of distribution and elimination.

2.2 Introduction

Antibody-drug conjugates (ADCs) are ushering in the next era of targeted therapy against cancer. An ADC for cancer therapy consists of a potent cytotoxic payload that is attached to a tumour-targeted antibody by a chemical linker, usually with an average drug-to-antibody ratio (DAR) of 3.5 – 4. The theory is to deliver potent cytotoxic payloads directly to tumour cells while sparing healthy cells. ADCs can be used to improve the therapeutic window of systemic chemotherapeutics and to open the door for chemotherapeutics that may have previously failed because of poor permeability or a lack of selectivity for tumour cell killing. When the ADC binds its target protein on the surface of tumour cells, it can be internalized by receptor-mediated endocytosis. It is subsequently degraded in the cell and the payload is released into the intracellular space. Current payloads under investigation primarily interfere with microtubule formation or crosslink DNA. Ideally, only cells that express the target

protein for the antibody will be exposed to the cytotoxic effects and systemic toxicity will be avoided. However, non-specific uptake occurs to a small degree in all tissues.

While the initial theory is simple, practical application has proven to be more difficult and only two ADCs are currently available for therapeutic use: trastuzumab emtansine[86] and brentuximab vedotin[87] (September 18, 2017). Nevertheless, as of 2016, approximately 50 ADCs are in the clinical pipeline.[88] Other forms of ADCs, such as radioimmunoconjugates and enzyme-immunoconjugates have been studied in preclinical contexts for many years and radioimmunotherapy is effective for hematologic malignancies.[89] These are once more emerging with promise for solid malignancies, though these are beyond the scope of this review.

For drug developers, academic researchers and clinicians alike, ADCs present unique pharmacokinetic opportunities and challenges. They are large molecules (~150kDa) with a distribution of the intact ADC that is mostly confined to the plasma, interstitial fluid and lymph.[90] They often possess long plasma residence times because of their dynamic interactions with the neonatal Fc receptor (FcRn) and are administered intravenously every 1-4 weeks.[91-93] In most but not all cases, they exhibit nonlinear pharmacokinetics and dose-dependent clearance due to saturable target binding and elimination.[94,95] No consistent pattern has yet been identified between the ADCs that exhibit dose-dependent clearance and those that do not.[94] In theory, the degree of nonlinearity will be proportional to the whole body target load. Figure 6 displays the mechanistic processes that are thought to affect the distribution and elimination of ADCs in humans. Physiologically-based pharmacokinetic (PBPK) models are emerging to describe the biodistribution of ADCs as a function of these key processes.[96]

A typical pharmacokinetic assessment of an ADC involves an analysis of multiple drug species in circulation, including the conjugated antibody, the total antibody (both conjugated and unconjugated) and the free payload, as well as any anti-drug antibodies (ADAs) that may have been generated.[97] While it is a standard of practice in industry,[97,98] the scientific value of this type of pharmacokinetic assessment is limited on its own. As with all drugs, plasma concentrations are only loosely correlated with efficacy at the tumour site.[99] The high inter-individual variability in plasma protein pharmacokinetics confounds predictions for dose-response relationships.[92,93] Plasma stability and the extent of deconjugation in circulation can be estimated with direct measurements of the conjugated fraction.[97] The free payload concentrations can be used to evaluate payload-dependent toxicity, though this toxicity is not easily distinguishable from the toxicity that occurs when the conjugated

antibody is taken up into normal tissues.[100] With respect to ADA analysis, it is important that ADCs possess low immunogenic potential – though with the increasing use of humanized or fully human IgG backbones and the low antigenicity of typical payloads, clinically-significant immunogenicity of ADCs is becoming a problem of the past.[101]

In the last decade there has been an explosion of options for ADC engineering to optimize target selection, Fc receptor interactions, linker, payload and more.[102] Evaluation of these strategies requires an understanding of the mechanistic underpinnings of ADC pharmacokinetics. Development of ADCs for use in cancer further requires an understanding of tumour properties and kinetics at the tumour site, and how the presence of cancer as a disease will impact distribution and elimination. Key pharmacokinetic considerations for the successful design and clinical application of ADCs in oncology will now be explored, with a focus on the mechanistic determinants of distribution and elimination (Table 2).

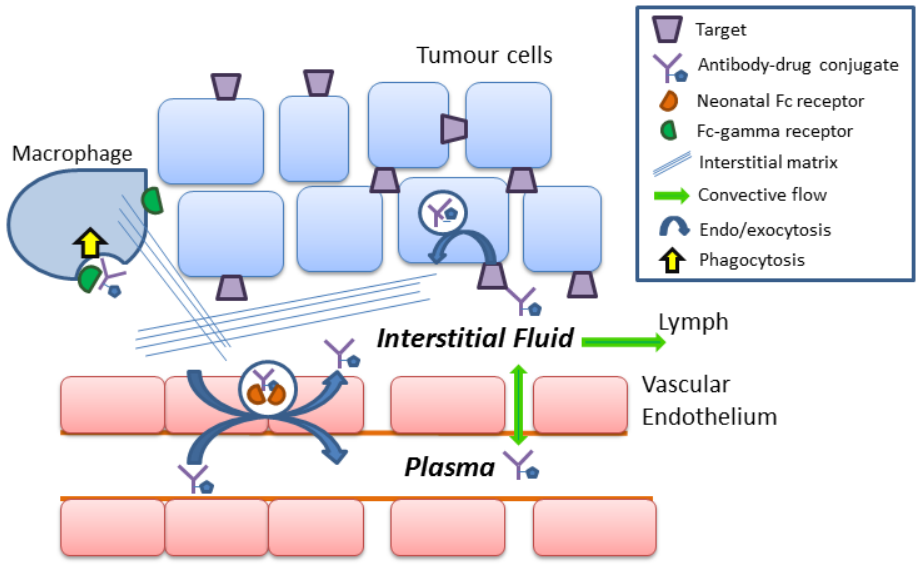

Figure 6. The main physiologic processes governing the disposition of ADCs. ADCs administered intravenously cross the blood vessel wall and enter tissues by convection through pores or (to a lesser extent) by transcytosis through the vascular endothelium. Movement through the interstitial matrix is slow and erratic. ADCs in the interstitial fluid bind their target receptor expressed on the cell surface and are internalized by receptor-mediated endocytosis. Internalized ADCs undergo lysosomal processing in cells and then release their cytotoxic payload. In endothelial, epithelial and hematopoietic cells, ADCs can be protected from lysosomal degradation through binding to the neonatal Fc receptor (FcRn). ADCs that fail to bind their target are mostly recycled through the lymph and back to the venous circulation. Macrophages, monocytes and other immunoregulatory cells that express the Fc-gamma family of receptors (FcγR) may phagocytose ADCs locally and in the circulation. In all tissues, ADCs may be degraded by non-specific proteases (not pictured).

Table 2. Pharmacokinetic considerations for antibody-drug conjugates against cancer

1. Target-Mediated Drug Disposition • High target expression in tumours and relatively low expression in normal tissues is required • Saturable target-mediated elimination contributes to nonlinear pharmacokinetics • The nature of binding to target at the tumour rim may hinder penetration into tumours (binding site barrier effect)	**2. Circulation and Tissue Distribution** • Tissue distribution is dependent on perfusion, vascular permeability and target expression • Recycling through the lymphatic system allows ADCs to avoid persisting in non-target-bearing tissues
3. Fc Receptor Interactions • FcRn may facilitate transcytosis of intact ADC across endothelial and epithelial layers • Affinity for FcRn influences plasma half-life • FcγR-mediated phagocytosis may contribute to elimination and toxicity	**4. Payload Kinetics** • The intracellularly-released payload must maintain nanomolar cytotoxic potency • Hydrophobic payloads diffuse to nearby cells, causing a bystander effect • Nonpolar payloads may be vulnerable to efflux by P-gp
5. Linker Kinetics • Site-specific conjugation maximizes homogeneity and avoids aggregation due to close packing of hydrophobic payloads • ADCs with high DARs are cleared quickly and accumulate in the liver	**6. Tumour Properties** • High interstitial fluid pressure hinders ADC penetration at the tumour rim • Normalizing tumour vasculature is a double-edged sword • Retention in tumours is mediated by poor lymphatic drainage and the dense extracellular matrix • Shifted extracellular pH may alter stability and binding kinetics

2.3 Target-Mediated Drug Disposition

ADCs are designed to bind to the extracellular domain of a membrane-bound target protein that can facilitate internalization into tumour cells by receptor-mediated endocytosis.[103] Because of the high affinity of the initial binding interaction, ADCs are said to undergo target-mediated drug disposition (TMDD), meaning that the properties of the target influence the pharmacokinetics of the drug.[19,95] TMDD can be observed on a small scale, affecting drug penetration into tumour tissue[104] and on a large scale, governing drug exposure across the whole body.[105] Target expression, internalization, turnover, accessibility and binding affinity all impact the pharmacokinetics of ADCs and must be considered for optimal target selection.

2.3.1 Target-Mediated Distribution

After administration, ADCs distribute to occupy target sites that are present in both normal and diseased tissue. Therapeutic doses often achieve maximum target occupancy around the body. If the dose is not enough to saturate all target sites, ADCs will distribute to target sites in tissues that are highly perfused and permeable[106,107] or have high target expression.[108]

For optimal specificity, the tumour target load (presence) should be as high as possible compared to the whole body target load. In reality, the tumour target load makes up less than 1% of the whole body load,[109] even with significant target overexpression and upregulation in tumours. New exploits target proteins that are uniquely mutated in tumour tissues so that uptake into normal tissues can be minimized.[110,111] In mice, high target expression in normal tissues can impede the distribution of an ADC into tumour tissue by forming a target sink.[108]

It has been suggested that this challenge can be obviated by pre-dosing patients with naked antibody before administration of the ADC to partially saturate the target sink so that ADC specificity for the tumour can be improved and also so that payload toxicity to normal tissues can be minimized.[112] When using this strategy, a proportion of target sites in the tumour tissue must be left unsaturated after the dose of the naked antibody or payload toxicity to tumours will also be compromised. However, feasibility would depend precisely on relative tissue perfusion and the nature of drug distribution after dosing. There is significant inter-individual variability in target expression and each patient would require a different dose of the naked antibody to achieve selective target saturation in normal tissues, making this strategy rather impractical. Furthermore, it is likely that the naked antibody itself will have activity, either by secondary effects through the immune system or by

target modulation (activation or internalization). We therefore do not anticipate this strategy will easily translate into clinical application.

The efficacy of ADCs is dependent on the degree of receptor occupancy or target saturation.[113] The notion of target accessibility is important, and this idea surfaced after the predicted doses required to saturate targets were much higher than observed clinically.[114] The density of cell-cell packing and the prevalence of tight junctions may limit the accessibility of targets on cell membranes. Target accessibility can also be impeded if targets form dimers or oligomers that block or hinder the antibody binding domain.[68]

2.3.2 Target-Mediated Elimination

Target-mediated elimination refers to the binding of an ADC to its target, internalization by receptor-mediated endocytosis and degradation within the cell. Saturable target-mediated elimination contributes to the nonlinear pharmacokinetic profile of ADCs. When target sites are saturated, elimination follows a zero order rate and when they are unsaturated, elimination follows a first order rate.

Along with target expression, the internalization rate of the drug-target complex also influences target-mediated elimination of ADCs. In contrast to small molecules, high target-mediated elimination – or in other words, a high rate of internalization into cells – could be desirable for ADCs because efficacy depends on internalization into tumour cells.[115,116] Antibodies of different sizes or antibodies directed against different epitopes of the same target may have drastically different internalization rates.[117] In some cases, binding of an antibody induces internalization of the target,[118] while in other cases it does not.[119] ADCs that induce internalization of the target, rather than passively internalize are predicted to have strong efficacy at first, but may struggle with sustained efficacy and tumour specificity if the target is quickly depleted on tumour cells. In that case, few target receptors would remain for ADC binding.

The extra-cellular domain (ECD) of membrane-bound targets can often be found in circulation in patients whose tumours overexpress the target.[120] A mathematical model suggests that the rate of shedding is influenced by target expression and the internalization rate.[121] Antibodies form immune complexes with circulating ECD proteins and are eliminated by immunoregulatory processes with a half-life of two days.[122,123] Pool et al. determine that antibodies bound to the ECD of EGFR

accumulate in the liver.[124] Therefore, ADCs against targets that have high shed ECD levels in plasma may incur more toxicity to the liver.

A population pharmacokinetic study of trastuzumab in breast cancer patients concludes that the serum ECD concentration is a significant covariate increasing clearance and volume of distribution.[125] However, both a mechanistic model[68] and a study in mice[126] demonstrate that the effects on plasma concentrations are marginal when antibodies are administered at therapeutic doses. It is likely that the significance of ECD concentrations as a covariate is related to its role as an indicator of more advanced disease in humans, rather than its role as a target sink.

2.3.3 Binding Site Barrier Effect

The effects of TMDD are prominent on a smaller scale in solid tumours.[104] The binding site barrier effect encompasses the cumulative effects of target expression, turnover and binding affinity that may hinder ADC penetration throughout solid tumours. If target expression in tumour tissue is exceptionally elevated and binding affinity is high, then large ADC concentrations are required in the tumour environment to saturate the available receptors at the tumour rim so that free ADC molecules can proceed to penetrate into the deeper layers.[127,128] ADCs face a similar kinetic challenge when target turnover is high and there is a quick replenishment of internalized targets.[127] The only modifiable component of the binding site barrier effect is target binding affinity. In the tumour environment, antibodies with high affinity are more likely to be sequestered by the first available targets, rather than to distribute to more distal targets.[129] However, a sufficient binding affinity is required for internalization and efficacy. It is a balance – there exists an optimal antibody affinity for each tumour size and target expression level to maximize distribution of ADCs within tumours while maintaining sufficient internalization and efficacy. This problem has been analytically addressed with modeling in the context of ADCs.[128]

The effects on conjugation on binding affinity must be investigated on a drug-by-drug basis. While in many cases the affinity is unaffected,[130] some results suggest otherwise. For example, Bondza et al. found that conjugation decreased binding affinity for cetuximab but did not affect binding affinity for an anti-CD44v6 antibody.[131] More research is required to determine the effects of conjugation site and payload properties on target binding affinity.

2.3.4 Circulating Lymphocyte Antigens

Of the two ADCs currently on the market, one is directed against HER2, a solid carcinoma target,[86] while the other is directed against CD30, a lymphocyte antigen in Hodgkin's lymphoma.[87] ADCs against lymphocyte antigens may require a unique pharmacokinetic approach because the target cells may be spread throughout different tissues, the lymphatic system or the peripheral circulation. Approximately 30% of ADCs in development are directed against hematologic and lymphoid cancers.[88] To date, there have been no clear pharmacokinetic differences in phase 1 trials between ADCs against solid carcinoma targets and those against hematologic or lymphoid cancers.[94] However this assessment is limited by the low sample sizes in phase 1 trials, the diversity of patients, the diversity of disease and the wide inter-individual variability in ADC pharmacokinetics. From a mechanistic standpoint, circulating lymphocytes may be highly accessible for ADCs because their distribution is similar to ADC distribution (see below).[132] In addition to payload-induced toxicity, binding of ADCs to circulating lymphocytes can cause elimination by immunoregulatory processes and activation of complement.[133] Mechanistic pharmacokinetic modeling of the two ADC subclasses may illuminate more subtle differences that can be observed through the lens of the pharmacokinetic profile in plasma.[132]

2.4 Circulation and Tissue Distribution

ADCs are large molecules with a molecular weight of approximately 150kDa. Because they are structurally similar to endogenous IgG, they have a distribution similar to IgG and they are affected by many of the same physiologic processes *in vivo*. Distribution is generally confined to the plasma, interstitial fluid and lymph.[90] Convective fluid flow facilitates the transport of ADCs through and between these physiologic mediums.[134]

After IV administration, the first method by which ADCs can pass through the capillary wall and into the interstitial fluid of tissues is by filtration, or the convective flow of plasma through vascular pores (junctions, fenestrae, sinusoids, etc.).[134] While there is fluid flow in both directions across the capillary wall, net flow of plasma proteins and ADCs in normal tissues is out of the blood vessels and into the interstitial fluid. The Starling equation describes the net movement of fluid across capillary walls as a function of opposing hydrostatic and osmotic pressures.[134] Once in the interstitial fluid, ADCs are free to interact with membrane-bound targets. ADCs that do not contact a target in the interstitial space are recycled to the venous circulation through the lymphatic system. Throughout

circulation, ADCs may be vulnerable to non-specific proteases, though this clearance mechanism is considered negligible for most IgG products.[135]

An analysis of the upper limit of pore size for capillaries and the blood perfusion in each tissue can be used to understand the tissue-specific distribution pattern of ADCs (Table 3).[136,137] The level of target expression also contributes to distribution by sequestering ADCs in tissues with prominent and accessible target loads.[108] Biodistribution studies in mice show that the liver, spleen, kidneys, lungs and heart are the dominant organs for tissue distribution shortly after administration; highly perfused tissues reach their Cmax quickly, while poorly perfused tissues reach their Cmax as long as 24 hours after IV administration.[106-108,112,138,139]

Table 3. Tissue-specific distribution profile of antibody-drug conjugates

Tissues	**Capillary Characteristics**	**Perfusion**	**Distribution**
Brain	Non-fenestrated capillaries with tight junctions	Minimal	Minimal
Muscle, skin, large intestine, adipose	Non-fenestrated capillaries with loose junctions	Low	Low
Thymus, small intestine, pancreas, bladder	Fenestrated capillaries	Moderate	Low
Bone marrow	Sinusoidal capillaries	Moderate	Moderate
Heart, lung	Non-fenestrated capillaries with loose junctions	High	Moderate
Kidney	Fenestrated capillaries	High	High
Liver, spleen	Sinusoidal capillaries	Maximal	Maximal

Resistance to flow through pores is due to the size, charge and hydrophilicity of an ADC. Because conjugation impacts these parameters, the degree of conjugation has been shown to alter biodistribution. At low drug-antibody ratios (DARs), there is no significant difference in tissue distribution between conjugated and unconjugated antibodies.[106,107,139] However, at DARs greater than four, conjugation induces a fast plasma clearance with a trend toward accumulation in the liver.[107,138] An explanatory hypothesis is that the hydrophobicity associated with increasing DARs may make ADCs more vulnerable to non-specific uptake into hepatocytes and Kupffer cells by pinocytosis and/or phagocytosis.

The filtration rate of antibodies and ADCs through vascular pores can be measured with visible tagging and *in vivo* imaging. Using such measurements, Parving and colleagues have demonstrated that the flow of plasma proteins through capillaries can change proportionally to blood pressure[140] and can be affected by such perturbations as liver cirrhosis,[141] diabetes,[142,143] congestive heart failure,[144] and inflammatory conditions.[145] Furthermore, the presence of cancer may impact the TER and the tissue uptake of ADCs. There are conflicting measurements of the TER in patients with cancer, though it can be up to two-fold higher in cachectic patients with cancer than in healthy subjects (Table 4).[146-148] Population pharmacokinetic analyses with both antibodies and ADCs in cancer have identified disease staging and tumour burden as significant covariates causing increased plasma clearance.[49,149] As mentioned earlier, the whole body target load is only marginally increased by a larger tumour burden[109] and would be unlikely to be responsible for such remarkable changes in the pharmacokinetic profile. The increased plasma clearance is likely indicative of high tissue uptake and facilitated by the systemic vascular hyperpermeability[150] that is attributable to the inflammatory burden of advanced cancer. ADCs may then have the highest tissue uptake and potential off-target toxicity in patients with advanced cancer and comorbid conditions that increase vascular permeability to plasma proteins (see Table 4).

Table 4. The transcapillary escape rate (TER) in patients with comorbid conditions

Condition	TER IgG (%/h, SD)	TER Albumin (%/h, SD)
Healthy[140]	3.0 (0.7)	5.2 (1.0)
Hypertension[a] [140]	4.7 (1.0)	7.8 (0.9)
Liver Cirrhosis[141]	8.4 (0.8)	7.4 (1.9)
Short-Term Type 1 Diabetes[b] [142]		5.5 (1.0)
Long-Term Type 1 Diabetes[c] [143]	4.4 (1.0)	7.4 (1.1)
Chronic Right Heart Failure[144]		8.3 (1.6)
Inflammatory Skin Disease[145]		8.6 (1.1)
Cancer[146-148]		5.5 – 12.1[d]

[a] mean arterial blood pressure: 193/119 mmHg
[b] mean duration: 2.6 years
[c] mean duration: 20 years with microangiopathy
[d] range of reported medians in three studies

Focused ultrasound (FUS) therapy can be used to induce enhanced permeability of tumour tissue to therapeutic antibodies by hyperthermia. When the temperature of tumour tissue in mice is increased to 42°C by FUS therapy for 3 – 5 minutes, the uptake of trastuzumab and other plasma proteins into

tumour tissue is increased up to two-fold.[151] Multiple short rounds of hyperthermia have additive effects on antibody uptake.[151]

The brain is the most inaccessible tissue for ADCs due to the complete restriction of convective flow through the blood-brain barrier. Researchers have explored osmotic, biochemical, radiological and focused ultrasound therapy methods for disrupting the blood-brain barrier and enabling convective flow of therapeutic antibodies into brain tissue, which are reviewed in detail by Chacko et al.[152] The most promising hypothesis for the route of entry of mAbs into the brain is via the circulation of the cerebrospinal fluid (CSF).[153]

The movement of ADCs and other macromolecules within the interstitial space is not consistent or predictable. The interstitium is a fibrous matrix of collagens, proteoglycans, laminins and other structural proteins woven around the blood and lymphatic capillaries.[134] The surrounding interstitial fluid is derived from plasma and contains ions, small solutes, plasma proteins and leukocytes.[134] Transport of ADCs through the interstitium is slow and erratic.[134] The movement of proteins and solutes is driven by hydrostatic pressure, osmotic pressure, chemical or electrical gradients and interactions with matrix components. Large pore microdialysis is being used to measure interstitial concentrations of antibodies[154] and may prove useful for evaluating the interstitial distribution of ADCs.

From the interstitium, ADCs can be taken up into lymphatic capillaries through cleft-like junctions.[134] They will be transported through the lymphatic system at a rate that is estimated to be 0.2% of the plasma flow rate.[135] After collection into the thoracic duct or the right lymphatic duct, ADCs will re-enter venous circulation at an interface with the left or right subclavian vein, respectively.[134] Recycling through the lymphatic system allows ADCs to avoid localizing in non-target-bearing tissues.

The mononuclear phagocyte system (MPS) is present throughout circulation and plays a role in the regulation of antibodies and the immune system.[155] It largely consists of monocytes in circulation and macrophages that are distributed in tissues.[155] Many of these mononuclear phagocytic cells express Fc-gamma receptors (FcγR), which can bind the Fc region of IgG molecules and clear them from circulation by phagocytosis.[156] The primary tissues involved in the MPS are the liver, spleen, lymph nodes, thymus and bone marrow.[155]

Subcutaneous administration has not yet been utilized for an ADC, but is common for unconjugated antibodies.[157] After subcutaneous administration, ADCs must reach the systemic circulation either through the lymphatic system, or by diffusion against the net fluid flux from interstitial space and into plasma at the local capillary beds.[158] The subcutaneous bioavailability of unconjugated antibodies ranges from 53-82%,[157] likely due to specific phagocytosis into cells of the MPS in lymphoid organs before reaching the venous circulation. This cellular uptake of ADCs could cause undue toxicity in lymphoid organs, limiting the subcutaneous administration route. Subcutaneous bioavailability of antibodies is correlated with FcRn affinity[159] (because cells of the MPS express FcRn) and can be as low as 28% in FcRn-deficient animals.[160]

2.5 Fc Receptor Interactions

Fc receptors are so named because they bind to the Fc region of antibodies and help to regulate their distribution and elimination in the body. The Fc receptors that interact with IgG-based drugs are the neonatal Fc receptor (FcRn) and the family of Fc-gamma receptors (FcγR). Each receptor subtype affects ADC pharmacokinetics in different ways.

FcRn is present in vascular endothelium, intestinal epithelium, the blood-brain barrier, placental syncytiotrophoblasts, kidney podocytes and macrophages.[161] Its primary purpose is to salvage IgG from intracellular degradation. It may also facilitate the endocytic transport of antibodies and ADCs across epithelial and endothelial boundaries, such as the intestinal wall in the neonate or the capillary wall. Figure 7 describes the main features of this transit. ADCs may be taken up by fluid-phase pinocytosis or receptor-mediated endocytosis from both apical and basolateral surfaces.[91,162] The method of uptake depends on the surrounding pH because FcRn binds ADCs in a pH-dependent manner, with high affinity below pH 6.5 and low affinity at pH 7.4.[161] During transit, FcRn binds to ADCs in a 2:1 conformation and acts as a shuttle protein to protect them from lysosomal degradation.[161] The pH-dependence of binding affinity causes ADCs to bind FcRn with highest affinity when the threat of degradation in lysosomes is highest. ADCs will compete with endogenous IgG for binding to FcRn, and the available concentrations are saturable.[109,135,163] Any ADCs that fail to bind FcRn in the endosome are degraded.[91,163] There is theoretical and experimental evidence to suggest that approximately two thirds of FcRn-bound ADCs in endothelial cells are shuttled to the apical surface and returned to the plasma, while one third is expelled into the interstitial fluid at the basolateral surface.[91,162] This recycling contributes to the prolonged plasma half-life of ADCs.

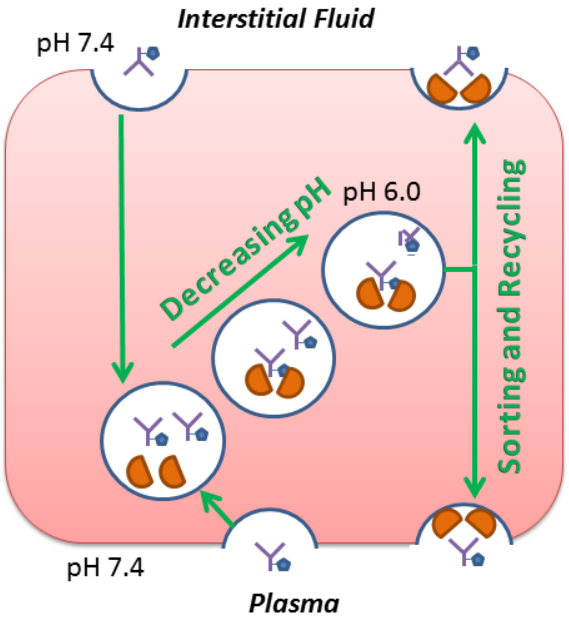

Figure 7. Summary of proposed mechanisms for transcytosis and FcRn binding. ADCs may pass through vascular endothelium by FcRn-mediated transcytosis. ADCs are taken up by fluid-phase endocytosis into vascular endothelial cells (and others). During endocytic trafficking and sorting, they may bind to the neonatal Fc receptor (FcRn) with pH-dependent affinity and in a 2:1 conformation, which protects them from lysosomal degradation. Mechanistic models suggest that approximately two-thirds of antibodies bound to FcRn are recycled to the plasma space, while one-third is shuttled to the interstitial fluid.

Antibody plasma half-life is correlated with its affinity for FcRn binding.[91,109,135] For ADCs in particular, increased FcRn affinity results in higher efficacy, a longer half-life and improved tolerability, as demonstrated by Hamblett et al. with four different ADCs in a mouse experimental model.[164] The Fc region is the site of conjugation for a number of ADCs[102] as well as the contact point for FcRn binding;[164] therefore the effect on conjugation on FcRn affinity must be assessed. A thermodynamic analysis concludes that FcRn affinity of ADCs may be decreased for ADCs with a high degree of conjugation to small hydrophilic payloads with PEG-based hydrophilic linkers.[165] A more recent *in vitro* assay explores the affinity of brentuximab for FcRn at varying ratios of conjugation with vedotin, a large hydrophobic payload.[166] Conjugation with 2-4 molecules of vedotin decreased FcRn affinity relative to the unconjugated antibody, while conjugation with 8 molecules of

vedotin actually increased FcRn affinity relative to the unconjugated antibody.[166] Further investigations are required to understand how the location and degree of conjugation and the nature of both the linker and payload affect FcRn affinity and plasma half-life.

FcγR receptors are present on monocytes, granulocytes (neutrophils, eosinophils, basophils and mast cells), lymphocytes (T cells, B cells and NK cells), antigen-presenting cells (macrophages, dendritic cells, Kupffer cells) and platelets.[167] The three major subtypes (I, II and III) are differentiated by their binding affinity for the Fc region, structure, function and tissue distribution.[167] Together they facilitate the antibody-dependent functions of the immune system, such as antibody-dependent cell-mediated cytotoxicity (ADCC) and the elimination of soluble immune complexes.[167] Binding of IgG to FcγRI occurs with nanomolar affinity and induces internalization of the IgG-receptor complex,[156] while binding of IgG to FcγRII and FcγRIII is 10-1000 times less efficient and internalization only occurs when receptors are crosslinked by interactions with multivalent circulating IgG complexes.[167] The majority of these interactions occur within the MPS (liver, spleen, lymph nodes, thymus and bone marrow).[167]

Pharmacokinetic studies with antibodies against both soluble and membrane-bound targets in FcγR knockout mice have determined that FcγR interactions have a negligible impact on plasma pharmacokinetics.[168,169] However, cytotoxicity to FcγR-bearing cells appears to be the main driver of dose-limiting toxicities for many ADCs,[100,170] supporting the hypothesis that this uptake may be clinically significant. For trastuzumab emtansine, the dose-limiting toxicity of thrombocytopenia is hypothesized to occur due to FcγRIIa-mediated uptake into megakaryocytes.[100,171,172] It has been suggested that FcγR interactions are most important when the antibody or ADC binds to a circulating target – either soluble or present on circulating lymphocytes – which can be opsonized with many IgG molecules and phagocytosed by FcγR-bearing cells more efficiently.[160] FcγR interactions may also be relevant for efficacy in the tumour microenvironment. Tumour-associated macrophages that express FcγR may phagocytose ADCs and release the payload to nearby tumour cells through the bystander effect (see Payload Kinetics).[173]

Fc affinity engineering is an effective method for achieving a desired pharmacokinetic profile for antibodies and ADCs. For example, Ko et al. engineered an antibody with increased FcRn affinity so that it achieved an extended plasma half-life and improved localization in intestinal epithelium in primates.[174] In this work, FcRn affinity was engineered without concurrent changes to FcγR affinity

so that the ADCC function was not compromised.[174] However, Grevys et al. note that concurrent changes to FcγR affinity should be expected.[175]

2.6 Payload Kinetics

The first payloads for ADCs were selected from among existing chemotherapeutic small molecules. Doxorubicin was one of these candidates.[176,177] However, the success of doxorubicin as a payload was limited by its poor potency at the tumour site and lack of overall efficacy compared to doxorubicin monotherapy.[176,177] Chemotherapeutic small molecules for direct use are evaluated with parameters in mind that do not cross over well to make them good candidates as payloads for ADCs.[178] Selection of optimal payloads requires an understanding of the intracellular processing of ADCs (Figure 8).

Ideal payloads must have tumour cell killing potencies (half maximal inhibitory concentration, IC_{50}) in the sub-nanomolar range because only a small number of molecules are internalized into each cell. Cytotoxic small molecules that show excessive toxicity when administered as monotherapy become possible candidates as payloads.[179-181] Directed delivery by antibodies will spare systemic toxicity and increase the therapeutic window.

Molecules that initially failed due to poor membrane permeability also become eligible as payloads for cancer because antibodies can facilitate internalization into tumour cells. For example, Ogitani et al. demonstrate tumour cell killing with a topoisomerase I inhibitor that has poor membrane permeability by linking it to a variety of antibodies against different targets to facilitate internalization.[182] Poor membrane permeability may be beneficial. If the linker holding the payload degrades or the payload spontaneously dissociates in systemic circulation, toxicity to normal tissues can occur if the free payload can easily pass into cells.

The two payloads currently approved for use are DM1, a maytansinoid derivative and MMAE, an auristatin derivative. Both compounds bind to tubulin and inhibit microtubule formation, inducing mitotic arrest.[183-185] A mechanism of action targeting intracellular components is desirable because that is where the payload is usually released.[186] Anti-microtubule activity makes these payloads somewhat selective to proliferating cells. A number of payloads are in development that target DNA, granting them activity against both proliferating and non-proliferating cells.[187]

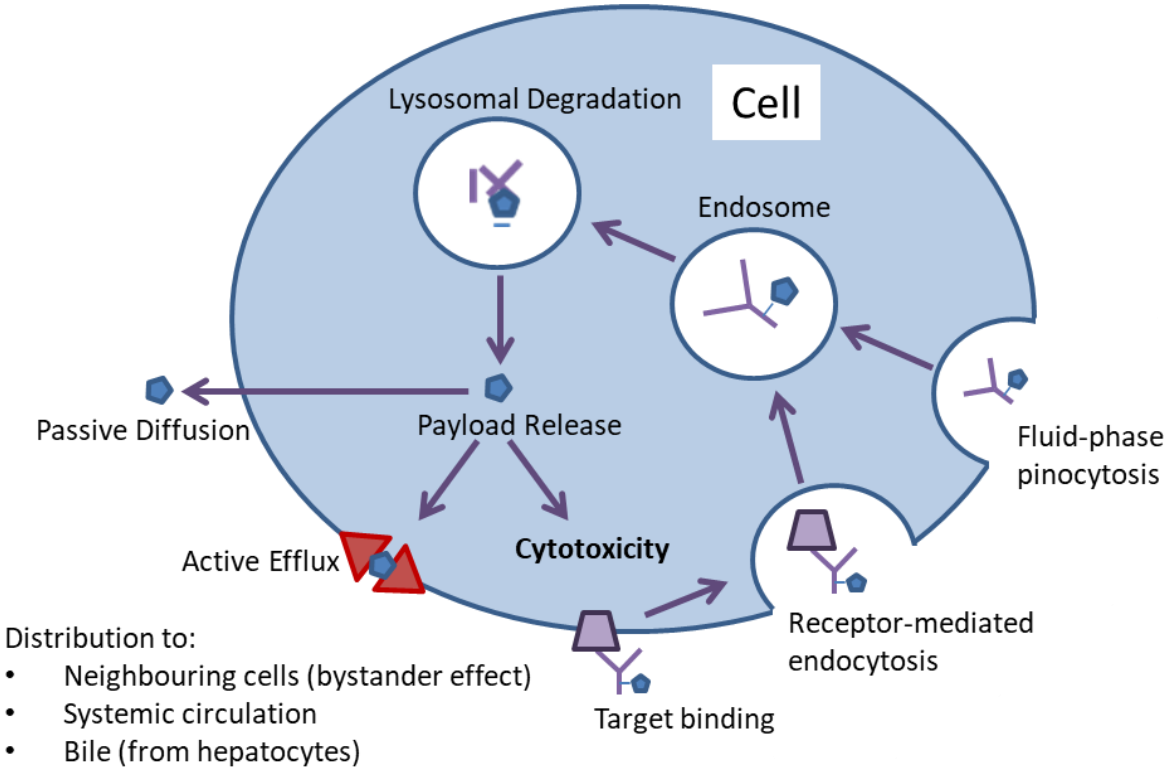

Figure 8. Summary of ADC cellular uptake and the bystander effect. Uptake of ADCs into cells occurs by receptor-mediated endocytosis after target binding or by pinocytosis. If FcRn is not present, ADCs are degraded in lysosomes and the cytotoxic payload is released into the intracellular space. A portion of the released payload may diffuse out of the cell or be transported out by efflux pumps to induce cytotoxicity in neighbouring cells (the bystander effect). The exit of permeable payloads cells may contribute to concentrations in systemic circulation or in the bile.

The catabolite or linker-payload fragment that is formed after linker degradation inside cells must retain its cytotoxic activity. DM1 is released from trastuzumab emtansine as lysine-SMCC-DM1.[188,189] This catabolite is charged and has poor membrane permeability, but retains its activity against tubulin.[190] MMAE is released cleanly from brentuximab vedotin with full activity.[186] In contrast to lysine-SMCC-DM1, MMAE is moderately permeable across membranes and causes toxicity in nearby cells[186] – a phenomenon that has been named the bystander effect.[191]

The bystander effect may be useful against tumours where target expression is heterogeneous or where high receptor occupancy in the tumour is difficult to achieve.[192] Kovtun et al. show that linkers can be manipulated to select for catabolites with varying permeability and bystander killing

potential.[193] With respect to heterogeneity, Golfier et al. report an 82% reduction in the size of tumour xenografts in which only 20% of cells express the target – a result that has been attributed to the lipophilicity and bystander effects of the reduced disulfide-DM4 catabolite.[192,194] Li et al. show a similar result against heterogeneous tumours using the permeable payload, MMAE.[195] They solidify the bystander effect by recording poor cell killing when using a less permeable payload as a control (MMAF).[195] A recent pharmacokinetic/pharmacodynamic model quantifies the effect based on *in vitro* tumour cell culture measurements.[196] The bystander effect in a heterogeneous tumour becomes less prominent over time as cells that express the target are killed.[196]

While leveraging the bystander effect may offer enhanced efficacy against heterogeneous tumours, there are concerns about safety. It may increase toxicity to healthy cells.[170] After experiments in mouse models, Ogitani et al. suggest that bystander killing is only observed in close neighbouring cells and that the risk for systemic toxicity is low.[197] However, more research is required to confirm this safety in humans. Generally, the amount of drug released for bystander effects is thought to be below the threshold for systemic effects. A comparison of the toxicity profiles of ADCs stratified by the potency of their bystander effects could shed light on this issue.

Cellular efflux transporters, such as P-glycoprotein (P-gp) affect the cellular disposition of many payloads.[198] Both of the payloads currently on the market are substrates for P-gp.[199,200] Nonpolar payloads are particularly vulnerable to efflux transporters. Kovtun et al. are able to minimize P-gp-mediated resistance for maytansinoid derivatives by using hydrophilic linkers which increase the polarity of the linker-payload catabolite that is released in the cell.[198] Toppmeyer et al. show that it is also possible to reduce P-gp-mediated drug resistance by administration of a competing co-substrate, such as verapamil.[200]

2.7 Linker Kinetics

Cytotoxic payloads are attached to the Fc region of antibodies by chemical linkers. A myriad of options for linker design and chemistry have emerged in recent years. Established linkers include hydrazones that are sensitive to pH, peptide linkers that are cleavable by cathepsin-B, disulfide bridges that are reducible by glutathione and other non-cleavable covalent attachments, such as thioether and maleimidocaproic acid linkers.[102] The field of available linkers has widened to include a multitude of other chemical technologies and each one must be evaluated from a pharmacokinetic standpoint.

The linker must be stable in the plasma, interstitial fluid and lymph to minimize off-target toxicity and to ensure maximal delivery to the intracellular space of tumours. These fluids have varying physicochemical properties and enzyme content throughout the body and within tumour tissue, making global stability difficult to achieve. Linker cleavage in circulation is responsible for the faster clearance that is observed for the conjugated antibody vs. the total antibody.[201,202]

The linker must efficiently release the payload in the intracellular space. Payload release should be predictable and consistent. Linkers can be grouped into cleavable and non-cleavable linkers. A cleavable linker depends on the intracellular pH, chemical conditions and the presence of proteases or other peptides to break the linker by hydrolysis or proteolysis. In contrast, a non-cleavable linker can only release the payload when the ADC has undergone intracellular processing within lysosomes. Increasing numbers of ADCs in development are being constructed with non-cleavable linkers.[102]

Whether cleavable or not, the metabolites that are formed must retain the cytotoxic activity of the original payload.[203] Non-cleavable linkers tend to release payload metabolites that include a residual amino acid, which may compromise activity and alter membrane permeability. Drug developers and clinicians may prefer that the active metabolites maintain poor permeability across cell membranes so that they remain in the cell to exert their cytotoxic effect.[190]

The drug-antibody ratio (DAR) is used to measure the degree of conjugation. Most ADCs in development have DARs between two and four. DARs up to 20 have been reported using branched polymer linkers with multiple payload molecules attached to each backbone by ester bonds.[204] The heterogeneity of an ADC is a measure of the distribution of DARs in the product and the variety in conjugation sites. Homogeneity achieved by site-specific conjugation enhances both safety in rats and efficacy in murine tumour xenograft models.[205]

Higher DARs are associated with stronger *in vitro* and *in vivo* potency against tumour cells.[206,207] However, the improvement in potency is offset by an increase in plasma clearance, with a trend toward accumulation in the liver.[107,206] The hydrophobicity of ADCs can be affected by close packing of four or more hydrophobic payloads.[206,208] Hydrophobic interactions and subsequent aggregation are thought to be largely responsible for the increase in plasma clearance that is observed.[166,206,208,209] Strop et al. avoid the limitations of hydrophobicity by strategically selecting conjugation sites that avoid close packing of payloads.[207] They are able to increase the therapeutic index of ADCs by improving the DAR and the potency.[207] Both the conjugation site and stoichiometry must be optimized to make homogenous ADCs with optimal therapeutic indices.

Site-specific conjugation has not yet been employed in an ADC product that is on the market (2017). Site-specific conjugation involves engineering the exact location on the Fc region where the linker and payload are attached, so as to create more homogenous drug molecules. Recent reviews describe the progress with these methods.[210-213] By using site-specific conjugation, Pillow et al. are able to improve the therapeutic activity and the plasma stability of trastuzumab emtansine in mice.[214] In similar fashion, Thompson et al. demonstrate that ADCs that employ site-specific conjugation have superior stability and efficacy compared to conventionally conjugated ADCs with the same DAR.[215] Based on various works, enhanced linker stability in plasma is likely responsible for the benefits of site-specific conjugation.[207,216-220] Payload release likely remains the same whether site-specific conjugation is used or not.[221]

Proper linker method selection must take into account many factors, including the biochemical predisposition of the payload and the antibody. The activity of the payload and the binding affinities of the antibody must be preserved. As mentioned before, there is conflicting evidence about whether the degree of conjugation impacts target or FcRn affinity.[130,131,165,166,222] Maruani et al. suggest that the internalization rate of ADC-target complexes is not impaired by conjugation of the ADC.[223]

2.8 Tumour Properties

The nature and structural properties of tumours present challenges and opportunities for antibody-drug conjugates targeted against cancer. This section elaborates on the unique tissue properties and fluid effects within the microenvironment of solid tumours that may impact exposure to ADCs. Thurber and Wittrup propose a theoretical model for antibody uptake into solid tumours that encompasses many of these considerations and enhances practical understanding.[224]

Conventional assumptions about plasma protein distribution and extravasation into tissues do not apply to solid tumours. Capillaries are the gatekeepers governing the entry of ADCs into tissues. The efficacy of antibody-based therapies depends on vascular access; biologic therapies are generally not effective against early stage tumours because significant capillary access to solid tumours is not achieved until stage 3. In contrast to normal vasculature, tumour capillaries have erratic and irregular architecture.[225,226] Blood supply is chaotic and inconsistent, with blood pools in some areas and hypoxic or acidic patches in others.[225,226] As a result, the distribution of antibodies in a tumour is highly heterogeneous.[227,228]

A variety of forces are at play along the walls of tumour capillaries. They often lack a basement membrane and are notoriously "leaky" due to large irregular fenestrae, wide intercellular junctions and poor support from pericytes.[226] In addition, vascular function may be compromised by tumour cells taking over the role of endothelial cells in certain locations of the vessel wall.[229] However, this leakiness does not necessarily lead to improved penetration of antibodies into tumours.[230] Jain explains that increased leakiness gives rise to high interstitial fluid pressure (IFP), which causes net convective flow to be directed out of tumours.[228,231,232] ADCs are large proteins which must rely on convective transport for penetration into solid tumours. Other barriers to convective transport include poor drainage of lymph from the tumour, interstitial fibrosis and irregularities in the extracellular matrix.[225,233] Reductions in IFP measurements have been shown to be correlated with therapeutic response to chemotherapy and radiation.[234-236] Further research is required to confirm the hypothesis that ADC exposure is a function of measured IFP in humans.

Attempts have been made to lower tumour IFP so that antibody penetration can be improved. High IFP can be alleviated by normalizing tumour vasculature.[237-239] Bevacizumab, an anti-VEGF antibody, blocks angiogenesis, restricts tumour vasculature and reduces IFP.[240-242] However, vascular normalization is a double-edged sword; even though bevacizumab can lower IFP, antibody penetration into tumours is not necessarily improved because vascular access is simultaneously compromised.[243-245] Other research using imatinib to reduce microvessel density and improve antibody penetration may be more promising in certain strains of tumours.[246,247] IFP can also be lowered by increasing plasma colloid osmotic pressure with systemic infusions of 20% human serum albumin as demonstrated by Hofmann et al. in mouse models.[248] A recent review by Baronzio, Parmar and Baronzio elaborates on other available methods to regulate IFP, such as inducing hyperthermia or using ultrasound therapy.[249]

Matsumura and Maeda describe an "enhanced permeability and retention (EPR) effect" in solid tumours for macromolecules larger than 48 kDa.[250,251] The hypotheses are that tumours have enhanced permeability to plasma proteins due to leaky tumour blood vessels and that plasma proteins are retained at the tumour site due to poor lymphatic drainage.[250,251] However, much of their information about enhanced permeability and its mechanism comes from infection models rather than solid tumours, which do not have high IFP as a barrier to convective flow.[252] Recent research into the EPR effect supports the IFP hypothesis regarding reduced convective flow in the tumour bulk and enhanced delivery and permeability only to the rim region of the tumour. Maeda and colleagues show

that the EPR effect is consistent for small tumours but not for larger tumours where the IFP barrier to delivery is significantly higher.[252] In these cases, they are able to boost the EPR effect by increasing blood pressure to overcome tumour IFP.[253]

Retention in tumours is also mediated in part by the properties of the extracellular matrix. The dense extracellular matrix present in desmoplastic tumours directly impairs the movement of antibodies through the interstitium.[254] Netti et al. show that this resistance can be mitigated by treatment with collagenase.[254]

Tumour cells have high demands for nutrients and amino acids. To meet these demands, macropinocytosis is upregulated in certain tumour cells to bring in large amounts of protein from the extracellular fluid that can be degraded into amino acids.[255] This mass internalization and quick protein degradation is ideal for the intracellular release of ADC payloads. Ha et al. propose that new ADCs can be targeted against macropinocytosis markers to achieve a degree of tumour-selective exposure.[256]

Broadly speaking, the location and size of solid tumours are important for predicting exposure to ADCs. Considering basic physiology, a melanoma on the skin would receive less exposure than a carcinoma in the liver after IV administration. An ideal solid tumour target for ADC therapy would be located in highly perfused tissue (e.g. liver, spleen, kidney, intestine, etc.). An inverse relationship between tumour size and antibody uptake per gram of tumour has been well established.[257-263] The highest antibody uptake per gram of tumour is seen in mouse xenografts weighing less than 200mg (range of tumour sizes studied: 30 – 1600mg), though this measurement cannot be easily extrapolated to humans.[257,261,262] The binding site barrier discussed above further hinders ADC penetration throughout solid tumour tissues.[104,128]

The physicochemical nature of the interstitial space in the tumour microenvironment poses an additional pharmacokinetic barrier for ADCs. Large tumours often have hypoxic regions and acidic interstitial fluid due to the lack of functional blood vessels and altered metabolism, and linkers may be unstable in these conditions. Moreover, the altered pH may affect or even compromise binding of ADC to the target.

Aside from physicochemical differences, the interstitial space in a solid tumour is often infiltrated with tumour-associated macrophages, dendritic cells, B cells, T cells and other members of the immune system. While it was originally thought that phagocytosis of ADCs into these non-target

cells would be a hindrance, adequate tumour cell-killing may still be achieved through the bystander effect. Furthermore, exposure of these immune cells to cytotoxic payloads has been shown to drive a beneficial anti-tumour immune response.[264]

2.9 Conclusion

The field of ADC development is expanding rapidly with contributions from many different research streams. The pharmacokinetic design and evaluation of the numerous ADCs in the clinical pipeline must be carefully thought out to ensure that ADCs reaching regulatory approval are both safe and effective. Due to the complexity of ADC pharmacokinetics and pharmacodynamics, the clinical value of a traditional pharmacokinetic assessment is low without a mechanistic understanding of disposition and elimination. This review serves as a consolidation of investigations from a multitude of disciplines into one foundation of pharmacokinetic understanding so that maximum value can be obtained from clinical trial data.

2.10 Study Highlights

In the context of this thesis, this chapter presents broad considerations on the mechanistic determinants of antibody pharmacokinetics in adults. In 2017, much of the concepts for antibodies had already been reviewed. This manuscript was written to expand that knowledge to cover antibody-drug conjugates, which were an emerging technology at the time.

Chapter 3
Population PBPK Modeling for Inter-Individual Variability in Trastuzumab Pharmacokinetics

3.1 Abstract

In this work we proposed a population physiologically-based pharmacokinetic (popPBPK) framework for quantifying and predicting inter-individual pharmacokinetic variability using the anti-HER2 monoclonal antibody (mAb) trastuzumab as an example. First, a PBPK model was developed to account for the possible mechanistic sources of variability. Within the model, five key factors that contribute to variability were identified and the nature of their contribution was quantified with local and global sensitivity analyses. The five key factors were the concentration of membrane-bound HER2 (Ag), the convective flow rate of mAb through vascular pores ($F2$), the endocytic transport rate of mAb through vascular endothelium (CL_{up}), the degradation rate of mAb-HER2 complexes (K_{deg}^{Ag}) and the concentration of shed HER2 extracellular domain in circulation (ECD). $F2$ was the most important parameter governing trastuzumab distribution into tissues and primarily affected variability in the first 500 hours post-administration. Ag was the most significant contributor to variability in clearance. These findings were used together with population generation methods to accurately predict the observed variability in four experimental trials with trastuzumab. To explore anthropometric sources of variability, virtual populations were created to represent participants in the four experimental trials. Using populations with only their expected anthropometric diversity resulted in under-prediction of the observed inter-individual variability. Adapting the populations to include literature-based variability around the five key parameters enabled accurate predictions of the variability in the four trials. Cancer increased variability in distribution and may increase the rate of extravasation or clearance of trastuzumab. The successful application of this framework demonstrates the utility of popPBPK methods to understand the mechanistic underpinnings of pharmacokinetic variability.

3.2 Introduction

With respect to pharmacokinetics, it is an impossible challenge to create one drug molecule that will be safe and effective for all people. A more realistic approach is to predict which subgroups of patients may be at risk of poor safety or efficacy. For this approach, the characteristics that may

predispose an individual to high or low exposure must be determined. In other words, we must determine the key factors that contribute to inter-individual pharmacokinetic variability.

Using conventional "top-down" pharmacokinetic (PopPK) modeling we can identify general pharmacokinetic differences between individuals based on covariates such as age, sex, size, ethnicity, organ function and disease progression. The main limitation of the PopPK method is that we cannot determine the impact of a covariate until it has been measured in a study population and the resulting clinical pharmacokinetic data has been analyzed.

In contrast, "bottom-up" population physiologically-based pharmacokinetic (popPBPK) modeling enables us to simulate the impact of covariates with virtual populations. General covariates identified through PopPK methods (e.g., ethnicity) may be surrogates for variability in underlying physiologic processes (e.g., genetic variant of a transporter). If a PBPK model accounts for all significant physiologic processes that affect the pharmacokinetics of the drug, then it follows that the total variability observed in pharmacokinetic data should be the output of inter-individual variability around each key process or parameter. This approach to quantifying variability is knowledge-driven rather than data-driven.

In this work we propose a framework for quantifying and predicting inter-individual pharmacokinetic variability. We demonstrate the utility of popPBPK modeling to complement conventional PopPK methods with a study of the anti-HER2 monoclonal antibody, trastuzumab. Key factors that contribute to variability will be identified and interpreted in tandem with a previous PopPK analysis by Bruno et al.[125] Conclusions will enhance our understanding of the mechanistic underpinnings of variability and prompt new questions about patient subgroups that may be at risk of poor safety or efficacy.

3.3 Methods

The primary aim of the research was to determine the factors that contribute to inter-individual variability in trastuzumab pharmacokinetics for both healthy volunteers and breast cancer patients using a population PBPK model.

3.3.1 Part One: Mean Analysis

1. Model Development: construction of an in silico whole-body PBPK model to describe the pharmacokinetics of trastuzumab in a mean individual.

2. Model Parameterization: estimation of model parameters based on existing literature.
3. Model Fitting: optimization of uncertain parameters by fitting the model to the mean concentration-time profiles in experimental data.
4. Model Evaluation: evaluation of the optimized model for a mean individual by predicting the mean concentration-time profiles from additional experimental data.

3.3.2 Part Two: Variability Analysis

5. Uncertainty and Sensitivity Analysis: identification of key parameters that contribute to inter-individual variability, characterization of their contribution and assessment of parameter correlation.
6. Population Simulation: development of a virtual population of unique individuals with literature-based variability around key parameters and simulation of plasma concentration-time data for the virtual population using the optimized model.
7. Analysis: comparison of the simulated inter-individual variability with the inter-individual variability observed in experimental data.

3.3.3 Software:

A MATLAB extension called SBToolbox2 was used to automate the simulation of the system of ordinary differential equations and model analysis.[265] The population generation tool was based in MATLAB and followed generally the method of Willmann et al.[266] Clinical data from literature was digitized using Plot Digitizer v2.6.8 by Joseph Huwaldt (plotdigitizer.sourceforge.net).

3.4 Results

3.4.1 Model Development

An *in silico* whole body model to describe the pharmacokinetics of trastuzumab in a mean individual was developed based on the platform model for a monoclonal antibody (mAb) by Shah and Betts.[135] A schematic for the structure of the model is shown in Figure 9. Figure 10 illustrates the mechanistic processes affecting mAb pharmacokinetics within each tissue compartment. Previous PBPK models by Cao and Jusko, Li et al., and Glassman and Balthasar have successfully characterized the nonlinear pharmacokinetic profile of trastuzumab.[109,267,268]

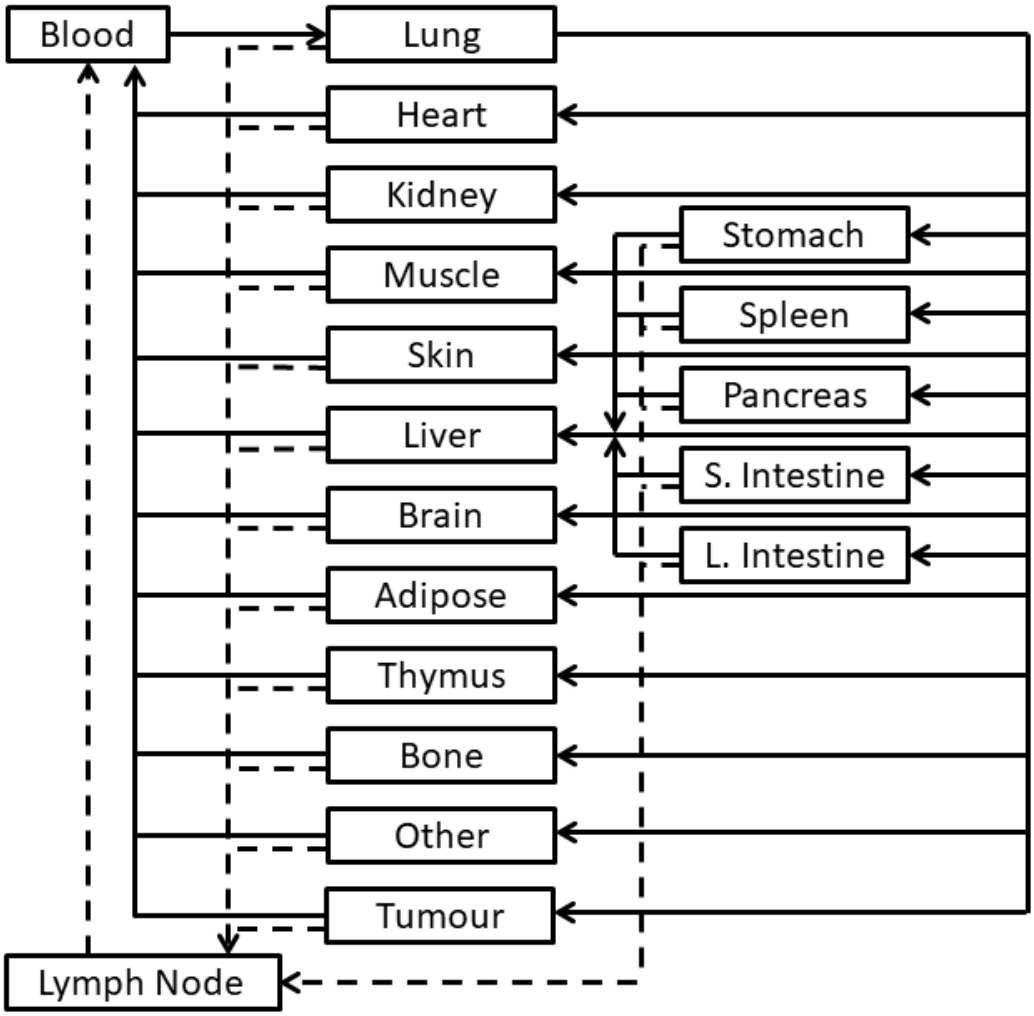

Figure 9. A schematic for the whole body PBPK model showing the connection of anatomical compartments by blood flow (solid line) and lymph flow (dashed line)

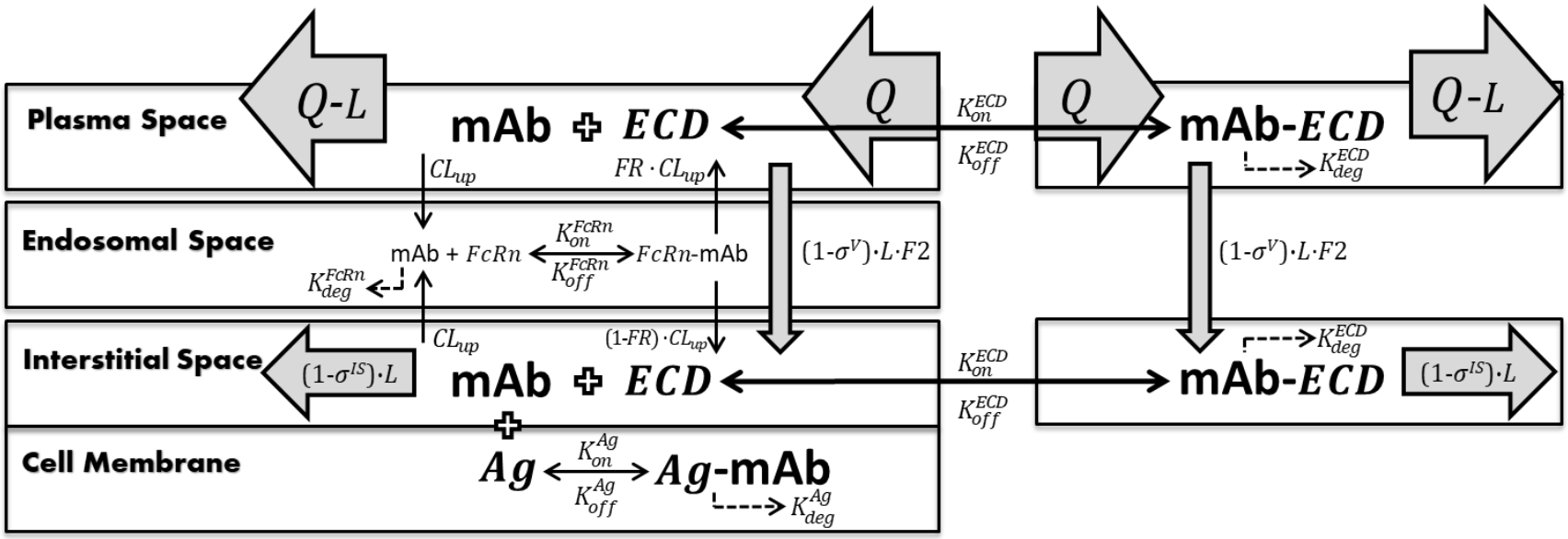

Figure 10. An illustration of the physiological processes affecting the movement of trastuzumab through each organ and sub-compartment

Shedding of the HER2 extracellular domain (ECD) was modeled as proposed by Li et al. with the following modifications:[268]

1. ECD concentrations were assumed constant (rate of synthesis equal to rate of degradation)
2. The concentration in the interstitial space was assumed equal to the measured concentration in plasma
3. mAb-ECD complex distribution was assumed to be similar to mAb distribution, and pinocytic uptake was lumped into a general degradation term for a circulating immune complex (K_{deg}^{ECD})

Antigen kinetics were determined from existing mechanistic models for HER2 trafficking that incorporated in vitro measurements.[269-274] Derivation of the antigen degradation term (K_{deg}^{Ag}) can be found in **Appendix A**. The concentration of membrane-bound HER2 antigen was kept constant (rate of synthesis equal to rate of degradation) because trastuzumab binding does not induce internalization or degradation of the receptor.[109,119,268-270,275,276] The model can apply to both healthy volunteers and breast cancer patients by toggling a tumour compartment on and off. The tumour compartment was connected by blood and lymph flow to the whole-body circulation for cancer simulations. Model equations can be found in **Appendix A**.

3.4.2 Model Parameterization

Reference values for anatomical parameters were obtained from BioDMET documents and can be found in **Appendix A**.[50,266] The volumes of the organ sub-compartments (plasma space, endosomal space and interstitial space) were calculated for each organ based on the fractions used in the platform model.[135] Lymph flow in each organ, aside from the lung, was set to 0.2% of plasma flow.[135] Lymph flow in the lung was set to 3% of total body lymph flow in agreement with Gill et al.[77]

Experimental plasma concentration-time data was collected from seven pharmacokinetic studies with trastuzumab and its biosimilars. Biosimilars are pharmacokinetic equivalents of trastuzumab and were included because of the sparse data available for trastuzumab. Table 5 lists the trials and corresponding demographic information.

Table 5. Experimental pharmacokinetic datasets collected for use with the PBPK model.

Trial	Dose (mg/kg)	N[a]	Sex	Cohort	ECD (ng/mL)	Age (years)
Trastuzumab						
Morita et al.[277]	6	35	M	Healthy Volunteers	8[d]	22.7 (6.8)
Wisman et al.[278]	6	46	M	Healthy Volunteers	8[d]	25 (6.8)
Wynne et al.[279]	6	6	M	Healthy Volunteers	8[d]	23 (19-26)
Yin et al.[280]	6	32	M	Healthy Volunteers	8[d]	35.3 (9.2)
Tokuda et al.[281]	1, 2, 4, 8	16	F	Breast Cancer	19.9	51 (32-64)
Baselga et al.[282]	8 then 6 q3w[b]	98	F	Breast Cancer	30	53.8 (23-84)
Cobleigh et al.[283]	4 then 2 q1w[c]	213	F	Breast Cancer	9.33	50 (28-81)
Leyland-Jones et al.[284]	8 then 6 q3w[b]	32	F	Breast Cancer	20	53 (31-70)
FTMB						
Wisman et al.[278]	0.5, 1.5, 3, 6	64	M	Healthy Volunteers	8[d]	25 (6.8)
DMB-3111						
Morita et al.[277]	6	35	M	Healthy Volunteers	8[d]	22.9 (3.2)
PF-05280014						
Yin et al.[280]	6	34	M	Healthy Volunteers	8[d]	34.5 (10.7)

[a] Number of patients
[b] Every 3 weeks thereafter
[c] Every 1 week thereafter
[d] Value not reported; assumed from literature[285,286]

When using the model to simulate the mean concentration-time profile with one representative virtual individual, anatomical parameters were scaled from the reference values so that the virtual individual's characteristics matched the mean height, weight, body mass index (BMI), body surface area (BSA), gender, cancer status and ECD level of individuals in the experimental trial. A tumour with a volume of 20mL was added to the representative individual for simulations of trials with breast cancer patients. Tumour parameters were extracted from a previous model for trastuzumab and are available in **Appendix A**.[109] A description of mechanistic model parameters can be found in Table 6.

Table 6. Mechanistic parameters used in the model including literature-based estimates and the reported variance for the parameter, expressed as a coefficient of variation (CV%)

Parameter	Description	Units	Estimate	CV%
σ^V	Vascular reflection coefficient	-	0.85-0.99[a] [135]	See $F2$
σ^{IS}	Lymph reflection coefficient	-	0.2[135]	-
CL_{up}	Rate of endocytic transport per L endosomal space	L/h/L	0.0366[135]	25[162,287]
$F2$ (h)	Convective flow scaling factor (healthy)	-	1[135]	25[140]
$F2$ (c)	Convective flow scaling factor (cancer)	-	1 (assumption)	50 (assumption)
$FcRn$	Accessible FcRn in endosomal space	nM	49800[135]	15[77,109,135]
FR	Fraction that recycles to vascular space	-	0.715[135]	5[162]
K_{deg}^{FcRn}	Degradation rate of FcRn-unbound mAb	1/h	42.9[135]	15[135]
K_{on}^{FcRn}	Association rate for FcRn binding	1/nM/h	0.8[288]	10[289]
K_{off}^{FcRn}	Dissociation rate for FcRn binding	1/h	618.4[288]	10[289]
K_{on}^{Ag}	Association rate for HER2 binding	1/nM/h	0.74[290,291]	5[290]
K_{off}^{Ag}	Dissociation rate for HER2 binding	1/h	4.07[290,291]	5[290]
K_{deg}^{Ag}	Degradation rate of HER2 and mAb-HER2 complexes	1/h	0.0789[270,273]	33.3[270]
Ag	Accessible membrane-bound HER2	nM	1.6[292]	100[293,294]
Ag_{Tumour}	Accessible HER2 on tumour cell membrane	nM	$25 \times Ag$[293]	100[293]
K_{on}^{ECD}	Association rate for ECD binding	1/nM/h	1[291]	5
K_{off}^{ECD}	Dissociation rate for ECD binding	1/h	0.1[291]	5
ECD	ECD in plasma and interstitial space	nM	Trial-specific	100[282]
K_{deg}^{ECD}	Degradation rate of mAb-ECD complexes	1/h	0.0144[122,123]	25[122]
BM	Body mass	kg	Trial-specific	12[266]

[a] Tissue-specific values are listed in **Appendix A**

The concentration of HER2 in normal tissues was measured to be 10,000 receptors/cell.[292] The following calculation was applied, assuming $3.27 \cdot 10^{13}$ cells/body and a cellular volume of 53.6 L/body, giving a concentration of 10.1 nM in cells.[295]

$$Ag_{body}^{C} = \frac{\left(1 \times 10^{4} \frac{receptors}{cell}\right)\left(3.27 \times 10^{13} \frac{cells}{body}\right)}{\left(6.02 \times 10^{23} \frac{receptors}{mol}\right)\left(53.6 \frac{L\ cells}{body}\right)}$$

However, HER2 is a membrane-bound protein and the concentration of HER2 (Ag) for the model input must be in terms of interstitial volume (V^{IS}) to enable stoichiometric binding of mAbs in the interstitial space. There are also limitations to HER2 accessibility. First, one third of HER2 receptors are internalized in the cell and inaccessible for binding while two thirds are present on the membrane.[269,270] Furthermore, accessibility is impaired by dimerization. Up to 95% of membrane-bound HER2 is homo- and heterodimerized with members of the HER family.[269,270] The HER2 extracellular domain is approximately 100kDa and trastuzumab is 145.5kDa in size.[296] Dimer linkages occur between the respective subdomain II regions of monomers. Trastuzumab binds to subdomain IV, which is closest to the membrane and is overshadowed by subdomain II.[296] An analysis of crystal structures suggests that subdomain IV is blocked when HER2 is dimerized by a linkage across subdomain II.[296] Therefore in our model, the concentration of membrane-bound HER2 available for high affinity binding in each organ was assumed to be the concentration of monomers only (~5% of membrane-bound HER2) and was calculated by:

$$Ag_{organ} = 10.1\ nM\ \times \frac{V_{organ}^{C}}{V_{organ}^{IS}} \times \frac{2}{3}\ membrane\text{-}bound \times 0.05\ monomers$$

3.4.3 Model Fitting

SBtoolbox2 was used to globally fit the model for a mean individual to the mean plasma concentration-time profiles for trastuzumab in the datasets from Wisman et al. and Yin et al. with a simulated annealing method (see Table 5).[278,280] Glassman and Balthasar identified that the rate of convective flow through pores and the rate of endocytic transport (CL_{up}) are drug-specific and require fitting.[109] A scaling factor ($F2$) was used for the fit to describe the convective flow through pores according to:

$$Convective\ Flow = \ F2 \times (1 - \sigma^{V}) \times L$$

The fitted values for $F2$ and CL_{up} were 3.35 and 0.0188 L/h/L respectively. Figure 11 shows two model-fitted profiles using data from Wisman et al. and Yin et al.[278,280] The optimized model for a mean individual accurately characterizes the non-linear shape of the mean pharmacokinetic profiles.

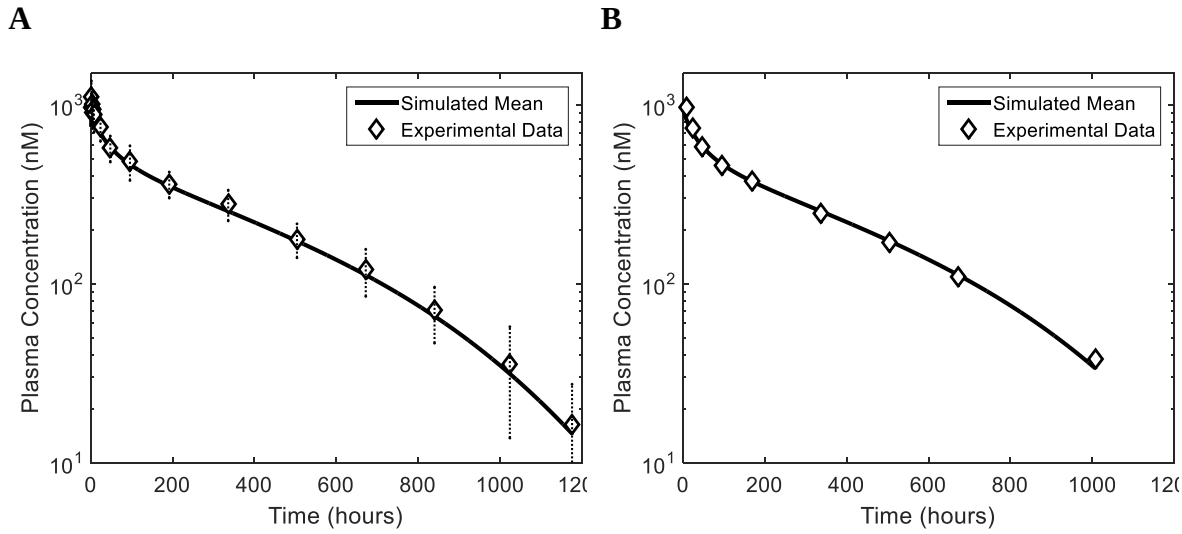

Figure 11. A comparison of the model-fitted profile for a mean individual (solid line) with the experimental data (diamond) in healthy males from Wisman et al. (A) and Yin et al. (B)[278,280]

3.4.4 Model Evaluation

The remaining datasets for trastuzumab and its biosimilars in Table 5 were used to validate the optimized model for mean individuals. Figure 12 shows a comparison of the observed mean plasma concentrations to the model-predicted mean plasma concentrations for all evaluation datasets, which include a variety of dose levels and administration protocols. Predictions for mean individuals were strong with an R^2 of 0.967 when simulating mean pharmacokinetic profiles for both healthy males and females with breast cancer. The model trended toward an overestimation of trastuzumab plasma concentrations at levels below 200 nM and an underestimation of trastuzumab plasma concentrations at levels above 1200 nM in patients with cancer.

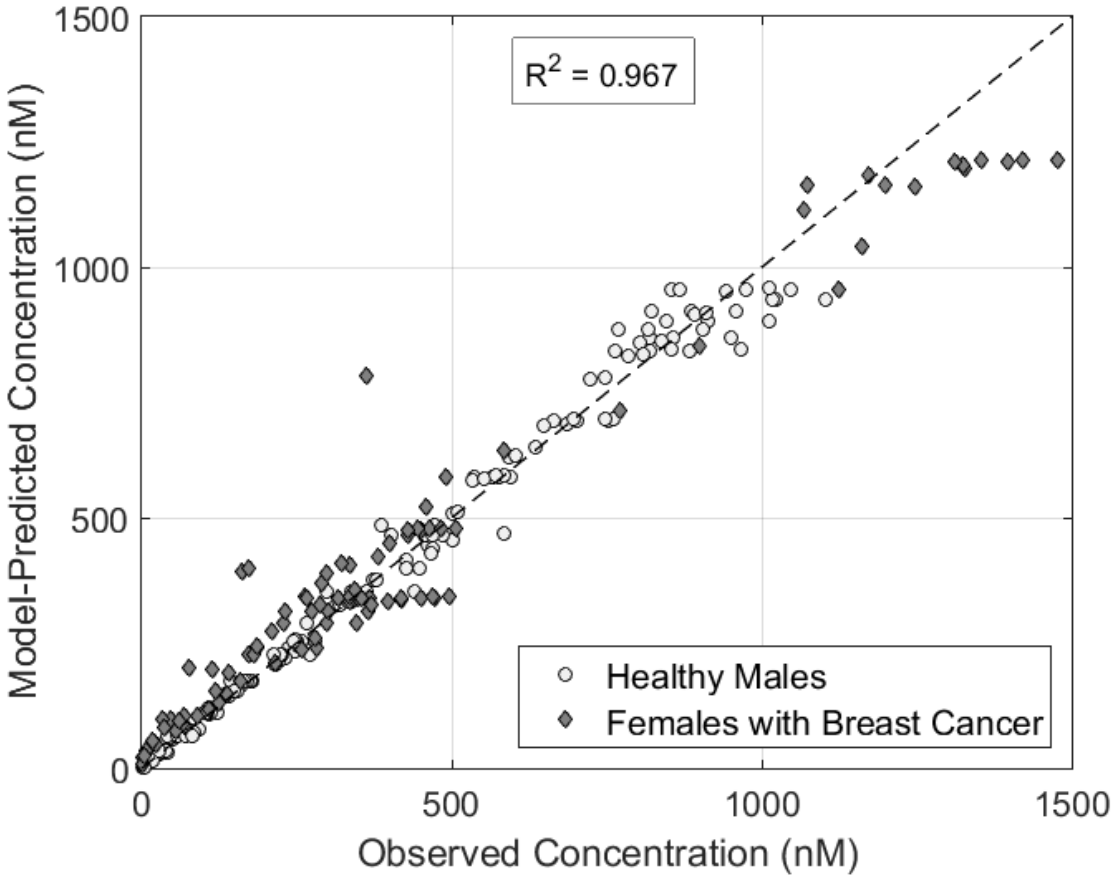

Figure 12. Model-predicted vs. observed concentrations for healthy males (circle) and females with breast cancer (diamond). The observed concentrations come from the experimental trials listed in Table 5 that were not used for model building.

With a validated model in place that adequately predicts mean concentration-time profiles, we turned our attention to analyze variability. Analyses were done with parameter values as determined for the validated model, which include the fitted values for $F2$ and CL_{up}. No changes were made to the mean parameter values.

3.4.5 Uncertainty and Sensitivity Analysis

A local sensitivity analysis that accounts for the variability around each parameter that is seen in a general population allows for an assessment of the importance of each parameter in defining total inter-individual variability (see Table 6). The sigma-normalized sensitivity coefficient (S_p^{σ}) is a

measure of the anticipated percent change in AUC with a perturbation of one standard deviation (σ_p) in the mean parameter value (p). The sigma-normalized sensitivity coefficient was calculated by:

$$S_p^{\sigma} = \left| \frac{AUC(p \pm \sigma_p) - AUC(p)}{AUC(p)} \right| \times 100\%$$

Key parameters that contribute to inter-individual variability were identified by $S_p^{\sigma} \geq 1$. If a parameter has a sigma-normalized sensitivity coefficient of 1, then an individual possessing a parameter value that is one standard deviation higher or lower than the mean value will have an AUC that is 1% different than the mean AUC of the population. We deem that this difference is the cut-off for declaring a parameter important for accounting for interindividual variability. The literature-defined variability in terms of a coefficient of variation (CV) for each parameter is listed in Table 6. Of note, the CV for FcRn is based on the variability in PBPK model estimates to date and the CV for $F2$ was dependent on cancer status. Figure 13 shows that the five key parameters are the rate of endocytic transport (CL_{up}), the rate of convective flow through pores ($F2$), the concentration of membrane-bound HER2 accessible for binding (Ag), the degradation rate of HER2 and mAb-HER2 complexes (K_{deg}^{Ag}) and the concentration of ECD (ECD). The magnitudes of the effects of the key parameters on the model remain similar whether the parameters are increased or decreased by one standard deviation. Body mass (BM) was included in this analysis for comparative purposes. The result suggests that physically varying body mass (changing organ size and flow rates) has a minor effect on plasma concentrations when dosing is normalized to body mass (mg/kg).

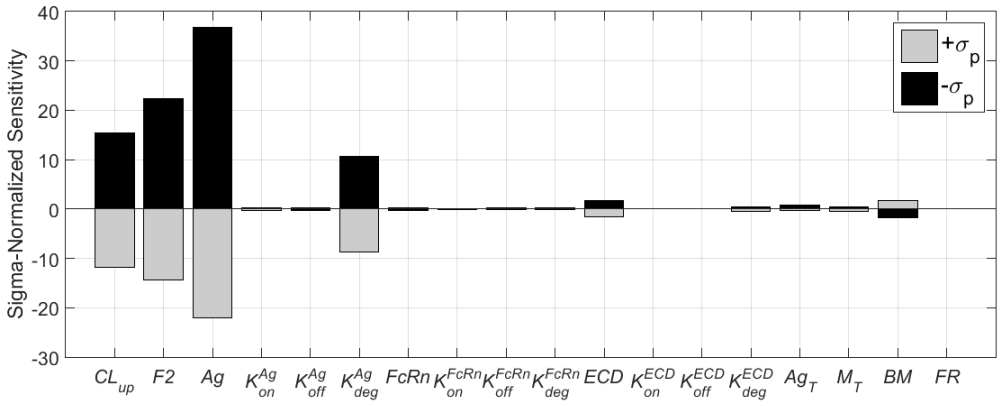

Figure 13. Sigma-normalized local sensitivity coefficients ($\boldsymbol{S_p^{\sigma}}$) determined for each mechanistic parameter in the model, and body mass (see Table 6). Key parameters were identified by $\boldsymbol{S_p^{\sigma} \geq 1}$

The sigma-normalized local sensitivity of the model to each key parameter over the entire time series was analyzed in Figure 14. The convective flow through pores ($F2$) was the most important parameter governing trastuzumab distribution into tissues and primarily affected variability in the first 500 hours post-administration. The concentration of HER2 (Ag) was the most significant contributor to variability in clearance. K_{deg}^{Ag} plays a significant role in elimination as expected. The effects of ECD are small overall.

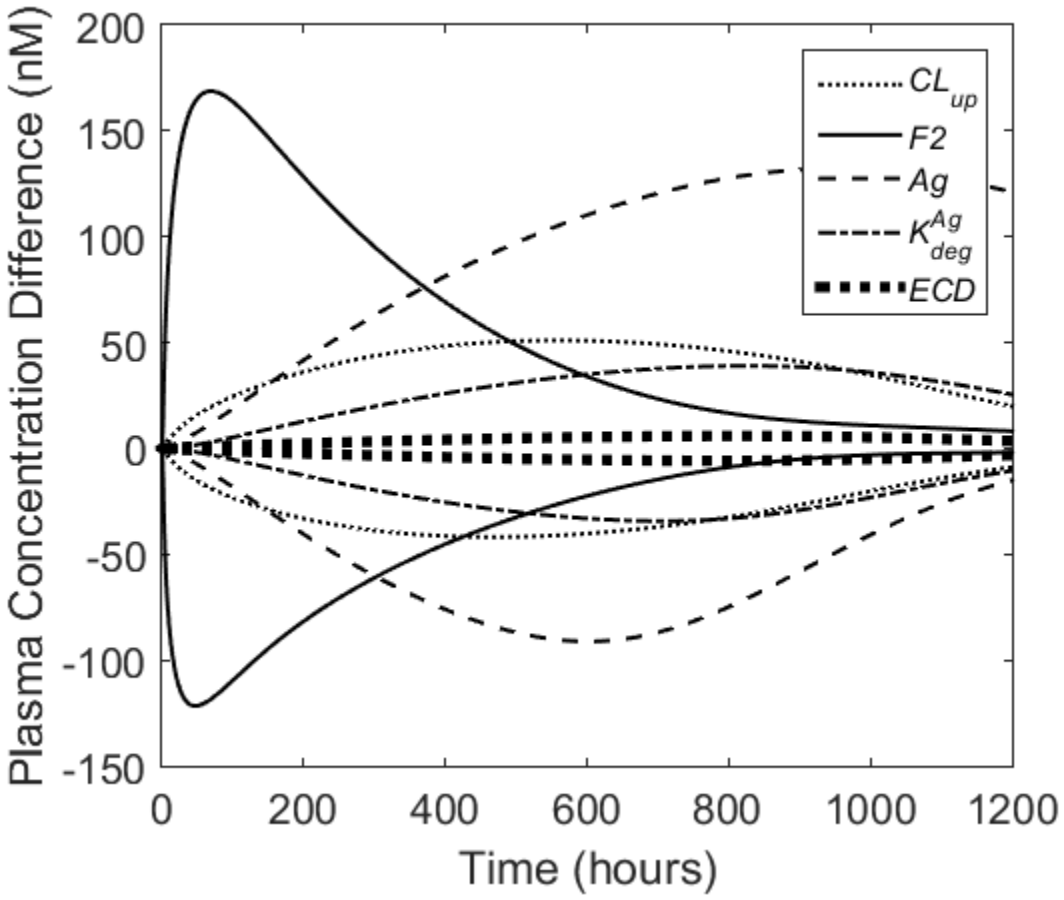

Figure 14. The effect of each key parameter on plasma concentration over time when perturbed by ± one standard deviation, expressed as the absolute difference in plasma concentration between the perturbed simulation and the nominal simulation at every time point.

Next, we carried out a global variance-based sensitivity analysis to quantify the contribution of select key parameters (CL_{up}, $F2$, K_{deg}^{Ag}, Ag, ECD and $FcRn$) to total variability in terms of the effect on plasma AUC. $FcRn$ was included as an insensitive parameter for a comparative control. The

global sensitivity analysis quantifies the variability attributed to each key parameter individually (first order effects) as well as the total variability caused by the parameter when additionally considering its interactions with every other input parameter (total effects). We used Sobol's method as proposed by Saltelli et al, which is described in **Appendix A**.[297,298]

Figure 15A shows that together, the first order effects of parameters CL_{up}, $F2$ and Ag account for most of the total variability observed when the six parameters in Table 7 are allowed to vary both individually and in possible combination with each other. Figure 15B contrasts the first order effects for each parameter with the total global effects, which occur when each parameter varies individually and in combination with the others. The first order effect of each parameter accounts for the vast proportion of its total effect. The difference between the total effect and first order effect sensitivity measure determines the degree of interaction between each parameter and the others. The difference between the total effects and first order effects are small, signifying a small degree of interaction between each of the analyzed parameters and the others.

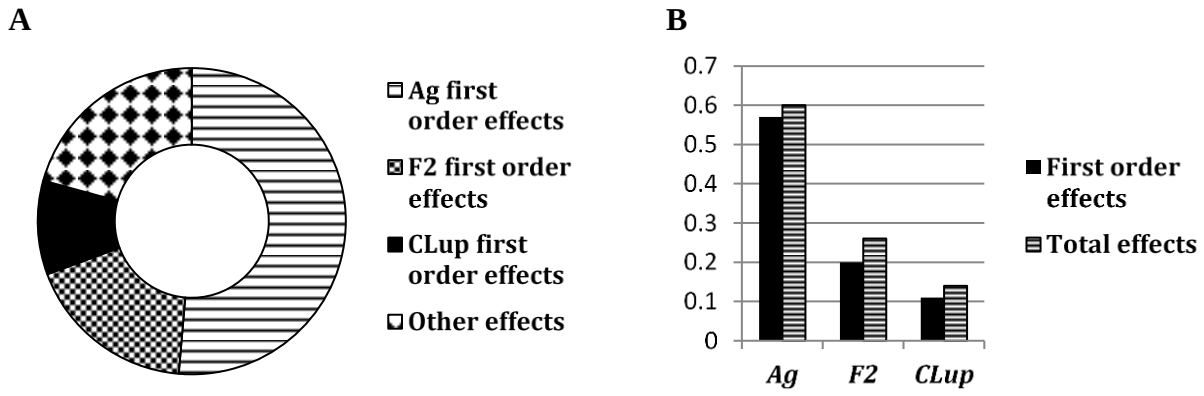

Figure 15. Panel (A) shows that the first order effects of $\boldsymbol{Ag}$, $\boldsymbol{F2}$ and $\boldsymbol{CL_{up}}$ make up most of the total variability. Panel (B) shows that the differences between the first order effects (solid fill) and total effects (stripe fill) for $\boldsymbol{Ag}$, $\boldsymbol{F2}$ and $\boldsymbol{CL_{up}}$ are small.

Table 7. A summary of the inputs and the results for Sobol's global sensitivity analysis

Parameter	Mean Value	Coefficient of variation (%)	First Order Sensitivity (S_j)	Total Sensitivity (S_{T_j})
CL_{up}	0.0188 L/h/L	25	0.11	0.14
$F2$ (cancer)	3.35	50	0.20	0.26
K_{deg}^{Ag}	0.0789 h^{-1}	33.3	0.02	0.06
Ag	1.6 nM	100	0.57	0.60
ECD	0.3 nM	100	~0	0.02
$FcRn$	49800 nM	15	~0	0.01

Lastly, it is important to assess the identifiability of the key parameters which gives a measure of the confidence we can have that the values in the model are the true values. A parameter is identifiable within a model if it is theoretically possible to learn the true value after observing the model for an infinitely long time. SBtoolbox2 was used to create a parameter correlation matrix based on the method by Jacquez and Greif (Figure 16).[299] Elements in the matrix that are close to 1 (white) indicate that it is not feasible to identify the true value of the corresponding parameters independently. Elements that are close to 0 (black) indicate that there is no correlation between the corresponding parameters and thus these parameters should be independently identifiable. As Figure 16 indicates, K_{deg}^{Ag} and Ag are correlated, meaning that we may be able to achieve a similar output profile with different combinations of values for these parameters. CL_{up} is also moderately correlated to these parameters. The information from Figure 14 strengthens the understanding of these correlations. Figure 14 shows that the three parameters affect the model in similar ways over similar time periods. However, the peak effect of CL_{up} on the pharmacokinetic profile occurs earlier than the peak effects for K_{deg}^{Ag} and Ag. Therefore, K_{deg}^{Ag} and Ag are highly correlated to each other. The correlations of CL_{up} to K_{deg}^{Ag} and Ag are weaker, but significant. This result stresses the importance of dense sampling schemes across the time profile if estimating a pair of these parameters.

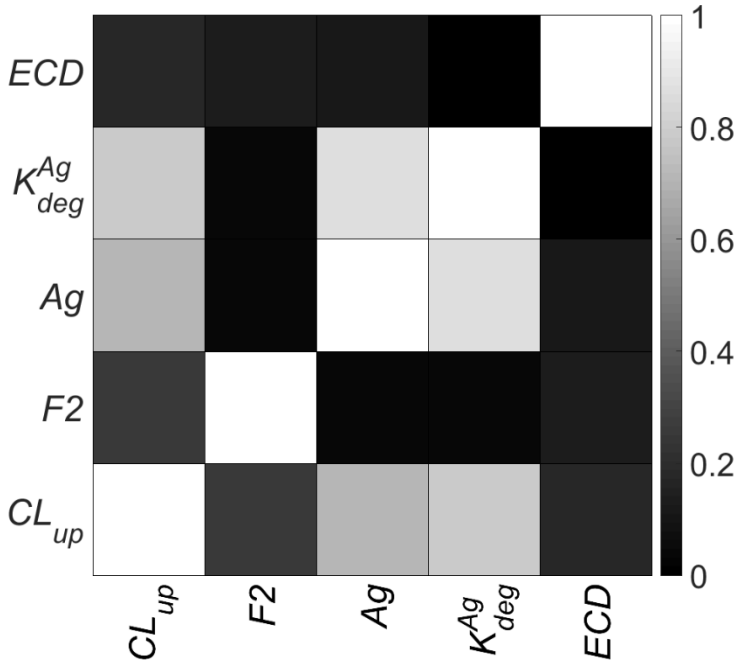

Figure 16. Matrix presenting the correlation between key parameters. A white colour suggests a strong correlation, while a black colour suggests no correlation between two parameters.

3.4.6 Population Simulations

Virtual populations with variability in anthropometric parameters (body mass, height, blood flow and hematocrit) similar to the anthropometric variability in each experimental sample were created using a population generation tool previously developed in the Edginton lab. Briefly, individuals for a population are randomly generated according to height and the associated standard deviation reported for the patient sample in the experimental trial. Organ masses are randomly generated from truncated distributions to prevent extreme outliers, and the resulting body mass and the BMI are calculated. If the calculated BMI is outside of the range provided for the patient sample in the experimental trial, this virtual individual is discarded. The resulting virtual population should have approximately the same mean and standard deviation for BMI, height and body mass as the patient sample.

Virtual individuals were used as inputs for the model and the simulated variability for the virtual population was compared to the actual observed variability in the datasets from Wisman et al., Morita et al., Baselga et al. and Cobleigh et al.[277,278,282,283] Figure 17 shows the minimal impact of

anthropometric variability alone on inter-individual variability in the presence of body-mass normalized dosing (mg/kg). As mentioned before, the model trended toward an over-prediction of trastuzumab plasma concentrations at levels below 200 nM in patients with cancer (Figure 12). These overestimations are compounded after multiple weekly low doses in the trial by Cobleigh et al., resulting in a significant over-prediction of the mean trough level until plasma concentrations reach steady state (Figure 17D).[283]

Next, individuals in the virtual populations were modified to have a normal or lognormal distribution around key model parameter values ($F2$, CL_{up}, Ag, K_{deg}^{Ag} and ECD) according to the coefficients of variation in Table 6. The distributions for Ag and ECD were lognormal to encompass the wide spread of values seen in the literature.[282,293,294] Since these five key parameters are the most important for describing variability, they should – in theory – capture most of the experimental variability together. The simulated variability was compared to the experimental variability in the datasets from Wisman et al., Morita et al., Baselga et al. and Cobleigh et al. in Figure 18.[277,278,282,283]

Overall, the framework enabled adequate predictions of the inter-individual variability in clinical trials by decomposing total variability into literature-based variability around each of the key parameters a priori (Figure 18). However, the population model under-predicted variability in the first 72 hours for healthy males (Figure 18A, Figure 18B) and in the first cycles before steady state for females with breast cancer (Figure 18C, Figure 18D). While the mean plasma concentration is over-predicted in the simulation for the trial by Cobleigh et al., an adequate prediction for the magnitude of the variability remains.[283]

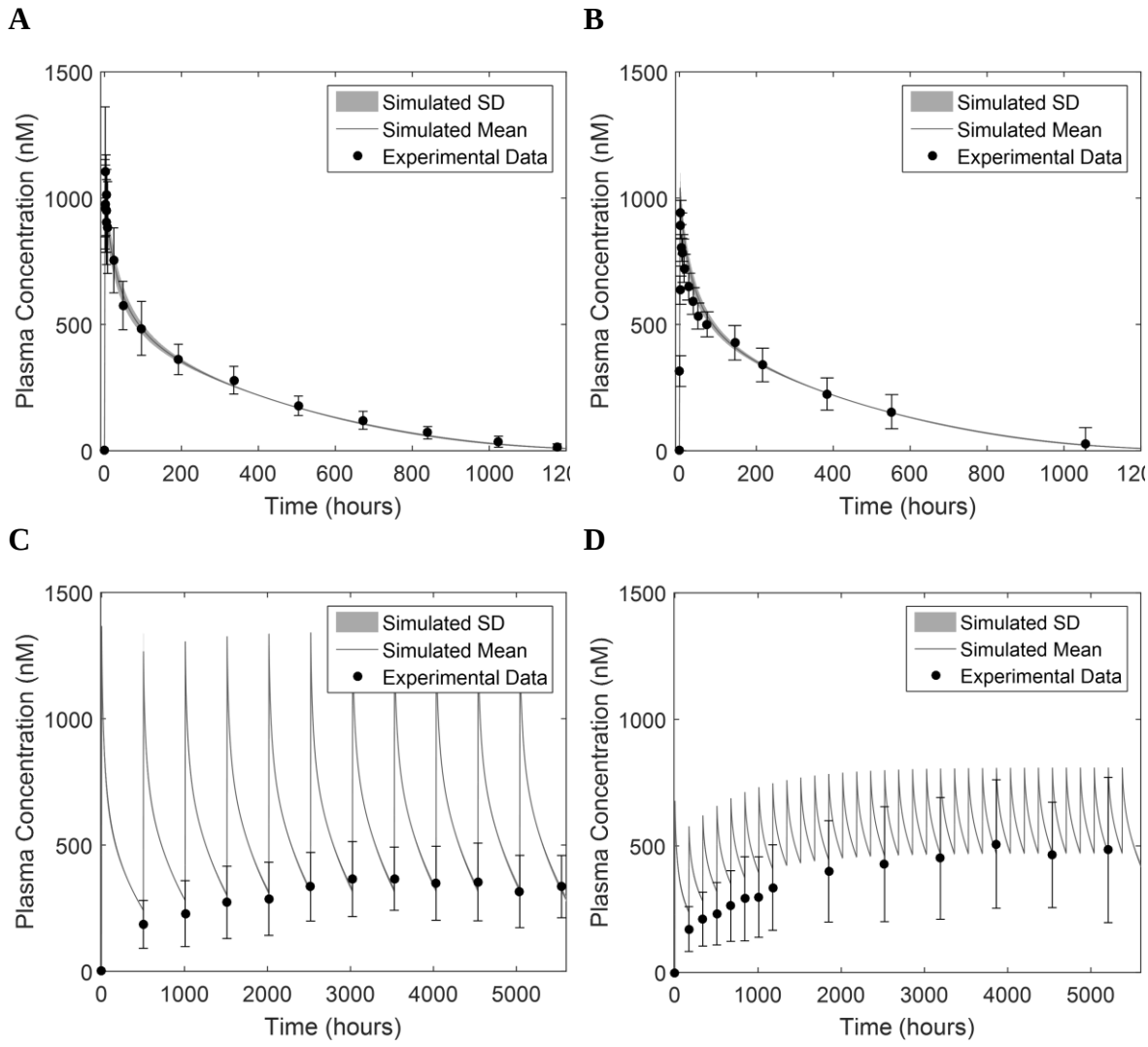

Figure 17. Plasma concentration vs. time profiles for a virtual population created with variability in anthropometric parameters alone. The resulting variability (shaded fill) was compared to the observed inter-individual variability (solid error bar) in Wisman et al. (A), Morita et al. (B), Baselga et al. (C) and Cobleigh et al. (D).[277,278,282,283] In all cases, variability is reported as an arithmetic standard deviation.

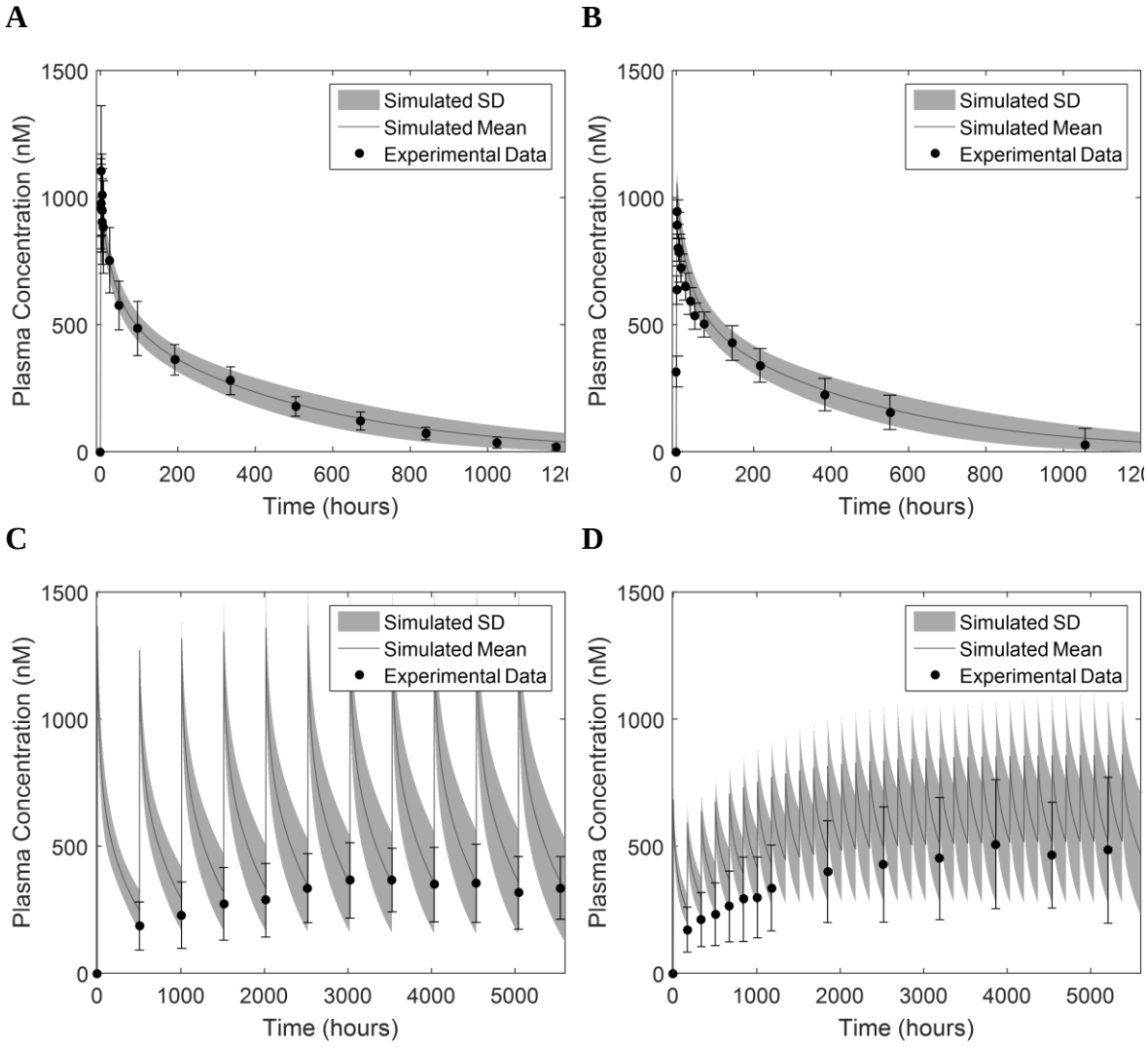

Figure 18. Plasma concentration vs. time profiles for a virtual population created with variability in anthropometric parameters plus literature-defined variability around the five key parameters ($\boldsymbol{F2}$, $\boldsymbol{CL_{up}}$, $\boldsymbol{Ag}$, $\boldsymbol{K_{deg}^{Ag}}$ and $\boldsymbol{ECD}$). The resulting variability (shaded fill) was compared to the observed inter-individual variability (solid error bar) in Wisman et al. (A), Morita et al. (B), Baselga et al. (C) and Cobleigh et al. (D).[277,278,282,283] In all cases, variability is reported as an arithmetic standard deviation.

3.5 Discussion

Using the population PBPK modeling framework, five key parameters that contribute to inter-individual variability in trastuzumab pharmacokinetics were identified. In other words, patients who are outliers with respect to these five key parameters:

1. The concentration of membrane-bound HER2 accessible for binding (Ag)
2. The rate of convective flow of mAb through vascular pores from plasma to interstitial space ($F2$)
3. The rate of endocytic transport of mAb into vascular endothelial cells (CL_{up})
4. The degradation rate of HER2 and mAb-HER2 complexes (K_{deg}^{Ag})
5. The concentration of shed HER2 ECD in the plasma and interstitial space (ECD)

may be at risk for poor safety or efficacy with trastuzumab.

The next task is to assess the clinical relevance of each parameter. Can these parameters be measured in patients and if not, how are these parameters related to more measurable characteristics? In a review of inter-individual variability for all mAbs, Gill et al. highlighted ways that physiologic processes affecting mAb pharmacokinetics could be correlated to general covariates such as age, body mass, ethnicity and disease state.[300] We expand on those insights here for trastuzumab.

Total concentrations of HER2 vary widely in healthy and cancer populations and can be measured with the HERmark assay.[292] This assay can also measure the concentration of HER2 homodimers, which enables a prediction for the concentration of HER2 that is accessible for mAb binding (Ag).[294] In the era of personalized medicine, measured levels of HER2 in normal tissues may be appropriate grounds for dose adjustments.

The rate of convective flow of mAb through pores ($F2$) is difficult to measure directly. However, Parving and colleagues have demonstrated that the flow of plasma proteins through capillaries can change proportionally to blood pressure and can be altered by liver cirrhosis, diabetes, congestive heart failure and inflammatory skin conditions.[140-144,146-148,301] The measured transcapillary escape rate (TER) of IgG and albumin in various disease states is summarized in Table 8.

Table 8. Values reported for the transcapillary escape rate (TER) of albumin and IgG in patients with various conditions

Condition	TER IgG (%/h, SD)	TER Albumin (%/h, SD)
Healthy[140]	3.0 (0.7)	5.2 (1.0)
Hypertension[a 140]	4.7 (1.0)	7.8 (0.9)
Short-Term Type 1 Diabetes[b 142]		5.5 (1.0)
Long-Term Type 1 Diabetes[c 143]	4.4 (1.0)	7.4 (1.1)
Liver Cirrhosis[141]	8.4 (0.8)	7.4 (1.9)
Chronic Right Heart Failure[144]		8.3 (1.6)
Inflammatory Skin Disease[301]		8.6 (1.1)
Cancer[146-148]		5.5 – 12.1[d]

[a] mean arterial blood pressure: 193/119 mmHg
[b] mean duration: 2.6 years
[c] mean duration: 20 years with microangiopathy
[d] range of reported medians in 3 studies

The presence of cancer impacts the TER and therefore likely increases the $F2$ parameter.[146-148] Cancer is an inflammatory disease that alters many homeostatic functions in the body. The TER of albumin is up to 2-fold faster in patients with cancer than healthy patients. Furthermore, the liver is a common site of metastasis and damage may increase the TER and $F2$ similar to cirrhosis.[282]

When $F2$ increases there is a shift in distribution from plasma to tissue, while the final plasma trough concentrations remain similar (Figure 14). Therefore, we anticipate that patients with the conditions listed in Table 8 may experience greater tissue exposure along with possibly increased efficacy and toxicity. For example, a cancer patient with diabetes who is receiving trastuzumab may have greater penetration of the drug into heart tissue and may be at an increased risk for cardiotoxicity compared to a cancer patient without diabetes, even while trough concentrations are within normal therapeutic ranges for both patients. The results of a recent meta-analysis by Leung and Chan may support this hypothesis.[302] They identify hypertension and diabetes (among other factors) as significant risk factors for cardiotoxicity in elderly females being treated with trastuzumab.[302]

The rate of endocytic transport (CL_{up}) of mAb into vascular endothelial cells is not well understood in modeling as estimates vary 10-fold between groups.[109,135] It is the gateway by which the mAb participates in FcRn binding and recycling. Genetic factors likely play the largest roles for determining CL_{up} for an individual.[287,300] Genotypic testing of FcRn, caveolin or other proteins involved in endocytosis may prove clinically relevant for dose adjustments.

Although not directly measurable, the degradation rate of HER2 and mAb-HER2 complexes (K_{deg}^{Ag}) is correlated with the internalization rate.[269,271] Hendriks showed that the internalization rate of HER2 depends on the presence of the epidermal growth factor (EGF) ligand and the relative concentrations of HER1-4 on the cell membrane.[269] The degradation rate may also be subject to genetic polymorphisms of the HER2 protein. Genotypic testing of HER2 may be useful for dosing to improve safety and efficacy.

The role of ECD as a predictor for response to trastuzumab therapy or tumour progression is still unknown. Carney et al. indicate that an increasing ECD level is a marker for poor prognosis, while a number of smaller studies show that an early increase in ECD level before trastuzumab treatment can predict a good response.[303-310] Because of the uncertainty and the overall small effect on variability, the clinical utility of ECD for predicting safety and efficacy is low.

Next, we compare our results from the popPBPK framework to existing results from a PopPK study by Bruno et al. in patients with metastatic breast cancer.[125] The group modeled the pharmacokinetics with a non-linear mixed effects model using two compartments.[125] Variability in patient body mass, the number of metastatic sites and the concentration of serum extracellular domain were determined to be the most important factors for predicting the observed variability, but together failed to predict the large variability in the data.[125] In the following analysis, we do not endeavour to contrast the work of Bruno et al. Rather we strive to gain a mechanistic understanding of their findings and of the overall variability in trastuzumab pharmacokinetics through PBPK modeling approaches.

First, they showed that the volume of distribution for trastuzumab changes as a function of body mass, ranging from 2.5L at 49 kg to 3.7L at 96 kg.[125] These volumes correspond to the predicted plasma volume changes as a function of body mass (65 mL blood/kg for females, hematocrit 0.36-0.48). Body mass-normalized dosing eliminates significant inter-individual variability, as shown in Figure 17.

Bruno et al. also demonstrated that patients with four or more metastatic sites had an 18% lower steady state exposure than those with up to three metastatic sites.[125] In our model, patients with a total tumour volume of 80 mL had a 1.75% lower AUC than patients with a total tumour volume of 20 mL. The covariate effect cannot be reproduced through mechanistic PBPK modeling. This result

suggests that the impact of more metastatic sites on clearance is not due to the physical effects of the tumour burden alone, but rather due to the increased disease burden on the whole body.

Because of its effects on clearance and volume of distribution, Bruno et al. predicted a 12% lower steady state exposure in a patient with a serum ECD level greater than 200 ng/mL compared to a patient with a serum ECD level of 8 ng/mL.[125] Our mechanistic model predicts an 8.3% lower AUC in a patient with a serum ECD level of 200 ng/mL compared to a patient with a serum ECD level of 8 ng/mL and a 12.0% lower AUC for a patient with a serum ECD level of 300 ng/mL. Therefore, it is likely that the overall effect of ECD on trastuzumab clearance is directly mechanistic in nature. In other words, the effect of ECD on clearance and volume and distribution as quantified by Bruno et al. can be fully attributed to the physical mechanism where trastuzumab binds to ECD in the plasma or the interstitial space and is then cleared as an immune complex.

A current challenge with virtual populations is a lack of information on inter-variability in the vascular and interstitial fractions of internal organs. Such information would be able to characterize the variability in peak concentrations, which is under-estimated in this work.

Some modeling limitations were encountered. First, the model was built using data from healthy males and the same mean parameter values were extrapolated to females with breast cancer.[281] While the model predictions were acceptable, improvements could be made by adjusting mean $F2$ values based on disease state. Figure 19 shows how increasing the mean $F2$ value by 50% for females with breast cancer relative to healthy males improves the accuracy of the model predictions for the mean data. Disease-specific mAb modeling using adjustments in the $F2$ parameter will be warranted in the future. However, at the moment there is no reliable way to proactively assign a mean $F2$ value for a population according to cancer severity.

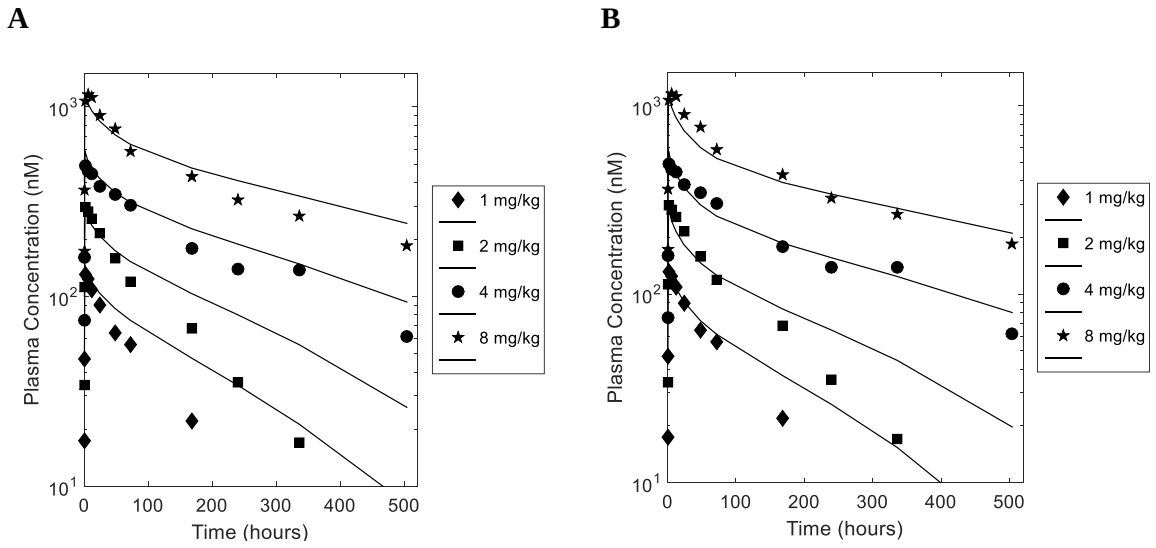

Figure 19. Panel (A) shows the model-predicted profiles and the experimental data in breast cancer patients from Tokuda et al.[281] Panel (B) shows the improved predictions when the mean ***F2*** value is increased by 50% to model the physiologic burden of cancer.

Further, there are limitations surrounding our assumptions for ECD kinetics that could be improved with additional physiologic data in the future. The concentration of ECD in the interstitial space is largely uncertain. Moreover, we assume that the convective flow of the mAb-ECD complex is the same as naked mAb. The mAb-ECD complex is much larger than the naked mAb and it is likely restricted by pore size to a greater degree. Data are not available to inform these two parameters at the present time.

Aside from the platform model by Shah and Betts, other recent models incorporate the competition of endogenous IgG for FcRn.[59,109,289] The overall effect is that the accessible concentration of FcRn decreases. Because the platform model was parameterized without endogenous IgG independently characterized, adding this feature would compromise the internal validity of the other model parameter estimates. Shah and Betts state that it is an advantage that they have removed the characterization of endogenous IgG from their model.[135] Figure 13 shows that the sensitivity of our model to accessible FcRn concentrations is relatively low in comparison to the key parameters and thus adding an FcRn modifier (i.e. endogenous IgG) would have little impact on model outcomes. The model could be improved by adding tissue-specific values for FcRn, though full measurements have only been established for mice.[311]

Finally, mass balance of fluid flow through the endosomal compartment requires the assumption that exactly half of the fluid taken up via endocytosis leaves endothelial cells via exocytosis, while the other half is sorted intracellularly for lysosomal processing before passively exiting the compartment. In the model equations, the fluid flow entering the endosomal compartment is $2 \times CL_{up}$ L·h^{-1}, while the fluid flow explicitly leaving the endosomal compartment is $FR \times CL_{up} + (1 - FR) \times CL_{up} = CL_{up}$ L·h^{-1}.

3.6 Conclusion

A popPBPK framework for quantifying inter-individual pharmacokinetic variability was proposed, tested and evaluated. Five key factors that contribute to inter-individual variability in trastuzumab pharmacokinetics were identified and the nature of their contribution was quantified with local and global sensitivity analyses. The clinical relevance of each of the five key parameters was explored. Simulations of plasma concentrations for virtual populations incorporating variability around each of the key parameters successfully predicted the inter-individual pharmacokinetic variability seen in experimental trials. The utility of popPBPK modeling to complement conventional PopPK methods was demonstrated. Overall, our understanding of inter-individual variability in trastuzumab pharmacokinetics has been enhanced with knowledge about the underlying key mechanistic processes. We look to the clinical research community to apply this information as they formulate dosing strategies for patient subgroups that may be at risk for poor safety or efficacy with mAb drugs.

3.7 Study Highlights

This study represents one of the early applications of whole body PBPK modeling to describe the pharmacokinetics of monoclonal antibodies in humans. The methods shown herein – both for mean model parameterization and population simulation – are performed in adults as workflow examples before the concepts are scaled to children. We also begin to discover the importance of modeling the effect of inflammatory disease states (such as cancer) on the pharmacokinetics of antibodies.

Chapter 4
PBPK Modeling vs. Allometric Scaling to Predict the Pharmacokinetics of Infliximab in Pediatric Patients

4.1 Abstract

The comparative performances of physiologically-based pharmacokinetic (PBPK) modeling and allometric scaling for predicting the pharmacokinetics of large molecules in pediatrics are unknown. Therefore, both methods were evaluated for accuracy in translating knowledge of infliximab pharmacokinetics from adults to children. PBPK modeling was performed using the base model for large molecules in PK-Sim v7.4 with modifications in Mobi. Eight population pharmacokinetic models from literature were reconstructed and scaled by allometry to pediatrics. Evaluation data included seven pediatric studies (~4 – 18 years). Both methods performed comparably with 66.7% and 68.6% of model-predicted concentrations falling within two-fold of the observed concentrations for PBPK modeling and allometry, respectively. Considerable variability was noted among the allometric models. Therefore, pediatric clinical trial planning would benefit from using approaches that require predictions depending on the specific question i.e., PBPK modeling and allometry.

4.2 Introduction

Physiologically-based pharmacokinetic (PBPK) modeling and allometric scaling are the two most common methods for translating knowledge of adult pharmacokinetics (PK) to the pediatric space for the planning of pediatric clinical trials.[312] While drug developers and regulatory agencies alike maintain high confidence in both methods for small molecule drugs, little is known about the performance and utility of either method for large molecule drugs.[70] Here we evaluate the two approaches for the prediction of large molecule PK in pediatric patients with infliximab as a working example, since plenty of adult and pediatric data are available in published literature for the exercise.

The practice of allometry applies an empiric and inherently simple method to perform body-weight-based scaling of adult PK parameters that have been derived from population pharmacokinetic (PopPK) studies (i.e. clearance and volume of distribution).[313] The accuracies of allometric models have been demonstrated with numerous small molecule drugs for children older than two years of age, when distribution and clearance processes have achieved adult performance.[15,314] Below this threshold empirical adjustments for maturation and ontogeny are required and the resulting functions

are not translatable between molecules.[315,316] In keeping with this observation, our evaluation of allometric scaling in the large molecule space first includes studies with children older than 4 years of age, when the mechanisms governing PK are thought to have reached full maturity.[34]

Physiologically-based pharmacokinetic (PBPK) models have long been recognized for offering translational utility by maintaining mechanistic approaches to distribution and clearance.[12] They enable PK predictions in unique populations or unknown exposure scenarios based on known physiological and anatomical characteristics, but are considerably more complex to develop. PBPK models must first be calibrated, informed and evaluated with PK data in adults before their predictions can become reliable in the pediatric space. The practice of PBPK modeling to support pediatric clinical trial planning in the context of small molecule drugs has achieved critical mass with regulatory support from both the US Food and Drug Administration (FDA) and the European Medicines Agency (EMA).[12] In contrast to allometric models, PBPK models can employ physiologic knowledge of growth and maturation to account for the ontogeny of key distribution and clearance processes in young children, even neonates and pre-term infants.[317]

The same confidence must yet be earned for large molecule drugs. The mechanisms governing the PK of large molecules are not at all similar to those of small molecules.[318] Platform PBPK models for large molecules in adults have emerged in the last 7 years and to date only one minimal PBPK modeling effort has been made to characterize PK in children.[66,135,319] We continue the exploration with a whole-body approach to the PK of infliximab in children since a large amount of pediatric PK data is available for this purpose in published literature. The assessment of pediatric PBPK modeling in older children and adolescents must be completed prior to considering children less than 4 years of age for proper evaluation of size-dependent scaling alone without additionally considering age-dependent factors, namely the maturation and ontogeny of key distribution and clearance mechanisms.[34]

Infliximab is a chimeric monoclonal antibody directed against tumour necrosis factor alpha (TNF) that is used to treat inflammation associated with many autoimmune conditions, such as inflammatory bowel disease, rheumatoid arthritis, psoriasis, ankylosing spondylitis and Kawasaki disease. It is most often dosed at 5 mg/kg by a 2-hour intravenous infusion at 0, 2 and 6 weeks for induction of remission and then every 8 weeks thereafter for maintenance of remission, though standard regimens may vary slightly among disease states and clinical treatment centres.

The drug exhibits complex but generally linear pharmacokinetics due to its large size, antibody-based design and low target burden. Two-compartment models are often used to describe its time-course in the adult body. The drug possesses an extensive plasma residence time due to poor permeability across blood vessel walls, with a mean plasma half-life of 9.5 days. High affinity interactions with the neonatal Fc receptor (FcRn) in endothelial, epithelial and hematopoietic cells further protect the drug from intracellular degradation. Infliximab neutralizes soluble TNF in most extracellular fluid domains, but most importantly in the interstitial spaces of inflamed organs. From the interstitial space, the lymphatic system recirculates infliximab via the thoracic duct to the venous blood, where the distribution cycle can begin again. Over time, and in part due to its make-up with portions of murine protein, the body may mount an immune response against infliximab. At sufficient titres, anti-drug antibodies (ADAs) can render infliximab undetectable in plasma.

Monoclonal antibodies are a rapidly expanding drug class and pediatric investigations are well underway. The FDA has recently highlighted the gaps in modeling and simulation efforts to support pediatric drug approvals.[70] By completing this work we aim to assess the confidence with which PBPK modeling and/or allometric scaling can be applied in the context of pediatric drug development and clinical trial planning.

4.3 Methods

4.3.1 Software

PBPK models were built and evaluated using the base model for large molecule drugs in PK-Sim and Mobi v7.4 (www.open-systems-pharmacology.org) with minor modifications.[66] PK data in scientific literature was digitized using Plot Digitizer v2.6.8 by Joseph Huwaldt (plotdigitizer.sourceforge.net). MATLAB R2018b and the Intiquian toolbox (IQMTools v1.2.2.2) by Henning Schmidt were used for reconstruction of PopPK models, allometric scaling and graphical presentation of results.

4.3.2 Pharmacokinetic Data

After a comprehensive literature search, seven pediatric PK trials were located and the data was digitized for evaluation of the pediatric PK predictions between PBPK modeling and allometric scaling (Table 9).[28,29,320-326] The datasets encompass children with inflammatory bowel disease or juvenile idiopathic arthritis almost exclusively between 4 and 18 years of age with infliximab doses ranging from 1 – 10 mg/kg IV.

4.3.3 Adult PBPK Model Development

PBPK modeling enables a mechanistic representation of drug disposition in virtual individuals with known anatomical and physiological properties. Virtual adults and children for the analysis were generated using PK-Sim v7.4. Algorithms for the generation of virtual individuals in PK-Sim are reported elsewhere.[266] In the PBPK modeling process, one virtual individual (whether adult or child) was created to represent the mean individual in each PK study. Each virtual individual had the same age, height, weight, sex and disease state as the mean individual in the corresponding real-world study along with all associated anatomical and physiological characteristics. Maturation was assumed not to have an impact on these characteristics in children older than 4 years of age.

In agreement with pediatric PBPK model development workflows for small molecules, an adult PBPK model was constructed for infliximab first to gain confidence in the global parameterization before scaling the model to pediatric individuals.

The base model for large molecule drugs in the software package has been described previously.[66] Fifteen organs were included in the model structure to represent a virtual human, and each organ compartment was further divided into plasma, endosomal, interstitial and cellular sub-compartments. The base model featured two-pore extravasation, endothelial uptake, salvage by FcRn and lymphatic recycling. The model structure was adapted in Mobi v7.4 to include target-mediated interactions with TNF and ADAs. Model parameters as inputted into PK-Sim and Mobi are presented in Table 10.

Table 9. Pharmacokinetic data evaluation of pediatric predictions

Study	**Dose** (mg/kg IV)	**N**	**Age** (years)	**Weight** (kg)
Inflammatory Bowel Disease				
Candon et al.[320]	Induction with 5	20	10.5 [0.5 – 15]	NA
Hyams et al.[28,29,321]	Induction with 5 then 5 q8w and q12w with dose escalation to 10	112	13.3 ± 2.5	43.8 ± 14.6
Hamalainen et al.[322]	Induction with 5 then 5 q8w	37	14 [5.6 – 18]	43.5 [19.6 – 67.1]
Baldassano et al.[323]	1, 5 and 10 single dose	21	15.1 [8 – 17]	49.1
Singh et al.[324]	Induction with 5 then 5 q8w	58	11.4 [6.6 – 18.4]	NA
Adedokun et al.[325]	Induction with 5 then 5 q8w and q12w with dose escalation	60	14.5 [6 – 17]	50.8 (36.3 – 59.4)
Juvenile Idiopathic Arthritis				
Ruperto et al.[326]	Induction with 3 or 6 then 3 or 6 q8w	122	11.2 [4 – 18]	NA

Data presented as mean or median and [range], (interquartile range) or ± standard deviation
'Induction' refers to intensive dosing at weeks 0, 2 and 6 before regular maintenance dosing

Table 10. Model parameters

Parameter	**Final Value**
Infliximab	
Molecular weight	149100 kDa
Hydrodynamic radius	5.34 nm[66]
Rate of uptake into endosomal space (k_{up})	**0.35 min^{-1}**
Dissociation constant for FcRn binding (K_D^{FcRn})	727 nM[288]
Dissociation constant for TNF binding (K_D^{TNF})	30 pM[327]
Dissociation constant for ADA binding (K_D^{ADA})	500 pM[328]
TNF	
TNF maximum plasma concentration[a] (TNF_{organ})	0.5 pM[329-331]
TNF factor for autoimmune disease	2[329,330,332,333]
TNF degradation rate (k_{deg}^{TNF})	0.0231 min^{-1} [334,335]
mAb-TNF complex degradation rate ($k_{deg}^{mAb-TNF}$)	0.0231 min^{-1}
ADA	
Duration of IgM production (T_{prod}^{IgM})	30.7 days[336]
Lag time prior to IgG production (T_{lag}^{IgG})	38.8 days[336]
IgM maximum plasma concentration[a] (E_{max}^{IgM})	$\frac{k_{deg}^{IgG} \times E_{max}^{IgG}}{k_{deg}^{IgM}}$
IgG maximum plasma concentration[a] (E_{max}^{IgG})	**136 nM**
ADA (IgM) degradation rate (k_{deg}^{IgM})	0.1 day^{-1} [336]
ADA (IgG) degradation rate in healthy (k_{deg}^{IgG})	0.014 day^{-1} [336]
ADA (IgG) degradation rate in autoimmune (k_{deg}^{IgG})	0.008 day^{-1} [336]
mAb-ADA complex degradation rate ($k_{deg}^{mAb-ADA}$)	0.48 day^{-1} [337]
Inflamed Organ	
Inflammation factor for inflamed pores (IF^{σ})	1.5[69,338,339]
TNF factor for inflamed organ	3[340,341]

[a] Zero order synthesis rates were calculated by multiplying the degradation rate by the maximum concentration of the molecule

Bolded values were mathematically optimized to their final value in the model building process

Infliximab binds to TNF in circulation with high affinity and the complex is later eliminated by the immune system.[342] In the PBPK model, TNF was present in all plasma and interstitial spaces with a relative expression of 1 across all organs. The natural synthesis (k_{syn}^{TNF}) and turnover (k_{deg}^{TNF}) of TNF were represented with zero order and first order rate constants, respectively. TNF molecules were non-circulating and stationary within each sub-compartment. Binding of infliximab to TNF caused the formation of a complex, which was eliminated from the system by a first order degradation rate ($k_{deg}^{mAb-TNF}$).

In PopPK studies, infliximab is often noted to exhibit faster clearance in individuals with severe inflammation, possibly mediated through higher TNF concentrations, vascular hyperpermeability or cachexia. In the PBPK model, the presence of autoimmune disease was represented with a global 2-fold increase in TNF concentrations.[329,330,332,333] In inflamed organs, local TNF concentrations were further increased by a factor of 3.[340,341]

Large molecule drugs abide by permeability-rate-limited distribution and are subject to vascular hyperpermeability in inflamed organs. To represent this effect, the pore sizes in inflamed organs were increased proportional to an inflammation factor in agreement with previous minimal PBPK models of inflammatory conditions by Jusko and colleagues, who observed the requirement for lower vascular reflection coefficients in inflamed organs.[69,338,339] The large intestine was inflamed in patients with inflammatory bowel disease, the bone was inflamed in patients with rheumatoid arthritis and ankylosing spondylitis, the skin was inflamed in patients with psoriasis and the lung was inflamed in patients with non-small cell lung cancer (NSCLC).

Immunogenicity is a key determinant of infliximab elimination. Results are conflicting due to inconsistency in ADA assays, though up to 60% of patients may express an immunogenic response against infliximab over the course of one year of therapy.[343] ADA molecules (IgM, IgG) bind to infliximab to form a complex, neutralizing its therapeutic potential and eventually resulting in degradation. In the PBPK model, ADA molecules (IgM, IgG) were synthesized, released and contained within the plasma of venous and arterial blood, similar to the assumptions made by Chen et al.[344] Mean ADA synthesis and degradation rates in the adult population were parameterized according to Ren et al., who quantified the typical immune response after first-dose exposure to four therapeutic proteins with a PopPK modeling approach.[336] In the absence of additional data, the zero order molar synthesis rates of IgM and IgG were assumed equal ($k_{syn}^{IgM} = k_{syn}^{IgG}$). The typical ADA profile featured an initial period of IgM synthesis, a lag phase and finally a sustained IgG response.

The group noted differences in IgG degradation rates between healthy and autoimmune individuals, which were implemented in the model.[336] Mechanistically, binding of infliximab to IgM or IgG caused the formation of a complex, which was eliminated from the system by a first order degradation rate ($k_{deg}^{mAb-ADA}$).

Two parameters in the adult PBPK model were uncertain and required optimization: the rate of uptake into endosomal space (k_{up}) and the zero order molar synthesis rate of ADA molecules against infliximab (k_{syn}^{IgG}), which was mediated via the maximum concentration of IgG parameter (E_{max}^{IgG}). Optimization was carried out in Mobi using a Monte-Carlo approach to exploring the parameter space. The parameters were optimized separately in two steps. First, k_{up} was optimized to ADA-negative PK data available in 4 studies (Table 11). Following this step, E_{max}^{IgG} was optimized to PK data available from 20 studies in healthy and diseased individuals (Table 11). Therefore, E_{max}^{IgG} represents the mean immunogenic response across the general adult population, including both ADA-positive and ADA-negative individuals.

Model accuracy following optimization was assessed statistically by the squared Pearson correlation coefficient (Pearson R^2), the absolute average fold error (AAFE) across all data points, the root mean squared error (RMSE) and the percent of model-predicted concentrations falling within two-fold of the corresponding observed concentrations. An external evaluation of the final adult model was not performed because the purpose of the model was to extrapolate knowledge of adult PK to pediatrics, and this workflow maximizes learning from adult datasets.

Table 11. Datasets used for adult PBPK model building

Study	**Cohort**	**Dose** (mg/kg IV)	**N**	**Age** (years)	**Weight** (kg)
Datasets with an ADA-Negative Subset (Model Building Step 1)					
Yoo et al.[345]	Rheumatoid Arthritis	Induction with 3 then 3 q8w	304	50 [21 – 74]	68 [36 – 136]
Brandse et al.[346]	Ulcerative Colitis	Induction with 5	19	36 (27 – 44)	70 (61 – 75)
Shin et al.[347]	Healthy	5 single dose	53	39.4 ± 9.9	79.1 ± 8.3
Takeuchi et al.[348]	Rheumatoid Arthritis	Induction with 3 then 3 q8w	47	53.8 ± 13.4	53.4 ± 10.1
Additional Datasets (Model Building Step 2)					
Lambert et al.[349]	Healthy	5 single dose	41	28.5 [18 – 45]	74.7 [62.3 – 88.6]
Udata et al.[350]	Healthy	10 single dose	48	[18 – 55]	NA
Park et al.[351]	Healthy	5 single dose	71	41 [18 – 55]	78.1 [55.4–99.9]
Maini et al.[352] St. Clair et al.[353]	Rheumatoid Arthritis	Induction with 3 and 10 then 3 and 10 q4w or q8w	197	53 [19 – 80]	NA
Park et al.[354,355]	Ankylosing Spondylitis	Induction with 5 then 5q8w	110	38 [18 – 66]	76.0 (45.5–122.7)
Gottlieb et al. [356,357]	Psoriasis	Induction with 5 and 10	17	43 [21 – 69]	91.5 [61 – 165]
Gottlieb et al. [357,358]	Psoriasis	Induction with 5 then 5 q8w	215	44.4 ± 13.3	93.5 ± 21.1
Adedokun et al.[359]	Ulcerative Colitis	Induction with 5 and 10 then 5 and 10 q8w	484	40 (30 – 52)	77 (66 – 89)
Rutgeerts et al.[360]	Crohn's Disease	5, 10 and 20 single dose then 10 q8w	37	34 [20 – 64]	66 [40 – 102]
Cornillie et al.[361]	Crohn's Disease	Induction with 5 then 5 and 10 q8w	284	36.8 [18 – 76]	NA
Rahman et al.[362]	Rheumatoid Arthritis	Induction with 3 then 3q8w	220	54 (44 – 62)	69.3 (60.1 – 81.0)
Hibi et al.[363]	Behcet Disease	Induction with 5 then 5 q8w	11	37.6 ± 7.4	67.8 ± 17.9
Jatoi et al.[364]	NSCLC	5 on weeks 0, 2, 4, 8, 12	4	72.25	NA
Choe et al.[365]	Rheumatoid Arthritis	Induction with 3 then 3 q8w	160	52.6 ± 11.7	71.9 ± 16.5
Bortlik et al.[366]	Crohn's Disease	Induction with 5 then 5 q8w	84	31 [17 – 62]	NA
Krzysiek et al.[367]	Ankylosing Spondylitis	Induction with 5 then 5 q6w	93	39.5 ± 12.0	NA
Torii et al.[357,368,369]	Psoriasis	Induction with 5 then 5 q8w	35	46.9 ± 13.0	68.5 ± 13.4
Sorrentino et al.[370]	Crohn's Disease	3 and 5 q8w	11	37.8	NA
Kavanaugh et al.[371]	Rheumatoid Arthritis	5, 10 and 20 single dose	21	45.5 ± 12.3	NA

Data presented as mean or median and [range], (interquartile range) or ± standard deviation
'Induction' refers to intensive dosing at weeks 0, 2 and 6 before regular maintenance dosing

4.3.4 Pediatric Extrapolation

After establishing confidence in the performance of the adult PBPK model, it was then translated to the pediatric space. In simple terms, the virtual adult individual was replaced with a pediatric individual with all associated anatomical and physiological parameters to explore the *a priori* PK predictions of the model in children. Physiological parameters related to disease pathology and immunogenicity were kept constant between adults and children, with some literature to inform this decision.[320,331,372] Observed PK data from seven pediatric clinical trials were available for evaluation of the predictions (Table 19). As above, prediction accuracy was assessed by four metrics: Pearson R^2, AAFE, RMSE and the percent of model-predicted concentrations falling within two-fold of the corresponding observed concentrations in children.

Allometric scaling offers a simple and empirical approach to translating the statistical knowledge gained from an adult PopPK study to a pediatric population by acknowledging differences in body weight. Many adult PopPK models for infliximab exist in published literature. In a typical drug development case only one model would exist, built after collation of PK data from two or three small studies. For this exercise, a total of eight adult PopPK models were reconstructed from literature for application of allometric scaling (Table 12).

Each PopPK model was constructed, scaled and evaluated independently. First, values for clearance (CL_{adult}), inter-compartmental clearance ($Q2_{adult}$), volume of distribution in the central compartment ($V1_{adult}$) and volume of distribution in the peripheral compartment ($V2_{adult}$) were extracted for the typical adult individual in each study (Table 12). The typical adult had mean or median covariate status for age, height, weight, sex, disease status, immunomodulator use and inflammatory biomarker concentration where applicable. The four PK parameters were then scaled by allometry from the typical adult to the typical child in each of the pediatric PK studies designated for evaluation (pediatric body weights presented in Table 19). Allometric scaling was implemented as described by Tod, Jullien and Pons.[313] Mathematically,

$$CL_{child} = CL_{adult} \times \left(\frac{BW_{child}}{BW_{adult}}\right)^{0.75}$$

$$Q2_{child} = Q2_{adult} \times \left(\frac{BW_{child}}{BW_{adult}}\right)^{0.75}$$

$$V1_{child} = V1_{adult} \times \left(\frac{BW_{child}}{BW_{adult}}\right)^{1.0}$$

$$V2_{child} = V2_{adult} \times \left(\frac{BW_{child}}{BW_{adult}}\right)^{1.0}$$

Pediatric PK predictions were only made in the context of the same or similar disease states. Seven PopPK models developed in adults with inflammatory bowel disease were used to make pediatric PK predictions for children with inflammatory bowel disease and one PopPK model developed in adults with rheumatoid arthritis was used to make pediatric PK predictions for children with juvenile rheumatoid arthritis. Pediatric PK profiles were simulated with the updated parameters and compared to the mean pediatric observed concentrations from literature (Table 19). Once again, the accuracy of PK profile prediction through allometric scaling was assessed by the same four statistical metrics for direct comparison to the PBPK model-driven predictions (Pearson R^2, AAFE, RMSE and percent of model-predicted concentrations falling within 2-fold of the corresponding observed concentrations).

Table 12. Adult infliximab PopPK studies used for allometric scaling

Study	**N**	**Age** (years)	**Weight** (kg)	**CL** (mL/h)	**Q2** (mL/h)	**V1** (L)	**V2** (L)
Inflammatory Bowel Disease							
Fasanmade et al.[27]	580	37.5 ± 11.9	71.1 ± 18.3	15.27	6.09	3.58	1.29
Fasanmade et al.[373]	482	41.2 ± 13.9	78.8 ± 18.4	16.96	297.5	3.29	4.13
Ternant et al.[374]	33	33 [19 – 53]	67 [44 – 110]	12	5.4	2.9	1.9
Dotan et al.[375]	54	35.6 [20 – 70]	NA	15.8	5.08	2.37	1.37
Aubourg et al.[376]	133	NA	60 [41 – 120]	14	83	2.6	4.5
Buurman et al.[377]	42	44 [19 – 80]	75 [51 – 145]	8.29	2.58	4.94	3.13
Brandse et al.[378]	332	38.6 ± 13.9	72.3 ± 16.3	14.96	2.9	4.72	2.4
Rheumatoid Arthritis							
Ternant et al.[379]	84	58 [27 – 84]	65	19	180	2.3	3.6

Data presented as mean or median and [range], (interquartile range) or ± standard deviation
CL = clearance, Q2 = intercompartmental clearance, V1 = volume of distribution in the central compartment, V2 = volume of distribution in the peripheral compartment.

4.4 Results

A comprehensive PBPK model was developed using the base model for large molecule drugs in PK-Sim and Mobi v7.4 with modifications to feature the effects of inflammation and target-mediated interactions with TNF and ADA molecules. The adult model was then scaled to represent children by updating all anatomical and physiological parameters accordingly. Additionally, eight two-compartment PopPK models from literature were reconstructed and scaled by allometry to the

pediatric space according to the methods proposed by Tod, Jullien and Pons.[313] Equipped with these tools, the performances of PBPK modeling and allometric scaling for the prediction of infliximab PK in children and adolescents were systematically evaluated.

4.4.1 Adult PBPK Model Development

In the first optimization step (the ADA negative scenarios), the final value for k_{up} was 0.35 min^{-1} (Figure 20). In the second optimization step, the final value for E_{max}^{IgG} was 136 nM. The adult PBPK model well-characterized the observed PK profiles from all datasets used in both optimization steps achieving a Pearson R^2 of 0.90, an AAFE of 1.16 and an RMSE of 30.9. Notably, 88.4% of the model-predicted infliximab concentrations were within 2-fold of the corresponding observed concentrations. Figure 21 shows sample PK profiles in healthy subjects, ankylosing spondylitis and rheumatoid arthritis, and a comparison of the model-predicted vs. observed concentrations across all studies. The possible effect of inflammation on clearance was modestly under-estimated for inflammatory bowel disease and psoriasis patients, though a significant portion of this observed data was obtained from non-responder subsets. Non-responders have lower trough concentrations than responders, possibly due to higher TNF concentrations, ADA positivity or severely inflamed, damaged or leaky organs.

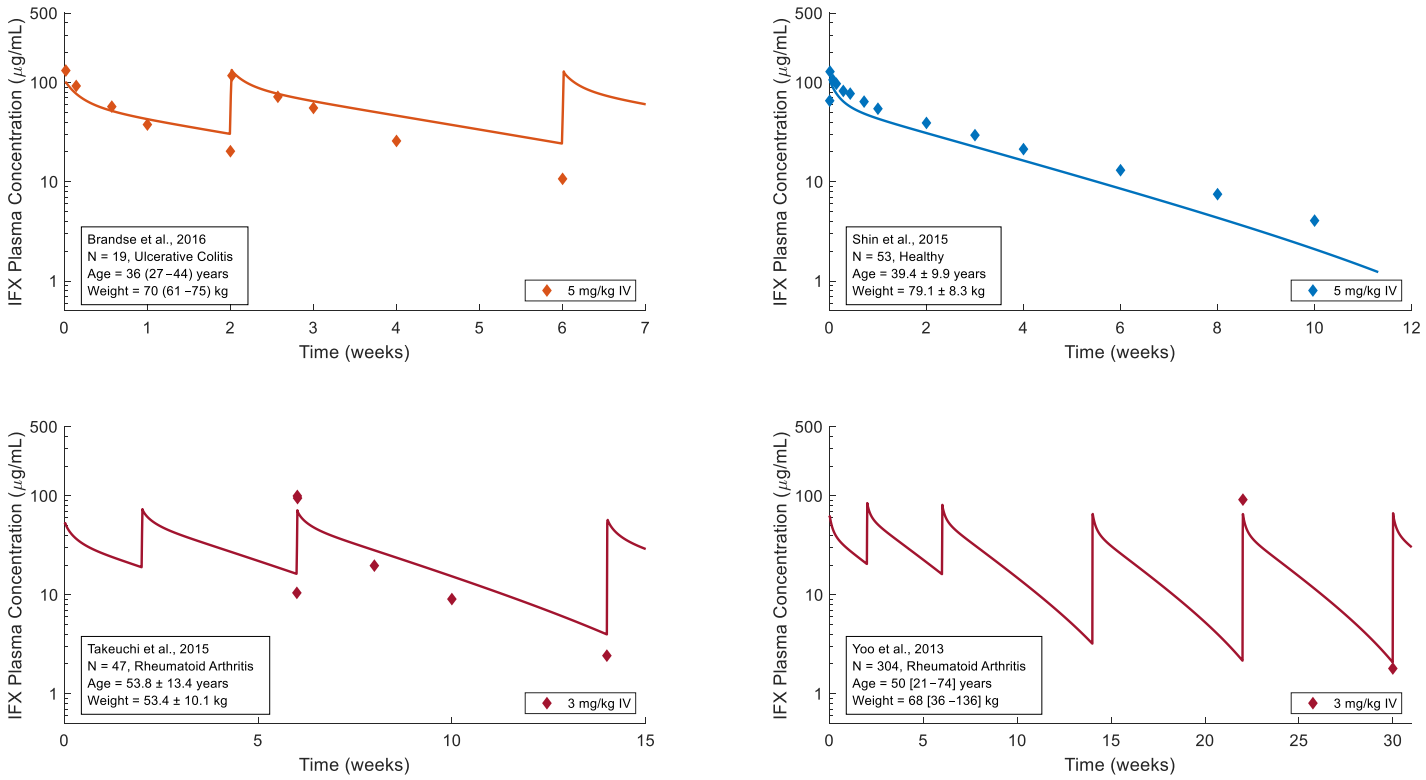

Figure 20. Comparison of model-fitted profiles to observed data after the first optimization step. References to observed data are provided in Table 11.

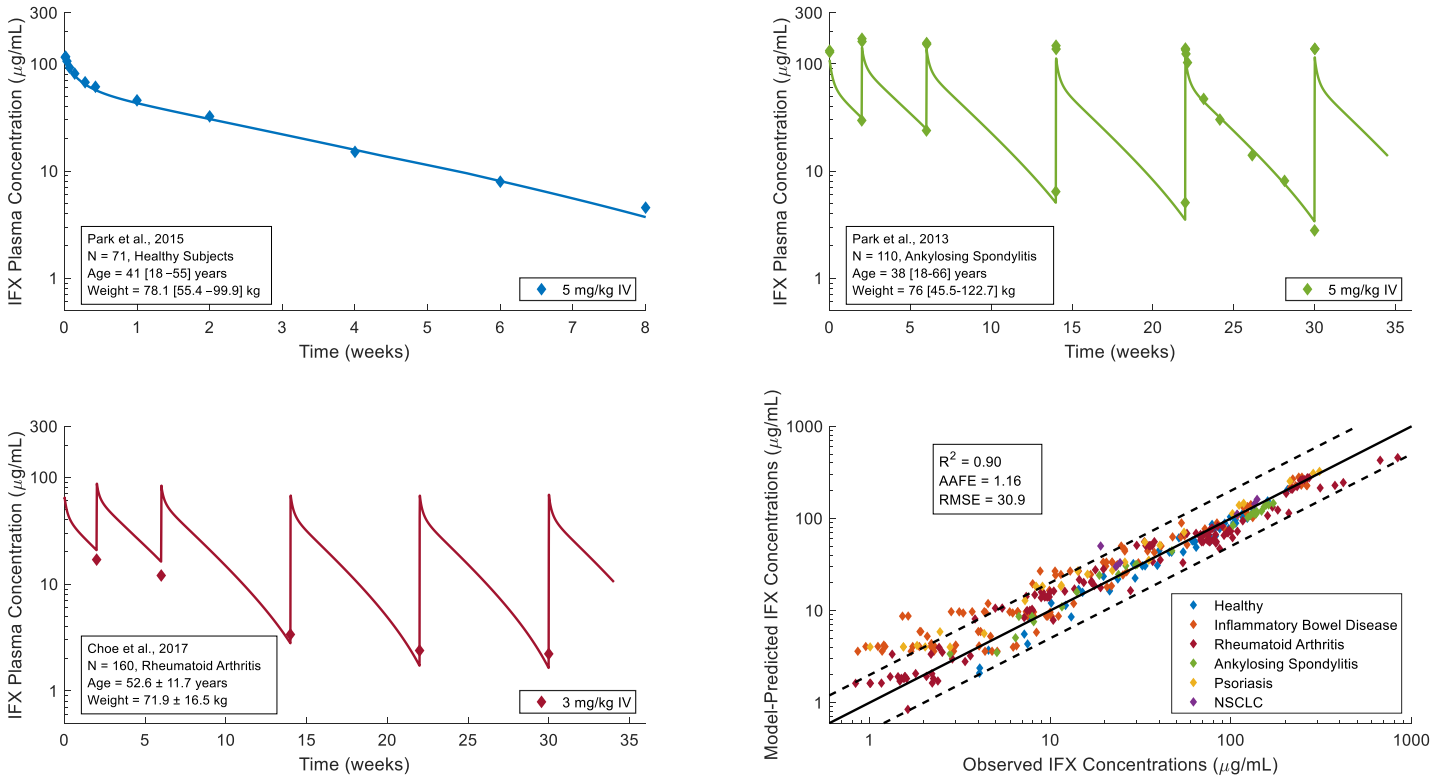

Figure 21. Sample fitted infliximab PK profiles in healthy subjects, ankylosing spondylitis and rheumatoid arthritis, and a comparison of model-predicted vs. observed infliximab concentrations (NSCLC = non-small cell lung cancer) after the second optimization step. References to observed data are provided in Table 11.

4.4.2 Evaluation of Pediatric Predictions

Both methods performed similarly for predicting the mean PK in children obtained from studies that included individuals almost exclusively between the ages of 4 and 18. Figure 22 displays a plot-by-plot comparison of allometrically-derived PK profiles, PBPK profiles and the mean pediatric observed concentrations from literature. Considerable differences were noted among the profiles derived from allometric scaling that stemmed from variable PK parameter values from the eight adult PopPK models. Visually, the pediatric PBPK model was more proficient for predicting peak concentrations after infusion and volume of distribution in the central compartment, while the allometrically-derived models performed better for predicting trough concentrations.

Across all allometric models, model-predicted concentrations were within 2-fold of the observed concentrations 68.6% of the time, while the best allometric model enabled predictions within 2-fold of the observed concentrations 84.3% of the time (Table 13).[378] The PBPK model performed similarly overall, achieving predictions within 2-fold of the observed concentrations 66.7% of the time (Table 13). No discernable correlations were detected between the sample size of a PopPK study (N) and the accuracy of its pediatric predictions. The Pearson R^2 and RMSE values identified trends in model performance but no conclusions could definitively be made about overall model performance from these metrics.

Finally, Figure 23 compares the model-predicted and observed infliximab concentrations across all pediatric studies. Low concentrations were over-predicted by both methods, though there is uncertainty in these data values with regard to the lower limits of quantification for the assays in the studies. Overall, the PBPK model predictions fell near the median of the allometric predictions for children.

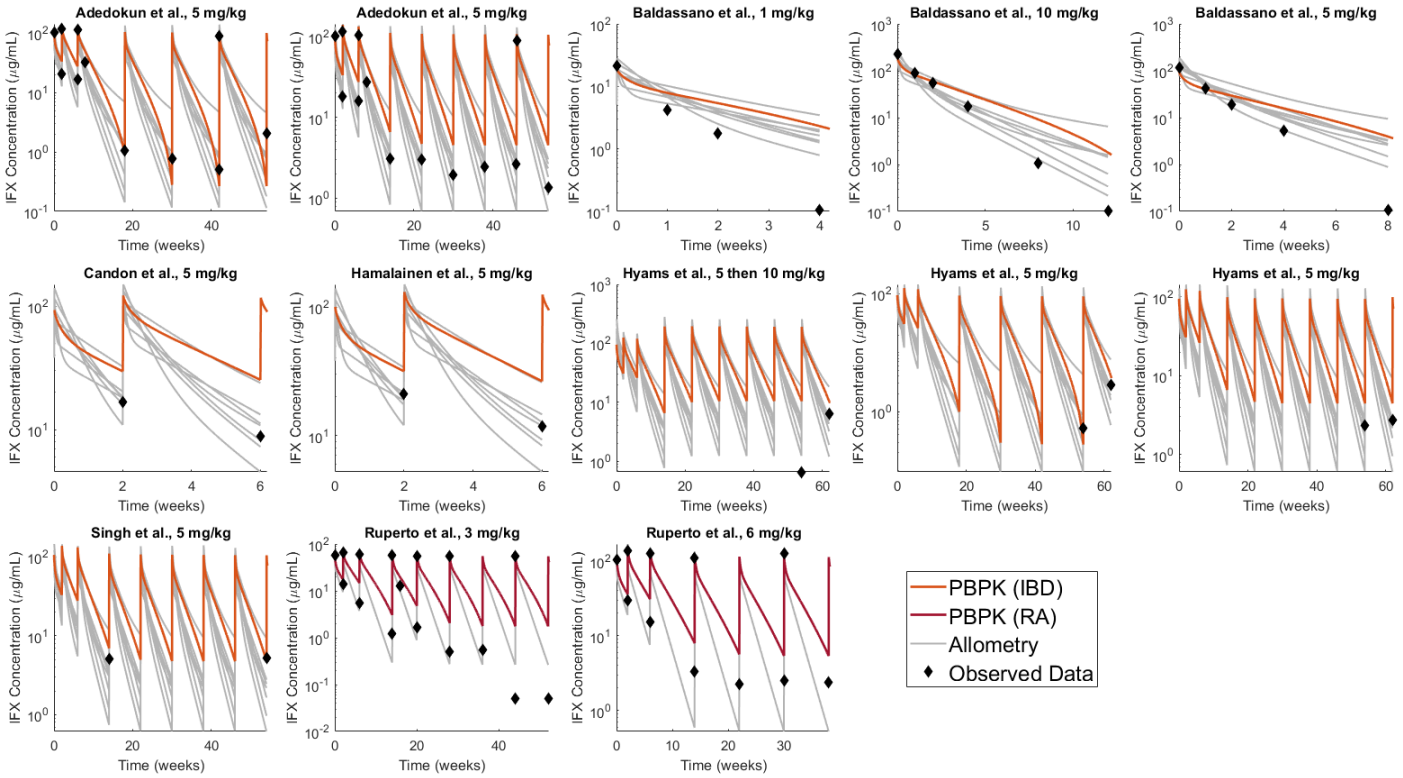

Figure 22. Comparison of pediatric PBK modeling and allometric scaling for the prediction of infliximab PK in children with inflammatory bowel disease or juvenile idiopathic arthritis; data digitized from seven pediatric studies (Table 19).

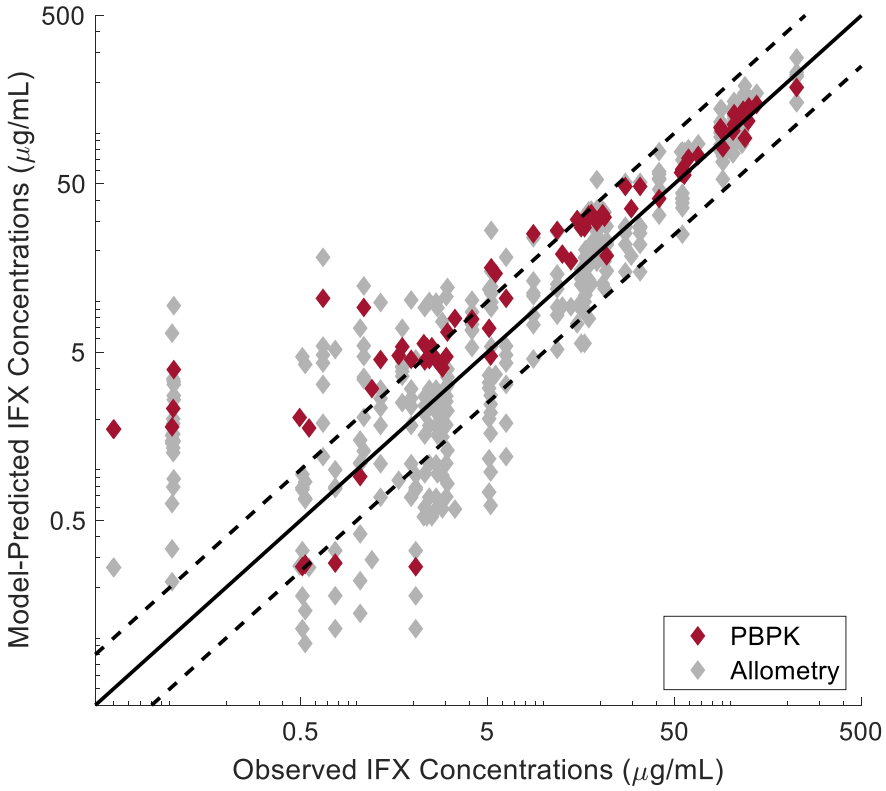

Figure 23. Model-predicted vs. observed infliximab concentrations in pediatrics.

Table 13. Statistical evaluation of pediatric PK model performance

Model	**N**	**AAFE**	**R^2**	**RMSE**	**2-Fold Error**
Inflammatory Bowel Disease					
Fasanmade et al.[27]	580	0.77	0.977	8.1	60.8%
Fasanmade et al.[373]	482	1.09	0.964	9.7	76.5%
Ternant et al.[374]	33	1.35	0.980	10.1	80.4%
Dotan et al.[375]	54	0.60	0.957	21.4	51.0%
Aubourg et al.[376]	133	1.36	0.973	8.5	82.4%
Buurman et al.[377]	42	2.82	0.913	17.0	47.0%
Brandse et al.[378]	332	1.18	0.970	14.0	84.3%
Rheumatoid Arthritis					
Ternant et al.[379]	84	0.83	0.987	20.7	66.7%
All Allometric Models					
		1.25		13.7	68.6%
PBPK Modeling					
This Study		1.79	0.96	7.0	66.7%

4.5 Discussion

The evaluations of PBPK modeling and allometric scaling for prediction of small molecule PK in children have been extensive.[15,314] Both methods are often reported to achieve predictions within 2-fold of the observed values up to 90% of the time for children older than 2 years of age. However, this evaluation has not yet been performed in the context of large molecule drugs. With infliximab as a case example, we demonstrate that PBPK modeling and allometric scaling in their current states provide similar pediatric PK predictions for children older than 4 years of age in known exposure scenarios. There is significant room for improvement in the large molecule space, as neither method in this example achieved the accuracies reported in small molecule evaluations (66.7% and 68.6% of model-predicted concentrations falling within 2-fold of the observed concentrations for PBPK modeling and allometric scaling, respectively). Refinement of allometric exponents for large molecule drugs and investigations into the relevance of pediatric physiology for predicting PK in young children are required to advance the predictive accuracy of these methods.[34]

A closer inspection of model performances may offer guidance about the utility of each method for specific purposes (Figure 22). The pediatric PBPK model performed stronger than the allometrically-derived models for the prediction of peak drug concentrations after infusion (Figure 23), suggesting that volume of distribution in the central compartment for children is most reliably estimated by physiological methods. Clearance in children older than 4 years of age was modestly underestimated by PBPK modeling, suggesting that there may be mild effects of maturation on anatomical and physiological parameters that govern elimination. Allometric scaling may more reliably estimate trough concentrations and clearance in known exposure scenarios. Lastly, allometric scaling was performed for eight different PopPK models in a small fraction of the time that was required to develop the pediatric PBPK model (~100 hours) and would be preferred when time is a constraint.

The findings from this study can be generalized to the pediatric PBPK modeling and allometric scaling of monoclonal antibodies with similar FcRn affinity and a low target burden to guide drug development and selection of first-in-pediatric doses. Antibodies with a high target burden often exhibit nonlinear kinetics and there is yet no reliable method for scaling the TMDD component of a non-linear PopPK model by allometry, especially when disease pathology may vary between adults and children. PBPK modeling would be highly desired in this case.

Wide variability was noted in the predictions among the eight allometric models and the accuracy among the models was independent of adult study sample size (Figure 22)(Table 12**,** Table 13). This

observation draws attention to the need for optimal sampling in the design of adult PopPK studies to increase confidence when applying allometric scaling. Without dense sampling and variable exposure scenarios, fundamental model structures cannot be determined. In the case of infliximab, estimates for PK parameters are highly variable among the eight models and are often poorly defined due to inadequate mid-profile sampling. Limited sampling analyses for large molecule drugs are beginning to be used to guide the sampling times for appropriate derivation of pivotal PK parameters, some of which govern curve shape.[380]

PBPK modeling for large molecules is gaining traction in academia, industry and regulatory agencies. Here we present the first evaluation of a whole-body PBPK model for a large molecule drug in pediatrics and the first PBPK model to incorporate immunogenicity. Infliximab is one of the oldest monoclonal antibodies and there is an abundance of PK data available for model parameterization, yet the drug has often been avoided due to uncertainty around modeling immunogenicity, which is a key driver of its elimination. The immunogenic response is a modelling challenge because ADA assays often do not quantify concentrations, only titres of ADA molecules.[24] As a first step toward quantifying the response, the ADA-negative PK data for infliximab available in literature combined with the parameterization of the time-course of ADA formation in humans by Ren et al. have enabled the first mechanistic representation of the immunogenic response to a therapeutic drug product.[336] Figure 24 displays the simulated profile of mean ADA formation following first dose administration in a typical population of adults with inflammatory bowel disease. The first phase is IgM formation, and the second phase is IgG formation. Not yet addressed mechanistically is the impact of concurrent drug therapy with immuno-modulators on ADA formation and clearance.

The adult PBPK model showed a modest under-prediction of clearance in inflammatory bowel disease, though a significant portion of this observed data was extracted from subsets including only non-responders to treatment. As previously mentioned, this result is expected since non-responders often have higher ADA concentrations, higher TNF levels and more severely inflamed tissues. Loss of infliximab into the feces is an alternate explanation for the error.[381]

For therapeutic proteins, the observation that children receive lower exposures than adults with the same weight-based doses has been reported before.[34] Drug developers are beginning to anticipate this phenomenon and derive pediatric-specific doses according to age or weight using PBPK modeling or allometric scaling.[56,70] The results of this study highlight the degree of error that can be expected

when only adult information is used to predict pediatric PK in maturation-independent age groups for the purposes of deriving age or weight-tiered doses with therapeutic proteins.[56]

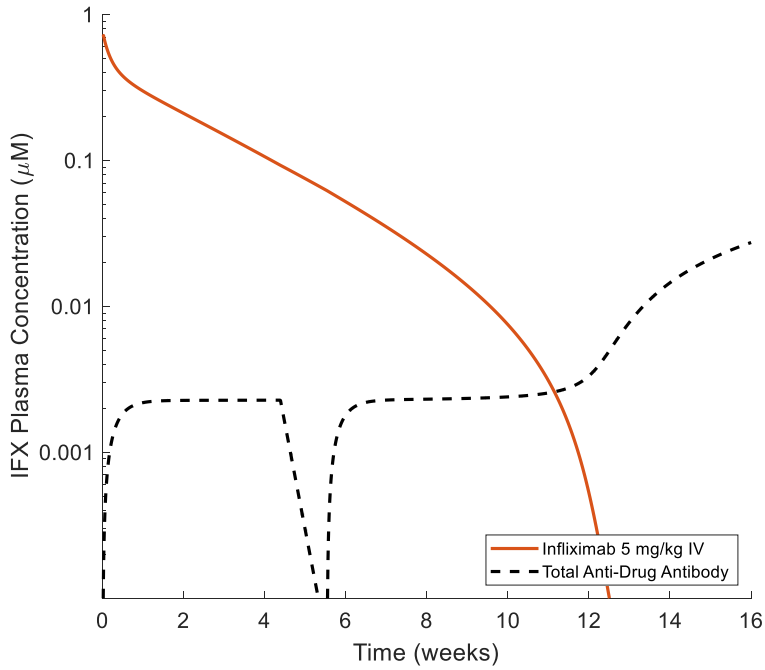

Figure 24. Simulated profile of mean ADA formation following first dose administration in a typical population of adults with inflammatory bowel disease

To summarize, the methods of PBPK modeling and allometric scaling were comprehensively evaluated in this work for their accuracy in translating infliximab pharmacokinetic knowledge from adults to children. Both methods performed comparably, yet neither method achieved the prediction accuracy that is recorded in studies with small molecule drugs. Considerable variability was noted among the predictions made by the eight allometric models and accuracy was not driven by the sample sizes from the parent PopPK studies. Therefore, a comprehensive pediatric clinical trial planning approach would benefit from both PBPK modeling and allometric scaling, being cognizant that PBPK modeling may be more appropriate for predicting peak concentrations and allometric scaling may be more appropriate for predicting trough concentrations in children.

4.6 Study Highlights

At present, pediatric drug development for large molecules is poorly supported by modeling and simulation. The comparative performances of physiologically-based pharmacokinetic (PBPK) modeling and allometric scaling for the prediction of large molecule pharmacokinetics in children are unknown.

This study addressed which method(s) for pediatric PK prediction could be used reliably in pediatric drug development and clinical trial planning for large molecules.

With infliximab as an example for the evaluation, PBPK modeling and allometric scaling had comparable accuracy in known exposure scenarios. Two-thirds of the model-predicted concentrations fell within two-fold of the observed concentrations. PBPK modeling was more accurate for predicting peak drug concentrations, while allometry was more accurate for predicting trough drug concentrations.

No pediatric PBPK modeling has been completed to support regulatory submissions to the FDA for a monoclonal antibody.[70] We highlight the opportunity for PBPK modeling to be used in tandem with allometry to contribute to this growing field of drug development.

Since a PBPK model with size-dependent anatomy alone failed to predict the elimination of infliximab in children, and since the disease physiology and exposure-response relationships are known to be similar between adults and children, we put forward the hypothesis that there are age-dependent physiological factors that must be considered when extrapolating PK even to adolescents with PBPK modeling.

Chapter 5
Pediatric Physiology in Relation to the Pharmacokinetics of Monoclonal Antibodies

5.1 Abstract

Dose designs for pediatric trials with monoclonal antibodies (mAbs) are often extrapolated from the adult dose according to weight, age or body-surface area. While these methods account for the size differences between adults and children, they do not account for the maturation of processes that may play a key role in the pharmacokinetics and/or pharmacodynamics of mAbs. With the same weight-based dose, infants and young children typically receive lower plasma exposures when compared to adults. In this review, the mechanistic features of mAb distribution, elimination and absorption are explored in detail and literature-based hypotheses are generated to describe their age-dependence. This knowledge can be incorporated into a physiologically-based pharmacokinetic (PBPK) modeling approach to pediatric dose determination.

5.2 Introduction

Increasing numbers of pediatric clinical trials are being performed under the pediatric regulations provided by the U.S. Food and Drug Administration and by the European Medicines Agency, which mandate and grant incentives to drug manufacturers for pursuing pediatric research. Dose designs for pediatric trials are often extrapolated from the adult dose according to weight, age or body-surface area (BSA). While these methods account for the size differences between adults and children, they do not account for the maturation of processes that may play a key role in pharmacokinetics and/or pharmacodynamics.[382] The therapeutic consequences are most pronounced for infants, who are small, immature and vulnerable to toxicity from dosing errors.[383] An alternative tool for dose determination in pediatric trials that explicitly accounts for age-related changes in anatomy and physiology is the physiologically based pharmacokinetic (PBPK) model. These mechanistic mathematical models attempt to recapitulate the anatomy and physiology of the human, at all stages of life, by compartmentalizing tissues and organs with knowledge of their size, composition and blood flow and connecting them to each other to simulate *in vivo* drug disposition. These models have utility in many areas of drug development, with pediatrics being a frequent use.[12,384]

Pharmacokinetic differences between adults and children have been linked to developmental differences in tissue composition, blood flow rates, enzyme and plasma protein concentrations and glomerular filtration rates.[14] These developmental differences can be incorporated into PBPK models to make predictions of pharmacokinetics in children and numerous examples of pediatric PBPK models for small molecules are published.[14,384-387] One use of the pediatric PBPK model is in the planning of pediatric clinical trials where it can be used to guide dosing regimen design, ensure efficient blood sampling times and potentially reduce the number of children required for the studies.[388]

In the last two decades there has been an explosion of large molecule drugs registered for use in children, a significant portion of which are monoclonal antibodies (mAbs).[80] They offer new avenues for targeted therapies against proteins that are involved in disease pathology. Most mAbs are structurally similar to endogenous IgG and share similar pharmacokinetic properties. For example, unlike small molecule drugs, many mAbs possess long plasma half-lives in part due to recycling by the neonatal Fc receptor (FcRn).[2] Consequently, we must endeavour to explore these new drivers of large molecule pharmacokinetics as they relate to children and cannot rely on our previous understanding of the factors related to small molecule pharmacokinetics.

A number of mAb therapies have been investigated in children for immunology, oncology, infectious disease and hematology. The general pharmacokinetic differences between adults and children (< 18 years) are reviewed by Edlund et al. and Zhang et al. and are most prominent in infants and young children, suggesting that maturation plays a key role.[4,80] Every mAb with published investigations that include infants (< 2 years) is listed in Table 14 (current as of January, 2018). Overall, infants and young children achieve lower plasma exposure than adults when the same weight-based doses are given.[3,4,80,389-391] Weight-normalized plasma clearance is faster and peak concentrations following an intravenous dose are lower.[3,4,80,389-391] BSA-based dosing regimens are less common and may cause higher exposures in infants.[3,4,42,80,389-391] The same general patterns are observed for other large molecule therapies that do not share the same IgG structure such as darbepoetin alfa, factor VII, recombinant factor VIII, and recombinant factor IX when administered to children, suggesting that the mechanisms responsible are not entirely specific to mAbs.[392-396]

Table 14. Pharmacokinetic studies with monoclonal antibodies involving infants (< 2 years)

Generic Name	Target	Indication	Dose	Age (years)	Year	Ref.
Basiliximab	IL-2Rα	Prophylaxis of transplant rejection	10 – 20 mg IV	1 – 15	2002	[397]
		Prophylaxis of transplant rejection	10 – 20 mg IV	1 – 16	2002	[398]
		Prophylaxis of transplant rejection	10 mg IV	1 – 12	2010	[399]
		Prophylaxis of transplant rejection	10 – 20 mg IV	1 – 16	2002	[400]
Bevacizumab	VEGF	Solid tumour	5 – 15 mg/kg IV	0.5 – 21	2016	[42]
		CNS tumour	10 mg/kg IV	< 3	2017	[401]
		Solid tumour	5 – 15 mg/kg IV	1 – 21	2008	[402]
		Retinopathy of prematurity	0.25 – 0.625 mg IVT	< 1	2015	[403]
		Retinopathy of prematurity	0.25 – 0.5 mg IVT	< 1	2012	[404]
Cetuximab	EGFR	Solid tumour	75 – 250 mg/m^2 IV	1 – 12	2009	[405]
Daclizumab	IL-2Rα	Prophylaxis of transplant rejection	1 mg/kg IV	0.9 – 5	2008	[406]
Dinutuximab	G_{D2}	Neuroblastoma	25 mg/m^2 IV	1.2 – 7.3	2014	[407]
		Neuroblastoma	20 – 40 mg/m^2 IV	1 – 14	2009	[408]
Eculizumab	C5	Atypical hemolytic-uremic syndrome	300 – 900 mg IV	0.4 – 17	2016	[409]
Gemtuzumab Ozogamicin	CD33	Acute myeloid leukemia	0.2 – 0.3 mg/kg IV	0 – 2	2004	[410]
Infliximab	TNFα	Kawasaki disease, Crohn's disease, ulcerative colitis, juvenile rheumatoid arthritis	5 mg/kg IV	0.2 – 17	2012	[411]
		Kawasaki disease	5 mg/kg IV	0.2 – 6	2008	[412]
		Crohn's disease	5 – 10 mg/kg IV	0.5 – 1	2006	[320]
MEDI8897	RSV-F	Respiratory syncytial virus infection	10 – 50 mg IM	0 – 2	2017	[413]
Motavizumab	RSV-F	Respiratory syncytial virus infection	15 mg/kg IM	< 2	2010	[414]
		Respiratory syncytial virus infection	3 – 15 mg/kg IM	< 2	2009	[415]
		Respiratory syncytial virus infection	15 mg/kg IM	< 2	2010	[416]
		Respiratory syncytial virus infection	3 – 30 mg/kg IV	< 2	2009	[417]
		Respiratory syncytial virus infection	15 mg/kg IM	< 2	2011	[418]
		Respiratory syncytial virus infection	15 mg/kg IM	< 0.5	2015	[419]
Pagibaximab	LTA	Coagulase-negative staphylococci infection	10 – 90 mg/kg IV	Neonate	2009	[52]
		Coagulase-negative staphylococci infection	60 – 90 mg/kg IV	Neonate	2011	[420]
		Coagulase-negative staphylococci infection	10 – 90 mg/kg IV	Neonate	2010	[421]
Palivizumab	RSV-F	Respiratory syncytial virus infection	15 mg/kg IM	< 2	2012	[35]
		Respiratory syncytial virus infection	3 – 15 mg/kg IV	< 2	1998	[422]
		Respiratory syncytial virus infection	5 – 15 mg/kg IV	< 2	2004	[423]
		Respiratory syncytial virus infection	5 – 15 mg/kg IM	< 2	1998	[424]
		Respiratory syncytial virus infection	15 mg/kg IM	< 0.5	2014	[425]
		Respiratory syncytial virus infection	15 mg/kg IM	< 2	2010	[416]
Rituximab	CD20	Opsoclonus-myoclonus syndrome	375 mg/m^2 IV	1.3 – 17	2010	[426]
SB 209763	RSV-F	Respiratory syncytial virus infection	0.25 – 10 mg/kg IM	< 0.5	1999	[427]
Urtoxazumab	Stx2	Hemolytic-uremic syndrome due to infection by Shiga-like toxin-producing *E. Coli*	1 – 3 mg/kg IV	1 – 15	2010	[428]

5.3 A Physiological Approach to Pharmacokinetics

A number of reviews describe the mechanistic processes governing the disposition of antibody-based drugs in the body (Figure 25).[2,429,430] The distribution of a protein-based drug is limited to the extracellular fluid. Uptake into cells generally leads to degradation. After intravenous administration into the plasma, mAbs can cross the vascular wall and enter the interstitial space of certain organs by extravasation through pores or (to a lesser extent) by transcytosis through the vascular endothelium. The rate of extravasation is tissue-specific and dependent on pore-size, vascular surface area and capillary permeability.[136] For mAbs, cellular uptake does not always lead to degradation. Inside endothelial, epithelial and hematopoietic cells, mAbs can bind reversibly with the neonatal Fc receptor (FcRn) during endosomal sorting, which protects them against lysosomal degradation.[431] From the interstitial space, mAbs can be drained through the lymphatic system and re-enter venous circulation. Transit within the interstitial space and through lymphatic circulation is slow, erratic and driven by convective flow. Drainage of interstitial fluid into the lymph helps to ensure that the interstitial spaces in tissues are not permanent traps for circulating mAbs. Catabolism by non-specific proteases in circulation may make a minor contribution to total elimination. Renal excretion is assumed negligible because the molecular weight exceeds 70 kDa.[64] Because mAbs are protein molecules, an immunogenic response and subsequent development of anti-drug antibodies may occur.[23] A full immunogenic response can render the drug near-undetectable in plasma.[320]

In cases of high target abundance and accessibility, mAbs may exhibit target-mediated drug disposition, meaning that the kinetics of the target directly impact the kinetics of the drug.[19] If the target is free and soluble, mAbs may contact it anywhere in the extracellular fluid. After binding, the neutralized mAb-target complex would circulate until it is cleared by the activation of complement and subsequent removal by phagocytosis. This phagocytosis could be mediated in part through binding to Fc-gamma receptors (FcγR) on the surface of macrophages. If the target is bound to the cell membrane, mAbs must often reach the interstitial space to contact it. After binding, the mAb-target complex may be internalized into the cell and degraded, initiating a major route of elimination for the drug. When a mAb is subject to significant target-mediated elimination, the *in vivo* pharmacokinetics can be noticeably non-linear (clearance can decrease with increasing doses).[19,20]

A physiological approach to mAb pharmacokinetics must be taken to ensure safe and effective dose design in the pediatric clinical trials to come. This review seeks to formulate hypotheses about the age-related differences in physiology that may be responsible for the observed pharmacokinetic

differences between adults and children. The major focus is on neonates (< 1 month) infants (< 2 years) and young children (2 – 6 years), where the pharmacokinetic differences are most prominent.

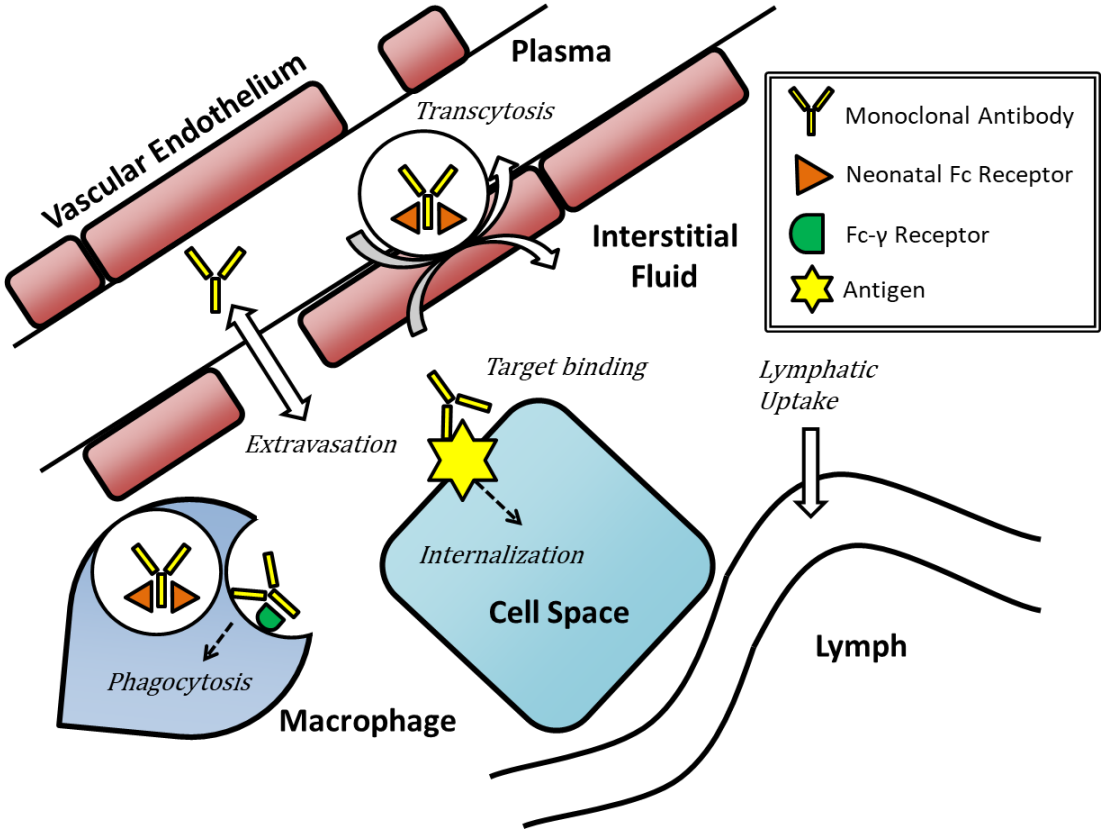

Figure 25. The main physiologic processes governing the disposition of mAbs. After IV administration, mAbs cross the vascular wall by extravasation or by transcytosis through the vascular endothelium. During this transcytosis, mAbs may bind reversibly with the neonatal Fc receptor (FcRn), which protects them from lysosomal degradation. If the target is membrane-bound, mAbs must reach the interstitial space in order to facilitate target binding. The mAb-target complex on the cell surface can be internalized and degraded. If the target is free and soluble, mAbs may contact the target anywhere in the extracellular fluid. The mAb-target complex will circulate until it is cleared by the activation of complement and subsequent phagocytosis. Phagocytosis of these complexes could be mediated in part through binding to Fc-gamma receptors (FcγR) on the surface of certain macrophages.

5.4 Distribution

As mentioned, the distribution of mAbs is limited to the extracellular fluid in the body due to their poor permeability across cellular membranes and vulnerability to intracellular catabolism. Therefore, it is possible to estimate the volume of distribution in different species or individuals based on known reference values for extracellular fluid volume and body composition. Table 15 summarizes the developmental biology of circulatory and hydrostatic parameters from infancy until adulthood. While the extracellular fluid volume fraction falls rapidly after birth, plasma volume rises incrementally. The net effect is that the proportion of total body volume available for distribution is higher in infants than in older children and adults.

Table 15 also highlights the fast rate of blood perfusion throughout the infant body in the first 6 months of life (cardiac output). On a per kilogram basis, young infants receive higher volumes of blood to tissues over time.[14,432] Consequently, distribution to tissues may occur faster in infants up to 6 months of age when compared to adults. However, the distribution of large molecules to tissue spaces is largely rate limited by permeability across capillary walls, rather than perfusion.

Table 15. Mean hydrostatic parameters for infants progressing until adulthood

Age	**Blood Pressure**[433] mmHg	**Heart Rate**[434] bpm	**Cardiac Output**[14,432] L/min	**Blood Volume**[435] mL/kg	**Hematocrit**[435,436] %	**Plasma Volume**[a] mL/kg	**ECW Fraction**[437] %
Birth	70/55	140	0.6 [0.174/kg]	85	53	40	45
1 month	85/52	120	0.7 [0.152/kg]	80	44	45	40
2 months	90/50	120	0.8 [0.139/kg]	80	44	45	32
3 months	90/50	120	0.9 [0.137/kg]	75	34	50	30
6 months	90/52	120	1.1 [0.134/kg]	75	34	50	29
12 months	90/55	120	1.3 [0.131/kg]	80	36	50	26
18 months	90/55	110	1.5	85	37	55	23
24 months	90/55	110	1.7	85	37	55	20
6 years	95/57	100	3.5	80	38	50	19
12 years	110/65	85	4.7	75	39	46	18
18 years	124/72 (M) 113/67 (F)	70 (M) 75 (F)	6.1 (M) 5.5 (F)	75 (M) 65 (F)	43 (M) 39 (F)	43 (M) 40 (F)	18

[a] calculated from blood volume and hematocrit
ECW = extracellular water

A number of mAbs have been recently approved or are in development for infectious disease prevention in neonates.[35,52,413,414,428] Therefore it is important to consider circulatory physiology during the fetal-to-neonatal circulatory transition period. In hours to days after birth, the neonatal circulatory system undergoes drastic structural changes.[438] Briefly, the placenta is replaced by the lungs as the location of gas exchange and the corresponding shift from a parallel circuit to a series circuit in the heart is accompanied by the closing of the ductus arteriosus, the foramen ovale and the ductus venosus. The pulmonary arteries dilate and the left ventricle strengthens as they each begin to accommodate the flow and volume of the entire cardiac output. These changes occur progressively and perfusion to the lungs and peripheral organs may not be strong in the first week of life. Generally speaking, there may be irregular distribution when mAbs are administered during the fetal-to-neonatal circulatory transition period.

While the rates of extravasation of therapeutic mAbs in children and adults have not been measured, there is data available for other plasma proteins, such as albumin.[439-450] Albumin and IgG are both plasma proteins that follow similar patterns of distribution and bind with high affinity to FcRn. The TER is measured by calculating the rate of disappearance of labelled albumin from plasma over time. The TER of IgG is typically 40% lower than the TER of albumin across a variety of disease states, as summarized by Malik et al.[68] Therefore, the transcapillary escape rate (TER) of albumin in infants and children can be used as a surrogate to explore how the rate of extravasation of IgG molecules into tissues may change with age.[449] Overall, the rate of extravasation of plasma proteins is approximately 3 times higher in healthy neonates than adults (Table 16). To make hypotheses about how these differences progress after birth and when adult extravasation rates are reached, the mechanism behind the increased rate of extravasation must be elucidated.

Extravasation of plasma proteins through pores occurs dynamically by filtration, convection and sieving.[150] The rate of extravasation is a function of capillary permeability – which itself is affected by the capillary pore size – and the vascular surface area available for plasma protein exchange. According to the Starling equation, capillary permeability and net flux of fluid is governed by competing hydrostatic (blood pressure, blood flow rate, fluid volumes, etc.) and colloidal osmotic (protein concentration gradients) fluid pressures on either side of the capillary wall:[150]

$$P_e = P_c - (P_t + P_o)$$

where P_e = effective filtration pressure, P_c = capillary hydrostatic pressure, P_t = opposing hydrostatic pressure, P_o = net colloid osmotic pressure

Table 16. Transcapillary escape rate of albumin in infants (< 2 years)

Study	Age	Condition	TER (%/h)	Label
Mollison et al.[439]	< 1 d	Healthy and hemolytic disease	20	EB
Steele[440]	< 1 d	Healthy	15.5	IHSA
Jegier et al.[441]	< 1 d	Healthy	19	IHSA
Cassady et al.[442]	< 1 d	Healthy	12.8	EB
Parving et al.[443]	< 1 d	Born to diabetic mothers	18.4	IHSA
Ingomar et al.[444]	< 1 d	Healthy	22.6	EB
Ingomar et al.[445]	< 1 d	Born to diabetic mothers	17.5	EB
Ingomar et al.[445]	< 1 d	IRDS	20.4	EB
Ingomar et al.[445]	< 1 d	Birth asphyxia	25.6	EB
Linderkamp et al.[446]	< 2 d	Premature	23	IHSA
Linderkamp et al.[446]	< 2 yr	Critically ill	11.3	IHSA
Tassani et al.[447]	< 14 d	Transposition of the Great Arteries	25.3	EB
Parving et al.[448]	Adult	Healthy	5.6	IHSA
Rossing et al.[449]	Adult	Healthy	5.4	IHSA
Wasserman and Mayerson[450]	Adult	Healthy	4.9	IHSA

TER – Transcapillary escape rate
EB – Evan's blue dye
IHSA – Iodinated human serum albumin

Hydrostatic pressure drives the movement of fluid out of capillaries and colloidal osmotic pressure draws fluid back into capillaries according to protein concentration gradients. The Landis model of fluid exchange suggests that net flux of fluid is out of capillaries at the arterial end of the capillary bed when hydrostatic pressure is highest and into capillaries at the venous end of the capillary bed when interstitial colloid osmotic pressure is able to overcome the diminishing hydrostatic pressure.[451] The movement of mAbs is expected to follow this flux, though there is significant resistance due to the large size and charge of the molecules. This model with filtration at the arterial end of the capillary bed and reabsorption at the venous end of the capillary bed is a simple approximation and both processes may not always be occurring.[451] For example, in renal tubular capillaries, the colloid osmotic pressure from the interstitial fluid is weak and cannot drive reabsorption because the renal tubular absorbate is being continuously flushed.[451] In addition, there are many dynamic factors to consider, such as the impact of transient vasoconstriction and vasodilation that may dictate the degrees of filtration and reabsorption.[451]

The developmental biology of transcapillary fluid balance has been explored in maturing animals, but there is limited data in human infants.[452-455] Where data is sparse, extrapolations of capillary

permeability in all tissues can be made by examining capillary permeability in the glomeruli. In animals, the net filtration rate of fluid across capillaries increases with age and approximately in proportion to the changes in arterial and venous pressures (Table 15).[452-455] This change is driven by discordant increases in the opposing forces of extravasation; although colloid osmotic pressure increases with age, hydrostatic pressure increases to a greater degree (Figure 26).[454] Even though plasma protein concentrations are much higher in adults than immature animals, colloid osmotic pressure only increases modestly with age due to the balance of protein concentrations that is maintained between the plasma and extracellular fluid.

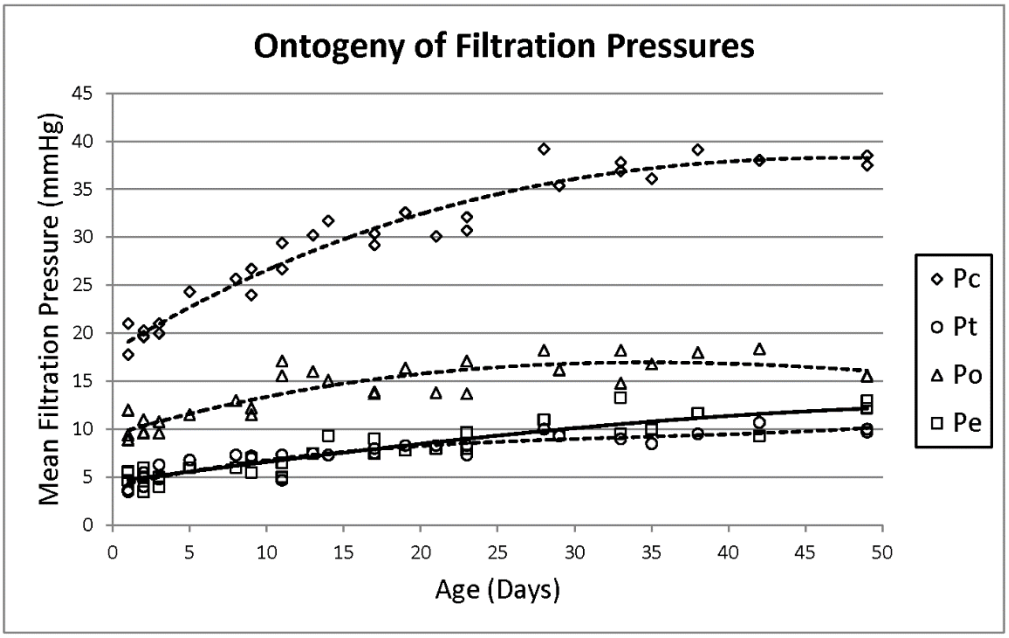

Figure 26. The ontogeny of filtration pressures in newborn guinea pigs until 7 weeks of age.[454] P_e = effective filtration pressure (solid line), P_c = capillary hydrostatic pressure, P_t = opposing hydrostatic pressure, P_o = net colloid osmotic pressure; $P_e = P_c - (P_t + P_o)$

Similar patterns of age-dependent capillary permeability and net filtration rate are observed in human infants. As evidence, the glomerular filtration rate of human infants per unit of kidney weight increases with age until reaching adult values after 6 months.[456,457] The mechanism of this change appears consistent between humans and animals. Though capillary hydrostatic pressure cannot be measured directly in humans, there is sufficient data regarding the modest age-dependent increase in colloid osmotic pressure that occurs during the first year of life to support this hypothesis.[458-463] Based on the ontogeny of glomerular filtration in humans and the maturation rates of factors in

transcapillary fluid balance observed in animals, we expect that capillary permeability to plasma proteins modestly increases with age until reaching adult values by six months.

The second component of extravasation is the capillary surface area available for plasma protein exchange. Neonatal tissues have high demands for oxygen and other nutrients after birth and during the subsequent period of rapid growth. To meet these demands, infants have a vast and dense capillary surface area available for fluid, oxygen, solute and protein exchange, most notably in the peritoneum, muscle and skin.[464-466] Further, infants have the largest skin surface area per unit volume, where capillary networks are dense.[466] Though capillary density is increased, the endothelial surface area is not compromised.[464] Capillary density decreases with age until puberty and then rises steadily throughout adulthood, though never reaching the extremes seen in infancy (Figure 27).[464,467] There is significant variability in capillary density at birth, and it can be even further elevated in preterm neonates or in those born to hypertensive mothers.[468,469]

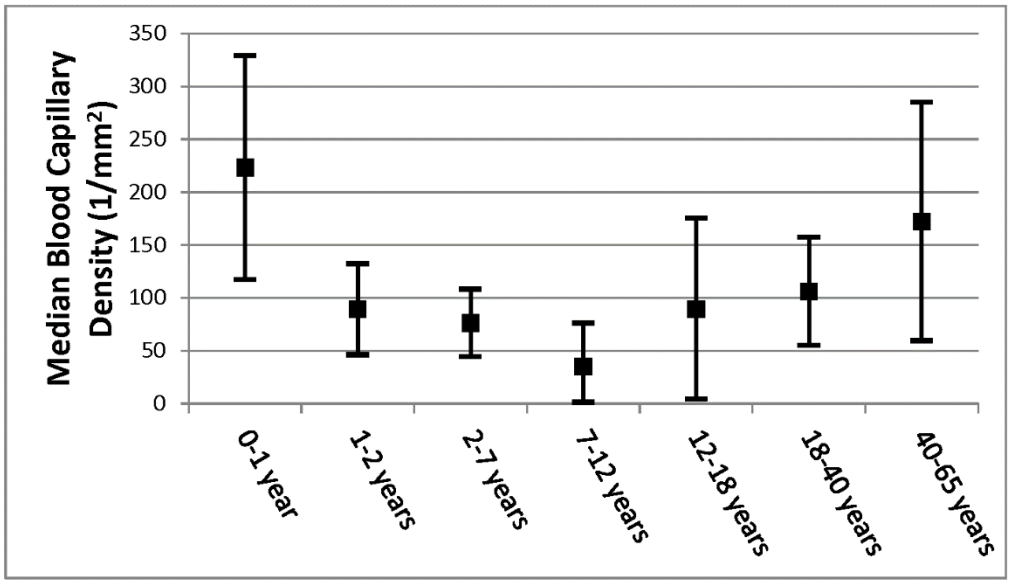

Figure 27. Median peritoneal capillary density in humans with interquartile ranges[464]

Finally, it is important to note that capillary endothelial structure is unique to each tissue. For example, the brain is largely impermeable to plasma proteins because of the tight intercellular junctions present between endothelial cells at the blood-brain barrier, while the liver, spleen and kidneys are highly permeable to plasma proteins due to the presence of sinusoidal or fenestrated capillaries.[136] These central organs are proportionally larger in infants, which may explain the faster rate of mAb distribution to tissues in infants when compared to adults.[443] For example, the liver

makes up 4% of the total body mass of infants, while in adults it makes up 2.5% of total body mass.[50] The ratio of "leaky" (liver, spleen, heart, lung, kidney, bone marrow, small intestine) to "tight" (brain, muscle, skin, adipose, large intestine, stomach, thymus, pancreas, bladder) tissue mass decreases by 30% from birth to adulthood and may partially explain the age-dependent pattern of weight-normalized clearance that is observed (Table 17). All things considered, the conclusion is that despite modestly lower capillary permeability, the overall rate of extravasation into tissues is higher in infants than in adults because infants have proportionally larger capillary surface area per unit volume available for plasma protein exchange and proportionally larger central organs, where sinusoidal or fenestrated capillaries are present.

Table 17. Ratio of leaky to tight tissue mass in humans from birth until adulthood[50,136]

Age (years)	**Leaky[a]:Tight[b] Tissue Mass Ratio**
Birth	0.129
1	0.115
5	0.118
10	0.116
15	0.102
Adult	0.098

[a] Leaky tissues: liver, spleen, heart (no blood), lung (no blood), kidney, bone marrow (active only) and small intestine.
[b] Tight tissues: brain, muscle, skin, adipose (separable), large intestine, stomach, thymus, pancreas and bladder

5.5 Elimination

Elimination of mAbs occurs predominantly through intracellular proteolysis and to a lesser extent, extracellular proteolysis (serum proteases, other non-specific interactions).

Uptake into cells that leads to intracellular degradation is accomplished by endocytosis, phagocytosis and in some cases, receptor-mediated endocytosis.[103,186,470-472] The major cell types implicated are endothelial and hematopoietic cells, including macrophages.[473] At present there is no evidence that these cellular uptake functions are different between adults and children. However, there is convincing evidence that the relative abundances of these major cell types are higher in children. As mentioned, children have high capillary density, particularly in muscle, skin and peritoneal tissues. This vascular network provides a greater number of vascular endothelial cells per unit volume for non-specific endocytosis and degradation of protein products. Moreover, reference values for complete blood counts show that there are also high numbers of circulating hematopoietic

cells in children, even up to an average of 3-fold higher than adult numbers shortly after birth (Table 18).[474-478] These high levels of circulating leukocytes and macrophages will contribute to the observed cellular uptake and clearance of protein products in children. Tissue-specific macrophages are also thought to be sites of mAb degradation and Fc-mediated recycling.[479] Tissue-specific macrophages can be detected very early during development in the fetal liver, spleen red pulp and bone marrow, and are known to be some of the first fully functioning cell types in the fetus.[480,481] Little is yet known about the relative abundance of tissue-specific macrophages in children.

Table 18. Summary of reference ranges for circulating leukocyte concentrations in children

Age	**Leukocyte Concentration**[a 474-478] (10^9 cells/L plasma)
Preterm	13.0 (5.0 – 21.0)[b]
Term	18.0 (11.0 – 28.0)
1 – 3 months	10.6 (7.2 – 18.0)
3 – 6 months	9.2 (6.7 – 14.0)
6 – 12 months	9.1 (6.4 – 13.0)
1 – 2 years	8.8 (6.4 – 12.0)
2 – 6 years	7.1 (5.2 – 11.0)
6 – 12 years	6.5 (4.4 – 9.5)
12 – 18 years	6.0 (4.4 – 9.1)
Adult	6.0 (4.0 – 9.0)

[a] Data reported as median (10th – 90th percentile)
[b] Premature infants who are small for gestational age may have leukocyte concentrations that are up to 50% lower than those who are appropriate for gestational age[482,483]

With regard to extracellular proteolysis, the comparative proteolytic activities of adult and infant sera against immunoglobulin are unknown.[484] Major protein modification pathways which may affect IgG stability and activity in serum include asparagine deamidation, methionine oxidation, Fc glycan interactions with mannosidases and reduction of disulfide bonds.[484] Certainly there is an opportunity for further investigation into the stability of IgG in infant serum.

Specific phagocytosis of IgG is mediated in part through contact with the FcγR family, named because they bind to the Fc region of IgG. These receptors are expressed in cells of the mononuclear phagocyte system and facilitate the antibody-dependent functions of the immune system, such as antibody-dependent cell-mediated cytotoxicity and the elimination of antibody-target complexes.[485] However, studies in mice and monkeys show no significant impact of FcγR binding on the pharmacokinetic profile of mAbs.[168,169,486] While there may be small differences in FcγR receptor

expression and activity between neonatal leukocytes and adult leukocytes,[487] the overall contribution to the age-dependence of elimination is expected to be low.

The effects of FcRn on the pharmacokinetics of mAbs in adults or infants are mediated by five factors:[488-491]

1. FcRn expression per cell
2. Relative abundance of FcRn-expressing cells
3. Affinity of FcRn for IgG
4. Concentration of endogenous IgG
5. Inflammation, which may alter the expression or function of FcRn

Organ-specific RT-PCR data from a study in rats reveals that FcRn expression varies from birth to puberty with sudden peaks and fluctuations.[492] A grouped representation of the FcRn expression in all organs is presented in Figure 28. This preliminary data suggests that FcRn expression may increase with age until the end of puberty (40 days of age for a rat). No consistent pattern of ontogeny can be determined after this point because there is considerable inter-individual and inter-organ variability.

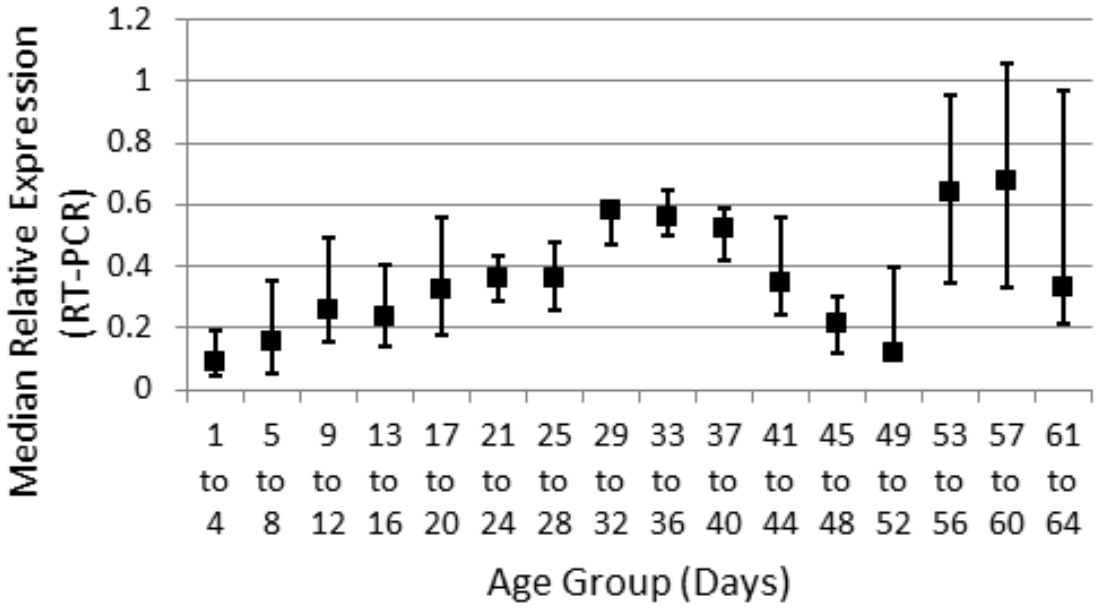

Figure 28. Grouped representation of the relative expression of FcRn mRNA in rat tissues. Tissue mRNA data was collected from the lung, intestine, heart, spleen, liver, kidney, skin and muscle

tissues of maturing rats (1-63 days old).[492] The red square denotes the median and the error bars mark the first and third quartiles.

Further investigations in immature rats with immunohistochemical staining show that FcRn is largely localized in epithelial cells and macrophages rather than endothelial cells, where expression is heterogeneous or sparse.[492] Cianga et al. discover a similar profile in human neonatal tissues.[493] However, these results may be limited by the poor sensitivity of immunohistochemical methods. If FcRn concentrations in vascular endothelium are indeed crucial to IgG homeostasis in humans, then a low concentration in infants may contribute to the increased weight-normalized clearance of mAbs that is observed.[473,489,490]

In addition to possible low FcRn concentrations, there are relatively high concentrations of endogenous IgG in infants available to compete for FcRn binding in the first month after birth. Placental transfer of maternal IgG occurs late in gestation and maternal IgG lingers for up to two months, based on a maximal plasma half-life of 28 days.[494] Maternal IgG transferred through breast milk also contributes to these levels. Endogenous IgG competes with exogenous mAb for binding to FcRn and this displacement would increase intracellular degradation of the mAb. Serum endogenous IgG levels in infants are relatively high at birth but fall in the first 3 months of life and then gradually rise to adult values before puberty (Figure 29).[495-497]

With the available data, it can be hypothesized that the increased weight-normalized clearance that is observed in infants and young children is related to a high relative abundance of circulating macrophages and vascular endothelial cells for cellular uptake, and a possible low level of FcRn expression in vascular endothelial cells (Figure 28). This effect may be more pronounced in the first month of life, when maternal IgG is present in relatively high amounts and may compete with therapeutic mAbs for the available FcRn salvage sites.

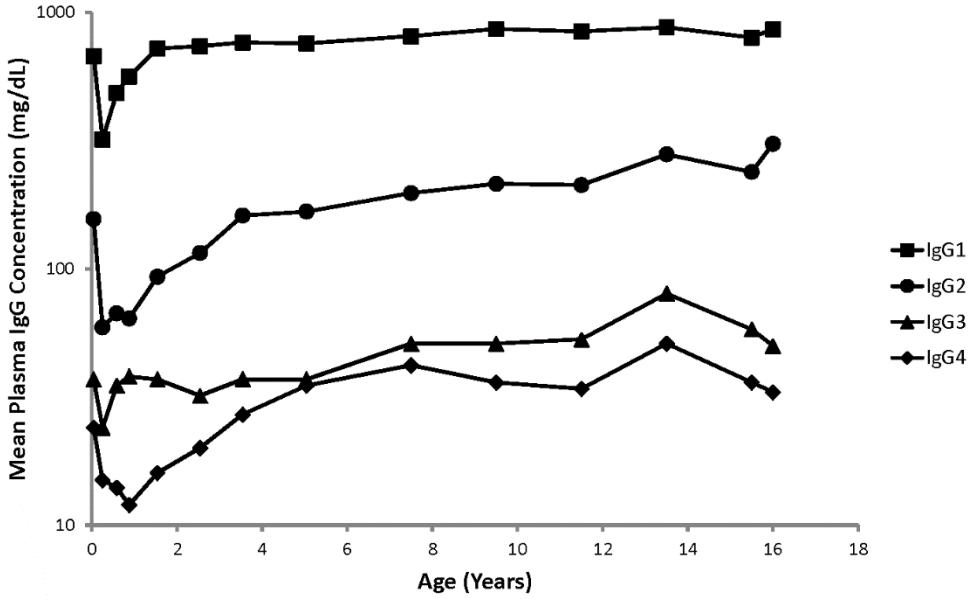

Figure 29. Plasma concentrations of IgG subclasses from birth to adulthood in human children.[497]

5.6 Absorption

Of the mAbs administered to infants, only a few are given by an extravascular route (Table 14). The mAbs for respiratory syncytial virus prophylaxis are given intramuscularly and the mAbs for retinopathy of prematurity are given intravitreally. While subcutaneous (SC) administration is preferred in adults for systemic biotherapeutics, intramuscular (IM) administration may be preferred in infants due to the ease of injection to the vastus lateralis muscle. In patients of all ages, absorption is slow with a time to maximal plasma concentration (Tmax) ranging from 1.7 – 13.5 days.[498] Both experimental evidence and mechanistic models in adults predict that while the rate and extent of absorption are largely comparable between the IM and SC routes for mAbs, the IM route may be associated with a higher Cmax and shorter Tmax.[498,499] For mAbs, bioavailability after extravascular administration ranges from 52 – 80%.[498,500]

There is moderate inter-individual variability in both the rate and extent of mAb absorption following extravascular administration due to factors related to body weight, gender, age, activity level, disease state, respiratory rate, and blood pressure.[2] There may also be variability in protein absorption depending on which injection site is used (e.g., abdomen, thigh, arm),[501] though the current evidence with mAbs in humans conflicts with the prevailing notions in the field of SC biotherapeutics.[499,502-505]

Mechanistically, absorption to the systemic circulation after either IM or SC administration occurs via two major pathways: immediate absorption into blood via fluid recirculation in the capillary beds of the local injection site, or slow lymphatic drainage and recirculation, which is the dominant pathway.[76,78,498] Sensitivity analyses with mechanistic models of SC mAb absorption suggest that the absorption rate is largely dependent on the lymph flow rate, which has been approximated to be 0.2% of the plasma flow rate in adults.[78,135,498] The extent of absorption and overall bioavailability are governed by the degree of pre-systemic elimination in the lymphatic system, the lymphatic transit time and the FcRn binding affinity.[498,506] Pre-systemic elimination is attributed to proteolytic degradation, endocytosis into endothelial and epithelial cells or phagocytosis into cells of the MPS that are present throughout the lymphatic system.[479,498]

Some data exist to inform predictions of the rate and extent of mAb absorption in infants and young children. One population pharmacokinetic (PopPK) study to date with palivizumab suggests that the rate of absorption after IM administration is two to three times faster in infants than adults and that the extent of absorption or bioavailability is similar between the two groups.[35] However, the results are limited due to the sparse nature of the pediatric data that was used, which included few data points in the early phases following administration. A fast rate of absorption in comparison to adults was also reported in a small study of SC adalimumab with five patients whose ages were 6, 9, 10, 13 and 13 years.[507] Studies with other large proteins, such as darbepoetin alfa, similarly suggest that absorption is more rapid in children 3 – 16 years of age with extravascular dosing.[392]

To potentially explain this observation of higher absorption rate in children as compared to adults, we examine the factors of lymph flow rate and extracellular fluid volume. Infants have a high fraction of extracellular fluid volume (Table 15) and enhanced tissue hydration when compared to adults.[508,509] This translates to a large fluid reservoir available for dispersion and absorption of protein therapeutics shortly after extravascular administration. Infants have greater cutaneous, subcutaneous and muscle perfusion due to the high density of capillaries present and immature vasomotor control, which improves access to the systemic circulation.[508,509]

When normalized for body weight, both local and whole body lymph flows are high in infants, which drives a fast rate of drug absorption.[510] In animal studies, newborn lambs had thoracic duct flow rates that were three times higher than the rates in adult sheep (7.4 vs. 2.3 mL·h-1·kg-1).[511] Locally, lymph flows from subcutaneous tissue and from the lungs have been measured to be higher in newborn anesthetized animals than in their adult counterparts.[512,513]

With respect to the extent of absorption, or bioavailability, it appears as if this property is similar to adults given the same route of administration.[35,392] Considering that the rate of absorption appears to be faster in young children, for bioavailability to remain similar, pre-systemic elimination must be higher. This elimination may be attributable to greater proteolytic degradation or phagocytosis by hematopoietic cells during lymphatic transport.[479]

The exact pathways of systemic absorption after intravitreal (IVT) administration are unknown. Two VEGF-inhibitors, bevacizumab (mAb) and ranibizumab (Fab) are known to reach systemic circulation after IVT administration in premature infants.[403,404,514] In adults, the systemic absorption of bevacizumab is significantly greater than the systemic absorption of ranibizumab.[515] FcRn is present in endothelial cells in the eye and may be responsible for the improved absorption of bevacizumab over ranibizumab, which does not bind FcRn.[516] FcRn binding may therefore be an important process governing systemic absorption after IVT administration. More research is required to elucidate the pathways of systemic absorption in the eye and how they may differ between premature infants and adults.

In summary, it is likely that the processes governing absorption are the most consistent between adults and children. There may be a faster rate of absorption and greater extent of pre-systemic elimination in children, but the same overall bioavailability.

5.7 Conclusion

A number of physiologic mechanisms may be responsible together for the unique pharmacokinetic profiles that are seen with mAbs in infants and young children. In particular, the faster rate of weight-normalized plasma clearance observed in children may be due to a higher burden of circulating hematopoietic cells, lower concentrations of FcRn in vascular endothelial cells, and/or high levels of maternal IgG that may compete for FcRn binding shortly after birth. The faster rate of extravasation is driven by a higher ratio of “leaky” to “tight” tissue mass and a greater capillary surface area per unit volume available for plasma protein exchange in young children. While overall bioavailability may appear similar, it is important to recognize that the rate of absorption can be much faster in children, especially infants. Further research is required to solidify these hypotheses and to explore their pharmacodynamic consequences.

5.8 Study Highlights

This review explores the age-dependence of the physiologic processes governing the disposition of monoclonal antibodies in infants.

1. The fraction of extracellular fluid volume in the body decreases with age and provides large weight-normalized volumes of distribution in infants.
2. Extravasation of antibodies into tissues occurs quickly in infants as they have a large capillary surface area per unit volume available for plasma protein exchange and a large proportion of "leaky" tissues, where capillary permeability is highest.
3. A fast rate of lymph flow in infants drives a fast rate of absorption after extravascular administration.
4. Infants have higher circulating concentrations of hematopoietic cells, which may contribute to extensive cellular uptake and fast elimination.
5. Intracellular metabolism and elimination may be increased due to low expression of FcRn – the neonatal salvage receptor – and the relatively high concentration of endogenous IgG competing for FcRn binding after birth.

Chapter 6
Integration of Ontogeny into a PBPK Model for Monoclonal Antibodies in Premature Infants

6.1 Abstract

An understanding of pediatric pharmacokinetics (PK) is essential for first-in-pediatric dose selection and clinical trial design. At present there is no reliable way to scale the PK of monoclonal antibodies and IgG drug products from adults to young children or to premature infants – a vulnerable population with a rapidly growing drug development pipeline.

In this work, pediatric PBPK models are constructed in PK-Sim and Mobi to explore the PK of pagibaximab, palivizumab, MEDI8897 and intravenous immunoglobulin (IVIG) in preterm infants. In addition to considering ontogeny in pediatric organ volumes, organ composition, blood flow rates and hematocrit, advanced ontogeny is applied for three key parameters: capillary surface area, hematopoietic cell concentration and lymph flow rate. The role and importance of each parameter for determining pediatric clearance and volume of distribution at steady state are quantitatively assessed with a local sensitivity analysis. In addition, the uncertainty around parameters with limited information in pediatrics is addressed (e.g. free FcRn concentration).

The full ontogeny parameterization yields pediatric PK predictions that are within 1.5-fold prediction error over 90% of the time for preterm infants, with an absolute average fold error of 1.05. This result suggests that many of the key factors related to ontogeny are appropriately addressed.

Overall, this study makes a first step toward developing a platform pediatric PBPK model for monoclonal antibodies and IgG drug products by solidifying existing parameterizations, integrating new concepts and drawing attention to unmet needs for physiologic knowledge in children.

6.2 Introduction

Monoclonal antibodies (mAbs) have solidified their position as the world's most popular class of drugs both on the market and in the drug development pipeline. The list of therapeutic applications is extensive and continues to grow, now featuring opportunities in a host of pediatric-specific disease states such as Kawasaki disease,[517] infectious syndromes of prematurity,[420,518] atypical hemolytic uremic syndrome,[409] and pediatric cancers.[407]

In pediatric drug development, safety is of utmost importance for first-in-pediatric (FIP) dose selection. However, if the FIP dose is too conservative, consequences may include exposing sick children to ineffective doses, wasting research expenditures or requiring additional children to be unnecessarily enrolled in the study. Conventionally, FIP doses are determined by establishing confidence in pharmacokinetics (PK), safety and efficacy in adults and then translating this knowledge to children by allometric scaling or physiologically-based pharmacokinetic (PBPK) modeling.[312]

Our recent work addresses the comparative performances of both methods for predicting infliximab PK in children between 4 and 18 years of age.[60] In the case of small molecule drugs, allometric scaling and PBPK modeling often achieve predictions within 2-fold error over 90% of the time for children over 2 years of age, when maturation and ontogeny do not critically influence drug disposition.[15,314] Below the age of two years there is more uncertainty. Allometric scaling with age-dependent exponents can match PBPK modeling in pediatric PK prediction for very young children, but the age-dependent exponents have to be learned with similar compounds in advance.[315,316,519]

At present there is no reliable way to scale the PK of mAbs from adults to younger children or to premature infants – neither PBPK modeling nor allometric scaling have been evaluated. At this stage of life, children are physiologically very different from adults and consequently achieve lower plasma exposures than adults when the same weight-based doses are given.[34] Our recent review highlights the key physiological drivers of this phenomenon in pediatrics.[34] The US Food and Drug Administration has stressed the importance of incorporating these physiological parameters into a PBPK modeling framework to support pediatric drug development for mAbs and Fc-fusion proteins.[70] To date, only one effort has been made to explore the PK of mAbs in pediatrics with a minimal PBPK modeling approach.[319]

In the same way as for small molecule drugs,[14] reviewing the literature[34] and integrating a quantitative understanding of pediatric physiology into a PBPK model are first steps toward the development of a platform pediatric PBPK model that can be used for FIP dose selection and drug development in the future. Here we synthesize literature-based ontogeny profiles for key physiological parameters relevant to mAb disposition, integrate them into pediatric PBPK models for four drug products in premature infants and quantify their impact on PK with a sensitivity analysis. Premature infants are first considered because they are the most different from the adult population and the majority of PK data available in literature for young children features this population.

6.3 Methods

6.3.1 Software

All PBPK models were constructed in PK-Sim and Mobi v8.0 using the base model for large molecules and therapeutic proteins (www.open-systems-pharmacology.org).[66] PK data from literature in the form of concentration-time profiles were digitized with PlotDigitizer v2.6.8 by Joseph Huwaldt. MATLAB R2018b was used for data analysis and graphical presentation of results.

6.3.2 Pharmacokinetic Data

Adult and pediatric concentration-time profiles featuring intravenous (IV) and intramuscular (IM) administrations were extracted from literature for pagibaximab, palivizumab, MEDI8897 and IVIG (Table 19). No adult PK data were available for palivizumab.

6.3.3 Virtual Individuals

As inputs to the PBPK models, virtual adults and premature infants were created in PK-Sim and Mobi v8.0 according to previously published algorithms.[14,266,317,520] For each real-world PK study (Table 19), a virtual individual was created for simulation with postnatal age, gestational age (if premature), height, weight and sex parameters according to the mean individual in that study. Additional physiological parameter adjustments were made for virtual premature infants to account for the ontogeny of key processes governing mAb disposition, as will be discussed.

6.3.4 Adult PBPK Model Development

The base model for large molecules and therapeutic proteins in PK-Sim features two-pore extravasation, endocytosis into vascular endothelium, binding to FcRn and lymph recirculation.[66] Intramuscular administration was implemented by applying the bioavailable dose ($Dose \cdot F$) as a bolus to the interstitial space of the muscle compartment. Modifications were made to address the contribution of hematopoietic cells to cellular uptake, as will be discussed. Target-mediated drug disposition and immunogenicity were considered negligible. The same model structure was used for both adults and children.

Table 19. Pharmacokinetic data for PBPK modeling

Study	Dose	Cohort	N	Age	Gestational Age	Weight
Pagibaximab						
Weisman et al. [53]	3 mg/kg IV 10 mg/kg IV	Healthy adults	8	34.7 [24-50] years	-	77.9 [61-113] kg
Weisman et al. [420]	60 mg/kg IV 90 mg/kg IV	Premature infants	42	[2-5] days	27.5 ± 1.7 weeks	0.99 ± 0.17 kg
Palivizumab						
Sáez-Llorens et al.[424]	15 mg/kg IV	Premature infants and infant with BPD	22	8.1 ± 1.69 months	Predominantly < 32 weeks	4.9 ± 0.74 kg
Sáez-Llorens et al.[424]	15 mg/kg IM	Premature infants and infant with BPD	48	6 months	Predominantly < 32 weeks	NR
MEDI8897						
Griffin et al.[521]	3000 mg IV 1000 mg IV 300 mg IV 300 mg IM 100 mg IM	Healthy adults	102	31 ± 7.8 years	-	78 ± 14.9 kg
Domachowske et al.[522]	50 mg IM 25 mg IM 10 mg IM	Premature infants	71	6.5 months	32 – 35 weeks	6.8 ± 1.9 kg
Intravenous Immunoglobulin (IVIG)						
Andresen et al. [523]	600 mg/kg IV	Healthy adults	30	26 [18-43] years	-	66 [52-86] kg
Chirico et al. [524]	500 mg/kg IV	Premature infants	23	[0-1] days	29.7 [24-34] weeks	1.1 [0.64-1.47] kg
Noya et al. [525]	500 mg/kg IV 750 mg/kg IV 1000 mg/kg IV	Premature infants	21	[1-5] days	29.1 [26-33] weeks	1.1 [0.75-1.5] kg
Noya et al. [526]	500 mg/kg IV 750 mg/kg IV	Premature infants	20	[1-5] days	28.9 [26-35] weeks	1.1 [0.75-1.5] kg

BPD = Bronchopulmonary dysplasia, data presented as mean or median ± standard deviation [range]

Adult models were constructed with drug-specific parameterizations for each molecule (Table 20). While the data for IVIG actually includes several brands of the product, the physicochemical parameters were assumed the same across all brands because no data was available to inform any product-specific differences. The affinities of pagibaximab and MEDI8897 for the neonatal Fc receptor (K_D^{FcRn}) and the bioavailable fractions in the muscle interstitium (F) for MEDI8897 were not available in literature and required optimization. The optimization was carried out in PK-Sim using a Monte-Carlo approach for exploring the parameter space. The bioavailable fraction of palivizumab in muscle interstitium was assumed the same as for MEDI8897 since no adult concentration-time data was available to perform an optimization and the molecules have similar parent derivations.

Table 20. Drug-specific parameters inputted into the PBPK model

Parameter	**Pagibaximab**	**Palivizumab**	**MEDI8897**	**IVIG**
Molecular Weight	146.1 kDa			150 kDa
Hydrodynamic Radius	5.34 nm	5.34 nm	5.34 nm	5.34 nm
FcRn Affinity	946 nM	750 nM	94 nM	630 nM
Bioavailable Fraction in Muscle Interstitium	-	0.85 *(assumed same as MEDI8897)*	0.85	-

Shaded parameters were optimized against the PK data from healthy adults

Success of the PBPK models for mechanistically representing the PK of the mAbs in adults was confirmed by comparing model predictions to observed concentration-time data from literature with a visual predictive check (Table 19).

6.3.5 Integration of Ontogeny

Adult parameters in the final models were adapted to pediatrics with careful consideration of physiological literature to date.[34] To begin, organ volume, organ composition, blood flow rate and hematocrit parameters were updated with values for preterm infants.[14,266,317,520]

Infant organs – particularly adipose and muscle tissues – are more "watery" than adult organs and provide large volumes of distribution (mL/kg) for protein-based drugs. The extracellular fluid fraction in the infant body decreases from 0.45 at birth to 0.18 in adulthood.[34,437] In addition, central "leaky" and macrophage-bearing organs such as the liver and spleen make up a large portion of the neonatal body when compared to adults (12.9% in infants vs. 9.8% in adults).[34] Virtual children are created by default in PK-Sim with these properties already accounted for.[14]

Moving forward, advanced ontogeny was considered in two additional domains: extravasation and lymph flow, and cellular uptake. Table 21 summarizes how advanced ontogeny was integrated into the PBPK model for premature infants.

Table 21. Summary of advanced ontogeny parameters in the PBPK model

Age	**Capillary Density** [464,467,468,527,528] (Fraction of Adult)	**Lymph Flow Rate** [34,511,513,529,530] (Fraction of Adult)	**Leukocyte Concentration**[a] [474-478,482] (10^9 cells/L plasma)
Preterm	1.6	2.0	13.0 (5.0 – 21.0)[b]
Term	1.3	2.0	18.0 (11.0 – 28.0)
1 – 3 months	1.1	2.0	10.6 (7.2 – 18.0)
3 – 6 months	1.0	2.0	9.2 (6.7 – 14.0)
6 – 12 months	0.9	2.0	9.1 (6.4 – 13.0)
1 – 2 years	0.8	-	8.8 (6.4 – 12.0)
2 – 6 years	0.8	-	7.1 (5.2 – 11.0)
6 – 12 years	0.9	-	6.5 (4.4 – 9.5)
12 – 18 years	1.0	1.0	6.0 (4.4 – 9.1)
Adult	1.0	1.0	6.0 (4.0 – 9.0)

[a] Data reported as median (10th – 90th percentile)
[b] Premature infants who are small for gestational age may have leukocyte concentrations that are up to 50% lower than those who are appropriate for gestational age[483,531]

The neonatal extravasation rate of IgG is three times faster than the adult extravasation rate as approximated by the transcapillary escape rates (TER) of plasma proteins[34] and the filtration capacity in skeletal muscle.[532] This phenomenon is governed by three factors:

1. "Leaky" organs (e.g., liver and spleen) are proportionally larger in children.[34]

2. Infant organs – particularly skin, muscle and adipose tissues – have dense capillary networks, providing greater surface areas for extravasation to occur.[34,464,467,468]

3. Neonatal lymph flow is two times faster than adult lymph flow as approximated from animal studies.[34,511,513,529,530]

Table 21 demonstrates the ontogeny profile for capillary density that was constructed from five definitive studies in humans representing the body of literature on the topic.[464,467,468,527,528] Similar data is available in animals.[533-535] For reference, the data and derivation are provided in **Appendix B**. In humans, the profile follows a U-shaped function with increasing age such that capillary density is high in the first 6 months after birth but falls as the body develops and then steadily increases until adulthood.

The convective flow terms in the two-pore equation[66] were updated with a surface area scaling factor ($F2$) to reflect that both convection and diffusion across capillary walls should increase in proportion to capillary surface area.

$$J_{vi,org} = F2 \cdot J_{L,org} \cdot \left(1 - \sigma_{L,org}\right) \cdot C_{v,org} + P_{L,org} \cdot SA_{org} \cdot \left(C_{v,org} - \frac{C_{i,org}}{K_{iv}}\right) \cdot \frac{Pe_{L,org}}{e^{Pe_{L,org}} - 1}$$
$$+ F2 \cdot J_{S,org} \cdot \left(1 - \sigma_{S,org}\right) \cdot C_{v,org} + P_{S,org} \cdot SA_{org} \cdot \left(C_{v,org} - \frac{C_{i,org}}{K_{iv}}\right) \cdot \frac{Pe_{S,org}}{e^{Pe_{S,org}} - 1}$$

where $F2 = \frac{SA_{org,child}}{SA_{org,adult}}$

Lymph flow (L) was doubled for preterm infants according to studies in newborn lambs.[34,511,513,529,530] Lymph flow is the key driver of the rate of absorption after IM administration.

The major route of mAb elimination is by cellular uptake and lysosomal degradation. Intracellular binding to the neonatal Fc receptor (FcRn) can protect the drug and prolong the plasma half-life. Animal studies have identified that vascular endothelial cells and hematopoietic cells (more specifically, leukocytes and macrophages) are the two major cell types contributing to cellular uptake and FcRn-mediated salvage.[473,490,536] Therefore, it is important to consider the concentrations of these cell populations in infants as compared to in adults.

The ontogeny of vascular endothelial cell concentration follows the ontogeny of capillary surface area, as previously discussed (Table 21). In a similar pattern, leukocyte cell concentrations – parameterized for the virtual child as a fraction of the adult concentration ($F1$) – are high at birth but decline with age (Table 21).[474,477]

In the base model for large molecules in PK-Sim, the vascular endothelial cell and leukocyte cell spaces are lumped together into one endosomal compartment. For this analysis, the endosomal compartment was split and attributed equally to vascular endothelial and leukocyte cell spaces according to observations from animal knock-out studies which suggest that each cell population contributes equally to mAb uptake and recycling.[473,490,536]

The availability of FcRn for intracellular salvage is a key determinant of plasma half-life. Some preliminary data may suggest lower FcRn concentrations in children, though no definitive argument can yet be made.[34,319,492,493,537] Three studies have examined FcRn expression in neonatal subjects relative to adults.[492,493,537] In rats, RT-PCR revealed a general trend across all organs of low FcRn mRNA expression at birth relative to adults,[492] though the intestine may be an exception.[537]

Physiologically this is plausible because FcRn expression in the intestine is important for the neonatal absorption of maternal IgG when breastfeeding. In humans, Cianga et al. discovered low and heterogeneous expression of FcRn in neonatal carcasses, especially in vascular endothelium.[493]

Volumes of organs of the mononuclear phagocyte system, such as the liver and spleen are of special consideration in relation to whole-body cell uptake rates because they house numerous leukocyte cell populations. The liver and spleen are proportionally larger in infants and this difference may contribute to more extensive cellular uptake of circulating mAbs. Again, these organ volumes for preterm infants are implemented appropriately in PK-Sim by default.

6.3.6 Dynamic Simulation of Growth

IgG-based molecules exhibit long plasma half-lives and the consequence is that even single dose PK trials for these drug products must be extended for weeks at a time. When modeling the PK of these long half-life products in preterm infants, the anatomy and physiology parameters in the model must be considered dynamic, rather than static, as the infants' bodies grow rapidly across the simulation time.

By selecting the "allow aging" option in PK-Sim, organ volume, organ composition, blood flow rate and hematocrit parameters for virtual preterm infants update at discrete intervals according to the data highlighted by Claassen et al.[317] Aging was manually implemented for capillary surface area, lymph flow rate and hematopoietic cell concentrations according to the intervals in Table 21.

In the absence of other data, preterm infants were assumed to possess the same capillary density and hematopoietic cell concentrations as term infants after 1 month of postnatal age.

6.3.7 Sensitivity Analysis

A local sensitivity analysis was performed for parameters relevant to ontogeny to quantify their impact on clearance and volume of distribution. Simulations were run for a mean premature infant (3 days old, 29 weeks gestational age) receiving a single dose of pagibaximab 60 mg/kg IV. Parameters related to ontogeny were varied by ±10% and the resulting percent changes in clearance ($CL = Dose \div AUC$) and volume of distribution at steady state ($V_{SS} = \frac{Dose \times AUMC}{AUC^2}$) were presented as sensitivity coefficients. The sensitivity analysis also directs attention to the parameters that are important to refine when developing a platform pediatric PBPK model and the degree of error that could be expected when those parameters are misinformed.

6.3.8 Pediatric Pharmacokinetics Assessment

The pediatric PK data from literature – both the concentration-time profiles and the calculated PK parameters – were compared to the predictions simulated by the full pediatric PBPK models. Model performance was assessed with a visual predictive check and by calculation of the absolute average fold error around each data point (AAFE), the root mean squared error (RMSE) and the percent of model-predicted plasma concentrations falling within 2-fold, 1.5-fold and 1.33-fold prediction error. Fold error at each datapoint was calculated as the predicted concentration divided by the observed concentration. 2-fold prediction error was defined as the range between 0.5- and 2.0 fold error. 1.5-fold prediction error was defined as the range between 0.667- and 1.5-fold error. Finally, 1.33-fold prediction error was defined as the range between 0.75- and 1.33-fold error.

6.4 Results

6.4.1 Adult PBPK Model Development

High confidence was established in the adult scenario for each drug except for palivizumab before approaching the pediatric scenario. Visual predictive checks for the optimized adult PBPK models revealed close fits with observed concentration-time data from literature (Figure 30).

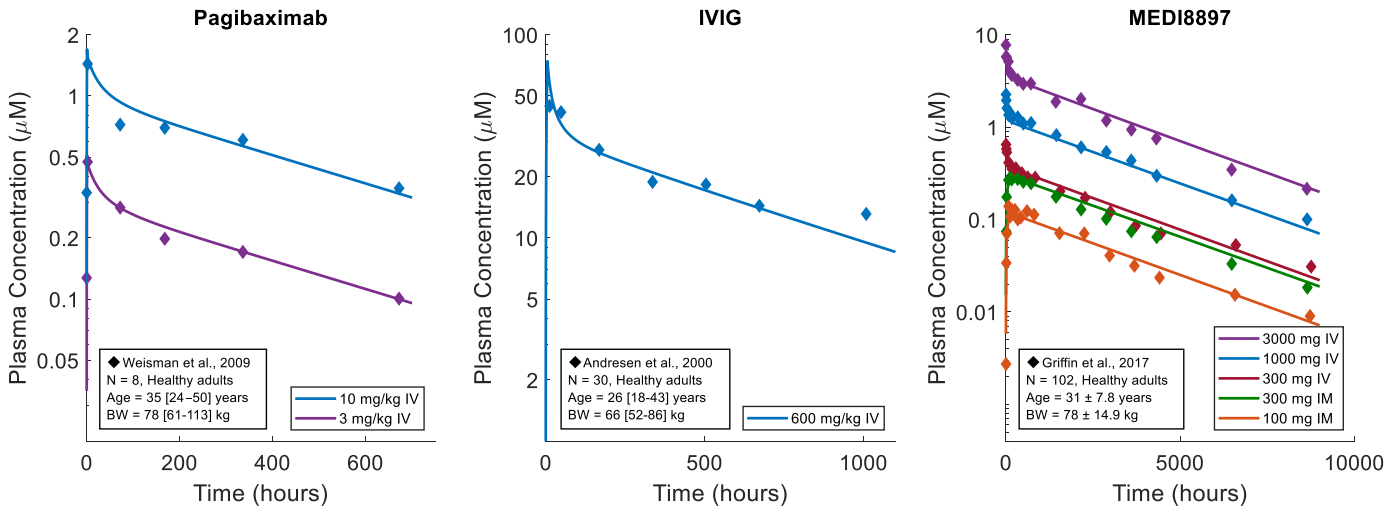

Figure 30. Performance of the final adult PBPK models for representing the observed pharmacokinetic data from literature for three antibody products.[53,521,523]

6.4.2 Sensitivity Analysis

The sensitivity analysis confirmed the importance of the advanced ontogeny parameters for predicting pediatric PK and gave insight into the roles that they play in defining clearance and V_{SS} (Figure 31). In the current structure and under the given assumptions, the sensitivity analysis reveals that high hematopoietic cell concentrations ($F1$) in children may be responsible for the increased clearance in children but have a minimal effect on V_{SS}. The capillary surface area ($F2$) is important for defining both clearance and V_{SS} in children since the parameter speeds extravasation and increases the volume of vascular endothelium available for cellular uptake. A fast lymph flow rate (L) in children mildly decreases V_{SS} due to faster recirculation from the interstitium to the venous blood. This parameter is most important when modeling mAb absorption after intramuscular or subcutaneous administration.

Figure 31. Results of the local sensitivity analysis reported as the percent changes in clearance and volume of distribution that were dictated by ±10% changes in input parameters relevant to ontogeny. $\boldsymbol{F1}$ = hematopoietic cell concentration ontogeny factor, $\boldsymbol{F2}$ = capillary surface area ontogeny factor, $\boldsymbol{L}$ = lymph flow rate, $\boldsymbol{FcRn}$ = free FcRn concentration in endosomal space, $\boldsymbol{V_{Liver}}$ = liver volume, $\boldsymbol{V^{E}_{Total}}$ = whole-body endosomal volume, $\boldsymbol{k_{up}}$= rate of cellular uptake, $\boldsymbol{r_{pore}}$ = capillary pore radius, $\boldsymbol{P}$ = capillary permeability.

Clearance in the pediatric model is most sensitive to the rate of cellular uptake (k_{up}) and there is no information available yet to assess potential differences in this parameter between adults and children. Vascular endothelial cells and leukocytes will be of interest for *in vitro* investigations. A fast rate of cellular uptake in children would increase clearance and vice versa. Interestingly, cellular uptake parameters have some relevance for predicting V_{SS} due to the mechanism where mAbs can be sequestered in endosomal spaces.

The sensitivity analysis also shows that if FcRn concentrations in children were lower than in adults as hypothesized elsewhere[34] – the difference would dictate a moderate increase in clearance.

Capillary pore radius (r_{pore}) and capillary permeability (P) are important contributors to describe extravasation and V_{SS}. Measurements of osmotic and hydrostatic pressures across capillary walls suggest that net capillary permeability in children is only slightly lower than in adults, but increases with age.[34] Conflicting observations are made showing increased permeability of new vessels formed by angiogenesis during wound healing, though the applicability to the developing blood vessels in children may be low.[538] A comprehensive quantitative expression of the ontogeny of capillary permeability is unlikely to be of significant importance for pediatric PK prediction since the effects on extravasation are strongly antagonized by the ontogeny of capillary surface area ($F2$).

Finally, proper parameterizations for the volumes and compositions of centrally vascularized, permeable and hematopoietic cell-bearing organs (such as V_{Liver}) are shown to have some importance for predicting both pediatric clearance and V_{SS}.

6.4.3 Pediatric Pharmacokinetics Assessment

After integration of ontogeny into the final pediatric PBPK models, PK predictions were strong for the four mAbs in premature infants from 1 day to 24 months of age (Figure 32). Across the observed drug concentrations, 93% of the corresponding model-predicted concentrations fell within 2-fold prediction error, 90% fell within 1.5-fold prediction error and 80% fell within 1.33-fold prediction error. This result suggests that many of the key factors related to ontogeny are appropriately addressed. Much of the error was driven by a failure to predict concentrations in the terminal phase of the IVIG profiles. Extravasation was also under-predicted after the first dose for pagibaximab. The rate of IM absorption was well-approximated for MEDI8897 but may be under-estimated for palivizumab.

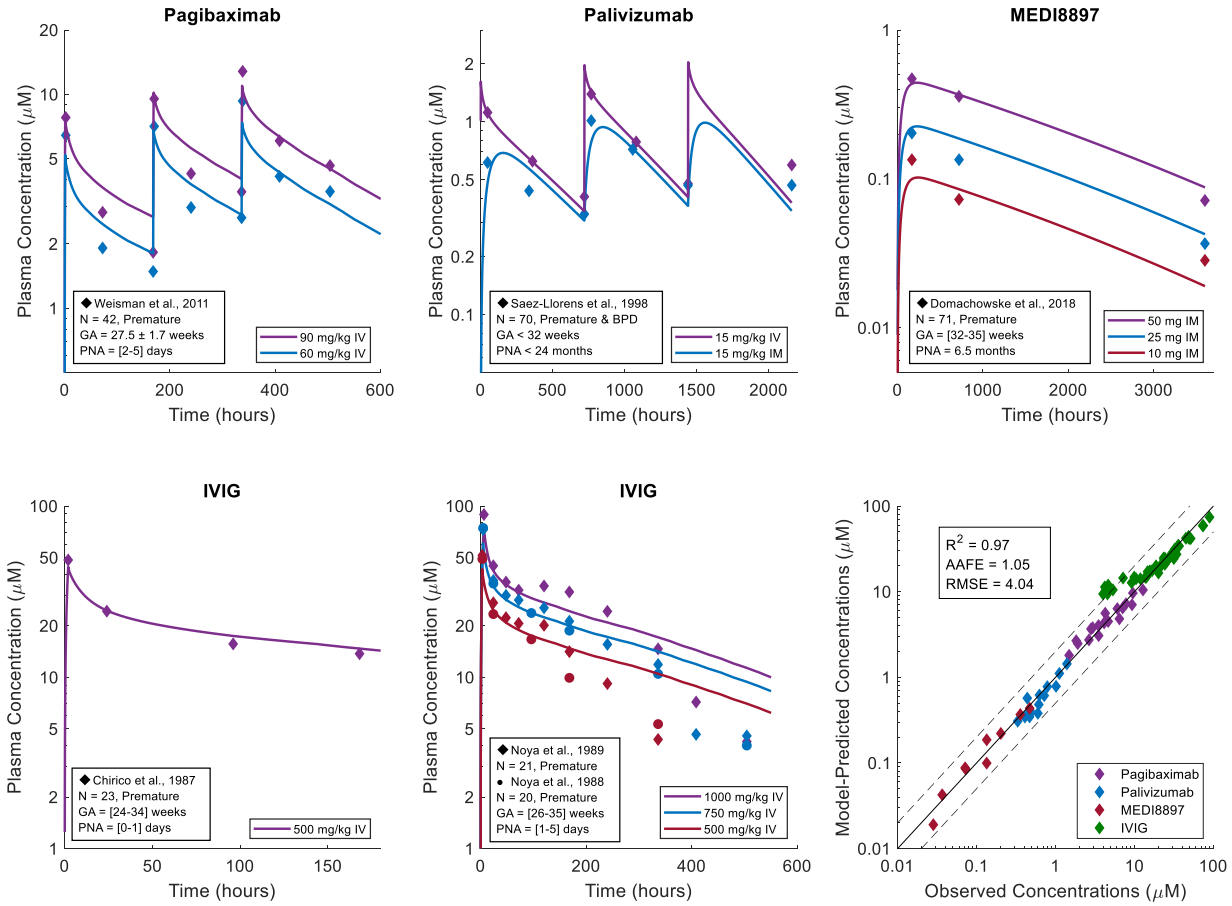

Figure 32. Performance of the final pediatric PBPK models for representing observed pharmacokinetic data from literature for pagibaximab, palivizumab, MEDI8897 and intravenous immunoglobulin (IVIG) in premature infants.[420,424,522,524-526]

Observed data in the terminal phase of the IVIG profiles should be interpreted with caution, as the reported values in the data for exogenous IgG are likely lower than the real values. In the literature, exogenous IgG concentrations are calculated as:

$$[IgG_{exo}] = [IgG_{Total}] - [IgG_{endo}]$$

However, endogenous IgG ($\boldsymbol{IgG_{endo}}$) is only measured at baseline in the first few days after birth. Endogenous IgG is shown to decrease from that point over the first two months of life for preterm infants.[539] The consequence of using the baseline measurement for endogenous IgG in the equation is that the terminal phase data points for exogenous IgG have low confidence and may be significantly under-reported. This phenomenon drives the decreasing predictive performance of the pediatric PBPK model over time for IVIG.

6.5 Discussion

Preterm infants are gaining increased therapeutic attention in drug development for mAbs and IgG products against infectious syndromes of prematurity (e.g. HIV, respiratory syncytial virus, cytomegalovirus, staphylococcal sepsis). The US FDA recently highlighted the need for pediatric PBPK modeling efforts to support drug development and clinical trial design for this vulnerable population, as is commonly done in the context of small molecules.[70] In response, we begin the first whole-body PBPK modeling assessment of mAbs in preterm infants, with pagibaximab, palivizumab, MEDI8897 and IVIG as working examples.

In this work, literature-based ontogeny for organ volumes, organ composition, blood flow rates, hematocrit, hematopoietic cell concentration, capillary surface area and lymph flow rates were integrated into a PBPK model for mAbs in premature infants. The importance of each parameter for determining clearance and V_{SS} was assessed quantitatively with a local sensitivity analysis. Furthermore, attention was drawn to other key parameters that are important to refine in the process of developing a platform PBPK model for mAbs and IgG products in premature infants. With over 90% of model-predicted concentrations falling within 1.5-fold prediction error, we can be confident that many of the important factors related to ontogeny have been appropriately addressed.

For the most part, analyses of the accuracy of PBPK modelling for predicting the PK of small molecule drugs in preterm infants report area-under-the-curve (AUC) and clearance as primary outcomes of interest.[540] However, it is the trough concentrations and the half-life that drive FIP dose selection for mAbs, especially those targeted against infectious antigens.[420,424,522] For these products, clinicians seek a dosing regimen that sustains a trough concentration above a target value. In doing

so, the patient achieves stronger immunity against the infectious antigen (RSV, HIV, bacterial antigens, etc.). Nevertheless, reporting the prediction error around AUC and clearance was not possible in this work because the observed values were rarely reported in the clinical studies and a manual non-compartmental analysis would be highly inaccurate with only three data points available for calculation.

This work also serves as an update on the state-of-the-art understanding of pediatric physiology in relation to mAb PK.[34] We refine this content with a quantitative presentation of the ontogeny of capillary surface area derived from five definitive studies.[464,467,468,527,528] Furthermore, knock-out animal studies[473,490,536] and recent PBPK models for FcRn inhibitors[541] highlight the important role that cells of hematopoietic origin may play in the cellular uptake, FcRn-mediated salvage and elimination of mAbs. The effects of a high concentration of hematopoietic cells at birth have been incorporated into the pediatric PBPK model for mAbs and characterized with a sensitivity analysis, showing that this parameter drives clearance but not V_{SS}.

The ontogenies of FcRn expression and endogenous IgG concentrations have yet to be addressed. They both moderate the availability of the free FcRn parameter. Previous minimal PBPK modeling work by Hardiansyah and Ng fully attributed the unique elimination profile of mAbs in children to altered FcRn expression.[319] However, similar patterns of pediatric exposure are observed for other protein-based drugs that do not bind to FcRn, such as erythropoietin stimulating agents and coagulation factor concentrates.[392-396] This observation suggests that the mechanisms responsible for fast elimination of mAbs in children are *not* attributable to FcRn ontogeny alone, or perhaps even at all. Here we uncover the impacts of ontogeny in foundational physiological parameters before considering the ontogeny of FcRn expression, which bears a high degree of uncertainty.

The conventional approach for using PBPK modeling to make a PK prediction in pediatric patients involves first evaluating the foundational model structure and parameters in adults before scaling select parameters to represent pediatrics according to known physiology.[387] For large molecules administered to patients in whom there is no ligand present, the drug-specific parameters are actually quite simplistic and a prediction of pediatric PK could be made without evaluating the parameters in the adult population first. For IVIG and palivizumab, no optimization or learning was performed at the adult modelling step. Unexpectedly, the a priori pediatric predictions are strong for palivizumab.

There are opportunities for further refinement of the parameterization. The capillary surface area ontogeny factor ($F2$) in the model is applied in the same way to every organ in the absence of organ-

specific data. The measurements from literature come from the abdominal peritoneum, buccal mucosa, skin, muscle and nail folds,[464,467,468,527,528] but are generalized to the central organs as well. Organ-specific estimates for the ontogeny of capillary surface area could be obtained from future animal studies.

Furthermore, the base model for large molecules and therapeutic proteins in PK-Sim does not explicitly include a hematopoietic cell compartment in addition to a vascular endothelial cell compartment, such as in the models put forward by Li and Balthasar[541] or Aborig et al.[542] Instead, the impacts of cellular uptake by vascular endothelial cells and hematopoietic cells are lumped together into one endosomal compartment. To correctly account for the ontogeny of this cell population we have split the relative contributions to cellular uptake equally between vascular endothelium and hematopoietic cells in the absence of specific data, though this fraction may vary among specific organs (e.g. spleen[542]).

While it is yet to be explored, PBPK modeling may even offer adequate pediatric PK predictions for molecules that are subject to target-mediated drug disposition and nonlinear elimination. As already mentioned, children and especially premature infants typically achieve much lower plasma exposures to biologic drugs than adults with the same mg/kg doses.[80] Since a PBPK model accounts for target-binding and nonlinear elimination mechanistically, such an approach would theoretically be able to classify when the drug would enter the linear clearance range in children.

At present, the PBPK modeling approach to pediatric PK assessment is limited by its inability to characterize or predict the variability in the PK data. In adults, population PBPK modeling has been proposed, which attributes overall PK variability to inter-subject variability in key physiological input parameters.[68] This approach enables a reproduction of the observed PK variability in clinical trials when simulations are conducted iteratively with parameter sets representing many virtual individuals as inputs.[68] The inter-subject variabilities in key parameters related to ontogeny and the correlations between them in children are not yet known for large molecules, but may be the subject of future research.

All models were constructed in the open-source software, PK-Sim and Mobi v8.0, enabling drug developers and academics to easily access and apply this parameterization. The parameterizations for full term infants and young children (1-4 years) were not evaluated explicitly in this work since limited or no data was available in literature for objective evaluation. Therefore, caution should be shown if used for pediatric PK prediction in these populations.

6.6 Conclusion

Overall, this work describes a literature-based integration of ontogeny into a PBPK model for mAbs in premature neonates coupled with a comprehensive assessment of the role that each parameter may play in the prediction of clearance and volume of distribution at steady state. It sets the stage for the development of a platform pediatric PBPK model by solidifying parameterizations for organ volumes, organ composition, blood flow rates and hematocrit, deriving parameterizations for hematopoietic cell concentration, capillary surface area and lymph flow, and drawing attention to unmet needs for physiologic knowledge in children.

6.7 Study Highlights

This manuscript integrates the ontogeny factors discovered in the literature review (Chapter 5) within a PBPK modeling framework to extrapolate monoclonal antibody pharmacokinetics from adults all the way down to preterm infants. This extrapolation was performed with the best knowledge that was available at that time (2019) to parameterize the PBPK model structure and the ontogeny profiles of relevant physiological factors in very young children. Assumptions about the role of hematopoietic cells in the pharmacokinetics of antibodies are investigated in the following chapter (Chapter 7).

Chapter 7

Model-Based Assessment of the Contribution of Hematopoietic Cells to the Pharmacokinetics of Monoclonal Antibodies

7.1 Abstract

The role of hematopoietic cells and in particular, monocytes and macrophages in the pharmacokinetics of monoclonal antibodies (mAbs) is currently not well understood. Uptake of mAbs into hematopoietic cells is of potential importance for anticipating the changes in pharmacokinetics that may occur when hematopoietic cells are present in relatively high concentrations in special populations, such as in children. A complicating factor is that children may also have lower availability of the neonatal Fc receptor (FcRn) for mAb protection. In this work, a minimal physiologically-based pharmacokinetic (PBPK) model is used to characterize mAb uptake into hematopoietic cells and associated FcRn-mediated recycling in the context of site-specific FcRn deletion and variable endogenous and exogenous IgG levels using data from mice. The model unifies experimental data from three studies in unique mouse models with site-specific FcRn deletion in macrophages or endothelial cells together with clodronate liposomes to achieve macrophage knockdown. The final model was verified by testing its predictive performance against experimental data describing the interaction between therapeutic mAb, endogenous IgG, high-dose exogenous IgG and FcRn in mice. A sensitivity analysis revealed the plasma AUC was highly sensitive to endothelial cell parameters, but had near-nil sensitivity to macrophage parameters, even in the scenario with 90% FcRn depletion. Overall, the model confirms the assertion that macrophages are indispensable for IgG homeostasis. In this regard, macrophages serve as highly efficient protectors of IgG in plasma, interstitial fluid and lymph. They are not, as previously thought, sinks for mAb degradation. In mice with normal FcRn expression, model simulations suggest that less than 2% of an intravenously administered dose is eliminated in macrophages, while endothelial cells are predicted to dominate mAb elimination. We conclude that it is very unlikely that a high concentration of circulating monocytes can contribute to explaining the fast weight-based clearance of mAbs in very young children, even if FcRn were depleted up to 90%.

7.2 Introduction

It is well known that Immunoglobulin G (IgG) and its therapeutic derivatives, termed monoclonal antibodies (mAbs) have long plasma residence times in the body spanning weeks to months.[2] The major route of elimination is by cellular uptake and subsequent endosomal catabolism.[2] Two major cell populations have been identified to be responsible for this uptake based on proximity to plasma and innate pinocytic or phagocytic activity – (1) vascular endothelial cells and (2) hematopoietic cells.[473] Fighting to protect IgG from catabolism in these cells is the neonatal Fc receptor (FcRn), a salvage protein that binds to IgG in the acidic conditions of endosomes and recycles back to the extracellular surface.[2] In the body, vascular endothelial cells make up the capillary walls and therefore have extensive access to mAb in plasma. Hematopoietic cells are present in plasma (e.g., monocytes), and are also located throughout the extravascular space and the lymph nodes.[479]

In 2018, data was presented from Richter et al. highlighting the contribution of hematopoietic cell uptake and FcRn-mediated recycling to mAb disposition in mice with site-specific FcRn knockouts.[479,536] The original conclusions from the work were that:

1. Hematopoietic cells and endothelial cells contribute about equally to the FcRn-mediated protection of mAbs
2. Hematopoietic cells and endothelial cells contribute about equally to the clearance of mAbs
3. Clearance of mAbs by endothelial cells occurs predominantly from plasma, while clearance of mAbs by hematopoietic cells occurs predominantly in the extravascular space
4. After extravascular administration, pre-systemic elimination or ‘first pass catabolism’ of mAbs occurs in hematopoietic cells

Based on these observations, our group hypothesized in 2019 that a higher concentration of circulating hematopoietic cells in very young children may explain in part why children have faster weight-based clearance of mAbs than adults.[65] It was revealed later in 2019 by Challa et al. that it was a specific hematopoietic cell subtype – the macrophages – that were predominantly responsible for the Fc-mediated recycling of mAbs.[490] Therefore our hypothesis evolved to consider that a higher concentration of monocytes (the circulating phagocytes) in children may contribute to this faster weight-based clearance. Indeed, monocytes are present at three to five times higher concentrations in infant blood when compared to adult blood, while tissue-resident macrophages are known to remain

largely constant in their abundance and activity throughout infancy to adulthood, even from the fetal stage.[478,480,543]

Complicating factors are the degree of FcRn expression and the circulating concentrations of endogenous IgG that may compete with therapeutic mAb for FcRn-mediated protection. With very limited evidence, it has been hypothesized that children may have lower FcRn concentrations in vascular endothelial and/or hematopoietic cells, which implies poor protection of mAbs *in vivo* and fast clearance.[34,63,492,493] The available FcRn is potentially further compromised by high concentrations of circulating IgG in the three months after birth from maternal sources.[34] Therefore it becomes of importance to understand the quaternary quantitative relationship between monocyte and macrophage concentrations, FcRn expression, endogenous IgG concentrations and mAb clearance.

In the presented work, a mechanistic model is developed using data from mice that characterizes mAb uptake into hematopoietic cells and associated FcRn-mediated recycling in the context of site-specific FcRn deletion and variable endogenous and exogenous IgG levels. The overall aim is to provide evidence towards accepting or rejecting the hypothesis that high concentrations of blood monocytes may contribute to the observed faster weight-normalized clearance of mAbs in young children.

7.3 Methods

7.3.1 Software

PBPK modeling was performed in MATLAB R2020a (Mathworks, Natick, MA) using the extension IQM Tools v1.2.2.2 by Henning Schmidt (Intiquan, www.intiquan.com). All datasets were digitized from literature using PlotDigitizer v2.6.8 by Joseph Huwaldt (plotdigitizer.sourceforge.net). Anatomical parameter values for a mouse were extracted from PKSim v9.1 (www.open-systems-pharmacology.org).

7.3.2 Pharmacokinetic Data

The first dataset for model building was from Garg et al.[91] In these experiments, C57BL/6J wild-type and global FcRn-knockout mice (GKO) were administered 8 mg/kg of mAb 7E3 by intravenous injection. Elimination of 7E3 was dramatically faster in GKO mice compared to controls. In an additional experiment, 7E3 was co-administered with 1 g/kg intravenous immunoglobulin (IVIG) to partially saturate FcRn, and elimination was moderately increased. This data was reserved for model

verification as it reflects the complex interplay between therapeutic mAb, endogenous IgG, exogenous IgG and FcRn.

The second dataset for model building was from Challa et al.[490] There were three populations of mice to consider: C57BL/6J wild-type mice, GKO mice, and macrophage-specific FcRn knockout mice (MKO). Mice were administered 10-15 μg of ^{125}I-labelled mAb D1.3 and whole-body radioactivity was measured at specific time points using an Atom Lab 100 dose calibrator. GKO mice exhibited the shortest whole-body mAb half-life (35.5 hours), followed by MKO (41.9 hours) mice and then wild-type mice (247.6 hours). In another set of experiments, macrophages in wild-type and GKO mice were knocked down by two 1.5 mg doses of clodronate liposomes injected 18 hours before and 30 hours after mAb administration. In wild-type mice, macrophage knockdown with clodronate did not significantly impact the whole-body mAb half-life. In GKO mice, however, macrophage knockdown increased the whole body mAb half-life (54 vs. 39 hours). Mice with endothelial-specific FcRn knockout were not successfully validated and so that data was excluded from this analysis. However, fast elimination was also observed in that mouse model.

The final dataset for model building was synthesized from experiments by Akilesh et al. and was digitized from the manuscript by Richter et al.[479,536] In these experiments, C57BL/6J wild-type mice and GKO mice were administered 4 mg/kg of mAb 1B7 by intraperitoneal injection. In addition, MKO mice were generated by subjecting C57BL/6 wild-type mice to high doses of radiation and then replacing hematopoietic cells with a bone marrow transplant from GKO mice. In similar fashion, endothelial-specific FcRn knockout mice (EKO) were generated by subjecting GKO mice to high doses of radiation and then replacing hematopoietic cells with a bone marrow transplant from C57BL/6 wild-type mice. Total exposures were highest in wild-type control mice, followed by EKO mice, MKO mice and then GKO mice.

7.3.3 Minimal PBPK Model Development

A minimal PBPK model is defined as one in which the whole body and its physiological mechanisms of drug disposition are simplified into one lumped organ compartment to test elementary pharmacokinetic hypotheses. For this model, whole body volume parameters for plasma, interstitial space and endothelial endosomes were extracted from PK-Sim v9.1 for a virtual mouse with 21 g body weight (V^P, V^{IS}, V^E). In the proposed physiological structure (Figure 33), mAb is deposited in the plasma space after intravenous administration. Lymph flow (L) drives convective transport across the vascular wall into the interstitial space, with resistance to flow through pores modeled by a

vascular reflection coefficient (σ^V). From the interstitial space, mAb may be returned by lymph flow back to the plasma space. Uptake into endothelial cells occurs from plasma (CL_{up}). Uptake into circulating macrophages and Kupffer cells occurs from plasma, and uptake into tissue-resident macrophages occurs from interstitial space (P_{up}). Within endosomes, unbound mAb is subject to degradation (CL_{spec}, P_{spec}). However, mAb that binds to the neonatal salvage receptor ($FcRn$) may be recycled back to the extracellular space (CL_{up}, P_{up}). Intracellular binding to FcRn was represented with first order binding rates determined from *in vitro* studies (k_{on}, k_{off}) and evaluated by Niederalt et al.[66] One FcRn concentration (nmol/L endosome) was applied consistently for endosomal spaces, regardless of cellular origin.[91,544] Full notation of the states, variables and parameters are presented in Table 22 with model equations following.

The volumes of three major macrophage populations were derived from literature: circulating hematopoietic macrophages (monocytes) (V_{circ}^M), Kupffer cells lining sinusoids in the liver ($V_{kupffer}^M$) and other tissue-resident macrophages (V_{tissue}^M), such as splenic red pulp macrophages, alveolar macrophages in the lung and Langerhans cells in the pancreas.[545] Monocytes are the dominant macrophage cell population in blood and make up approximately 2% of the murine white blood cell count.[545-549] As such, the circulating macrophage volume was calculated based on a murine white blood cell count of 9000 cells/µL and employing a 20 µm spherical radius for monocytes.[548] Kupffer cells make up 10-16% of cells in the murine liver and are largely derived from circulating monocytes.[543,549-551] With challenges due to their irregular shape, Kupffer cell volume was assumed to be the same as that calculated for the monocyte parent. The total Kupffer cell volume in mouse was then calculated based on the cellularity of 135 million cells per gram liver tissue.[552] Tissue-resident macrophage volume was fixed at 2% of non-blood volume according to a previous derivation by Aborig & Malik et al.[542,553] The endosomal fraction (f_{endo}) of 0.2 was assigned the same for macrophages as for endothelial cells.[66]

Intraperitoneal administration was described by adding a local injection site compartment and allowing mAb to enter the plasma compartment by a first order absorption rate constant (k_a). This process represents the flow of lymph from the local site to the interface of the thoracic duct with the subclavian vein. In transit, mAb is subject to pre-systemic elimination. In FcRn transgenic mice, Richter et al. observe that EKO mice have similar bioavailability to wild-type mice, but that MKO and GKO mice have marked lower bioavailability.[479] The exact intraperitoneal bioavailability of 1B7

in the wild-type (F_{WT}^{IP}) and macrophage knockout (F_{MKO}^{IP}) scenarios could not be calculated as there was no intravenous data for comparison.

Endogenous IgG is present in parallel within the system and competes with therapeutic mAb for binding to FcRn. Each model run requires a baseline phase (0-500 hours) that allows endogenous IgG levels in the body to acclimate to steady state, and then a dosing phase, where therapeutic mAb is administered. Endogenous IgG levels in plasma of C57BL/6J mice and various knockout mice were used for each experiment as measured by Challa et al.[490]

In this "middle-out" approach, nine parameters were optimized using a simulated annealing temperature-based global optimization method ($CL_{up}, CL_{spec}, P_{up}, P_{spec}, L, \sigma^V, k_a, F_{WT}^{IP}, F_{MKO}^{IP}$). Ten optimizations were run from randomized start values within physiologically relevant parameter bounds to assess identifiability of a unique solution. To absolve potential correlations between uptake and degradation, the endosomal degradation rates were optimized using a scaling factor multiplied by the uptake rate ($CL_{spec} = CL_{spec}^{factor} \times CL_{up}$, $P_{spec} = P_{spec}^{factor} \times P_{up}$). In the beginning of the optimization process, it was found that three constants trended to solutions that were lower than those physiological plausible (σ^V, F_{WT}^{IP}, F_{MKO}^{IP}). Therefore, they were fixed to the lower limit of physiological plausibility and the remaining six parameters were optimized freely.

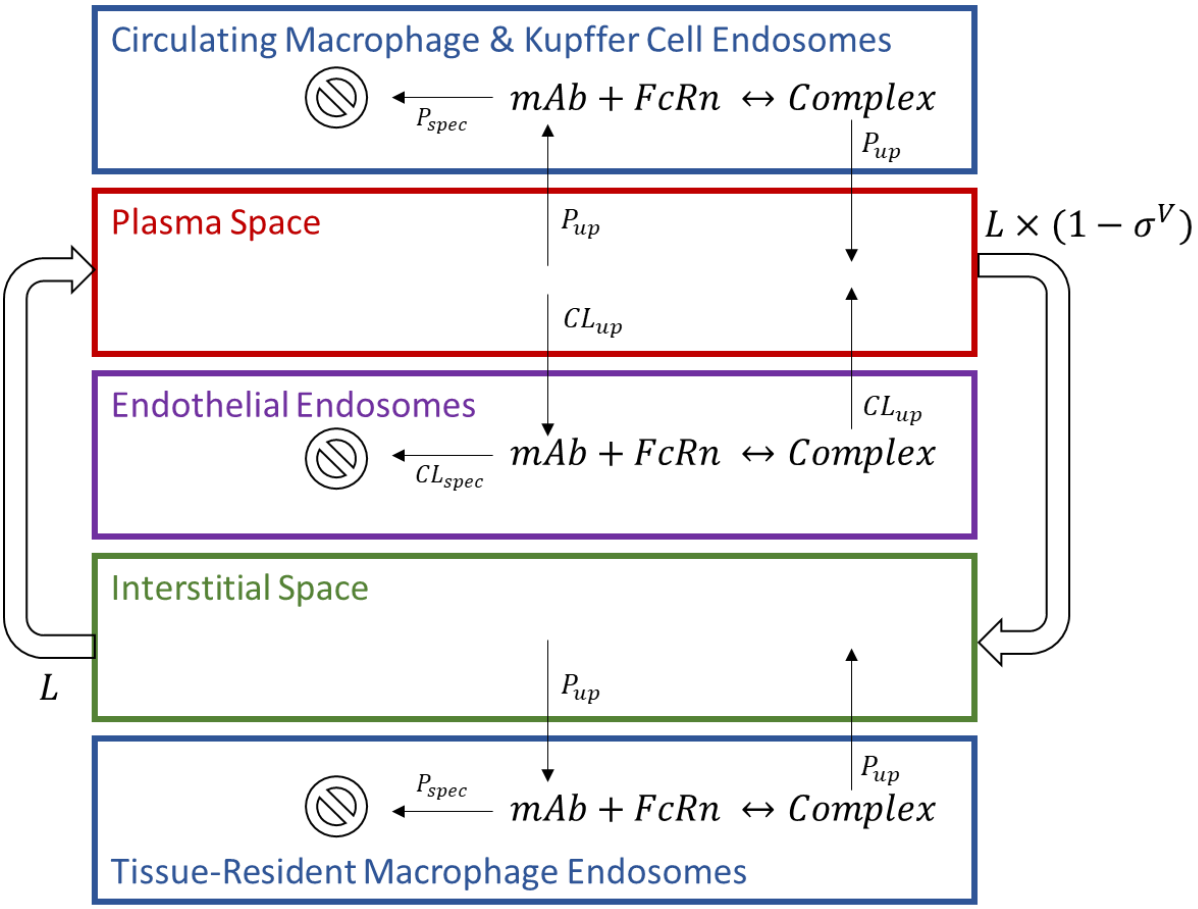

Figure 33. Minimal PBPK model structure

Table 22. State and parameter notation for the minimal PBPK model

Term	Units	Definition
States		
C^P	pmol/mL	Concentration of mAb in plasma space
C^E	pmol/mL	Concentration of unbound mAb in endothelial endosomes
$C^{E:Bound}$	pmol/mL	Concentration of FcRn-bound mAb in endothelial endosomes
C^{IS}	pmol/mL	Concentration of mAb in interstitial space
C_i^M	pmol/mL	Concentration of unbound mAb in macrophage endosomes (i = circulating. Kupffer or tissue)
$C_i^{M:Bound}$	pmol/mL	Concentration of FcRn-bound mAb in macrophage endosomes (i = circulating, Kupffer or tissue)
$FcRn^E$	pmol/mL	State for the negative value of mAb-FcRn complex concentration in endothelial endosomes
$FcRn_i^M$	pmol/mL	State for the negative value of mAb-FcRn complex concentration in macrophage endosomes (i = circulating, Kupffer or tissue)
Parameters		
L	mL/h	Organ lymph flow
σ^V	-	Vascular reflection coefficient
V^P	mL	Volume of plasma space
V^E	mL	Volume of endothelial endosomes
V^{IS}	mL	Volume of interstitial space
V_i^M	mL	Volume of macrophage endosomes (i = circulating, Kupffer or tissue)
CL_{up}	mL/h/mL	Rate of pinocytosis and exocytosis per mL of endothelial endosomes
CL_{spec}	mL/h/mL	Rate of degradation in endothelial endosomes
P_{up}	mL/h/mL	Rate of phagocytosis and exocytosis per mL of macrophage endosomes
P_{spec}	mL/h/mL	Rate of degradation in macrophage endosomes
$FcRn$	pmol/mL	Maximum concentration of the neonatal Fc receptor in endosomes (constant)
k_{on}^{FcRn}	mL/pmol/h	Association rate constant for mAb binding to FcRn
k_{off}^{FcRn}	h^{-1}	Dissociation rate constant for mAb binding to FcRn
K_D^{FcRn}	pmol/mL	Equilibrium dissociation constant for mAb binding to FcRn
F_{WT}^{IP}	-	Bioavailabilty of D1.3 from intraperitoneal space in WT and EKO mice
F_{MKO}^{IP}	-	Bioavailability of D1.3 from intraperitoneal space in MKO and GKO mice
k_a	h^{-1}	Absorption rate constant from intraperitoneal space

Plasma

Equation Set 7.1: Amount of mAb in Plasma

$$V^P \times \frac{dC^P}{dt} = -(1-\sigma^V) \times L \times C^P + L \times C^{IS} - P_{up} \times V_{circ}^M \times C^P + P_{up} \times V_{circ}^M \times C_{circ}^{M:Bound}$$

$$- P_{up} \times V_{kupffer}^M \times C^P + P_{up} \times V_{kupffer}^M \times C_{kupffer}^{M:Bound} + A^{IP} \times k_a$$

$$C^P(0) = \frac{Dose^{IV}}{V^P}$$

Circulating Macrophage Endosomes

Equation Set 7.2: Concentration of mAb and FcRn in Circulating Macrophage Endosomes

$$\frac{dC_{circ}^M}{dt} = P_{up} \times C^P - k_{on}^{FcRn} \times C_{circ}^M \times \left(FcRn_{circ}^M + FcRn\right) + k_{off}^{FcRn} \times C_{circ}^{M:Bound} - P_{spec} \times C_{circ}^M$$

$$\frac{dC_{circ}^{M:Bound}}{dt} = k_{on}^{FcRn} \times C_{circ}^M \times \left(FcRn_{circ}^M + FcRn\right) - k_{off}^{FcRn} \times C_{circ}^{M:Bound} - P_{up} \times C_{circ}^{M:Bound}$$

$$\frac{dFcRn_{circ}^M}{dt} = -k_{on}^{FcRn} \times C_{circ}^M \times \left(FcRn_{circ}^M + FcRn\right) + k_{off}^{FcRn} \times C_{circ}^{M:Bound} + P_{up} \times C_{circ}^{M:Bound}$$

Endothelial Endosomes

Equation Set 7.3: Concentration of mAb and FcRn in Endothelial Endosomes

$$\frac{dC^E}{dt} = CL_{up} \times C^P - k_{on}^{FcRn} \times C^E \times (FcRn^E + FcRn) + k_{off}^{FcRn} \times C^{E:Bound} - CL_{spec} \times C^E$$

$$\frac{dC^{E:Bound}}{dt} = k_{on}^{FcRn} \times C^E \times (FcRn^E + FcRn) - k_{off}^{FcRn} \times C^{E:Bound} - CL_{up} \times C^{E:Bound}$$

$$\frac{dFcRn^E}{dt} = -k_{on}^{FcRn} \times C^E \times (FcRn^E + FcRn) + k_{off}^{FcRn} \times C^{E:Bound} + CL_{up} \times C^{E:Bound}$$

Interstitial Space

Equation Set 7.4: Amount of mAb in Interstitial Space

$$V^{IS} \times \frac{dC^{IS}}{dt} = (1 - \sigma^{V}) \times L \times C^{P} - L \times C^{IS} - P_{up} \times V_{tissue}^{M} \times C^{IS} + P_{up} \times V_{tissue}^{M} \times C_{tissue}^{M:Bound}$$

Tissue-Resident Macrophage Endosomes

Equation Set 7.5: Concentration of mAb and FcRn in Tissue-Resident Macrophage Endosomes

$$\frac{dC_{tissue}^{M}}{dt} = P_{up} \times C^{IS} - k_{on}^{FcRn} \times C_{tissue}^{M} \times \left(FcRn_{tissue}^{M} + FcRn\right) + k_{off}^{FcRn} \times C_{tissue}^{M:Bound} - P_{spec} \times C_{tissue}^{M}$$

$$\frac{dC_{tissue}^{M:Bound}}{dt} = k_{on}^{FcRn} \times C_{tissue}^{M} \times \left(FcRn_{tissue}^{M} + FcRn\right) - k_{off}^{FcRn} \times C_{tissue}^{M:Bound} - P_{up} \times C_{tissue}^{M:Bound}$$

$$\frac{dFcRn_{tissue}^{M}}{dt} = -k_{on}^{FcRn} \times C_{tissue}^{M} \times \left(FcRn_{tissue}^{M} + FcRn\right) + k_{off}^{FcRn} \times C_{tissue}^{M:Bound} + P_{up} \times C_{tissue}^{M:Bound}$$

Kupffer Cell Endosomes

Equation Set 7.6: Concentration of mAb and FcRn in Kupffer Cell Endosomes

$$\frac{dC_{kupffer}^{M}}{dt} = P_{up} \times C^{P} - k_{on}^{FcRn} \times C_{kupffer}^{M} \times \left(FcRn_{kupffer}^{M} + FcRn\right) + k_{off}^{FcRn} \times C_{kupffer}^{M:Bound} - P_{spec} \times C_{kupffer}^{M}$$

$$\frac{dC_{kupffer}^{M:Bound}}{dt} = k_{on}^{FcRn} \times C_{kupffer}^{M} \times \left(FcRn_{kupffer}^{M} + FcRn\right) - k_{off}^{FcRn} \times C_{kupffer}^{M:Bound} - P_{up} \times C_{kupffer}^{M:Bound}$$

$$\frac{dFcRn_{kupffer}^{M}}{dt} = -k_{on}^{FcRn} \times C_{kupffer}^{M} \times \left(FcRn_{kupffer}^{M} + FcRn\right) + k_{off}^{FcRn} \times C_{kupffer}^{M:Bound} + P_{up} \times C_{kupffer}^{M:Bound}$$

Intraperitoneal Injection Site

Equation Set 7.7: Amount of mAb in the Intraperitoneal Injection Site (i = wild-type or MKO)

$$\frac{dA^{IP}}{dt} = -A^{IP} \times k_a$$

$$A^{IP}(0) = Dose^{IP} \times F_{IP}^{i}$$

7.3.4 Minimal PBPK Model Verification

The final model was verified by evaluating its predictive performance against the dataset from Garg et al. that was not used during the model building process.[91] In this scenario, mAb 7E3 was administered intravenously at 8 mg/kg to C57BL/6J mice along with high dose IVIG (1 g/kg). Strong performance in this scenario reflects appropriate characterization of the complex interplay between therapeutic mAb, endogenous IgG, exogenous IgG and FcRn *in vivo*.

7.3.5 Model Projections

Simulations were conducted to refine the overall understanding on the contribution of hematopoietic cell uptake and FcRn-mediated recycling to mAb pharmacokinetics. The original conclusions postulated by Richter et al. were tested by simulating the amount cleared by each of the cell populations over time in wild-type and GKO mice.[479]

7.3.6 Sensitivity Analysis

A one-at-a-time (OAT) sensitivity analysis was conducted with the final model to quantify the contribution of the three macrophage cell populations (circulating monocytes, Kupffer cells and tissue-resident macrophages) to the clearance of mAbs in mice. Separate sensitivity analyses were conducted for the wild-type model and for adaptations featuring 50% FcRn depletion and 90% FcRn depletion to anticipate the effects if FcRn were partially or near-fully depleted in children. Parameters hypothesized to have relevance to the ontogeny of mAb pharmacokinetics were varied individually by +50% and –50% of the nominal value and the resulting percent changes in the area-under-the-curve of the plasma concentration-time profile ($AUC_{0\text{-}500h}$) were reported as sensitivity coefficients (S_p^{50}).

$$S_p^{50} = \frac{AUC(p \pm 0.5 \times p) - AUC(p)}{AUC(p)} \times 100$$

To explore if monocyte blood concentration may be a plausible explanation to the observed faster weight-normalized clearance of mAbs in young children, the monocyte volume in blood (V_{circ}^{M}) was increased 5-fold and compared against the nominal profile.

7.4 Results

7.4.1 Minimal PBPK Model Development

A minimal PBPK model was developed that describes mAb extravasation, flow via lymph, uptake into endothelial cells, uptake into macrophages, salvage through binding to FcRn and competition with endogenous IgG for FcRn in a series of wild-type of site-specific FcRn knockout mouse models. The final model fit is presented in Figure 34 and the final parameterization is presented in Table 23. The coefficients of variation on estimated parameters among solutions from multiple optimizations with randomized start values were less than 0.2%, confirming that the solution is uniquely identifiable (Figure 35). The fit analysis is presented in Figure 36. Fold error at every data point was calculated as the predicted value divided by the observed value. The absolute average fold error across all datapoints was 1.00 and 90.3% of points fell within the 1.5-fold error boundaries (0.667 – 1.5-fold error).

The model fit was poor only when characterizing the plasma profile of GKO mice from Garg et al.[91] However the fit to this dataset must be balanced against the mild under-fitting of the GKO profiles in the other two datasets.[479,490,536] Indeed this analysis assumes that all three of the studied mAbs (7E3, D1.3 and 1B7) have the same cellular uptake rates, but there is notable heterogeneity in cellular uptake among other mAbs that may explain the interstudy variation in observed data for GKO mice.[554] The subgroup analysis by experiment type confirms that the error in the GKO datasets is balanced across the median fold-error of 1, with the Garg et al. dataset being over-estimated and the rest being modestly under-estimated (Figure 36).

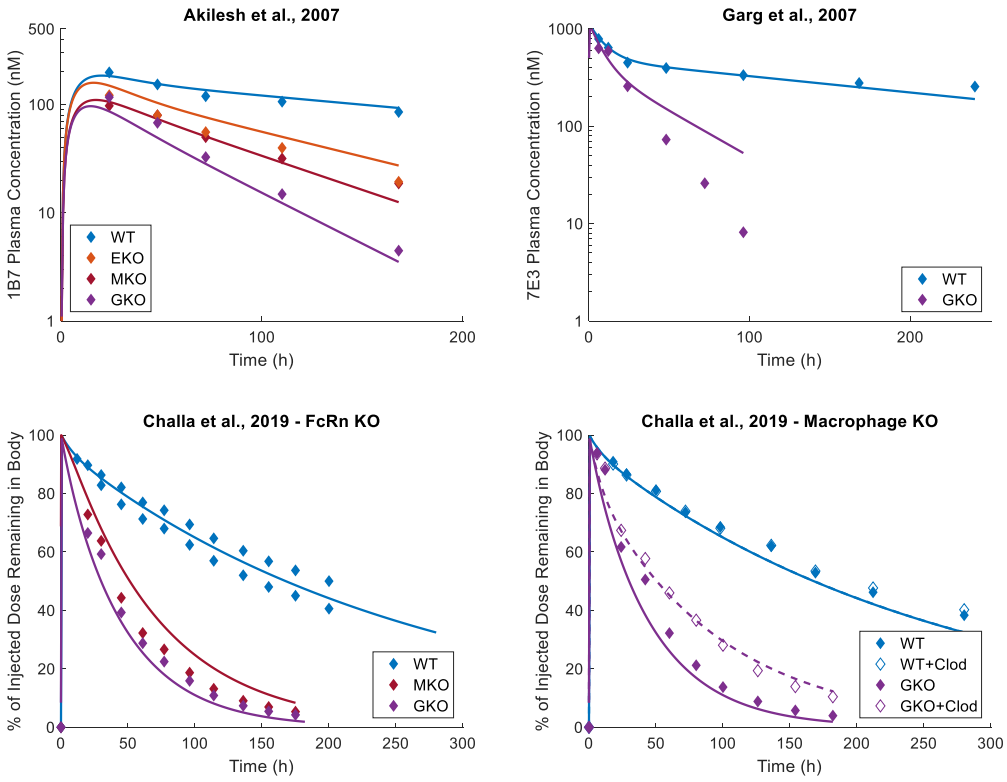

Figure 34. Fitted model performance against observed data in various FcRn knockout mice (WT, EKO, MKO, GKO) and macrophage knockdown scenarios (WT+Clod, GKO+Clod). WT = wild-type control mice, EKO = endothelial-specific FcRn knoc006Bout mice, MKO = macrophage-specific FcRn knockout mice, GKO = global FcRn knockout mice, Clod = co-administration of clodronate liposomes to knock down macrophages. Observed data presented from Akilesh et al.,[479,536] Garg et al.,[91] and Challa et al.[490]

Table 23. Final parameter values for the minimal PBPK model

Term	Units	Value (estimation CV%)	Reference
Fixed Parameters			
V^P	mL	0.99	Niederalt et al.[66]
V^E	mL	0.0051	Niederalt et al.[66]
V^{IS}	mL	3.165	Niederalt et al.[66]
V^M_{circ}	mL	0.00028	Derived
$V^M_{kupffer}$	mL	0.0176	Derived
V^M_{tissue}	mL	0.08	Derived
k^{FcRn}_{on}	mL/pmol/h	0.0522	Niederalt et al.[66]
K^{FcRn}_D	pmol/mL	750	Niederalt et al.[66]
σ^V	-	0.65	Fixed during estimation
F^{IP}_{WT}	-	0.70	Fixed during estimation
F^{IP}_{MKO}	-	0.45	Fixed during estimation
$FcRn$	pmol/mL	33000	Garg et al.,[91] Li et al.[544]
Serum IgG in WT mice	pmol/mL	8600	Challa et al.[490]
Serum IgG in EKO mice	pmol/mL	3600	Challa et al.[490]
Serum IgG in MKO mice	pmol/mL	3200	Challa et al.[490]
Serum IgG in GKO mice	pmol/mL	850	Challa et al.[490]
Optimized Parameters			
CL_{up}	mL/h/mL	5.05 (0.02%)	-
CL_{spec}	mL/h/mL	79.7 (0.07%)	-
P_{up}	mL/h/mL	0.480 (0.015%)	-
P_{spec}	mL/h/mL	0.150 (0.18%)	-
L	mL/h	0.152 (0.04%)	-
k_a	h^{-1}	0.0788 (0.12%)	-

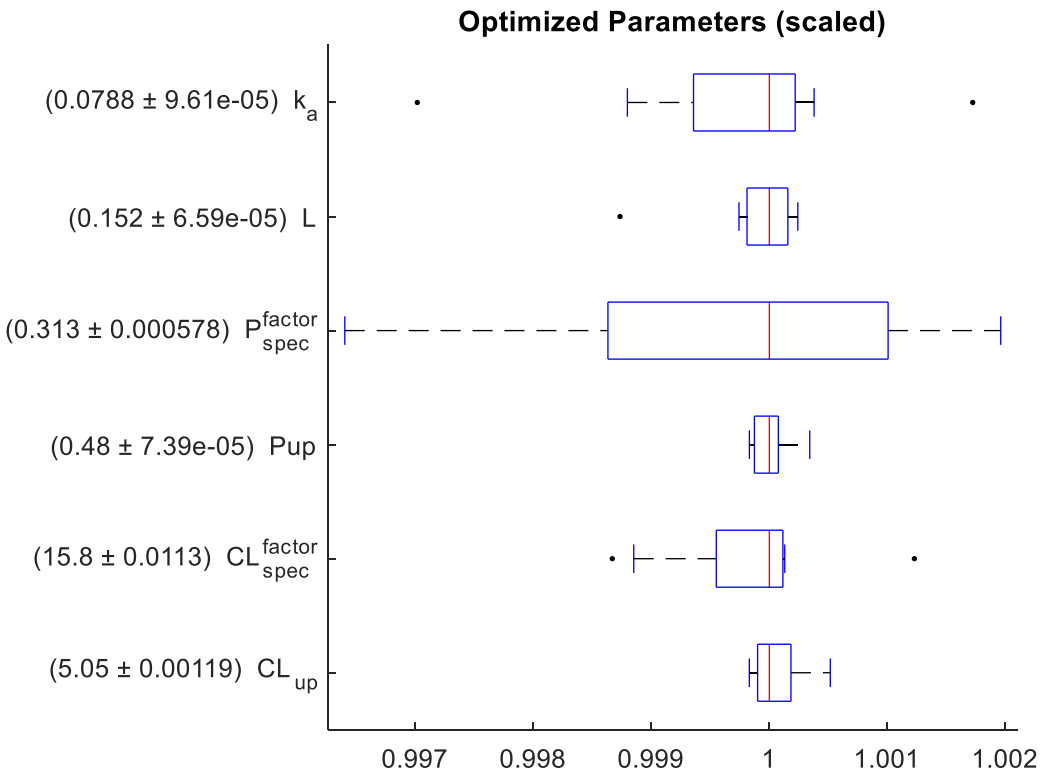

Figure 35. Box-and-whisker diagram for the estimation data visualizing the spread in the parameter estimation results. Parameters presented on y-axis with mean and arithmetic standard deviation. Red lines note the median, boxes note the first and third quartiles, error bars note the minimum and maximum, and outliers are plotted as single dots (defined as a value further than 1.5 times the interquartile range from the median). To normalize the data for the box-and-whisker diagram, the parameters are scaled such that the median of each single parameter is 1.

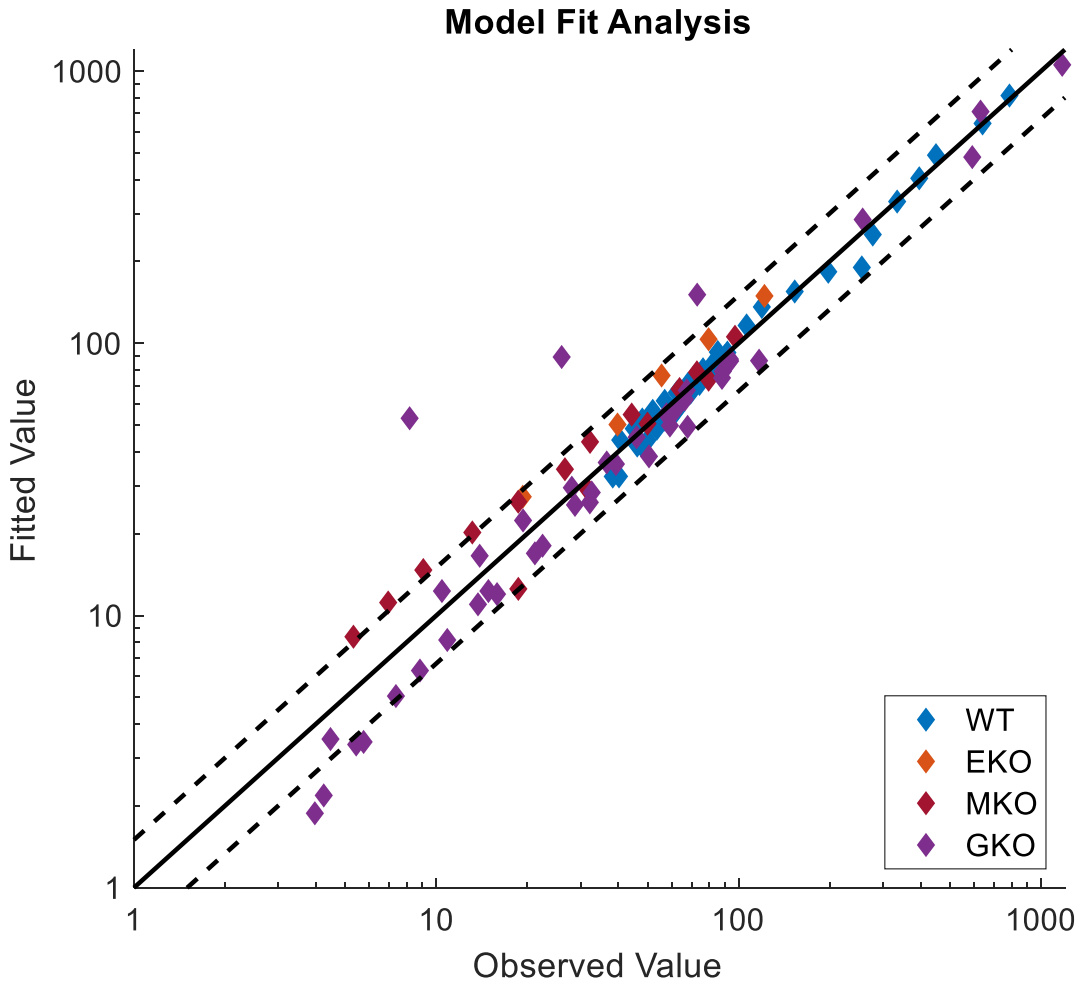

Figure 36. Model fit analysis. Fitted values are plotted against observed values for each experiment type (colored diamonds). WT = wild-type, EKO = endothelial-specific FcRn knockout, MKO = macrophage-specific FcRn knockout, GKO = global FcRn knockout. The solid black line marks the line of equality, and the dashed black lines mark the boundaries of 1.5 fold error.

7.4.2 Minimal PBPK Model Verification

The final model was verified with respect to its Fc-receptor mediated interactions by making a successful prediction for the plasma concentration-time profile of 7E3 when co-administered with 1 g/kg IVIG in the study by Garg et al.[91] The prediction is presented in Figure 37.

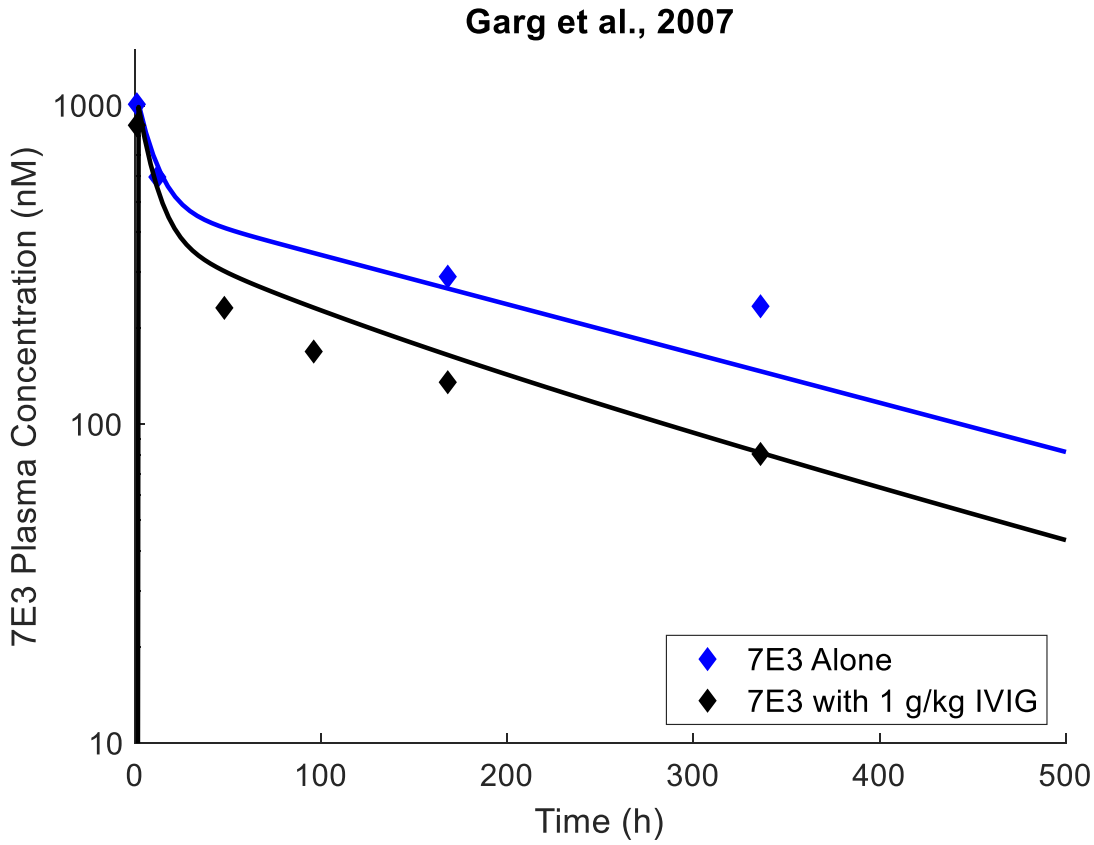

Figure 37. Prediction of 7E3 pharmacokinetics when co-administered with 1 g/kg intravenous immunoglobulin (IVIG) to verify the Fc-dependent interactions in the final model. Observed data presented from Garg et al.[91] over the period of exogenous IVIG persistence (500 hours).

7.4.3 Model Projections

Simulations with the final model were used to revisit existing hypotheses about the contribution of hematopoietic cell uptake and FcRn-mediated recycling to the pharmacokinetics of mAbs in mice. The model suggests that in individuals with normal FcRn expression, macrophages largely act as protectors of mAb in the body, rather than degraders. Instead, degradation occurs predominantly in non-hematopoietic cells. In the wild-type scenario, the model predicts that at 500 hours, 84% of the administered mAb dose is eliminated in endothelial cells while 2% is eliminated in macrophages (Figure 38). However in the GKO scenario, the model predicts that at 500 hours, 57% of the administered mAb dose is eliminated in endothelial cells while 43% is eliminated in macrophages (Figure 38). This observation also changes the understanding of the pre-systemic elimination of mAbs after extravascular administration. Instead of degraders, hematopoietic cells can be thought of as protectors enabling safe transit of mAb through the lymphatic system. When FcRn is knocked out in these cells, bioavailability decreases because the protection is only afforded through binding to FcRn.

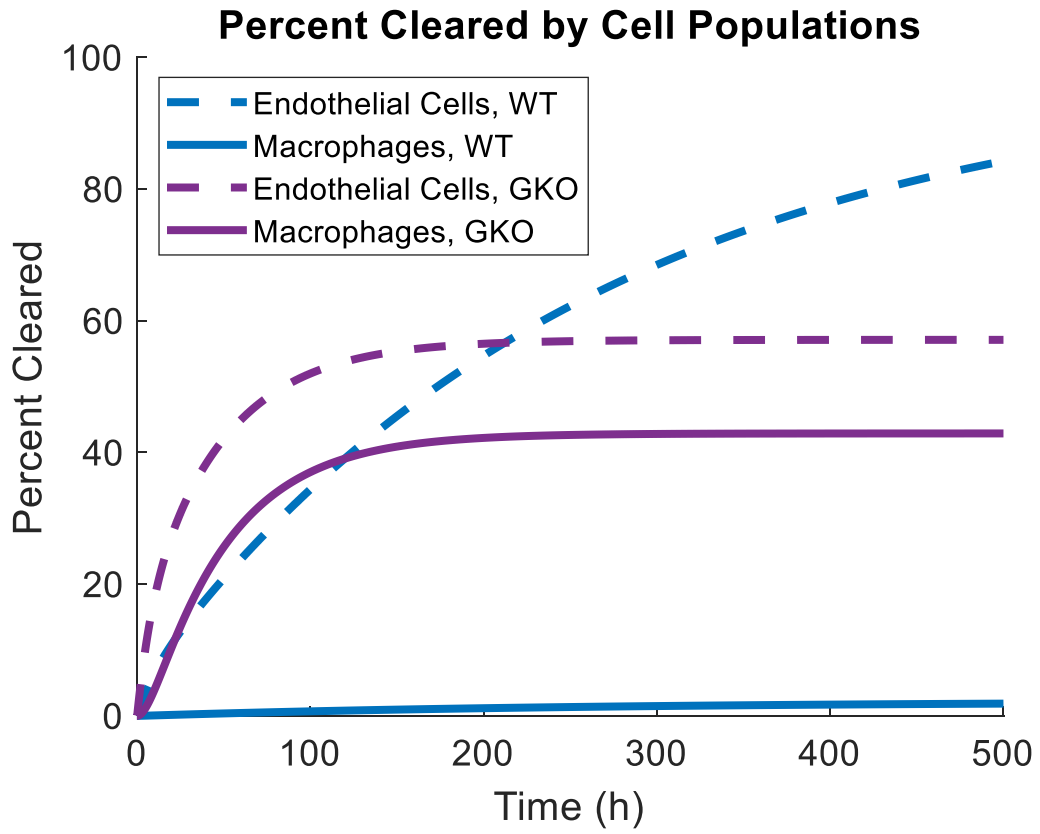

Figure 38. Simulation for percent of injected dose cleared by endothelial cells (dashed line) and macrophages (solid line) in wild-type mice (blue) and global FcRn-knockout mice (purple).

7.4.4 Sensitivity Analysis

The OAT sensitivities of the simulated plasma AUC to select model parameters across the wild-type, 50% FcRn depleted and 90% FcRn depleted scenarios are presented in Figure 39. Across all scenarios, the plasma AUC is most sensitive to endothelial clearance parameters, namely the volume of endothelial cells (V^E), the rate of uptake into endothelial cells (CL_{up}) and the rate of degradation in endothelial cells (CL_{spec}). The vascular reflection coefficient between plasma and interstitial space had a mild impact on the AUC as it governs the distributional equilibrium between plasma and interstitial fluid, and therefore the availability of mAb for uptake into endothelial cells. Parameters related to macrophage volume or uptake had virtually no impact on the plasma profile even in the scenario with 90% FcRn depletion – circulating monocyte volume least of all (V_{circ}^M). This result suggests that the FcRn-mediated recycling of mAbs in hematopoietic cells is highly efficient. To confirm this observation, a simulation was run where the monocyte volume was increased 5-fold from its nominal value, and the plasma AUC did not change. Therefore it is very unlikely that a high concentration of circulating monocytes may contribute to the fast weight-based clearance in young children, even if children were to have up to 90% depletion of FcRn.

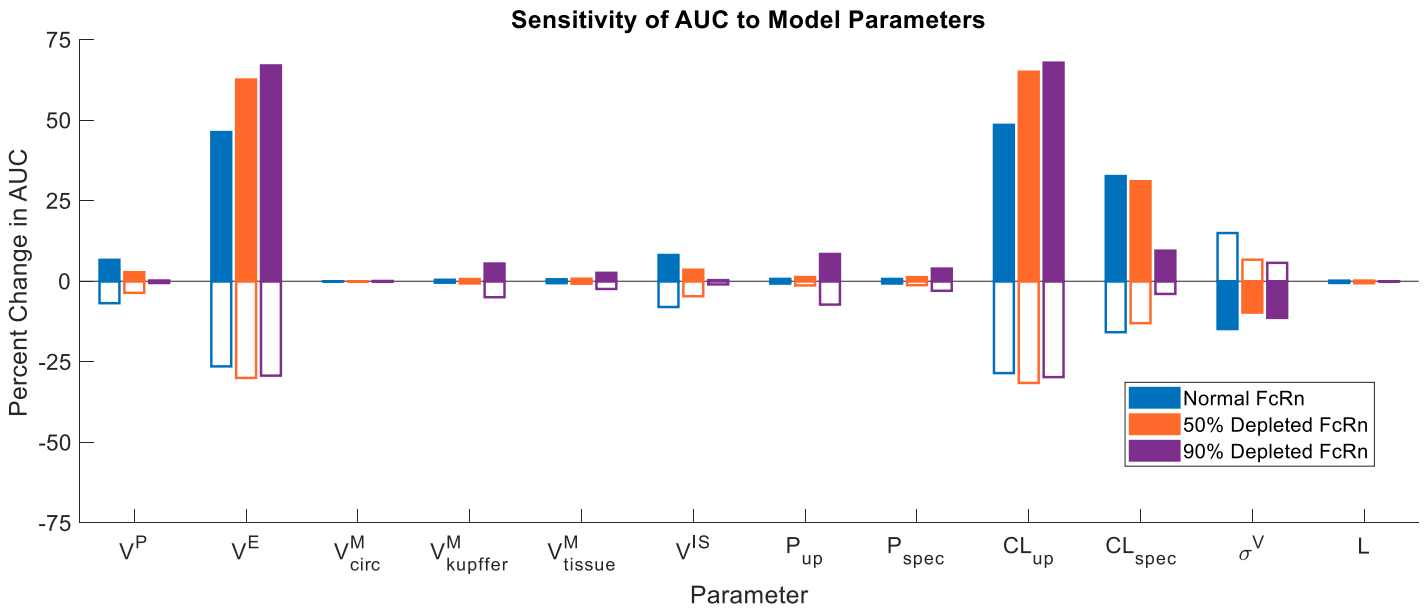

Figure 39. One-at-a-time sensitivity of the simulated plasma AUC to select model parameters in scenarios with normal FcRn expression (blue), 50% depletion of FcRn (orange) and 90% depletion of FcRn (purple). Parameters were varied by -50% (solid bar) and +50% (empty bar) of the nominal value and the resulting percent changes in AUC are reported as sensitivity coefficients. See Table 22 for parameter definitions.

7.5 Discussion

The role of hematopoietic cells and in particular, monocytes and macrophages in the pharmacokinetics of mAbs is currently not well understood. Recent mouse PK data with site-specific FcRn deletion and macrophage knockdown with clodronate liposomes have been enlightening toward this end.[479,490,536] In the current work, a minimal PBPK model has been developed to unify the datasets and a model-based analysis has been conducted to bring clarity to the issue. A model-based analysis is valuable for this exercise because of the degree of experimental complexity. Experiments in mice with site-specific FcRn deletion are further complicated by simultaneous macrophage knockdown with clodronate liposomes, intraperitoneal administration and experiment-specific endogenous IgG concentrations competing for FcRn binding. Overall, the model confirms the assertion by Challa et al. that macrophages are indispensable for IgG homeostasis. In this regard, macrophages serve as highly efficient protectors of IgG in plasma, interstitial fluid and lymph. They are not, as previously thought, sinks for mAb degradation. In fact, model simulations suggest that with normal FcRn expression less than 2% of an intravenously administered dose is eliminated in macrophages, while endothelial cells are predicted to dominate mAb elimination. The near-nil sensitivity of the models with up to 90% FcRn depletion to monocyte and macrophage parameters suggests that it is very unlikely that a high concentration of circulating monocytes can contribute to explaining the fast weight-based clearance of mAbs in very young children.

This work inspires new questions about the importance of hematopoietic cell uptake toward the biodistribution and organ-specific accumulation of mAbs, especially in the context of an expansion of this work to a full body PBPK model. The relative abundance of macrophages in various organs is well known in mice.[553,555] One full body PBPK model for mAbs has incorporated hematopoietic cell uptake as relevant for IgG homeostasis in the context of therapeutic FcRn inhibition, but this parameterization was not built with biodistribution data or the knockout data used here.[544] The present minimal model does not allow significant accumulation of mAb inside endothelial cells or macrophages outside of FcRn binding due to the assumption of equal cellular influx and efflux rates. Nevertheless, the conceptual strides that have been made toward understanding the role of each cell type in the uptake and elimination of mAbs will assist future efforts for modeling organ accumulation as potentially dependent on uptake into macrophages. Such expansion is debatably necessary for mAbs alone, but certainly necessary for characterizing the PK of other large molecule species that are vulnerable to macrophage uptake, such as nanoparticles, liposomes and lysosomal protein replacement therapies.

The collected datasets have particular strengths in that they all feature the same foundational mouse model that is not immunodeficient and does not have human transgenic FcRn, the C57BL/6 athymic nude mouse. The mice were otherwise healthy and did not have tumour xenografts, which increases mAb clearance.[556,557] The administered mAbs showed linear kinetics and demonstrated negligible target binding in mice to avoid the potentially confounding effects of target-mediated drug disposition. However, some challenges were met when unifying the datasets under one model parameterization. While each study used a unique mAb, none of the studies reported the FcRn affinity of their drug product. Different mAbs are also known to show different propensities for extravasation and cellular uptake dependent on their charge, glycosylation, and other physicochemical properties.[554,558,559] In this work, none of these drug-specific parameters were able to be accounted for.

Finally, it is important to acknowledge that this PBPK model is limited by its structural assumptions. All compartments are assumed to be well-stirred and representative of the sum of the respective organ sub-compartments across the whole body. Cellular uptake is limited to FcRn-expressing cells only (endothelial cells and macrophages), and FcRn binding is mathematically described with 1:1 stoichiometry, though 2:1 stoichiometry is observed *in vitro*. Cellular uptake and recycling are assumed to occur at equal rates to improve identifiability, though *in vitro* experiments may prove useful for establishing a relationship between these parameters.

7.6 Conclusion

The model-based analysis of experimental data in mice suggests that the role of macrophages in IgG homeostasis includes highly efficient FcRn-mediated protection but not degradation as previously thought. The relevance of this finding for hypotheses related to high concentrations of circulating monocytes in pediatrics has been discussed.

7.7 Study Highlights

This manuscript revisits the assumptions that were used to perform the pediatric extrapolation in Chapter 6 and reveals that a high concentration of circulating hematopoietic cells is likely not responsible for the observed fast weight-based clearance of monoclonal antibodies in children.

Chapter 8
Conclusions and Future Directions

With the body of pediatric data growing, it is becoming increasingly possible to scale the pharmacokinetics of a mAb from adults to children older than 2 years of age empirically, especially one that is administered intravenously and displays linear kinetics *in vivo*. On the other hand, a physiologically-based extrapolation to children will be preferred when accounting for non-linear behaviour, when disease pathophysiology impacts pharmacokinetics in children, when scaling to infants (where only sparse data exist) or when asking mechanistic research questions. The efforts in this thesis have been directed to making a physiologically-based extrapolation a feasible reality for drug developers, regulators and academics alike.

Four hypotheses remain that may account for the observed fast clearance and high volumes of distribution in children on a per kg basis. First, high extracellular water fractions in young children contribute to a large volume of distribution for mAbs.[61,437] Extravasation of mAbs occurs quickly in children due to dense capillary networks and proportionally larger central and leaky organs.[50,464,560] A fast rate of lymph flow drives fast absorption – and even potentially higher bioavailability after extravascular administration.[36,511] Finally, it cannot be ruled out that the free concentration of the neonatal Fc receptor (FcRn) is present in lower concentrations in the endothelial cells and macrophages of infants and children, leading to faster clearance.[492]

Future research will be directed to the continued testing of these hypotheses and the generation of new ones to eventually complete the full picture of mAb absorption, distribution and elimination in children. As shown by the results of the last chapter, the mechanistic determinants of mAb disposition in humans (even adults) are still not fully understood. Yet to be addressed is the potential for mAbs to deposit or adhere to the endothelial glycocalyx, the potential for fast clearance in liver sinusoidal endothelial cells, or the drivers of hematopoietic cell uptake and accumulation in the spleen.[556,561] To make physiologically based tools that can support pediatric clinical trial planning, the final parameterizations must be expanded to a population approach, similar to the example shown for trastuzumab. Pharmacokinetic variability in peak concentrations remains unaccounted for by the current understanding of variability in virtual individuals, and among experts it has been suggested that the vascular volume fraction or varying potentials for endothelial adherence in the post-injection period may be the key determinants to investigate. Encouragingly, the advances made for mAbs in

pediatrics will also contribute to the wider field of all therapeutic protein use in children. Even nanoparticles and liposomes share similar disposition patterns in children.[562]

Of course, none of this work was done in a vacuum. Multiple research groups contributed literature over the same years that together brought about the evolution of this field. Hardiansyah and Ng published the first physiologically-based pediatric extrapolation for mAbs in 2018.[319] They concluded that FcRn concentrations would be higher in children than adults. In 2020, the commercial team at SimCyp released a pediatric PBPK model for therapeutic proteins by Pan et al., which has been discussed in Chapter 1.[63] They attribute the ontogeny in mAb clearance to a lower concentration of free FcRn in children. A significant portion of our work would not be possible without the use of the generic model for large molecules by Niederalt et al. that was released in 2018.[66] Basu et al. subsequently trialed the generic model for extrapolation of bevacizumab and palivizumab pharmacokinetics to children considering only size-dependent anatomy and physiology.[563] Similar to our work, they came to the conclusion that immature physiology likely contributes to faster clearance even for older children. Temrikar and Meibohm published a notable review of the clinical pharmacology of monoclonal antibodies including a summary of the ontogenic hypotheses in 2020, who then became our collaborators for the review on pediatric dose selection for therapeutic proteins in 2021.[25] Now in 2021, the platform PBPK model by Shah and Betts is being translated to pediatrics with infliximab as an example.[564,565] It has been a privilege to be a part of these pioneering efforts.

Letters of Copyright Permissions

Chapter 2

Order Completed

Thank you for your order.

This Agreement between University of Waterloo -- Paul Malik ("You") and Springer Nature ("Springer Nature") consists of your license details and the terms and conditions provided by Springer Nature and Copyright Clearance Center.

Your confirmation email will contain your order number for future reference.

Printable Details

License Number	5047360151226
License date	Apr 13, 2021

Licensed Content

Licensed Content Publisher	Springer Nature
Licensed Content Publication	Pharmaceutical Research
Licensed Content Title	Pharmacokinetic Considerations for Antibody-Drug Conjugates against Cancer
Licensed Content Author	Paul Malik et al
Licensed Content Date	Sep 18, 2017

Order Details

Type of Use	Thesis/Dissertation
Requestor type	academic/university or research institute
Format	electronic
Portion	full article/chapter
Will you be translating?	no
Circulation/distribution	1 - 29
Author of this Springer Nature content	yes

About Your Work

Title	Physiologically Based Tools to Support Pediatric Dose Selection for Therapeutic Proteins
Institution name	University of Waterloo
Expected presentation date	Jun 2021

Additional Data

Requestor Location

Requestor Location	University of Waterloo 10A Victoria St S Kitchener, ON N2G 1C5 Canada Attn: University of Waterloo

Tax Details

$ Price

Total	0.00 USD

Chapter 3

Order Completed

Thank you for your order.

This Agreement between University of Waterloo -- Paul Malik ("You") and Springer Nature ("Springer Nature") consists of your license details and the terms and conditions provided by Springer Nature and Copyright Clearance Center.

Your confirmation email will contain your order number for future reference.

Printable Details

License Number	5047351299134
License date	Apr 13, 2021

Licensed Content

Licensed Content Publisher	Springer Nature
Licensed Content Publication	Journal of Pharmacokinetics and Pharmacodynamics
Licensed Content Title	Population PBPK modelling of trastuzumab: a framework for quantifying and predicting inter-individual variability
Licensed Content Author	Paul R. V. Malik et al
Licensed Content Date	Mar 4, 2017

Order Details

Type of Use	Thesis/Dissertation
Requestor type	academic/university or research institute
Format	electronic
Portion	full article/chapter
Will you be translating?	no
Circulation/distribution	1 - 29
Author of this Springer Nature content	yes

About Your Work

Title	Physiologically Based Tools to Support Pediatric Dose Selection for Therapeutic Proteins
Institution name	University of Waterloo
Expected presentation date	Jun 2021

Additional Data

Requestor Location

Requestor Location	University of Waterloo 10A Victoria St S Kitchener, ON N2G 1C5 Canada Attn: University of Waterloo

Tax Details

Price

Total	0.00 CAD

Chapter 5

Pediatric physiology in relation to the pharmacokinetics of monoclonal antibodies

Author: Paul Malik, , Andrea Edginton
Publication: Expert Opinion on Drug Metabolism & Toxicology
Publisher: Taylor & Francis
Date: Jun 3, 2018

Rights managed by Taylor & Francis

Thesis/Dissertation Reuse Request

Taylor & Francis is pleased to offer reuses of its content for a thesis or dissertation free of charge contingent on resubmission of permission request if work is published.

BACK CLOSE

Chapter 6

Order Completed

Thank you for your order.

This Agreement between University of Waterloo -- Paul Malik ("You") and John Wiley and Sons ("John Wiley and Sons") consists of your license details and the terms and conditions provided by John Wiley and Sons and Copyright Clearance Center.

Your confirmation email will contain your order number for future reference.

Printable Details

License Number	5047360346044
License date	Apr 13, 2021

Licensed Content

Licensed Content Publisher	John Wiley and Sons
Licensed Content Publication	The Journal of Clinical Pharmacology
Licensed Content Title	Integration of Ontogeny Into a Physiologically Based Pharmacokinetic Model for Monoclonal Antibodies in Premature Infants
Licensed Content Author	Andrea N. Edginton, Paul R. V. Malik
Licensed Content Date	Nov 14, 2019
Licensed Content Volume	60
Licensed Content Issue	4
Licensed Content Pages	11

Order Details

Type of use	Dissertation/Thesis
Requestor type	Author of this Wiley article
Format	Electronic
Portion	Full article
Will you be translating?	No

About Your Work

Title	Physiologically Based Tools to Support Pediatric Dose Selection for Therapeutic Proteins
Institution name	University of Waterloo
Expected presentation date	Jun 2021

Additional Data

Requestor Location

	University of Waterloo 10A Victoria St S
Requestor Location	Kitchener, ON N2G 1C5 Canada Attn: University of Waterloo

Tax Details

Publisher Tax ID	EU826007151

Bibliography

1. Malik PRV, Phipps C, Edginton AN, Blay J. Pharmacokinetic considerations for antibody-drug conjugates against cancer. *Pharm Res.* 2017;34(12):2579-2595.
2. Ryman JT, Meibohm B. Pharmacokinetics of monoclonal antibodies. *CPT Pharmacometrics Syst Pharmacol.* 2017;6(9):576-588.
3. Xu Z, Davis HM, Zhou H. Rational development and utilization of antibody-based therapeutic proteins in pediatrics. *Pharmacol Ther.* 2013;137(2):225-247.
4. Zhang Y, Wei X, Bajaj G, et al. Challenges and considerations for development of therapeutic proteins in pediatric patients. *J Clin Pharmacol.* 2015;55 Suppl 3:S103-115.
5. Dunne J, Rodriguez WJ, Murphy MD, et al. Extrapolation of adult data and other data in pediatric drug-development programs. *Pediatrics.* 2011;128(5):E1242-E1249.
6. Bhattacharya I, Manukyan Z, Chan P, Heatherington A, Harnisch L. Application of quantitative pharmacology approaches in bridging pharmacokinetics and pharmacodynamics of domagrozumab from adult healthy subjects to pediatric patients with Duchenne muscular disease. *J Clin Pharmacol.* 2018;58(3):314-326.
7. Suri A, Mould DR, Song G, Kinley J, Venkatakrishnan K. Population pharmacokinetics of brentuximab vedotin in adult and pediatric patients with relapsed/refractory hematologic malignancies: Model-informed hypothesis generation for pediatric dosing regimens. *J Clin Pharmacol.* 2020;60(12):1585-1597.
8. Diao L, Meibohm B. Pharmacometric applications and challenges in the development of therapeutic antibodies in immuno-oncology. *Curr Pharmacol Rep.* 2018;4(4):285-291.
9. Kleiber M. Body size and metabolic rate. *Physiol Rev.* 1947;27(4):511-541.
10. Abernethy D, Burckart G. Pediatric dose selection. *Clin Pharmacol Ther.* 2010;87(3):270-271.
11. Meibohm B, Läer S, Panetta JC, Barrett JS. Population pharmacokinetic studies in pediatrics: Issues in design and analysis. *AAPS J.* 2005;7(2):E475-E487.
12. Yellepeddi V, Rower J, Liu X, Kumar S, Rashid J, Sherwin CM. State-of-the-art review on physiologically based pharmacokinetic modeling in pediatric drug development. *Clin Pharmacokinet.* 2019;58(1):1-13.
13. Maharaj AR, Edginton AN. Physiologically based pharmacokinetic modeling and simulation in pediatric drug development. *CPT Pharmacometrics Syst Pharmacol.* 2014;3(11):e148.
14. Edginton AN, Schmitt W, Willmann S. Development and evaluation of a generic physiologically based pharmacokinetic model for children. *Clin Pharmacokinet.* 2006;45(10):1013-1034.
15. Wu Q, Peters SA. A retrospective evaluation of allometry, population pharmacokinetics, and physiologically-based pharmacokinetics for pediatric dosing using clearance as a surrogate. *CPT Pharmacometrics Syst Pharmacol.* 2019;8(4):220-229.
16. Mould DR, Meibohm B. Drug development of therapeutic monoclonal antibodies. *BioDrugs.* 2016;30(4):275-293.
17. Bai S, Jorga K, Xin Y, et al. A guide to rational dosing of monoclonal antibodies. *Clin Pharmacokinet.* 2012;51(2):119-135.
18. Thomas VA, Balthasar JP. Understanding inter-individual variability in monoclonal antibody disposition. *Antibodies (Basel).* 2019;8(4):56.
19. Mager DE, Jusko WJ. General pharmacokinetic model for drugs exhibiting target-mediated drug disposition. *J Pharmacokinet Pharmacodyn.* 2001;28(6):507-532.

20. Peletier LA, Gabrielsson J. Dynamics of target-mediated drug disposition: Characteristic profiles and parameter identification. *J Pharmacokinet Pharmacodyn.* 2012;39(5):429-451.
21. Pardeo M, Bracaglia C, De Benedetti F. Systemic juvenile idiopathic arthritis: New insights into pathogenesis and cytokine directed therapies. *Best Pract Res Clin Rheumatol.* 2017;31(4):505-516.
22. De Benedetti F, Brunner HI, Ruperto N, et al. Randomized trial of tocilizumab in systemic juvenile idiopathic arthritis. *N Engl J Med.* 2012;367(25):2385-2395.
23. Chirmule N, Jawa V, Meibohm B. Immunogenicity to therapeutic proteins: Impact on PK/PD and efficacy. *AAPS J.* 2012;14(2):296-302.
24. Gunn GR, 3rd, Sealey DCF, Jamali F, Meibohm B, Ghosh S, Shankar G. From the bench to clinical practice: understanding the challenges and uncertainties in immunogenicity testing for biopharmaceuticals. *Clin Exp Immunol.* 2016;184(2):137-146.
25. Temrikar ZH, Suryawanshi S, Meibohm B. Pharmacokinetics and clinical pharmacology of monoclonal antibodies in pediatric patients. *Paediatr Drugs.* 2020;22(2):199-216.
26. Hofmekler T, Bertha M, McCracken C, et al. Infliximab optimization based on therapeutic drug monitoring in pediatric inflammatory bowel disease. *J Pediatr Gastroenterol Nutr.* 2017;64(4):580-585.
27. Fasanmade AA, Adedokun OJ, Blank M, Zhou H, Davis HM. Pharmacokinetic properties of infliximab in children and adults with Crohn's disease: A retrospective analysis of data from 2 phase III clinical trials. *Clin Ther.* 2011;33(7):946-964.
28. Hyams J, Crandall W, Kugathasan S, et al. Induction and maintenance infliximab therapy for the treatment of moderate-to-severe Crohn's disease in children. *Gastroenterology.* 2007;132(3):863-873.
29. Hyams JS, Lerer T, Griffiths A, et al. Long-term outcome of maintenance infliximab therapy in children with Crohn's disease. *Inflamm Bowel Dis.* 2009;15(6):816-822.
30. Singh N, Dubinsky MC. Therapeutic drug monitoring in children and young adults with inflammatory bowel disease: A practical approach. *Gastroenterol Hepatol.* 2015;11(1):48-55.
31. Jongsma MME, Winter DA, Huynh HQ, et al. Infliximab in young paediatric IBD patients: It is all about the dosing. *Eur J Pediatr.* 2020;179:1935-1944.
32. Winter DA, Joosse ME, de Wildt SN, Taminiau J, de Ridder L, Escher JC. Pharmacokinetics, pharmacodynamics, and immunogenicity of infliximab in pediatric inflammatory bowel disease: A systematic review and revised dosing considerations. *J Pediatr Gastroenterol Nutr.* 2020;70(6):763-776.
33. Frymoyer A, Piester TL, Park KT. Infliximab dosing strategies and predicted trough exposure in children with Crohn's disease. *J Pediatr Gastroenterol Nutr.* 2016;62(5):723-727.
34. Malik P, Edginton A. Pediatric physiology in relation to the pharmacokinetics of monoclonal antibodies. *Expert Opin Drug Metab Toxicol.* 2018;14(6):585-599.
35. Robbie GJ, Zhao L, Mondick J, Losonsky G, Roskos LK. Population pharmacokinetics of palivizumab, a humanized anti-respiratory syncytial virus monoclonal antibody, in adults and children. *Antimicrob Agents Chemother.* 2012;56(9):4927-4936.
36. Li J, Nikanjam M, Cunningham CK, et al. Model informed development of VRC01 in newborn infants using a population pharmacokinetics approach. *Clin Pharmacol Ther.* 2020;[epub ahead of print].
37. Abrantes JA, Nielsen EI, Korth-Bradley J, Harnisch L, Jönsson S. Elucidation of factor VIII activity pharmacokinetics: A pooled population analysis in patients with Hemophilia A treated with moroctocog alfa. *Clin Pharmacol Ther.* 2017;102(6):977-988.
38. Björkman S, Oh M, Spotts G, et al. Population pharmacokinetics of recombinant factor VIII: the relationships of pharmacokinetics to age and body weight. *Blood.* 2012;119(2):612-618.

39. Chelle P, Yeung CHT, Bonanad S, et al. Routine clinical care data for population pharmacokinetic modeling: The case for Fanhdi/Alphanate in Hemophilia A patients. *J Pharmacokinet Pharmacodyn.* 2019;46(5):427-438.
40. Clements JD, Zhu M, Kuchimanchi M, Terminello B, Doshi S. Population pharmacokinetics of blinatumomab in pediatric and adult patients with hematological malignancies. *Clin Pharmacokinet.* 2020;59(4):463-474.
41. Garmann D, McLeay S, Shah A, Vis P, Maas Enriquez M, Ploeger BA. Population pharmacokinetic characterization of BAY 81-8973, a full-length recombinant factor VIII: Lessons learned - importance of including samples with factor VIII levels below the quantitation limit. *Haemophilia.* 2017;23(4):528-537.
42. Han K, Peyret T, Quartino A, et al. Bevacizumab dosing strategy in paediatric cancer patients based on population pharmacokinetic analysis with external validation. *Br J Clin Pharmacol.* 2016;81(1):148-160.
43. Jodele S, Fukuda T, Mizuno K, et al. Variable eculizumab clearance requires pharmacodynamic monitoring to optimize therapy for thrombotic microangiopathy after hematopoietic stem cell transplantation. *Biol Blood Marrow Transplant.* 2016;22(2):307-315.
44. Preijers T, Hazendonk H, Liesner R, et al. Population pharmacokinetics of factor IX in Hemophilia B patients undergoing surgery. *J Thromb Haemost.* 2018;16(11):2196-2207.
45. Shemesh CS, Chanu P, Jamsen K, et al. Population pharmacokinetics, exposure-safety, and immunogenicity of atezolizumab in pediatric and young adult patients with cancer. *J Immunother Cancer.* 2019;7(1):314.
46. Suzuki A, Tomono Y, Korth-Bradley JM. Population pharmacokinetic modelling of factor IX activity after administration of recombinant factor IX in patients with Haemophilia B. *Haemophilia.* 2016;22(5):e359-366.
47. Zhang Y, Roberts J, Tortorici M, et al. Population pharmacokinetics of recombinant coagulation factor VIII-SingleChain in patients with severe Hemophilia A. *J Thromb Haemost.* 2017;15(6):1106-1114.
48. Xu Y, Langevin BA, Zhou H, Xu Z. Model-aided adults-to-children pharmacokinetic extrapolation and empirical body size-based dosing exploration for therapeutic monoclonal antibodies - Is allometry a reasonable choice? *J Clin Pharmacol.* 2020;60(12):1573-1584.
49. Dirks NL, Meibohm B. Population pharmacokinetics of therapeutic monoclonal antibodies. *Clin Pharmacokinet.* 2010;49(10):633-659.
50. Valentin J. Basic anatomical and physiological data for use in radiological protection: Reference values. *Ann ICRP.* 2002;32(3):1-277.
51. McEneny-King A, Foster G, Iorio A, Edginton AN. Data analysis protocol for the development and evaluation of population pharmacokinetic models for incorporation into the Web-Accessible Population Pharmacokinetic Service - Hemophilia (WAPPS-Hemo). *JMIR Res Protoc.* 2016;5(4):e232.
52. Weisman LE, Thackray HM, Garcia-Prats JA, et al. Phase 1/2 double-blind, placebo-controlled, dose escalation, safety, and pharmacokinetic study of pagibaximab (BSYX-A110), an antistaphylococcal monoclonal antibody for the prevention of staphylococcal bloodstream infections, in very-low-birth-weight neonates. *Antimicrob Agents Chemother.* 2009;53(7):2879-2886.
53. Weisman LE, Fischer GW, Thackray HM, et al. Safety and pharmacokinetics of a chimerized anti-lipoteichoic acid monoclonal antibody in healthy adults. *Int Immunopharmacol.* 2009;9(5):639-644.
54. Wu YW, Bauer LA, Ballard RA, et al. Erythropoietin for neuroprotection in neonatal encephalopathy: safety and pharmacokinetics. *Pediatrics.* 2012;130(4):683-691.

55. Veng-Pedersen P, Widness JA, Pereira LM, Peters C, Schmidt RL, Lowe LS. Kinetic evaluation of nonlinear drug elimination by a disposition decomposition analysis. Application to the analysis of the nonlinear elimination kinetics of erythropoietin in adult humans. *J Pharm Sci.* 1995;84(6):760-767.
56. Hanke N, Kunz C, Thiemann M, Fricke H, Lehr T. Translational PBPK modeling of the protein therapeutic and CD95L inhibitor asunercept to develop dose recommendations for its first use in pediatric glioblastoma patients. *Pharmaceutics.* 2019;11(4):152.
57. Sun H, Van LM, Floch D, et al. Pharmacokinetics and pharmacodynamics of canakinumab in patients with systemic juvenile idiopathic arthritis. *J Clin Pharmacol.* 2016;56(12):1516-1527.
58. Lowe PJ, Renard D. Omalizumab decreases IgE production in patients with allergic (IgE-mediated) asthma; PKPD analysis of a biomarker, total IgE. *Br J Clin Pharmacol.* 2011;72(2):306-320.
59. Chetty M, Li L, Rose R, et al. Prediction of the pharmacokinetics, pharmacodynamics, and efficacy of a monoclonal antibody, using a physiologically based pharmacokinetic FcRn model. *Front Immunol.* 2014;5:670.
60. Malik PRV, Edginton AN. Physiologically-based pharmacokinetic modeling vs. allometric scaling for the prediction of infliximab pharmacokinetics in pediatric patients. *CPT Pharmacometrics Syst Pharmacol.* 2019;8(11):835-844.
61. Stake G, Monclair T. A single plasma sample method for estimation of the glomerular filtration rate in infants and children using iohexol, I: Establishment of a body weight-related formula for the distribution volume of iohexol. *Scand J Clin Lab Invest.* 1991;51(4):335-342.
62. Friis-Hansen B. Water distribution in the foetus and newborn infant. *Acta Paediatr Scand Suppl.* 1983;305:7-11.
63. Pan X, Stader F, Abduljalil K, et al. Development and application of a physiologically-based pharmacokinetic model to predict the pharmacokinetics of therapeutic proteins from full-term neonates to adolescents. *AAPS J.* 2020;22(4):76.
64. Meibohm B, Zhou H. Characterizing the impact of renal impairment on the clinical pharmacology of biologics. *J Clin Pharmacol.* 2012;52(1 Suppl):54S-62S.
65. Malik PRV, Edginton AN. Integration of ontogeny into a physiologically based pharmacokinetic model for monoclonal antibodies in premature infants. *J Clin Pharmacol.* 2019;60(4):466-476.
66. Niederalt C, Kuepfer L, Solodenko J, et al. A generic whole body physiologically based pharmacokinetic model for therapeutic proteins in PK-Sim. *J Pharmacokinet Pharmacodyn.* 2018;45(2):235-257.
67. Wong YC, Centanni M, de Lange ECM. Physiologically based modeling approach to predict dopamine D2 receptor occupancy of antipsychotics in brain: Translation from rat to human. *J Clin Pharmacol.* 2019;59(5):731-747.
68. Malik PRV, Hamadeh A, Phipps C, Edginton AN. Population PBPK modelling of trastuzumab: A framework for quantifying and predicting inter-individual variability. *J Pharmacokinet Pharmacodyn.* 2017;44(3):277-290.
69. Chen X, DuBois DC, Almon RR, Jusko WJ. Biodistribution of etanercept to tissues and sites of inflammation in arthritic rats. *Drug Metab Dispos.* 2015;43(6):898-907.
70. Liu XI, Dallmann A, Wang YM, et al. Monoclonal antibodies and Fc-fusion proteins for pediatric use: Dosing, immunogenicity, and modeling and simulation in data submitted to the US Food and Drug Administration. *J Clin Pharmacol.* 2019;59(8):1130-1143.

71. Ternant D, Azzopardi N, Raoul W, Bejan-Angoulvant T, Paintaud G. Influence of antigen mass on the pharmacokinetics of therapeutic antibodies in humans. *Clin Pharmacokinet.* 2019;58(2):169-187.
72. Admiraal R, van Kesteren C, Jol-van der Zijde CM, et al. Population pharmacokinetic modeling of Thymoglobulin in children receiving allogeneic-hematopoietic cell transplantation: towards improved survival through individualized dosing. *Clin Pharmacokinet.* 2015;54(4):435-446.
73. Admiraal R, Jol-van der Zijde CM, Furtado Silva JM, et al. Population pharmacokinetics of alemtuzumab (Campath) in pediatric hematopoietic cell transplantation: Towards individualized dosing to improve outcome. *Clin Pharmacokinet.* 2019;58(12):1609-1620.
74. Li Y, Kassir N, Chen N, Wang X, Palmisano M, Zhou S. Population pharmacokinetics and exposure-response analysis of nab-paclitaxel in pediatric patients with recurrent or refractory solid tumors. *Clin Pharmacol Drug Dev.* 2020;[epub ahead of print].
75. Dong JQ, Salinger DH, Endres CJ, et al. Quantitative prediction of human pharmacokinetics for monoclonal antibodies: retrospective analysis of monkey as a single species for first-in-human prediction. *Clin Pharmacokinet.* 2011;50(2):131-142.
76. Richter WF, Bhansali SG, Morris ME. Mechanistic determinants of biotherapeutics absorption following subcutaneous administration. *AAPS J.* 2012;14(3):559-570.
77. Gill KL, Gardner I, Li L, Jamei M. A bottom-up whole-body physiologically based pharmacokinetic model to mechanistically predict tissue distribution and the rate of subcutaneous absorption of therapeutic proteins. *AAPS J.* 2016;18(1):156-170.
78. Hu S, D'Argenio DZ. Predicting monoclonal antibody pharmacokinetics following subcutaneous administration via whole-body physiologically-based modeling. *J Pharmacokinet Pharmacodyn.* 2020;47(5):385-409.
79. Varkhede N, Forrest ML. Understanding the monoclonal antibody disposition after subcutaneous administration using a minimal physiologically based pharmacokinetic model. *J Pharm Pharm Sci.* 2018;21(1s):130S-148S.
80. Edlund H, Melin J, Parra-Guillen ZP, Kloft C. Pharmacokinetics and pharmacokinetic-pharmacodynamic relationships of monoclonal antibodies in children. *Clin Pharmacokinet.* 2015;54(1):35-80.
81. *Humira (Adalimumab) Prescribing Information.* North Chicago, IL: Abbvie, Inc.
82. *Actemra (Tocilizumab) Prescribing Information.* South San Francisco, CA: Genentech, Inc.
83. Honma W, Gautier A, Paule I, Yamaguchi M, Lowe PJ. Ethnic sensitivity assessment of pharmacokinetics and pharmacodynamics of omalizumab with dosing table expansion. *Drug Metab Pharmacokinet.* 2016;31(3):173-184.
84. Bi Y, Liu J, Wang J, et al. Model-informed drug development approach supporting approval of adalimumab (Humira) in adolescent patients with hidradenitis suppurativa: A regulatory perspective. *AAPS J.* 2019;21(5):91.
85. Dubinsky MC, Phan BL, Singh N, Rabizadeh S, Mould DR. Pharmacokinetic dashboard-recommended dosing is different than standard of care dosing in infliximab-treated pediatric IBD patients. *AAPS J.* 2017;19(1):215-222.
86. Verma S, Miles D, Gianni L, et al. Trastuzumab emtansine for HER2-positive advanced breast cancer. *N Engl J Med.* 2012;367(19):1783-1791.
87. Younes A, Gopal AK, Smith SE, et al. Results of a pivotal phase II study of brentuximab vedotin for patients with relapsed or refractory Hodgkin's lymphoma. *J Clin Oncol.* 2012;30(18):2183-2189.
88. Diamantis N, Banerji U. Antibody-drug conjugates - An emerging class of cancer treatment. *Br J Cancer.* 2016;114(4):362-367.

89. Kraeber-Bodere F, Bodet-Milin C, Rousseau C, et al. Radioimmunoconjugates for the treatment of cancer. *Semin Oncol.* 2014;41(5):613-622.
90. Han TH, Zhao B. Absorption, distribution, metabolism, and excretion considerations for the development of antibody-drug conjugates. *Drug Metab Dispos.* 2014;42(11):1914-1920.
91. Garg A, Balthasar JP. Physiologically-based pharmacokinetic (PBPK) model to predict IgG tissue kinetics in wild-type and FcRn-knockout mice. *J Pharmacokinet Pharmacodyn.* 2007;34(5):687-709.
92. Nolin TD. Chapter 4 - Drug Metabolism in Kidney Disease. In: Xie W, ed. *Drug Metabolism in Diseases.* Boston: Academic Press; 2017:91-113.
93. Lu D, Girish S, Gao Y, et al. Population pharmacokinetics of trastuzumab emtansine (T-DM1), a HER2-targeted antibody-drug conjugate, in patients with HER2-positive metastatic breast cancer: clinical implications of the effect of covariates. *Cancer Chemother Pharmacol.* 2014;74(2):399-410.
94. Deslandes A. Comparative clinical pharmacokinetics of antibody-drug conjugates in first-in-human phase 1 studies. *mAbs.* 2014;6(4):859-870.
95. Levy G. Pharmacologic target-mediated drug disposition. *Clin Pharmacol Ther.* 1994;56(3):248-252.
96. Khot A, Tibbitts J, Rock D, Shah DK. Development of a translational physiologically based pharmacokinetic model for antibody-drug conjugates: A case study with T-DM1. *AAPS J.* 2017;19(6):1715-1734.
97. Kraynov E, Kamath AV, Walles M, et al. Current approaches for absorption, distribution, metabolism, and excretion characterization of antibody-drug conjugates: An industry white paper. *Drug Metab Dispos.* 2016;44(5):617-623.
98. Gorovits B, Alley SC, Bilic S, et al. Bioanalysis of antibody–drug conjugates: American Association of Pharmaceutical Scientists Antibody–Drug Conjugate Working Group position paper. *Bioanalysis.* 2013;5(9):997-1006.
99. Singh AP, Shah DK. Application of a PK-PD modeling and simulation-based strategy for clinical translation of antibody-drug conjugates: A case study with trastuzumab emtansine (T-DM1). *AAPS J.* 2017;19(4):1054-1070.
100. Poon KA, Flagella K, Beyer J, et al. Preclinical safety profile of trastuzumab emtansine (T-DM1): Mechanism of action of its cytotoxic component retained with improved tolerability. *Toxicol Appl Pharmacol.* 2013;273(2):298-313.
101. Hock MB, Thudium KE, Carrasco-Triguero M, Schwabe NF. Immunogenicity of antibody drug conjugates: Bioanalytical methods and monitoring strategy for a novel therapeutic modality. *AAPS J.* 2015;17(1):35-43.
102. Beck A, Goetsch L, Dumontet C, Corvaia N. Strategies and challenges for the next generation of antibody-drug conjugates. *Nat Rev Drug Discov.* 2017;16(5):315-337.
103. Ritchie M, Tchistiakova L, Scott N. Implications of receptor-mediated endocytosis and intracellular trafficking dynamics in the development of antibody drug conjugates. *mAbs.* 2013;5(1):13-21.
104. Fujimori K, Covell DG, Fletcher JE, Weinstein JN. A modeling analysis of monoclonal antibody percolation through tumors: A binding-site barrier. *J Nucl Med.* 1990;31(7):1191-1198.
105. Peletier LA, Gabrielsson J. Dynamics of target-mediated drug disposition: Characteristic profiles and parameter identification. *J Pharmacokinet Pharmacodyn.* 2012;39(5):429-451.
106. Giddabasappa A, Gupta VR, Norberg R, et al. Biodistribution and targeting of anti-5T4 antibody-drug conjugate using fluorescence molecular tomography. *Mol Cancer Ther.* 2016;15(10):2530-2540.

107. Sun X, Ponte JF, Yoder NC, et al. Effects of drug-antibody ratio on pharmacokinetics, biodistribution, efficacy, and tolerability of antibody-maytansinoid conjugates. *Bioconjug Chem.* 2017;28(5):1371-1381.
108. Boswell CA, Mundo EE, Firestein R, et al. An integrated approach to identify normal tissue expression of targets for antibody-drug conjugates: Case study of TENB2. *Br J Pharmacol.* 2013;168(2):445-457.
109. Glassman PM, Balthasar JP. Physiologically-based pharmacokinetic modeling to predict the clinical pharmacokinetics of monoclonal antibodies. *J Pharmacokinet Pharmacodyn.* 2016;43(4):427-446.
110. Reardon DA, Lassman AB, van den Bent M, et al. Efficacy and safety results of ABT-414 in combination with radiation and temozolomide in newly diagnosed glioblastoma. *Neuro Oncol.* 2017;19(7):965-975.
111. Tolcher AW, Ochoa L, Hammond LA, et al. Cantuzumab mertansine, a maytansinoid immunoconjugate directed to the CanAg antigen: A phase I, pharmacokinetic, and biologic correlative study. *J Clin Oncol.* 2003;21(2):211-222.
112. Boswell CA, Mundo EE, Zhang C, et al. Differential effects of predosing on tumor and tissue uptake of an 111In-labeled anti-TENB2 antibody-drug conjugate. *J Nucl Med.* 2012;53(9):1454-1461.
113. Boswell CA, Bumbaca D, Fielder PJ, Khawli LA. Compartmental tissue distribution of antibody therapeutics: Experimental approaches and interpretations. *AAPS J.* 2012;14(3):612-618.
114. Grimm HP. Gaining insights into the consequences of target-mediated drug disposition of monoclonal antibodies using quasi-steady-state approximations. *J Pharmacokinet Pharmacodyn.* 2009;36(5):407-420.
115. Williams SP, Ogasawara A, Tinianow JN, et al. ImmunoPET helps predicting the efficacy of antibody-drug conjugates targeting TENB2 and STEAP1. *Oncotarget.* 2016;7(18):25103-25112.
116. Ingle GS, Chan P, Elliott JM, et al. High CD21 expression inhibits internalization of anti-CD19 antibodies and cytotoxicity of an anti-CD19-drug conjugate. *Br J Haematol.* 2008;140(1):46-58.
117. Pincus SH, Song K, Maresh GA, et al. Identification of human anti-HIV gp160 monoclonal antibodies that make effective immunotoxins. *J Virol.* 2017;91(3):e01955-01916.
118. Berger C, Madshus IH, Stang E. Cetuximab in combination with anti-human IgG antibodies efficiently down-regulates the EGF receptor by macropinocytosis. *Exp Cell Res.* 2012;318(20):2578-2591.
119. Longva KE, Pedersen NM, Haslekas C, Stang E, Madshus IH. Herceptin-induced inhibition of ErbB2 signaling involves reduced phosphorylation of Akt but not endocytic down-regulation of ErbB2. *Int J Cancer.* 2005;116(3):359-367.
120. Dello Sbarba P, Rovida E. Transmodulation of cell surface regulatory molecules via ectodomain shedding. *Biol Chem.* 2002;383(1):69-83.
121. Pak Y, Pastan I, Kreitman RJ, Lee B. Effect of antigen shedding on targeted delivery of immunotoxins in solid tumors from a mathematical model. *PLoS One.* 2014;9(10):e110716.
122. Weigle WO. Elimination of antigen-antibody complexes from sera of rabbits. *J Immunol.* 1958;81(3):204-213.
123. Berson SA, Yalow RS. Quantitative aspects of the reaction between insulin and insulin-binding antibody. *J Clin Invest.* 1959;38(11):1996-2016.

124. Pool M, Kol A, Lub-de Hooge MN, et al. Extracellular domain shedding influences specific tumor uptake and organ distribution of the EGFR PET tracer 89Zr-imgatuzumab. *Oncotarget.* 2016;7(42):68111-68121.
125. Bruno R, Washington CB, Lu JF, Lieberman G, Banken L, Klein P. Population pharmacokinetics of trastuzumab in patients with HER2+ metastatic breast cancer. *Cancer Chemother Pharmacol.* 2005;56(4):361-369.
126. Pastuskovas CV, Mallet W, Clark S, et al. Effect of immune complex formation on the distribution of a novel antibody to the ovarian tumor antigen CA125. *Drug Metab Dispos.* 2010;38(12):2309-2319.
127. Ackerman ME, Pawlowski D, Wittrup KD. Effect of antigen turnover rate and expression level on antibody penetration into tumor spheroids. *Mol Cancer Ther.* 2008;7(7):2233-2240.
128. Vasalou C, Helmlinger G, Gomes B. A mechanistic tumor penetration model to guide antibody drug conjugate design. *PLoS One.* 2015;10(3):e0118977.
129. Rudnick SI, Lou J, Shaller CC, et al. Influence of affinity and antigen internalization on the uptake and penetration of anti-HER2 antibodies in solid tumors. *Cancer Res.* 2011;71(6):2250-2259.
130. Phillips AC, Boghaert ER, Vaidya KS, et al. ABT-414, an antibody–drug conjugate targeting a tumor-selective EGFR epitope. *Mol Cancer Ther.* 2016;15(4):661-669.
131. Bondza S, Stenberg J, Nestor M, Andersson K, Bjorkelund H. Conjugation effects on antibody-drug conjugates: evaluation of interaction kinetics in real time on living cells. *Mol Pharm.* 2014;11(11):4154-4163.
132. Glassman PM, Balthasar JP. Physiologically-based modeling to predict the clinical behavior of monoclonal antibodies directed against lymphocyte antigens. *mAbs.* 2017;9(2):297-306.
133. Beum PV, Lindorfer MA, Beurskens F, et al. Complement activation on B lymphocytes opsonized with rituximab or ofatumumab produces substantial changes in membrane structure preceding cell lysis. *J Immunol.* 2008;181(1):822-832.
134. Wiig H, Swartz MA. Interstitial fluid and lymph formation and transport: Physiological regulation and roles in inflammation and cancer. *Physiol Rev.* 2012;92(3):1005-1060.
135. Shah DK, Betts AM. Towards a platform PBPK model to characterize the plasma and tissue disposition of monoclonal antibodies in preclinical species and human. *J Pharmacokinet Pharmacodyn.* 2012;39(1):67-86.
136. Sarin H. Physiologic upper limits of pore size of different blood capillary types and another perspective on the dual pore theory of microvascular permeability. *J Angiogenes Res.* 2010;2:14.
137. Hossler FE, Monson FC. Microvasculature of the rabbit urinary bladder. *Anat Rec.* 1995;243(4):438-448.
138. Boswell CA, Mundo EE, Zhang C, et al. Impact of drug conjugation on pharmacokinetics and tissue distribution of anti-STEAP1 antibody-drug conjugates in rats. *Bioconjug Chem.* 2011;22(10):1994-2004.
139. Xie H, Audette C, Hoffee M, Lambert JM, Blattler WA. Pharmacokinetics and biodistribution of the antitumor immunoconjugate, cantuzumab mertansine (huC242-DM1), and its two components in mice. *J Pharmacol Exp Ther.* 2004;308(3):1073-1082.
140. Parving HH, Jensen HA, Westrup M. Increased transcapillary escape rate of albumin and IgG in essential hypertension. *Scand J Clin Lab Invest.* 1977;37(3):223-227.
141. Parving HH, Ranek L, Lassen NA. Increased transcapillary escape rate of albumin in patients with cirrhosis of the liver. *Scand J Clin Lab Invest.* 1977;37(7):643-648.
142. Parving HH. Increased microvascular permeability to plasma proteins in short- and long-term juvenile diabetics. *Diabetes.* 1976;25(2 Suppl):884-889.

143. Parving HH, Rossing N. Simultaneous determination of the transcapillary escape rate of albumin and IgG in normal and long-term juvenile diabetic subjects. *Scand J Clin Lab Invest.* 1973;32(3):239-244.
144. Hesse B, Parving HH, Lund-Jacobsen H, Noer I. Transcapillary escape rate of albumin and right atrial pressure in chronic congestive heart failure before and after treatment. *Circ Res.* 1976;39(3):358-362.
145. Parving HH, Worm AM, Rossing N. Plasma volume, intravascular albumin and its transcapillary escape rate in patients with extensive skin disease. *Br J Dermatol.* 1976;95(5):519-214.
146. Fleck A, Hawker F, Wallace PI, et al. Increased vascular permeability: A major cause of hypoalbuminemia in disease and injury. *Lancet.* 1985;325(8432):781-784.
147. Ballmer PE, Ochsenbein AF, Schütz-Hofmann S. Transcapillary escape rate of albumin positively correlates with plasma albumin concentration in acute but not in chronic inflammatory disease. *Metabolism.* 1994;43(6):697-705.
148. Pedersen LM, Terslev L, PG SL, Stokholm KH. Urinary albumin excretion and transcapillary escape rate of albumin in malignancies. *Med Oncol.* 2000;17(2):117-122.
149. Gupta M, Lorusso PM, Wang B, et al. Clinical implications of pathophysiological and demographic covariates on the population pharmacokinetics of trastuzumab emtansine, a HER2-targeted antibody-drug conjugate, in patients with HER2-positive metastatic breast cancer. *J Clin Pharmacol.* 2012;52(5):691-703.
150. Nagy JA, Benjamin L, Zeng H, Dvorak AM, Dvorak HF. Vascular permeability, vascular hyperpermeability and angiogenesis. *Angiogenesis.* 2008;11(2):109-119.
151. Centelles MN, Wright M, Gedroyc W, Thanou M. Focused ultrasound induced hyperthermia accelerates and increases the uptake of anti-HER-2 antibodies in a xenograft model. *Pharmacol Res.* 2016;114:144-151.
152. Chacko AM, Li C, Pryma DA, Brem S, Coukos G, Muzykantov V. Targeted delivery of antibody-based therapeutic and imaging agents to CNS tumors: Crossing the blood-brain barrier divide. *Expert Opin Drug Deliv.* 2013;10(7):907-926.
153. Chang HY, Wu S, Meno-Tetang G, Shah DK. A translational platform PBPK model for antibody disposition in the brain. *J Pharmacokinet Pharmacodyn.* 2019;46(4):319-338.
154. Jadhav SB, Khaowroongrueng V, Fueth M, Otteneder MB, Richter W, Derendorf H. Tissue distribution of a therapeutic monoclonal antibody determined by large pore microdialysis. *J Pharm Sci.* 2017;106(9):2853-2859.
155. van Furth R, Cohn ZA, Hirsch JG, Humphrey JH, Spector WG, Langevoort HL. The mononuclear phagocyte system: A new classification of macrophages, monocytes, and their precursor cells. *Bull World Health Organ.* 1972;46(6):845-852.
156. Harrison PT, Davis W, Norman JC, Hockaday AR, Allen JM. Binding of monomeric immunoglobulin G triggers Fc gamma RI-mediated endocytosis. *J Biol Chem.* 1994;269(39):24396-24402.
157. Richter WF, Jacobsen B. Subcutaneous absorption of biotherapeutics: Knowns and unknowns. *Drug Metab Dispos.* 2014;42(11):1881-1889.
158. Richter WF, Bhansali SG, Morris ME. Mechanistic determinants of biotherapeutics absorption following SC administration. *AAPS J.* 2012;14(3):559-570.
159. Deng R, Meng YG, Hoyte K, et al. Subcutaneous bioavailability of therapeutic antibodies as a function of FcRn binding affinity in mice. *mAbs.* 2012;4(1):101-109.
160. Wang W, Wang EQ, Balthasar JP. Monoclonal antibody pharmacokinetics and pharmacodynamics. *Clin Pharmacol Ther.* 2008;84(5):548-558.

161. Roopenian DC, Akilesh S. FcRn: The neonatal Fc receptor comes of age. *Nat Rev Immunol.* 2007;7(9):715-725.
162. McCarthy KM, Yoong Y, Simister NE. Bidirectional transcytosis of IgG by the rat neonatal Fc receptor expressed in a rat kidney cell line: A system to study protein transport across epithelia. *J Cell Sci.* 2000;113(Pt 7):1277-1285.
163. Fuhrmann S, Kloft C, Huisinga W. Impact of altered endogenous IgG on unspecific mAb clearance. *J Pharmacokinet Pharmacodyn.* 2017;44(4):351-374.
164. Hamblett KJ, Le T, Rock BM, et al. Altering antibody-drug conjugate binding to the neonatal Fc receptor impacts efficacy and tolerability. *Mol Pharm.* 2016;13(7):2387-2396.
165. Acchione M, Kwon H, Jochheim CM, Atkins WM. Impact of linker and conjugation chemistry on antigen binding, Fc receptor binding and thermal stability of model antibody-drug conjugates. *mAbs.* 2012;4(3):362-372.
166. Brachet G, Respaud R, Arnoult C, et al. Increment in drug loading on an antibody-drug conjugate increases its binding to the human neonatal Fc receptor in vitro. *Mol Pharm.* 2016;13(4):1405-1412.
167. Gessner JE, Heiken H, Tamm A, Schmidt RE. The IgG Fc receptor family. *Ann Hematol.* 1998;76:231-248.
168. Abuqayyas L, Balthasar JP. Application of knockout mouse models to investigate the influence of FcgammaR on the tissue distribution and elimination of 8C2, a murine IgG1 monoclonal antibody. *Int J Pharm.* 2012;439(1-2):8-16.
169. Abuqayyas L, Zhang X, Balthasar JP. Application of knockout mouse models to investigate the influence of FcgammaR on the pharmacokinetics and anti-platelet effects of MWReg30, a monoclonal anti-GPIIb antibody. *Int J Pharm.* 2013;444(1-2):185-192.
170. Donaghy H. Effects of antibody, drug and linker on the preclinical and clinical toxicities of antibody-drug conjugates. *mAbs.* 2016;8(4):659-671.
171. Krop IE, Beeram M, Modi S, et al. Phase I study of trastuzumab-DM1, an HER2 antibody-drug conjugate, given every 3 weeks to patients with HER2-positive metastatic breast cancer. *J Clin Oncol.* 2010;28(16):2698-2704.
172. Uppal H, Doudement E, Mahapatra K, et al. Potential mechanisms for thrombocytopenia development with trastuzumab emtansine (T-DM1). *Clin Cancer Res.* 2015;21(1):123-133.
173. Li F, Ulrich M, Jonas M, et al. Tumor associated macrophages can contribute to antitumor activity through FcgammaR-mediated processing of antibody-drug conjugates. *Mol Cancer Ther.* 2017;16(7):1347-1354.
174. Ko SY, Pegu A, Rudicell RS, et al. Enhanced neonatal Fc receptor function improves protection against primate SHIV infection. *Nature.* 2014;514(7524):642-645.
175. Grevys A, Bern M, Foss S, et al. Fc engineering of human IgG1 for altered binding to the neonatal Fc receptor affects Fc effector functions. *J Immunol.* 2015;194(11):5497-5508.
176. Tolcher AW, Sugarman S, Gelmon KA, et al. Randomized phase II study of BR96-doxorubicin conjugate in patients with metastatic breast cancer. *J Clin Oncol.* 1999;17(2):478-484.
177. Comereski CR, Peden WM, Davidson TJ, Warner GL, Hirth RS, Frantz JD. BR96-doxorubicin conjugate (BMS-182248) versus doxorubicin: A comparative toxicity assessment in rats. *Toxicol Pathol.* 1994;22(5):473-488.
178. Senter PD. Potent antibody drug conjugates for cancer therapy. *Curr Opin Chem Biol.* 2009;13(3):235-244.
179. Sessa C, Weigang-Köhler K, Pagani O, et al. Phase I and pharmacological studies of the cryptophycin analogue LY355703 administered on a single intermittent or weekly schedule. *Eur J Cancer.* 2002;38(18):2388-2396.

180. Edelman MJ, Gandara DR, Hausner P, et al. Phase 2 study of cryptophycin 52 (LY355703) in patients previously treated with platinum based chemotherapy for advanced non-small cell lung cancer. *Lung Cancer.* 2003;39(2):197-199.
181. Verma VA, Pillow TH, DePalatis L, et al. The cryptophycins as potent payloads for antibody drug conjugates. *Bioorg Med Chem Lett.* 2015;25(4):864-868.
182. Ogitani Y, Abe Y, Iguchi T, et al. Wide application of a novel topoisomerase I inhibitor-based drug conjugation technology. *Bioorg Med Chem Lett.* 2016;26(20):5069-5072.
183. Lopus M, Oroudjev E, Wilson L, et al. Maytansine and cellular metabolites of antibody-maytansinoid conjugates strongly suppress microtubule dynamics by binding to microtubules. *Mol Cancer Ther.* 2010;9(10):2689-2699.
184. Oroudjev E, Lopus M, Wilson L, et al. Maytansinoid-antibody conjugates induce mitotic arrest by suppressing microtubule dynamic instability. *Mol Cancer Ther.* 2010;9(10):2700-2713.
185. Alley SC, Zhang X, Okeley NM, et al. The pharmacologic basis for antibody-auristatin conjugate activity. *J Pharmacol Exp Ther.* 2009;330(3):932-938.
186. Okeley NM, Miyamoto JB, Zhang X, et al. Intracellular activation of SGN-35, a potent anti-CD30 antibody-drug conjugate. *Clin Cancer Res.* 2010;16(3):888-897.
187. Mantaj J, Jackson PJM, Rahman KM, Thurston DE. From anthramycin to pyrrolobenzodiazepine (PBD)-containing antibody–drug conjugates (ADCs). *Angew Chem Int Ed Engl.* 2017;56(2):462-488.
188. Erickson HK, Widdison WC, Mayo MF, et al. Tumor delivery and in vivo processing of disulfide-linked and thioether-linked antibody-maytansinoid conjugates. *Bioconjug Chem.* 2010;21(1):84-92.
189. Erickson HK, Lewis Phillips GD, Leipold DD, et al. The effect of different linkers on target cell catabolism and pharmacokinetics/pharmacodynamics of trastuzumab maytansinoid conjugates. *Mol Cancer Ther.* 2012;11(5):1133-1142.
190. Erickson HK, Lambert JM. ADME of antibody-maytansinoid conjugates. *AAPS J.* 2012;14(4):799-805.
191. Allen TM. Ligand-targeted therapeutics in anticancer therapy. *Nat Rev Cancer.* 2002;2(10):750-763.
192. Erickson HK, Park PU, Widdison WC, et al. Antibody-maytansinoid conjugates are activated in targeted cancer cells by lysosomal degradation and linker-dependent intracellular processing. *Cancer Res.* 2006;66(8):4426-4433.
193. Kovtun YV, Audette CA, Ye Y, et al. Antibody-drug conjugates designed to eradicate tumors with homogeneous and heterogeneous expression of the target antigen. *Cancer Res.* 2006;66(6):3214-3221.
194. Golfier S, Kopitz C, Kahnert A, et al. Anetumab ravtansine: A novel mesothelin-targeting antibody-drug conjugate cures tumors with heterogeneous target expression favored by bystander effect. *Mol Cancer Ther.* 2014;13(6):1537-1548.
195. de Souza EG, Hara CC, Fagundes DL, et al. Maternal-foetal diabetes modifies neonatal Fc receptor expression on human leucocytes. *Scand J Immunol.* 2016;84(4):237-244.
196. Singh AP, Sharma S, Shah DK. Quantitative characterization of in vitro bystander effect of antibody-drug conjugates. *J Pharmacokinet Pharmacodyn.* 2016;43(6):567-582.
197. Ogitani Y, Aida T, Hagihara K, et al. DS-8201a, a novel HER2-targeting ADC with a novel DNA topoisomerase I inhibitor, demonstrates a promising antitumor efficacy with differentiation from T-DM1. *Clin Cancer Res.* 2016;22(20):5097-5108.
198. Kovtun YV, Audette CA, Mayo MF, et al. Antibody-maytansinoid conjugates designed to bypass multidrug resistance. *Cancer Res.* 2010;70(6):2528-2537.

199. Tang R, Cohen S, Perrot J-Y, et al. P-gp activity is a critical resistance factor against AVE9633 and DM4 cytotoxicity in leukaemia cell lines, but not a major mechanism of chemoresistance in cells from acute myeloid leukaemia patients. *BMC Cancer.* 2009;9:199-199.
200. Toppmeyer DL, Slapak CA, Croop J, Kufe DW. Role of p-glycoprotein in dolastatin 10 resistance. *Biochem Pharmacol.* 1994;48(3):609-612.
201. Beeram M, Krop IE, Burris HA, et al. A phase 1 study of weekly dosing of trastuzumab emtansine (T-DM1) in patients with advanced human epidermal growth factor 2-positive breast cancer. *Cancer.* 2012;118(23):5733-5740.
202. Wang H, Rangan VS, Sung MC, et al. Pharmacokinetic characterization of BMS-936561, an anti-CD70 antibody-drug conjugate, in preclinical animal species and prediction of its pharmacokinetics in humans. *Biopharm Drug Dispos.* 2016;37(2):93-106.
203. Widdison W, Wilhelm S, Veale K, et al. Metabolites of antibody-maytansinoid conjugates: characteristics and in vitro potencies. *Mol Pharm.* 2015;12(6):1762-1773.
204. Yurkovetskiy AV, Yin M, Bodyak N, et al. A polymer-based antibody-vinca drug conjugate platform: Characterization and preclinical efficacy. *Cancer Res.* 2015;75(16):3365-3372.
205. Behrens CR, Ha EH, Chinn LL, et al. Antibody-drug conjugates derived from interchain cysteine cross-linking demonstrate improved homogeneity and other pharmacological properties over conventional heterogeneous ADCs. *Mol Pharm.* 2015;12(11):3986-3998.
206. Hamblett KJ, Senter PD, Chace DF, et al. Effects of drug loading on the antitumor activity of a monoclonal antibody drug conjugate. *Clin Cancer Res.* 2004;10(20):7063-7070.
207. Strop P, Delaria K, Foletti D, et al. Site-specific conjugation improves therapeutic index of antibody drug conjugates with high drug loading. *Nat Biotechnol.* 2015;33(7):694-696.
208. Lyon RP, Bovee TD, Doronina SO, et al. Reducing hydrophobicity of homogeneous antibody-drug conjugates improves pharmacokinetics and therapeutic index. *Nat Biotech.* 2015;33(7):733-735.
209. Zhao RY, Wilhelm SD, Audette C, et al. Synthesis and evaluation of hydrophilic linkers for antibody-maytansinoid conjugates. *J Med Chem.* 2011;54(10):3606-3623.
210. Schumacher D, Hackenberger CP, Leonhardt H, Helma J. Current status: Site-specific antibody drug conjugates. *J Clin Immunol.* 2016;36 Suppl 1:100-107.
211. Behrens CR, Liu B. Methods for site-specific drug conjugation to antibodies. *mAbs.* 2014;6(1):46-53.
212. Chudasama V, Maruani A, Caddick S. Recent advances in the construction of antibody-drug conjugates. *Nat Chem.* 2016;8(2):114-119.
213. Sochaj AM, Swiderska KW, Otlewski J. Current methods for the synthesis of homogeneous antibody-drug conjugates. *Biotechnol Adv.* 2015;33(6 Pt 1):775-784.
214. Pillow TH, Tien J, Parsons-Reponte KL, et al. Site-specific trastuzumab maytansinoid antibody-drug conjugates with improved therapeutic activity through linker and antibody engineering. *J Med Chem.* 2014;57(19):7890-7899.
215. Thompson P, Fleming R, Bezabeh B, et al. Rational design, biophysical and biological characterization of site-specific antibody-tubulysin conjugates with improved stability, efficacy and pharmacokinetics. *J Control Release.* 2016;236:100-116.
216. Strop P, Tran TT, Dorywalska M, et al. RN927C, a site-specific Trop-2 antibody-drug conjugate with enhanced stability, is highly efficacious in preclinical solid tumor models. *Mol Cancer Ther.* 2016;15(11):2698-2708.
217. Shen BQ, Xu K, Liu L, et al. Conjugation site modulates the in vivo stability and therapeutic activity of antibody-drug conjugates. *Nat Biotechnol.* 2012;30(2):184-189.

218. Strop P, Liu SH, Dorywalska M, et al. Location matters: Site of conjugation modulates stability and pharmacokinetics of antibody drug conjugates. *Chem Biol.* 2013;20(2):161-167.
219. Dorywalska M, Strop P, Melton-Witt JA, et al. Site-dependent degradation of a non-cleavable auristatin-based linker-payload in rodent plasma and its effect on ADC efficacy. *PLoS One.* 2015;10(7):e0132282.
220. Dorywalska M, Strop P, Melton-Witt JA, et al. Effect of attachment site on stability of cleavable antibody drug conjugates. *Bioconjug Chem.* 2015;26(4):650-659.
221. Gikanga B, Adeniji NS, Patapoff TW, Chih HW, Yi L. Cathepsin B cleavage of vcMMAE-based antibody-drug conjugate is not drug location or monoclonal antibody carrier specific. *Bioconjug Chem.* 2016;27(4):1040-1049.
222. Bryant P, Pabst M, Badescu G, et al. In vitro and in vivo evaluation of cysteine rebridged trastuzumab-MMAE antibody drug conjugates with defined drug-to-antibody ratios. *Mol Pharm.* 2015;12(6):1872-1879.
223. Maruani A, Smith ME, Miranda E, Chester KA, Chudasama V, Caddick S. A plug-and-play approach to antibody-based therapeutics via a chemoselective dual click strategy. *Nat Commun.* 2015;6:6645.
224. Thurber GM, Dane Wittrup K. A mechanistic compartmental model for total antibody uptake in tumors. *J Theor Biol.* 2012;314:57-68.
225. Minchinton AI, Tannock IF. Drug penetration in solid tumours. *Nat Rev Cancer.* 2006;6(8):583-592.
226. Carmeliet P, Jain RK. Angiogenesis in cancer and other diseases. *Nature.* 2000;407(6801):249-257.
227. Baker JH, Lindquist KE, Huxham LA, Kyle AH, Sy JT, Minchinton AI. Direct visualization of heterogeneous extravascular distribution of trastuzumab in human epidermal growth factor receptor type 2 overexpressing xenografts. *Clin Cancer Res.* 2008;14(7):2171-2179.
228. Jain RK, Baxter LT. Mechanisms of heterogeneous distribution of monoclonal antibodies and other macromolecules in tumors: Significance of elevated interstitial pressure. *Cancer Res.* 1988;48(24 Pt 1):7022-7032.
229. Dudley AC. Tumor endothelial cells. *Cold Spring Harb Perspect Med.* 2012;2(3):a006536.
230. Heine M, Freund B, Nielsen P, et al. High interstitial fluid pressure is associated with low tumour penetration of diagnostic monoclonal antibodies applied for molecular imaging purposes. *PLoS One.* 2012;7(5):e36258.
231. Jain RK. Transport of molecules in the tumor interstitium: A review. *Cancer Res.* 1987;47(12):3039-3051.
232. Jain RK. Transport of molecules across tumor vasculature. *Cancer Metastasis Rev.* 1987;6(4):559-593.
233. Heldin C-H, Rubin K, Pietras K, Ostman A. High interstitial fluid pressure - An obstacle in cancer therapy. *Nat Rev Cancer.* 2004;4(10):806-813.
234. Curti BD, Urba WJ, Alvord WG, et al. Interstitial pressure of subcutaneous nodules in melanoma and lymphoma patients: Changes during treatment. *Cancer Res.* 1993;53(10 Suppl):2204-2207.
235. Roh HD, Boucher Y, Kalnicki S, Buchsbaum R, Bloomer WD, Jain RK. Interstitial hypertension in carcinoma of uterine cervix in patients: Possible correlation with tumor oxygenation and radiation response. *Cancer Res.* 1991;51(24):6695-6698.
236. Milosevic M, Fyles A, Hedley D, et al. Interstitial fluid pressure predicts survival in patients with cervix cancer independent of clinical prognostic factors and tumor oxygen measurements. *Cancer Res.* 2001;61(17):6400-6405.

237. Jain RK. Normalization of tumor vasculature: An emerging concept in antiangiogenic therapy. *Science.* 2005;307(5706):58-62.
238. Mohammadi M, Chen P. Effect of microvascular distribution and its density on interstitial fluid pressure in solid tumors: A computational model. *Microvasc Res.* 2015;101:26-32.
239. Gremonprez F, Descamps B, Izmer A, et al. Pretreatment with VEGF(R)-inhibitors reduces interstitial fluid pressure, increases intraperitoneal chemotherapy drug penetration, and impedes tumor growth in a mouse colorectal carcinomatosis model. *Oncotarget.* 2015;6(30):29889-29900.
240. O'Connor JP, Carano RA, Clamp AR, et al. Quantifying antivascular effects of monoclonal antibodies to vascular endothelial growth factor: Insights from imaging. *Clin Cancer Res.* 2009;15(21):6674-6682.
241. Yuan F, Chen Y, Dellian M, Safabakhsh N, Ferrara N, Jain RK. Time-dependent vascular regression and permeability changes in established human tumor xenografts induced by an anti-vascular endothelial growth factor/vascular permeability factor antibody. *Proc Natl Acad Sci USA.* 1996;93(25):14765-14770.
242. Yang AD, Bauer TW, Camp ER, et al. Improving delivery of antineoplastic agents with anti-vascular endothelial growth factor therapy. *Cancer.* 2005;103(8):1561-1570.
243. Arjaans M, Oude Munnink TH, Oosting SF, et al. Bevacizumab-induced normalization of blood vessels in tumors hampers antibody uptake. *Cancer Res.* 2013;73(11):3347-3355.
244. Pastuskovas CV, Mundo EE, Williams SP, et al. Effects of anti-VEGF on pharmacokinetics, biodistribution, and tumor penetration of trastuzumab in a preclinical breast cancer model. *Mol Cancer Ther.* 2012;11(3):752-762.
245. Abuqayyas L, Balthasar JP. Pharmacokinetic mAb-mAb interaction: Anti-VEGF mAb decreases the distribution of anti-CEA mAb into colorectal tumor xenografts. *AAPS J.* 2012;14(3):445-455.
246. Rajkumar VS, Boxer G, Robson M, Muddle J, Papastavrou Y, Pedley RB. A comparative study of PDGFR inhibition with imatinib on radiolabeled antibody targeting and clearance in two pathologically distinct models of colon adenocarcinoma. *Tumour Biol.* 2012;33(6):2019-2029.
247. Baranowska-Kortylewicz J, Abe M, Pietras K, et al. Effect of platelet-derived growth factor receptor-β inhibition with STI571 on radioimmunotherapy. *Cancer Res.* 2005;65(17):7824-7831.
248. Hofmann M, McCormack E, Mujic M, et al. Increased plasma colloid osmotic pressure facilitates the uptake of therapeutic macromolecules in a xenograft tumor model. *Neoplasia.* 2009;11(8):812-822.
249. Baronzio G, Parmar G, Baronzio M. Overview of methods for overcoming hindrance to drug delivery to tumors, with special attention to tumor interstitial fluid. *Front Oncol.* 2015;5:165.
250. Matsumura Y, Maeda H. A new concept for macromolecular therapeutics in cancer chemotherapy: Mechanism of tumoritropic accumulation of proteins and the antitumor agent smancs. *Cancer Res.* 1986;46(12 Part 1):6387-6392.
251. Noguchi Y, Wu J, Duncan R, et al. Early phase tumor accumulation of macromolecules: A great difference in clearance rate between tumor and normal tissues. *Jpn J Cancer Res.* 1998;89(3):307-314.
252. Maeda H. Vascular permeability in cancer and infection as related to macromolecular drug delivery, with emphasis on the EPR effect for tumor-selective drug targeting. *Proc Jpn Acad Ser B Phys Biol Sci.* 2012;88(3):53-71.

253. Nagamitsu A, Greish K, Maeda H. Elevating blood pressure as a strategy to increase tumor-targeted delivery of macromolecular drug SMANCS: Cases of advanced solid tumors. *Jpn J Clin Oncol.* 2009;39(11):756-766.
254. Netti PA, Berk DA, Swartz MA, Grodzinsky AJ, Jain RK. Role of extracellular matrix assembly in interstitial transport in solid tumors. *Cancer Res.* 2000;60(9):2497-2503.
255. Commisso C, Davidson SM, Soydaner-Azeloglu RG, et al. Macropinocytosis of protein is an amino acid supply route in Ras-transformed cells. *Nature.* 2013;497(7451):633-637.
256. Ha KD, Bidlingmaier SM, Zhang Y, Su Y, Liu B. High-content analysis of antibody phage-display library selection outputs identifies tumor selective macropinocytosis-dependent rapidly internalizing antibodies. *Mol Cell Proteomics.* 2014;13(12):3320-3331.
257. Hagan PL, Halpern SE, Dillman RO, et al. Tumor size: Effect on monoclonal antibody uptake in tumor models. *J Nucl Med.* 1986;27(3):422-427.
258. Pedley RB, Boden J, Keep PA, Harwood PJ, Green AJ, Rogers GT. Relationship between tumour size and uptake of radiolabelled anti-CEA in a colon tumour xenograft. *Eur J Nucl Med.* 1987;13(4):197-202.
259. Williams LE, Duda RB, Proffitt RT, et al. Tumor uptake as a function of tumor mass: A mathematic model. *J Nucl Med.* 1988;29(1):103-109.
260. Kinuya S, Yokoyama K, Kawashima A, et al. Radioimmunotherapy with 186Re-labeled monoclonal antibody to treat liver metastases of colon cancer cells in nude mice. *Cancer Biother Radiopharm.* 2002;17(6):681-687.
261. Kinuya S, Li X-F, Yokoyama K, et al. Intraperitoneal radioimmunotherapy in treating peritoneal carcinomatosis of colon cancer in mice compared with systemic radioimmunotherapy. *Cancer Sci.* 2003;94(7):650-654.
262. Li X-F, Kinuya S, Yokoyama K, et al. Benefits of combined radioimmunotherapy and anti-angiogenic therapy in a liver metastasis model of human colon cancer cells. *Eur J Nucl Med Mol Imaging.* 2002;29(12):1669-1674.
263. Dearling JL, Flynn AA, Qureshi U, et al. Localization of radiolabeled anti-CEA antibody in subcutaneous and intrahepatic colorectal xenografts: Influence of tumor size and location within host organ on antibody uptake. *Nucl Med Biol.* 2009;36(8):883-894.
264. Muller P, Kreuzaler M, Khan T, et al. Trastuzumab emtansine (T-DM1) renders HER2+ breast cancer highly susceptible to CTLA-4/PD-1 blockade. *Sci Transl Med.* 2015;7(315):315ra188.
265. Schmidt H. SBPOP Package: efficient support for model based drug development—from mechanistic models to complex trial simulation. *PAGE meeting, Glasgow.* 2013.
266. Willmann S, Hohn K, Edginton A, et al. Development of a physiology-based whole-body population model for assessing the influence of individual variability on the pharmacokinetics of drugs. *J Pharmacokinet Pharmacodyn.* 2007;34(3):401-431.
267. Cao Y, Jusko WJ. Incorporating target-mediated drug disposition in a minimal physiologically-based pharmacokinetic model for monoclonal antibodies. *J Pharmacokinet Pharmacodyn.* 2014;41(4):375-387.
268. Li L, Gardner I, Rose R, Jamei M. Incorporating target shedding into a minimal PBPK-TMDD model for monoclonal antibodies. *CPT Pharmacometrics Syst Pharmacol.* 2014;3(1):e96.
269. Hendriks BS, Opresko LK, Wiley HS, Lauffenburger D. Quantitative analysis of HER2-mediated effects on HER2 and epidermal growth factor receptor endocytosis: distribution of homo- and heterodimers depends on relative HER2 levels. *J Biol Chem.* 2003;278(26):23343-23351.

270. Hendriks BS, Opresko LK, Wiley HS, Lauffenburger D. Coregulation of epidermal growth factor receptor/human epidermal growth factor receptor 2 (HER2) levels and locations: quantitative analysis of HER2 overexpression effects. *Cancer Res.* 2003;63(5):1130-1137.
271. Shankaran H, Wiley HS, Resat H. Modeling the effects of HER/ErbB1-3 coexpression on receptor dimerization and biological response. *Biophys J.* 2006;90(11):3993-4009.
272. Resat H, Ewald JA, Dixon DA, Wiley HS. An integrated model of epidermal growth factor receptor trafficking and signal transduction. *Biophys J.* 2003;85(2):730-743.
273. Valabrega G, Montemurro F, Sarotto I, et al. TGFalpha expression impairs trastuzumab-induced HER2 downregulation. *Oncogene.* 2005;24(18):3002-3010.
274. Stancovski I, Hurwitz E, Leitner O, Ullrich A, Yarden Y, Sela M. Mechanistic aspects of the opposing effects of monoclonal antibodies to the ERBB2 receptor on tumor growth. *Proc Natl Acad Sci USA.* 1991;88(19):8691-8695.
275. Zhu W, Okollie B, Artemov D. Controlled internalization of Her-2/neu receptors by cross-linking for targeted delivery. *Cancer Biol Ther.* 2007;6(12):1960-1966.
276. Austin CD, De Maziere AM, Pisacane PI, et al. Endocytosis and sorting of ErbB2 and the site of action of cancer therapeutics trastuzumab and geldanamycin. *Mol Biol Cell.* 2004;15(12):5268-5282.
277. Morita J, Tanaka M, Nomoto M, et al. Pharmacokinetic bioequivalence, safety, and immunogenicity of DMB-3111, a trastuzumab biosimilar, and trastuzumab in healthy japanese adult males: results of a randomized trial. *BioDrugs.* 2016;30(1):17-25.
278. Wisman LA, De Cock EP, Reijers JA, et al. A phase I dose-escalation and bioequivalence study of a trastuzumab biosimilar in healthy male volunteers. *Clin Drug Investig.* 2014;34(12):887-894.
279. Wynne C, Harvey V, Schwabe C, Waaka D, McIntyre C, Bittner B. Comparison of subcutaneous and intravenous administration of trastuzumab: A phase I/Ib trial in healthy male volunteers and patients with HER2-positive breast cancer. *J Clin Pharmacol.* 2013;53(2):192-201.
280. Yin D, Barker KB, Li R, et al. A randomized phase 1 pharmacokinetic trial comparing the potential biosimilar PF-05280014 with trastuzumab in healthy volunteers. *Br J Clin Pharmacol.* 2014;78(6):1281-1290.
281. Tokuda Y, Watanabe T, Omuro Y, et al. Dose escalation and pharmacokinetic study of a humanized anti-HER2 monoclonal antibody in patients with HER2/neu-overexpressing metastatic breast cancer. *Br J Cancer.* 1999;81(8):1419-1425.
282. Baselga J, Carbonell X, Castaneda-Soto NJ, et al. Phase II study of efficacy, safety, and pharmacokinetics of trastuzumab monotherapy administered on a 3-weekly schedule. *J Clin Oncol.* 2005;23(10):2162-2171.
283. Cobleigh MA, Vogel CL, Tripathy D, et al. Multinational study of the efficacy and safety of humanized anti-HER2 monoclonal antibody in women who have HER2-overexpressing metastatic breast cancer that has progressed after chemotherapy for metastatic disease. *J Clin Oncol.* 1999;17(9):2639-2648.
284. Leyland-Jones B, Gelmon K, Ayoub JP, et al. Pharmacokinetics, safety, and efficacy of trastuzumab administered every three weeks in combination with paclitaxel. *J Clin Oncol.* 2003;21(21):3965-3971.
285. Di Gioia D, Dresse M, Mayr D, et al. Serum HER2 supports HER2-testing in tissue at the time of primary diagnosis of breast cancer. *Clinica Chimica Acta.* 2014;430:86-91.
286. Lam L, Czerniecki BJ, Fitzpatrick E, et al. Interference-free HER2 ECD as a serum biomarker in breast cancer. *J Mol Biomark Diagn.* 2014;4(3):151.

287. McCarthy KM, Lam M, Subramanian L, et al. Effects of mutations in potential phosphorylation sites on transcytosis of FcRn. *J Cell Sci.* 2001;114(Pt 8):1591-1598.
288. Suzuki T, Ishii-Watabe A, Tada M, et al. Importance of neonatal FcR in regulating the serum half-life of therapeutic proteins containing the Fc domain of human IgG1: A comparative study of the affinity of monoclonal antibodies and Fc-fusion proteins to human neonatal FcR. *J Immunol.* 2010;184(4):1968-1976.
289. Li L, Gardner I, Dostalek M, Jamei M. Simulation of monoclonal antibody pharmacokinetics in humans using a minimal physiologically based model. *AAPS J.* 2014;16(5):1097-1109.
290. Lua W-H, Gan SK-E, Lane DP, Verma CS. A search for synergy in the binding kinetics of trastuzumab and pertuzumab whole and F(ab) to HER2. *NPJ Breast Cancer.* 2015;1:15012.
291. Troise F, Cafaro V, Giancola C, D'Alessio G, De Lorenzo C. Differential binding of human immunoagents and Herceptin to the ErbB2 receptor. *FEBS J.* 2008;275(20):4967-4979.
292. Larson JS, Goodman LJ, Tan Y, et al. Analytical validation of a highly quantitative, sensitive, accurate, and reproducible assay (HERmark) for the measurement of HER2 total protein and HER2 homodimers in FFPE breast cancer tumor specimens. *Patholog Res Int.* 2010;2010:814176.
293. Olsen DA, Ostergaard B, Bokmand S, et al. HER1-4 protein concentrations in normal breast tissue from breast cancer patients are expressed by the same profile as in the malignant tissue. *Clin Chem Lab Med.* 2009;47(8):977-984.
294. Huang W, Reinholz M, Weidler J, et al. Comparison of central HER2 testing with quantitative total HER2 expression and HER2 homodimer measurements using a novel proximity-based assay. *Am J Clin Pathol.* 2010;134(2):303-311.
295. Bianconi E, Piovesan A, Facchin F, et al. An estimation of the number of cells in the human body. *Ann Hum Biol.* 2013;40(6):463-471.
296. Cho H-S, Mason K, Ramyar KX, et al. Structure of the extracellular region of HER2 alone and in complex with the Herceptin Fab. *Nature.* 2003;421(6924):756-760.
297. Saltelli A, Annoni P, Azzini I, Campolongo F, Ratto M, Tarantola S. Variance based sensitivity analysis of model output: Design and estimator for the total sensitivity index. *Comput Phys Commun.* 2010;181(2):259-270.
298. Homma T, Saltelli A. Importance measures in global sensitivity analysis of nonlinear models. *Reliab Eng Syst Saf.* 1996;52(1):1-17.
299. Jacquez JA, Greif P. Numerical parameter identifiability and estimability: Integrating identifiability, estimability, and optimal sampling design. *Math Biosci.* 1985;77(1):201-227.
300. Gill KL, Machavaram KK, Rose RH, Chetty M. Potential sources of inter-subject variability in monoclonal antibody pharmacokinetics. *Clin Pharmacokinet.* 2016;55(7):789-805.
301. Parving HH, Worm AM, Rossing N. Plasma volume, intravascular albumin and its transcapillary escape rate in patients with extensive skin disease. *Br J Dermatol.* 1976;95(5):519-524.
302. Leung HWC, Chan ALF. Trastuzumab-induced cardiotoxicity in elderly women with HER-2-positive breast cancer: A meta-analysis of real-world data. *Expert Opin Drug Saf.* 2015;14(11):1661-1671.
303. Carney WP. Circulating oncoproteins HER2/neu, EGFR and CAIX (MN) as novel cancer biomarkers. *Expert Rev Mol Diagn.* 2007;7(3):309-319.
304. Carney WP, Neumann R, Lipton A, Leitzel K, Ali S, Price CP. Potential clinical utility of serum HER-2/neu oncoprotein concentrations in patients with breast cancer. *Clin Chem.* 2003;49(10):1579-1598.

305. Ghedini GC, Ciravolo V, Tortoreto M, et al. Shed HER2 extracellular domain in HER2-mediated tumor growth and in trastuzumab susceptibility. *J Cell Physiol.* 2010;225(1):256-265.
306. Esteva FJ, Cheli CD, Fritsche H, et al. Clinical utility of serum HER2/neu in monitoring and prediction of progression-free survival in metastatic breast cancer patients treated with trastuzumab-based therapies. *Breast Cancer Res.* 2005;7(4):R436-443.
307. Tse C, Brault D, Gligorov J, et al. Evaluation of the quantitative analytical methods real-time PCR for HER-2 gene quantification and ELISA of serum HER-2 protein and comparison with fluorescence in situ hybridization and immunohistochemistry for determining HER-2 status in breast cancer patients. *Clin Chem.* 2005;51(7):1093-1101.
308. Fornier MN, Seidman AD, Schwartz MK, et al. Serum HER2 extracellular domain in metastatic breast cancer patients treated with weekly trastuzumab and paclitaxel: association with HER2 status by immunohistochemistry and fluorescence in situ hybridization and with response rate. *Ann Oncol.* 2005;16(2):234-239.
309. Kostler WJ, Schwab B, Singer CF, et al. Monitoring of serum Her-2/neu predicts response and progression-free survival to trastuzumab-based treatment in patients with metastatic breast cancer. *Clin Cancer Res.* 2004;10(5):1618-1624.
310. Bethune-Volters A, Labroquere M, Guepratte S, et al. Longitudinal changes in serum HER-2/neu oncoprotein levels in trastuzumab-treated metastatic breast cancer patients. *Anticancer Res.* 2004;24(2C):1083-1089.
311. Chen Y, Balthasar JP. Evaluation of a catenary PBPK model for predicting the in vivo disposition of mAbs engineered for high-affinity binding to FcRn. *AAPS J.* 2012;14(4):850-859.
312. Edginton AN. Knowledge-driven approaches for the guidance of first-in-children dosing. *Paediatr Anaesth.* 2011;21(3):206-213.
313. Tod M, Jullien V, Pons G. Facilitation of drug evaluation in children by population methods and modelling. *Clin Pharmacokinet.* 2008;47(4):231-243.
314. Mahmood I, Tegenge MA. A comparative study between allometric scaling and physiologically based pharmacokinetic modeling for the prediction of drug clearance from neonates to adolescents. *J Clin Pharmacol.* 2019;59(2):189-197.
315. Wang J, Edginton AN, Avant D, Burckart GJ. Predicting neonatal pharmacokinetics from prior data using population pharmacokinetic modeling. *J Clin Pharmacol.* 2015;55(10):1175-1183.
316. Mansoor N, Ahmad T, Alam Khan R, Sharib SM, Mahmood I. Prediction of clearance and dose of midazolam in preterm and term neonates: A comparative study between allometric scaling and physiologically based pharmacokinetic modeling. *Am J Ther.* 2019;26(1):e32-e37.
317. Claassen K, Thelen K, Coboeken K, et al. Development of a physiologically-based pharmacokinetic model for preterm neonates: Evaluation with in vivo data. *Curr Pharm Des.* 2015;21(39):5688-5698.
318. Ferl GZ, Theil FP, Wong H. Physiologically based pharmacokinetic models of small molecules and therapeutic antibodies: a mini-review on fundamental concepts and applications. *Biopharm Drug Dispos.* 2016;37(2):75-92.
319. Hardiansyah D, Ng CM. Effects of the FcRn developmental pharmacology on the pharmacokinetics of therapeutic monoclonal IgG antibody in pediatric subjects using minimal physiologically-based pharmacokinetic modelling. *mAbs.* 2018;10(7):1144-1156.

320. Candon S, Mosca A, Ruemmele F, Goulet O, Chatenoud L, Cézard J-P. Clinical and biological consequences of immunization to infliximab in pediatric Crohn's disease. *Clin Immunol.* 2006;118(1):11-19.
321. Hyams J, Walters TD, Crandall W, et al. Safety and efficacy of maintenance infliximab therapy for moderate-to-severe Crohn's disease in children: REACH open-label extension. *Curr Med Res Opin.* 2011;27(3):651-662.
322. Hämäläinen A, Sipponen T, Kolho K-L. Serum infliximab concentrations in pediatric inflammatory bowel disease. *Scand J Gastroenterol.* 2013;48(1):35-41.
323. Baldassano R, Braegger CP, Escher JC, et al. Infliximab (Remicade) therapy in the treatment of pediatric Crohn's disease. *Am J Gastroenterol.* 2003;98(4):833-838.
324. Singh N, Rosenthal CJ, Melmed GY, et al. Early infliximab trough levels are associated with persistent remission in pediatric patients with inflammatory bowel disease. *Inflamm Bowel Dis.* 2014;20(10):1708-1713.
325. Adedokun OJ, Xu Z, Padgett L, et al. Pharmacokinetics of infliximab in children with moderate-to-severe ulcerative colitis: Results from a randomized, multicenter, open-label, phase 3 study. *Inflamm Bowel Dis.* 2013;19(13):2753-2762.
326. Ruperto N, Lovell DJ, Cuttica R, et al. A randomized, placebo-controlled trial of infliximab plus methotrexate for the treatment of polyarticular-course juvenile rheumatoid arthritis. *Arthritis Rheum.* 2007;56(9):3096-3106.
327. Kaymakcalan Z, Sakorafas P, Bose S, et al. Comparisons of affinities, avidities, and complement activation of adalimumab, infliximab, and etanercept in binding to soluble and membrane tumor necrosis factor. *Clin Immunol.* 2009;131(2):308-316.
328. van Schie KA, Kruithof S, Ooijevaar-de Heer P, et al. Restricted immune activation and internalisation of anti-idiotype complexes between drug and antidrug antibodies. *Ann Rheum Dis.* 2018;77(10):1471-1479.
329. Manicourt DH, Triki R, Fukuda K, Devogelaer JP, Nagant de Deuxchaisnes C, Thonar EJ. Levels of circulating tumor necrosis factor alpha and interleukin-6 in patients with rheumatoid arthritis - Relationship to serum levels of hyaluronan and antigenic keratan sulfate. *Arthritis Rheum.* 1993;36(4):490-499.
330. Bal A, Unlu E, Bahar G, Aydog E, Eksioglu E, Yorgancioglu R. Comparison of serum IL-1 beta, sIL-2R, IL-6, and TNF-alpha levels with disease activity parameters in ankylosing spondylitis. *Clin Rheumatol.* 2007;26(2):211-215.
331. Kleiner G, Marcuzzi A, Zanin V, Monasta L, Zauli G. Cytokine levels in the serum of healthy subjects. *Mediators Inflamm.* 2013;2013:434010.
332. Korolkova OY, Myers JN, Pellom ST, Wang L, M'Koma AE. Characterization of serum cytokine profile in predominantly colonic inflammatory bowel disease to delineate ulcerative and Crohn's colitides. *Clin Med Insights Gastroenterol.* 2015;8:29-44.
333. Arican O, Aral M, Sasmaz S, Ciragil P. Serum levels of TNF-alpha, IFN-gamma, IL-6, IL-8, IL-12, IL-17, and IL-18 in patients with active psoriasis and correlation with disease severity. *Mediators Inflamm.* 2005;2005(5):273-279.
334. Stepensky D. Local versus systemic anti-tumour necrosis factor-alpha effects of adalimumab in rheumatoid arthritis. *Clin Pharmacokinet.* 2012;51(7):443-455.
335. Chen X, DuBois DC, Almon RR, Jusko WJ. Characterization and interspecies scaling of tumour necrosis factor-alpha pharmacokinetics with minimal physiologically based pharmacokinetic models. *Drug Metab Dispos.* 2017;45(7):798-806.
336. Ren Y, Li L, Kirshner S, Wang Y, Sahajwalla C, Ji P. A model-based approach to quantify the time-course of anti-drug antibodies for therapeutic proteins. *Clin Pharmacol Ther.* 2019;105(4):970-978.

337. Rojas JR, Taylor RP, Cunningham MR, et al. Formation, distribution, and elimination of infliximab and anti-infliximab immune complexes in cynomolgus monkeys. *J Pharmacol Exp Ther.* 2005;313(2):578-585.
338. Li X, Jusko WJ, Cao Y. Role of interstitial fluid turnover on target suppression by therapeutic biologics using a minimal physiologically based pharmacokinetic model. *J Pharmacol Exp Ther.* 2018;367(1):1-8.
339. Chen X, Jiang X, Jusko WJ, Zhou H, Wang W. Minimal physiologically-based pharmacokinetic (mPBPK) model for a monoclonal antibody against interleukin-6 in mice with collagen-induced arthritis. *J Pharmacokinet Pharmacodyn.* 2016;43(3):291-304.
340. Olsen T, Goll R, Cui G, et al. Tissue levels of tumor necrosis factor-alpha correlates with grade of inflammation in untreated ulcerative colitis. *Scand J Gastroenterol.* 2007;42(11):1312-1320.
341. Olszewski WL, Pazdur J, Kubasiewicz E, Zaleska M, Cooke CJ, Miller NE. Lymph draining from foot joints in rheumatoid arthritis provides insight into local cytokine and chemokine production and transport to lymph nodes. *Arthritis Rheum.* 2001;44(3):541-549.
342. Chen X, DuBois DC, Almon RR, Jusko WJ. Interrelationships between infliximab and recombinant tumor necrosis factor-alpha in plasma using minimal physiologically-based pharmacokinetic (mPBPK) models. *Drug Metab Dispos.* 2017;45(7):790-797.
343. Baert F, Noman M, Vermeire S, et al. Influence of immunogenicity on the long-term efficacy of infliximab in Crohn's disease. *N Engl J Med.* 2003;348(7):601-608.
344. Chen X, Hickling TP, Vicini P. A mechanistic, multiscale mathematical model of immunogenicity for therapeutic proteins: Part 1 - theoretical model. *CPT Pharmacometrics Syst Pharmacol.* 2014;3(9):e133.
345. Yoo DH, Hrycaj P, Miranda P, et al. A randomised, double-blind, parallel-group study to demonstrate equivalence in efficacy and safety of CT-P13 compared with innovator infliximab when coadministered with methotrexate in patients with active rheumatoid arthritis: The PLANETRA study. *Ann Rheum Dis.* 2013;72(10):1613-1620.
346. Brandse JF, Mathôt RA, van der Kleij D, et al. Pharmacokinetic features and presence of antidrug antibodies associate with response to infliximab induction therapy in patients with moderate to severe ulcerative colitis. *Clin Gastroenterol Hepatol.* 2016;14(2):251-258.e252.
347. Shin D, Kim Y, Kim YS, Kornicke T, Fuhr R. A randomized, phase I pharmacokinetic study comparing SB2 and infliximab reference product (Remicade) in healthy subjects. *BioDrugs.* 2015;29(6):381-388.
348. Takeuchi T, Yamanaka H, Tanaka Y, et al. Evaluation of the pharmacokinetic equivalence and 54-week efficacy and safety of CT-P13 and innovator infliximab in Japanese patients with rheumatoid arthritis. *Mod Rheumatol.* 2015;25(6):817-824.
349. Lambert J, Wyand M, Lassen C, et al. Bioavailability, safety and immunogenicity of biosimilar infliximab (BOW015) compared to reference infliximab. *Int J Clin Pharmacol Ther.* 2016;54(4):315-322.
350. Udata C, Hua SY, Yin D, Salts S, Meng X, Rehman MI. A phase I pharmacokinetics trial comparing PF-06438179 (a potential biosimilar) and infliximab in healthy volunteers. *Ann Rheum Dis.* 2014;73(Suppl 2):494.
351. Park W, Lee SJ, Yun J, Yoo DH. Comparison of the pharmacokinetics and safety of three formulations of infliximab (CT-P13, EU-approved reference infliximab and the US-licensed reference infliximab) in healthy subjects: A randomized, double-blind, three-arm, parallel-group, single-dose, phase I study. *Expert Rev Clin Immunol.* 2015;11 Suppl 1:S25-S31.

352. Maini R, St Clair EW, Breedveld F, et al. Infliximab (chimeric anti-tumour necrosis factor alpha monoclonal antibody) versus placebo in rheumatoid arthritis patients receiving concomitant methotrexate: A randomised phase III trial. *Lancet.* 1999;354(9194):1932-1939.
353. St. Clair EW, Wagner CL, Fasanmade AA, et al. The relationship of serum infliximab concentrations to clinical improvement in rheumatoid arthritis: Results from ATTRACT, a multicenter, randomized, double-blind, placebo-controlled trial. *Arthritis Rheum.* 2002;46(6):1451-1459.
354. Park W, Hrycaj P, Jeka S, et al. A randomised, double-blind, multicentre, parallel-group, prospective study comparing the pharmacokinetics, safety, and efficacy of CT-P13 and innovator infliximab in patients with ankylosing spondylitis: The PLANETAS study. *Ann Rheum Dis.* 2013;72(10):1605-1612.
355. Park W, Yoo DH, Jaworski J, et al. Comparable long-term efficacy, as assessed by patient-reported outcomes, safety and pharmacokinetics, of CT-P13 and reference infliximab in patients with ankylosing spondylitis: 54-week results from the randomized, parallel-group PLANETAS study. *Arthritis Res Ther.* 2016;18(1):25.
356. Gottlieb AB, Masuda S, Ramamurthi R, et al. Pharmacodynamic and pharmacokinetic response to anti-tumor necrosis factor-alpha monoclonal antibody (infliximab) treatment of moderate to severe psoriasis vulgaris. *J Am Acad Dermatol.* 2003;48(1):68-75.
357. Dannepond C, Maruani A, Machet L, Ternant D, Paintaud G, Samimi M. Serum infliximab concentrations in psoriatic patients treated with infliximab: A systematic review. *Acta Derm Venereol.* 2015;95(4):401-406.
358. Gottlieb AB, Kalb RE, Blauvelt A, et al. The efficacy and safety of infliximab in patients with plaque psoriasis who had an inadequate response to etanercept: Results of a prospective, multicenter, open-label study. *J Am Acad Dermatol.* 2012;67(4):642-650.
359. Adedokun OJ, Sandborn WJ, Feagan BG, et al. Association between serum concentration of infliximab and efficacy in adult patients with ulcerative colitis. *Gastroenterology.* 2014;147(6):1296-1307.e1295.
360. Rutgeerts P, D'Haens G, Targan S, et al. Efficacy and safety of retreatment with anti-tumor necrosis factor antibody (infliximab) to maintain remission in Crohn's disease. *Gastroenterology.* 1999;117(4):761-769.
361. Cornillie F, Hanauer SB, Diamond RH, et al. Postinduction serum infliximab trough level and decrease of C-reactive protein level are associated with durable sustained response to infliximab: a retrospective analysis of the ACCENT I trial. *Gut.* 2014;63(11):1721-1727.
362. Rahman MU, Strusberg I, Geusens P, et al. Double-blinded infliximab dose escalation in patients with rheumatoid arthritis. *Ann Rheum Dis.* 2007;66(9):1233-1238.
363. Hibi T, Hirohata S, Kikuchi H, et al. Infliximab therapy for intestinal, neurological, and vascular involvement in Behcet disease: Efficacy, safety, and pharmacokinetics in a multicenter, prospective, open-label, single-arm phase 3 study. *Medicine.* 2016;95(24):e3863.
364. Jatoi A, Jett JR, Sloan J, et al. A pilot study on safety and pharmacokinetics of infliximab for the cancer anorexia/weight loss syndrome in non-small-cell lung cancer patients. *Support Care Cancer.* 2004;12(12):859-863.
365. Choe J-Y, Prodanovic N, Niebrzydowski J, et al. A randomised, double-blind, phase III study comparing SB2, an infliximab biosimilar, to the infliximab reference product Remicade in patients with moderate to severe rheumatoid arthritis despite methotrexate therapy. *Ann Rheum Dis.* 2017;76(1):58-64.
366. Bortlik M, Duricova D, Malickova K, et al. Infliximab trough levels may predict sustained response to infliximab in patients with Crohn's disease. *J Crohns Colitis.* 2013;7(9):736-743.

367. Krzysiek R, Breban M, Ravaud P, et al. Circulating concentration of infliximab and response to treatment in ankylosing spondylitis: Results from a randomized control study. *Arthritis Rheum.* 2009;61(5):569-576.
368. Torii H, Nakagawa H. Infliximab monotherapy in Japanese patients with moderate-to-severe plaque psoriasis and psoriatic arthritis - A randomized, double-blind, placebo-controlled multicenter trial. *J Dermatol Sci.* 2010;59(1):40-49.
369. Torii H, Sato N, Yoshinari T, Nakagawa H. Dramatic impact of a Psoriasis Area and Severity Index 90 response on the quality of life in patients with psoriasis: An analysis of Japanese clinical trials of infliximab. *J Dermatol.* 2012;39(3):253-259.
370. Sorrentino D, Marino M, Dassopoulos T, Zarifi D, Del Bianco T. Low dose infliximab for prevention of postoperative recurrence of Crohn's disease: Long term follow-up and impact of infliximab trough levels and antibodies to infliximab. *PLoS One.* 2015;10(12):e0144900.
371. Kavanaugh A, St Clair EW, McCune WJ, Braakman T, Lipsky P. Chimeric anti-tumor necrosis factor-alpha monoclonal antibody treatment of patients with rheumatoid arthritis receiving methotrexate therapy. *J Rheumatol.* 2000;27(4):841-850.
372. Kosmač M, Avčin T, Toplak N, Simonini G, Cimaz R, Šerbec VČ. Exploring the binding sites of anti-infliximab antibodies in pediatric patients with rheumatic diseases treated with infliximab. *Pediatr Res.* 2011;69(3):243-248.
373. Fasanmade AA, Adedokun OJ, Ford J, et al. Population pharmacokinetic analysis of infliximab in patients with ulcerative colitis. *Eur J Clin Pharmacol.* 2009;65(12):1211-1228.
374. Ternant D, Aubourg A, Magdelaine-Beuzelin C, et al. Infliximab pharmacokinetics in inflammatory bowel disease patients. *Ther Drug Monit.* 2008;30(4):523-529.
375. Dotan I, Ron Y, Yanai H, et al. Patient factors that increase infliximab clearance and shorten half-life in inflammatory bowel disease: A population pharmacokinetic study. *Inflamm Bowel Dis.* 2014;20(12):2247-2259.
376. Aubourg A, Picon L, Lecomte T, Bejan-Angoulvant T, Paintaud G, Ternant D. A robust estimation of infliximab pharmacokinetic parameters in Crohn's disease. *Eur J Clin Pharmacol.* 2015;71(12):1541-1542.
377. Buurman D, Maurer J, Keizer R, Kosterink J, Dijkstra G. Population pharmacokinetics of infliximab in patients with inflammatory bowel disease: potential implications for dosing in clinical practice. *Aliment Pharmacol Ther.* 2015;42(5):529-539.
378. Brandse JF, Mould D, Smeekes O, et al. A real-life population pharmacokinetic study reveals factors associated with clearance and immunogenicity of infliximab in inflammatory bowel disease. *Inflamm Bowel Dis.* 2017;23(4):650-660.
379. Ternant D, Ducourau E, Perdriger A, et al. Relationship between inflammation and infliximab pharmacokinetics in rheumatoid arthritis. *Br J Clin Pharmacol.* 2014;78(1):118-128.
380. Brekkan A, Berntorp E, Jensen K, Nielsen EI, Jönsson S. Population pharmacokinetics of plasma-derived factor IX: Procedures for dose individualization. *J Thromb Haemost.* 2016;14(4):724-732.
381. Brandse JF, van den Brink GR, Wildenberg ME, et al. Loss of infliximab into feces is associated with lack of response to therapy in patients with severe ulcerative colitis. *Gastroenterology.* 2015;149(2):350-355.e352.
382. Kearns GL, Abdel-Rahman SM, Alander SW, Blowey DL, Leeder JS, Kauffman RE. Developmental pharmacology - Drug disposition, action, and therapy in infants and children. *N Engl J Med.* 2003;349(12):1157-1167.
383. Koren G. Therapeutic drug monitoring principles in the neonate. *Clin Chem.* 1997;43(1):222-227.

384. Maharaj AR, Barrett JS, Edginton AN. A workflow example of PBPK modeling to support pediatric research and development: Case study with lorazepam. *AAPS J.* 2013;15(2):455-464.
385. Hornik CP, Wu H, Edginton AN, Watt K, Cohen-Wolkowiez M, Gonzalez D. Development of a pediatric physiologically-based pharmacokinetic model of clindamycin using opportunistic pharmacokinetic data. *Clin Pharmacokinet.* 2017;56(11):1343-1353.
386. Emoto C, Fukuda T, Johnson TN, Adams DM, Vinks AA. Development of a pediatric physiologically based pharmacokinetic model for sirolimus: Applying principles of growth and maturation in neonates and infants. *CPT Pharmacometrics Syst Pharmacol.* 2015;4(2):e17.
387. Delaney SR, Malik PRV, Stefan C, Edginton AN, Colantonio DA, Ito S. Predicting escitalopram exposure to breastfeeding infants: Integrating analytical and in silico techniques. *Clin Pharmacokinet.* 2018;57(12):1603-1611.
388. Edginton AN, Theil FP, Schmitt W, Willmann S. Whole body physiologically-based pharmacokinetic models: Their use in clinical drug development. *Expert Opin Drug Metab Toxicol.* 2008;4(9):1143-1152.
389. Shi R, Derendorf H. Pediatric dosing and body size in biotherapeutics. *Pharmaceutics.* 2010;2(4):389.
390. Yanni S. Disposition and interaction of biotherapeutics in pediatric populations. *Curr Drug Metab.* 2012;13(7):882-900.
391. Mahmood I. Pharmacokinetic considerations in designing pediatric studies of proteins, antibodies, and plasma-derived products. *Am J Ther.* 2016;23(4):e1043-e1056.
392. Lerner G, Kale AS, Warady BA, et al. Pharmacokinetics of darbepoetin alfa in pediatric patients with chronic kidney disease. *Pediatr Nephrol.* 2002;17(11):933-937.
393. Villar A, Aronis S, Morfini M, et al. Pharmacokinetics of activated recombinant coagulation factor VII (NovoSeven) in children vs. adults with haemophilia A. *Haemophilia.* 2004;10(4):352-359.
394. Blanchette VS, Shapiro AD, Liesner RJ, et al. Plasma and albumin-free recombinant factor VIII: Pharmacokinetics, efficacy and safety in previously treated pediatric patients. *J Thromb Haemost.* 2008;6(8):1319-1326.
395. Monahan PE, Liesner R, Sullivan ST, Ramirez ME, Kelly P, Roth DA. Safety and efficacy of investigator-prescribed BeneFIX prophylaxis in children less than 6 years of age with severe haemophilia B. *Haemophilia.* 2010;16(3):460-468.
396. Bjorkman S, Shapiro AD, Berntorp E. Pharmacokinetics of recombinant factor IX in relation to age of the patient: Implications for dosing in prophylaxis. *Haemophilia.* 2001;7(2):133-139.
397. Kovarik JM, Gridelli BG, Martin S, et al. Basiliximab in pediatric liver transplantation: A pharmacokinetic-derived dosing algorithm. *Pediatr Transplant.* 2002;6(3):224-230.
398. Offner G, Broyer M, Niaudet P, et al. A multicenter, open-label, pharmacokinetic/pharmacodynamic safety, and tolerability study of basiliximab (Simulect) in pediatric de novo renal transplant recipients. *Transplantation.* 2002;74(7):961-966.
399. Nagai T, Gotoh Y, Watarai Y, Tajima T, Arai K, Uchida K. Pharmacokinetics and pharmacodynamics of basiliximab in Japanese pediatric renal transplant patients. *Int J Clin Pharmacol Ther.* 2010;48(3):214-223.
400. Kovarik JM, Offner G, Broyer M, et al. A rational dosing algorithm for basiliximab (Simulect) in pediatric renal transplantation based on pharmacokinetic-dynamic evaluations. *Transplantation.* 2002;74(7):966-971.

401. Gojo J, Sauermann R, Knaack U, Slavc I, Peyrl A. Pharmacokinetics of bevacizumab in three patients under the age of 3 years with CNS malignancies. *Drugs R D.* 2017;17(3):469-474.
402. Glade Bender JL, Adamson PC, Reid JM, et al. Phase I trial and pharmacokinetic study of bevacizumab in pediatric patients with refractory solid tumors: A Children's Oncology Group Study. *J Clin Oncol.* 2008;26(3):399-405.
403. Kong L, Bhatt AR, Demny AB, et al. Pharmacokinetics of bevacizumab and its effects on serum VEGF and IGF-1 in infants with retinopathy of prematurity. *Invest Ophthalmol Vis Sci.* 2015;56(2):956-961.
404. Sato T, Wada K, Arahori H, et al. Serum concentrations of bevacizumab (Avastin) and vascular endothelial growth factor in infants with retinopathy of prematurity. *Am J Ophthalmol.* 2012;153(2):327-333.e321.
405. Trippett TM, Herzog C, Whitlock JA, et al. Phase I and pharmacokinetic study of cetuximab and irinotecan in children with refractory solid tumors: A study of the pediatric oncology experimental therapeutic investigators' consortium. *J Clin Oncol.* 2009;27(30):5102-5108.
406. Pescovitz MD, Knechtle S, Alexander SR, et al. Safety and pharmacokinetics of daclizumab in pediatric renal transplant recipients. *Pediatr Transplant.* 2008;12(4):447-455.
407. Desai AV, Fox E, Smith LM, Lim AP, Maris JM, Balis FM. Pharmacokinetics of the chimeric anti-GD2 antibody, ch14.18, in children with high-risk neuroblastoma. *Cancer Chemother Pharmacol.* 2014;74(5):1047-1055.
408. Gilman AL, Ozkaynak MF, Matthay KK, et al. Phase I study of ch14.18 with granulocyte-macrophage colony-stimulating factor and interleukin-2 in children with neuroblastoma after autologous bone marrow transplantation or stem-cell rescue: A report from the Children's Oncology Group. *J Clin Oncol.* 2009;27(1):85-91.
409. Greenbaum LA, Fila M, Ardissino G, et al. Eculizumab is a safe and effective treatment in pediatric patients with atypical hemolytic uremic syndrome. *Kidney Int.* 2016;89(3):701-711.
410. Buckwalter M, Dowell JA, Korth-Bradley J, Gorovits B, Mayer PR. Pharmacokinetics of gemtuzumab ozogamicin as a single-agent treatment of pediatric patients with refractory or relapsed acute myeloid leukemia. *J Clin Pharmacol.* 2004;44(8):873-880.
411. Xu Z, Mould D, Hu C, et al. Population pharmacokinetic analysis of infliximab in pediatrics using integrated data from six clinical trials. *Clin Pharmacol Drug Dev.* 2012;4:203.
412. Burns JC, Best BM, Mejias A, et al. Infliximab treatment of intravenous immunoglobulin–resistant Kawasaki disease. *J Pediatr.* 2008;153(6):833-838.e836.
413. Domachowske JB, Khan A, Esser MT, et al. A single dose monoclonal antibody immunoprophylaxis strategy to prevent RSV disease in all infants: Results of the first in infant study with MEDI8897. *Open Forum Infect Dis.* 2017;4(Suppl 1):S37-S37.
414. Zhao L, Roskos L, Griffin P, et al. Population pharmacokinetics analysis of motavizumab in children at risk for respiratory syncytial virus infection. *Pediatr Res.* 2010;68(S1):447-447.
415. Abarca K, Jung E, Fernandez P, et al. Safety, tolerability, pharmacokinetics, and immunogenicity of motavizumab, a humanized, enhanced-potency monoclonal antibody for the prevention of respiratory syncytial virus infection in at-risk children. *Pediatr Infect Dis J.* 2009;28(4):267-272.
416. Fernández P, Trenholme A, Abarca K, et al. A phase 2, randomized, double-blind safety and pharmacokinetic assessment of respiratory syncytial virus (RSV) prophylaxis with motavizumab and palivizumab administered in the same season. *BMC Pediatr.* 2010;10(1):38.
417. Lagos R, DeVincenzo JP, Muñoz A, et al. Safety and antiviral activity of motavizumab, a respiratory syncytial virus (RSV)-specific humanized monoclonal antibody, when administered to RSV-infected children. *Pediatr Infect Dis J.* 2009;28(9):835-837.

418. Feltes TF, Sondheimer HM, Tulloh RMR, et al. A randomized controlled trial of motavizumab versus palivizumab for the prophylaxis of serious respiratory syncytial virus disease in children with hemodynamically significant congenital heart disease. *Pediatr Res.* 2011;70(2):186-191.
419. O'Brien KL, Chandran A, Weatherholtz R, et al. Efficacy of motavizumab for the prevention of respiratory syncytial virus disease in healthy Native American infants: a phase 3 randomised double-blind placebo-controlled trial. *Lancet Infect Dis.* 2015;15(12):1398-1408.
420. Weisman LE, Thackray HM, Steinhorn RH, et al. A randomized study of a monoclonal antibody (pagibaximab) to prevent staphylococcal sepsis. *Pediatrics.* 2011;128(2):271-279.
421. Kokai-Kun JF, Mould D, Weisman LE, et al. Predicted and measured pagibaximab serum levels in high-risk neonates. *Pediatr Res.* 2010;68:683.
422. Subramanian KN, Weisman LE, Rhodes T, et al. Safety, tolerance and pharmacokinetics of a humanized monoclonal antibody to respiratory syncytial virus in premature infants and infants with bronchopulmonary dysplasia. *Pediatr Infect Dis J.* 1998;17(2):110-115.
423. Saez-Llorens X, Moreno MT, Ramilo O, Sanchez PJ, Top FH, Jr., Connor EM. Safety and pharmacokinetics of palivizumab therapy in children hospitalized with respiratory syncytial virus infection. *Pediatr Infect Dis J.* 2004;23(8):707-712.
424. Saez-Llorens X, Castano E, Null D, et al. Safety and pharmacokinetics of an intramuscular humanized monoclonal antibody to respiratory syncytial virus in premature infants and infants with bronchopulmonary dysplasia. *Pediatr Infect Dis J.* 1998;17(9):787-791.
425. Robbie GJ, Makari D, Harris B, Losonsky GA, Jafri HS. Randomized, double-blind study of the pharmacokinetics and safety of palivizumab liquid formulation compared with lyophilized formulation. *Infect Dis Ther.* 2014;3(2):203-214.
426. Pranzatelli MR, Tate ED, Verhulst SJ, et al. Pediatric dosing of rituximab revisited: Serum concentrations in opsoclonus-myoclonus syndrome. *J Pediatr Hematol Oncol.* 2010;32(5):e167-172.
427. Meissner HC, Groothuis JR, Rodriguez WJ, et al. Safety and pharmacokinetics of an intramuscular monoclonal antibody (SB 209763) against respiratory syncytial virus (RSV) in infants and young children at risk for severe RSV disease. *Antimicrob Agents Chemother.* 1999;43(5):1183-1188.
428. Lopez EL, Contrini MM, Glatstein E, et al. Safety and pharmacokinetics of urtoxazumab, a humanized monoclonal antibody, against Shiga-like toxin 2 in healthy adults and in pediatric patients infected with Shiga-like toxin-producing Escherichia coli. *Antimicrob Agents Chemother.* 2010;54(1):239-243.
429. Wang W, Wang EQ, Balthasar JP. Monoclonal antibody pharmacokinetics and pharmacodynamics. *Clin Pharmacol Ther.* 2008;84(5):548-558.
430. Lobo ED, Hansen RJ, Balthasar JP. Antibody pharmacokinetics and pharmacodynamics. *J Pharm Sci.* 2004;93(11):2645-2668.
431. Pyzik M, Rath T, Lencer WI, Baker K, Blumberg RS. FcRn: The architect behind the immune and non-immune functions of IgG and albumin. *J Immunol.* 2015;194(10):4595-4603.
432. Sholler GF, Celermajer JM, Whight CM, Bauman AE. Echo Doppler assessment of cardiac output and its relation to growth in normal infants. *Am J Cardiol.* 1987;60(13):1112-1116.
433. Task force on blood pressure control in children, National Heart, Lung, and Blood Institute. Report of the second task force on blood pressure control in children. . *Pediatrics.* 1987;79(1):1-25.

434. Fleming S, Thompson M, Stevens R, et al. Normal ranges of heart rate and respiratory rate in children from birth to 18 years: a systematic review of observational studies. *Lancet.* 2011;377(9770):1011-1018.
435. Linderkamp O, Versmold HT, Riegel KP, Betke K. Estimation and prediction of blood volume in infants and children. *Eur J Pediatr.* 1977;125(4):227-234.
436. Jopling J, Henry E, Wiedmeier SE, Christensen RD. Reference ranges for hematocrit and blood hemoglobin concentration during the neonatal period: Data from a multihospital health care system. *Pediatrics.* 2009;123(2):e333-e337.
437. Friis-Hansen B. Body water compartments in children: Changes during growth and related changes in body composition. *Pediatrics.* 1961;28(2):169-181.
438. Heymann MA, Iwamoto HS, Rudolph AM. Factors affecting changes in the neonatal systemic circulation. *Annu Rev Physiol.* 1981;43:371-383.
439. Mollison PL, Veall N, Cutbush M. Red cell and plasma volume in newborn infants. *Arch Dis Child.* 1950;25(123):242-253.
440. Steele MW. Plasma volume changes in the neonate. *Am J Dis Child.* 1962;103:10-18.
441. Jegier W, Maclaurin J, Blankenship W, Lind J. Comparative study of blood volume estimation in the newborn infant using I-131 labeled human serum albumin (IHSA) and T-1824. *Scand J Clin Lab Invest.* 1964;16:125-132.
442. Cassady G. Plasma volume studies in low birth weight infants. *Pediatrics.* 1966;38(6):1020-1027.
443. Parving HH, Klebe JG, Ingomar CJ. Simultaneous determination of plasma volume and transcapillary escape rate with 131 I-labelled albumin and T-1824 in the newborn. *Acta Paediatr Scand.* 1973;62(3):248-252.
444. Ingomar CJ, Klebe JG, BÆKgaard P. The transcapillary escape rate of T-1824 in healthy newborn infants. The influence of the placental transfusion. *Acta Paediatr Scand.* 1973;62(6):617-620.
445. Ingomar CJ, Klebe JG. The transcapillary escape rate of T-1824 in newborn infants of diabetic mothers and newborn infants with respiratory distress or birth asphyxia. *Acta Paediatr Scand.* 1974;63(4):565-570.
446. Linderkamp O, Mader T, Butenandt O, Riegel KP. Plasma volume estimation in severely ill infants and children using a simplified Evans blue method. *Eur J Pediatr.* 1977;125(2):135-141.
447. Tassani P, Schad H, Schreiber C, et al. Extravasation of albumin after cardiopulmonary bypass in newborns. *J Cardiothorac Vasc Anesth.* 2007;21(2):174-178.
448. Parving HH, Gyntelberg F. Transcapillary escape rate of albumin and plasma volume in essential hypertension. *Circ Res.* 1973;32(5):643-651.
449. Rossing N, Parving H-H, Lassen NA. Albumin transcapillary escape rate as an approach to microvascular physiology in health and disease. In: Bianchi R, Mariani G, McFarlane AS, eds. *Plasma protein turnover.* London: Palgrave Macmillan UK; 1976:357-370.
450. Wasserman K, Mayerson HS. Dynamics of lymph and plasma protein exchange. *Cardiology.* 1952;21(4-5):296-307.
451. Levick JR. Chapter 9 - Circulation of fluid between plasma, interstitium and lymph. In: *An introduction to cardiovascular physiology.* Butterworth-Heinemann; 1991:142-170.
452. Reed RK, Aukland K. Transcapillary fluid balance in immature rats. Interstitial fluid pressure, serum and interstitial protein concentration, and colloid osmotic pressure. *Microvasc Res.* 1977;14(1):37-43.

453. Turner AJ, Brown RD, Carlström M, Gibson KJ, Persson AEG. Mechanisms of neonatal increase in glomerular filtration rate. *Am J Physiol Regul Integr Comp Physiol.* 2008;295(3):R916-R921.
454. Spitzer A, Edelmann CM, Jr. Maturational changes in pressure gradients for glomerular filtration. *Am J Physiol.* 1971;221(5):1431-1435.
455. Brace RA, Christian JL. Transcapillary Starling pressures in the fetus, newborn, adult, and pregnant adult. *Am J Physiol.* 1981;240(6):H843-H847.
456. Spitzer A, Schwartz GJ. The kidney during development. In: *Comprehensive Physiology.* John Wiley & Sons, Inc.; 2010.
457. Rubin MI, Bruck E, Rapoport M, Snively M, McKay H, Baumler A. Maturation of renal function in childhood: Clearance studies. *J Clin Invest.* 1949;28(5 Pt 2):1144-1162.
458. Sola A, Gregory GA. Colloid osmotic pressure of normal newborns and premature infants. *Crit Care Med.* 1981;9(8):568-572.
459. Delivoria-Papadopoulos M, Battaglia FC, Meschia G. A comparison of fetal versus maternal plasma colloidal osmotic pressure in man. *Proc Soc Exp Biol Med.* 1969;131(1):84-87.
460. Sussmane JB, de Soto M, Torbati D. Plasma colloid osmotic pressure in healthy infants. *Crit Care.* 2001;5(5):261-264.
461. Wu PYK, Rockwell G, Chan L, Wang S-M, Udani V. Colloid osmotic pressure in newborn infants: Variations with birth weight, gestational age, total serum solids, and mean arterial pressure. *Pediatrics.* 1981;68(6):814-819.
462. Baum JD, Eisenberg C, Franklin jFA, Meschia G, Battaglia FC. Studies on colloid osmotic pressure in the fetus and newborn infant. *Biol Neonate.* 1971;18(3):311-320.
463. Bhat R, Javed S, Malalis L, Vidyasagar D. Critical care problems in neonates. Colloid osmotic pressure in healthy and sick neonates. *Crit Care Med.* 1981;9(8):563-567.
464. Schaefer B, Bartosova M, Macher-Goeppinger S, et al. Quantitative histomorphometry of the healthy peritoneum. *Sci Rep.* 2016;6:21344.
465. Celander O, Marild K. Regional circulation and capillary filtration in relation to capillary exchange in the foot and calf of the newborn infant. *Acta Paediatr.* 1962;51(3):385-400.
466. Perera P, Kurban AK, Ryan TJ. The development of the cutaneous microvascular system in the newborn. *Br J Dermatol.* 1970;82(s5):86-91.
467. Top AP, van Dijk M, van Velzen JE, Ince C, Tibboel D. Functional capillary density decreases after the first week of life in term neonates. *Neonatology.* 2011;99(1):73-77.
468. D'Souza R, Raghuraman RP, Nathan P, Manyonda IT, Antonios TF. Low birth weight infants do not have capillary rarefaction at birth: implications for early life influence on microcirculation. *Hypertension.* 2011;58(5):847-851.
469. Antonios TFT, Raghuraman RP, D'Souza R, Nathan P, Wang D, Manyonda IT. Capillary remodeling in infants born to hypertensive pregnancy: Pilot study. *Am J Hypertens.* 2012;25(8):848-853.
470. Xu S. Internalization, trafficking, intracellular processing and actions of antibody-drug conjugates. *Pharm Res.* 2015;32(11):3577-3583.
471. Deissler HL, Lang GK, Lang GE. Internalization of bevacizumab by retinal endothelial cells and its intracellular fate: Evidence for an involvement of the neonatal Fc receptor. *Exp Eye Res.* 2016;143:49-59.
472. Shih LB, Lu HHZ, Xuan H, Goldenberg DM. Internalization and intracellular processing of an anti B-cell lymphoma monoclonal antibody, ll2. *Int J Cancer.* 1994;56(4):538-545.
473. Montoyo HP, Vaccaro C, Hafner M, Ober RJ, Mueller W, Ward ES. Conditional deletion of the MHC class I-related receptor FcRn reveals the sites of IgG homeostasis in mice. *Proc Natl Acad Sci USA.* 2009;106(8):2788-2793.

474. Shearer WT, Rosenblatt HM, Gelman RS, et al. Lymphocyte subsets in healthy children from birth through 18 years of age: The pediatric AIDS clinical trials group P1009 study. *J Allergy Clin Immunol.* 2003;112(5):973-980.
475. Wakeman L, Al-Ismail S, Benton A, et al. Robust, routine haematology reference ranges for healthy adults. *Int J Lab Hematol.* 2007;29(4):279-283.
476. Stulnig T, Maczek C, Böck G, Majdic O, Wick G. Reference intervals for human peripheral blood lymphocyte subpopulations from 'healthy' young and aged subjects. *Int Arch Allergy Immunol.* 1995;108(3):205-210.
477. Newman TB, Puopolo KM, Wi S, Draper D, Escobar GJ. Interpreting complete blood counts soon after birth in newborns at risk for sepsis. *Pediatrics.* 2010;126(5):903-909.
478. *Nathan and Oski's hematology and oncology of infancy and childhood.* 8th ed. Philadelphia, PA: Elsevier; 2015.
479. Richter WF, Christianson GJ, Frances N, Grimm HP, Proetzel G, Roopenian DC. Hematopoietic cells as site of first-pass catabolism after subcutaneous dosing and contributors to systemic clearance of a monoclonal antibody in mice. *mAbs.* 2018;10(5):803-813.
480. Morris L, Graham CF, Gordon S. Macrophages in haemopoietic and other tissues of the developing mouse detected by the monoclonal antibody F4/80. *Development.* 1991;112(2):517-526.
481. Park J-E, Jardine L, Gottgens B, Teichmann SA, Haniffa M. Prenatal development of human immunity. *Science.* 2020;368(6491):600-603.
482. Ochiai M, Matsushita Y, Inoue H, et al. Blood reference intervals for preterm low-birth-weight infants: A multicenter cohort study in Japan. *PloS One.* 2016;11(8):E0161439.
483. Wirbelauer J, Thomas W, Rieger L, Speer CP. Intrauterine growth retardation in preterm infants less than 32 weeks of gestation is associated with low white blood cell counts. *Am J Perinatol.* 2010;27(10):819-824.
484. Correia IR. Stability of IgG isotypes in serum. *mAbs.* 2010;2(3):221-232.
485. Gessner JE, Heiken H, Tamm A, Schmidt RE. The IgG Fc receptor family. *Ann Hematol.* 1998;76(6):231-248.
486. Leabman MK, Meng YG, Kelley RF, DeForge LE, Cowan KJ, Iyer S. Effects of altered FcgammaR binding on antibody pharmacokinetics in cynomolgus monkeys. *mAbs.* 2013;5(6):896-903.
487. Maeda M, van Schie RC, Yuksel B, et al. Differential expression of Fc receptors for IgG by monocytes and granulocytes from neonates and adults. *Clin Exp Immunol.* 1996;103(2):343-347.
488. Martins JP, Kennedy PJ, Santos HA, Barrias C, Sarmento B. A comprehensive review of the neonatal Fc receptor and its application in drug delivery. *Pharmacol Ther.* 2016;161:22-39.
489. Challa DK, Velmurugan R, Ober RJ, Sally Ward E. FcRn: From molecular interactions to regulation of IgG pharmacokinetics and functions. *Curr Top Microbiol Immunol.* 2014;382:249-272.
490. Challa DK, Wang X, Montoyo HP, Velmurugan R, Ober RJ, Ward ES. Neonatal Fc receptor expression in macrophages is indispensable for IgG homeostasis. *mAbs.* 2019;11(5):848-860.
491. Sand KMK, Bern M, Nilsen J, Noordzij HT, Sandlie I, Andersen JT. Unraveling the interaction between FcRn and albumin: Opportunities for design of albumin-based therapeutics. *Front Immunol.* 2014;5:682.
492. Tian Z, Sutton BJ, Zhang X. Distribution of rat neonatal Fc receptor in the principal organs of neonatal and pubertal rats. *J Recept Signal Transduct Res.* 2014;34(2):137-142.

493. Cianga C, Cianga P, Plamadeala P, Amalinei C. Nonclassical major histocompatibility complex I-like Fc neonatal receptor (FcRn) expression in neonatal human tissues. *Hum Immunol.* 2011;72(12):1176-1187.
494. Mankarious S, Lee M, Fischer S, et al. The half-lives of IgG subclasses and specific antibodies in patients with primary immunodeficiency who are receiving intravenously administered immunoglobulin. *J Lab Clin Med.* 1988;112(5):634-640.
495. Oxelius V-A. IgG subclass levels in infancy and childhood. *Acta Paediatr Scand.* 1979;68(1):23-27.
496. Schur PH, Rosen F, Norman ME. Immunoglobulin subclasses in normal children. *Pediatr Res.* 1979;13(3):181-183.
497. Aksu G, Genel F, Koturoglu G, Kurugol Z, Kutukculer N. Serum immunoglobulin (IgG, IgM, IgA) and IgG subclass concentrations in healthy children: A study using nephelometric technique. *Turk J Pediatr.* 2006;48(1):19-24.
498. Zhao L, Ji P, Li Z, Roy P, Sahajwalla CG. The antibody drug absorption following subcutaneous or intramuscular administration and its mathematical description by coupling physiologically based absorption process with the conventional compartment pharmacokinetic model. *J Clin Pharmacol.* 2013;53(3):314-325.
499. Ortega H, Yancey S, Cozens S. Pharmacokinetics and absolute bioavailability of mepolizumab following administration at subcutaneous and intramuscular sites. *Clin Pharmacol Drug Dev.* 2014;3(1):57-62.
500. Richter WF, Jacobsen B. Subcutaneous absorption of biotherapeutics: Knowns and unknowns. *Drug Metab Dispos.* 2014;42(11):1881-1889.
501. Kota J, Machavaram KK, McLennan DN, Edwards GA, Porter CJ, Charman SA. Lymphatic absorption of subcutaneously administered proteins: Influence of different injection sites on the absorption of darbepoetin alfa using a sheep model. *Drug Metab Dispos.* 2007;35(12):2211-2217.
502. Wang EQ, Plotka A, Salageanu J, Sattler C, Yunis C. Pharmacokinetics and pharmacodynamics of bococizumab, a monoclonal antibody to PCSK9, after single subcutaneous injection at three sites. *Cardiovasc Ther.* 2017;35(5):e12278.
503. Lunven C, Paehler T, Poitiers F, et al. A randomized study of the relative pharmacokinetics, pharmacodynamics, and safety of alirocumab, a fully human monoclonal antibody to PCSK9, after single subcutaneous administration at three different injection sites in healthy subjects. *Cardiovasc Ther.* 2014;32(6):297-301.
504. Cai WW, Fiscella M, Chen C, Zhong ZJ, Freimuth WW, Subich DC. Bioavailability, pharmacokinetics, and safety of belimumab administered subcutaneously in healthy subjects. *Clin Pharmacol Drug Dev.* 2013;2(4):349-357.
505. Xu Z, Wang Q, Zhuang Y, et al. Subcutaneous bioavailability of golimumab at 3 different injection sites in healthy subjects. *J Clin Pharmacol.* 2010;50(3):276-284.
506. Deng R, Meng YG, Hoyte K, et al. Subcutaneous bioavailability of therapeutic antibodies as a function of FcRn binding affinity in mice. *mAbs.* 2012;4(1):101-109.
507. Ternant D, Paintaud G, Trachtman H, Gipson DS, Joy MS. A possible influence of age on absorption and elimination of adalimumab in focal segmental glomerulosclerosis (FSGS). *Eur J Clin Pharmacol.* 2016;72(2):253-255.
508. Ku LC, Smith PB. Dosing in neonates: Special considerations in physiology and trial design. *Pediatr Res.* 2015;77(1-1):2-9.
509. Rakhmanina NY, van den Anker JN. Pharmacological research in pediatrics: From neonates to adolescents. *Adv Drug Deliv Rev.* 2006;58(1):4-14.

510. Bellini C, Boccardo F, Bonioli E, Campisi C. Lymphodynamics in the fetus and newborn. *Lymphology.* 2006;39(3):110-117.
511. Johnson SA, Vander Straten MC, Parellada JA, Schnakenberg W, Gest AL. Thoracic duct function in fetal, newborn, and adult sheep. *Lymphology.* 1996;29(2):50-56.
512. Holman R. The flow and protein content of subcutaneous lymph in dogs of different ages. *Am J Physiol.* 1937;118(2):354-358.
513. Boston RW, Humphreys PW, Reynolds EOR, Strang LB. Lymph-flow and clearance of liquid from the lungs of the foetal lamb. *Lancet.* 1965;286(7410):473-474.
514. Wu WC, Shih CP, Lien R, et al. Serum vascular endothelial growth factor after bevacizumab or ranibizumab treatment for retinopathy of prematurity. *Retina.* 2017;37(4):694-701.
515. Avery RL, Castellarin AA, Steinle NC, et al. Systemic pharmacokinetics and pharmacodynamics of intravitreal aflibercept, bevacizumab, and ranibizumab. *Retina.* 2017;37(10):1847-1858.
516. Kim H, Fariss RN, Zhang C, Robinson SB, Thill M, Csaky KG. Mapping of the neonatal Fc receptor in the rodent eye. *Invest Ophthalmol Vis Sci.* 2008;49(5):2025-2029.
517. Tremoulet AH, Jain S, Jaggi P, et al. Infliximab for intensification of primary therapy for Kawasaki disease: A phase 3 randomised, double-blind, placebo-controlled trial. *Lancet.* 2014;383(9930):1731-1738.
518. Group TI-RS. Palivizumab, a humanized respiratory syncytial virus monoclonal antibody, reduces hospitalization from respiratory syncytial virus infection in high-risk infants. *Pediatrics.* 1998;102(3 Pt 1):531-537.
519. Mahmood I. Prediction of drug clearance in premature and mature neonates, infants, and children less than 2 years of age: A comparison of the predictive performance of 4 allometric models. *J Clin Pharmacol.* 2016;56(6):733-739.
520. Troutman JA, Sullivan MC, Carr GJ, Fisher J. Development of growth equations from longitudinal studies of body weight and height in the full term and preterm neonate: From birth to four years postnatal age. *Birth Defects Res.* 2018;110(11):916-932.
521. Griffin MP, Khan AA, Esser MT, et al. Safety, tolerability, and pharmacokinetics of MEDI8897, the respiratory syncytial virus prefusion F-targeting monoclonal antibody with an extended half-life, in healthy adults. *Antimicrob Agents Chemother.* 2017;61(3):E01714-01716.
522. Domachowske JB, Khan AA, Esser MT, et al. Safety, tolerability and pharmacokinetics of MEDI8897, an extended half-life single-dose respiratory syncytial virus prefusion F-targeting monoclonal antibody administered as a single dose to healthy preterm infants. *Pediatr Infect Dis J.* 2018;37(9):886-892.
523. Andresen I, Kovarik JM, Spycher M, Bolli R. Product equivalence study comparing the tolerability, pharmacokinetics, and pharmacodynamics of various human immunoglobulin-G formulations. *J Clin Pharmacol.* 2000;40(7):722-730.
524. Chirico G, Rondini G, Plebani A, Chiara A, Massa M, Ugazio AG. Intravenous gammaglobulin therapy for prophylaxis of infection in high-risk neonates. *J Pediatr.* 1987;110(3):437-442.
525. Noya FJ, Rench MA, Courtney JT, Feldman S, Baker CJ. Pharmacokinetics of intravenous immunoglobulin in very low birth weight neonates. *Pediatr Infect Dis J.* 1989;8(11):759-763.
526. Noya FJ, Rench MA, Garcia-Prats JA, Jones TM, Baker CJ. Disposition of an immunoglobulin intravenous preparation in very low birth weight neonates. *J Pediatr.* 1988;112(2):278-283.
527. Ingegnoli F, Herrick AL. Nailfold capillaroscopy in pediatrics. *Arthritis Care Res (Hoboken).* 2013;65(9):1393-1400.

528. Dolezalova P, Young SP, Bacon PA, Southwood TR. Nailfold capillary microscopy in healthy children and in childhood rheumatic diseases: a prospective single blind observational study. *Ann Rheum Dis.* 2003;62(5):444-449.
529. Bland RD, McMillan DD. Lung fluid dynamics in awake newborn lambs. *J Clin Invest.* 1977;60(5):1107-1115.
530. Humphreys PW, Normand IC, Reynolds EO, Strang LB. Pulmonary lymph flow and the uptake of liquid from the lungs of the lamb at the start of breathing. *J Physiol.* 1967;193(1):1-29.
531. Troger B, Muller T, Faust K, et al. Intrauterine growth restriction and the innate immune system in preterm infants of less than 32 weeks gestation. *Neonatology.* 2013;103(3):199-204.
532. Gamble J, Bethell D, Day NP, et al. Age-related changes in microvascular permeability: a significant factor in the susceptibility of children to shock? *Clin Sci (Lond).* 2000;98(2):211-216.
533. Sillau AH, Banchero N. Effect of maturation on capillary density, fiber size and composition in rat skeletal muscle. *Proc Soc Exp Biol Med.* 1977;154(3):461-466.
534. Aquin L, Banchero N. The cytoarchitecture and capillary supply in the skeletal muscle of growing dogs. *J Anat.* 1981;132(Pt 3):341-356.
535. Aquin L, Sillau AH, Lechner AJ, Banchero N. Growth and skeletal muscle microvascularity in the guinea pig. *Microvasc Res.* 1980;20(1):41-50.
536. Akilesh S, Christianson GJ, Roopenian DC, Shaw AS. Neonatal FcR expression in bone marrow-derived cells functions to protect serum IgG from catabolism. *J Immunol.* 2007;179(7):4580-4588.
537. Martin MG, Wu SV, Walsh JH. Ontogenetic development and distribution of antibody transport and Fc receptor mRNA expression in rat intestine. *Dig Dis Sci.* 1997;42(5):1062-1069.
538. Schoefl GI. Studies on inflammation. *Virchows Arch Path Anat.* 1963;337(2):97-141.
539. Fanaroff AA, Korones SB, Wright LL, et al. A controlled trial of intravenous immune globulin to reduce nosocomial infections in very-low-birth-weight infants. *N Engl J Med.* 1994;330(16):1107-1113.
540. Abduljalil K, Pan X, Pansari A, Jamei M, Johnson TN. Preterm physiologically based pharmacokinetic model. Part II: Applications of the model to predict drug pharmacokinetics in the preterm population. *Clin Pharmacokinet.* 2020;59(4):501-518.
541. Li T, Balthasar JP. Development and evaluation of a physiologically based pharmacokinetic model for predicting the effects of anti-FcRn therapy on the disposition of endogenous IgG in humans. *J Pharm Sci.* 2019;108(1):714-724.
542. Aborig M, Malik PRV, Nambiar S, et al. Biodistribution and physiologically-based pharmacokinetic modeling of gold nanoparticles in mice with interspecies extrapolation. *Pharmaceutics.* 2019;11(4):179.
543. Lopez BG, Tsai MS, Baratta JL, Longmuir KJ, Robertson RT. Characterization of Kupffer cells in livers of developing mice. *Comp Hepatol.* 2011;10(1):2.
544. Li T, Balthasar JP. Application of physiologically based pharmacokinetic modeling to predict the effects of FcRn inhibitors in mice, rats, and monkeys. *J Pharm Sci.* 2019;108(1):701-713.
545. Sheng J, Ruedl C, Karjalainen K. Most tissue-resident macrophages except microglia are derived from fetal hematopoietic stem cells. *Immunity.* 2015;43(2):382-393.
546. Austyn JM, Gordon S. F4/80, a monoclonal antibody directed specifically against the mouse macrophage. *Eur J Immunol.* 1981;11(10):805-815.

547. O'Connell KE, Mikkola AM, Stepanek AM, et al. Practical murine hematopathology: A comparative review and implications for research. *Comp Med.* 2015;65(2):96-113.
548. Schenkel AR, Chew TW, Muller WA. Platelet endothelial cell adhesion molecule deficiency or blockade significantly reduces leukocyte emigration in a majority of mouse strains. *J Immunol.* 2004;173(10):6403-6408.
549. Helk E, Bernin H, Ernst T, et al. TNF alpha-mediated liver destruction by kupffer cells and Ly6Chi monocytes during Entamoeba histolytica infection. *PLoS Pathog.* 2013;9(1):e1003096.
550. Baratta JL, Ngo A, Lopez B, Kasabwalla N, Longmuir KJ, Robertson RT. Cellular organization of normal mouse liver: A histological, quantitative immunocytochemical, and fine structural analysis. *Histochem Cell Biol.* 2009;131(6):713-726.
551. Jenne CN, Kubes P. Immune surveillance by the liver. *Nat Immunol.* 2013;14(10):996-1006.
552. Sohlenius-Sternbeck AK. Determination of the hepatocellularity number for human, dog, rabbit, rat and mouse livers from protein concentration measurements. *Toxicol In Vitro.* 2006;20(8):1582-1586.
553. Lee SH, Starkey PM, Gordon S. Quantitative analysis of total macrophage content in adult mouse tissues. Immunochemical studies with monoclonal antibody F4/80. *J Exp Med.* 1985;161(3):475-489.
554. Chung S, Nguyen V, Lin YL, et al. An in vitro FcRn- dependent transcytosis assay as a screening tool for predictive assessment of nonspecific clearance of antibody therapeutics in humans. *mAbs.* 2019;11(5):942-955.
555. Yu Y-RA, O'Koren EG, Hotten DF, et al. A protocol for the comprehensive flow cytometric analysis of immune cells in normal and inflamed murine non-lymphoid tissues. *PLoS One.* 2016;11(3):e0150606.
556. Chang HP, Kim SJ, Shah DK. Whole-body pharmacokinetics of antibody in mice determined using enzyme-linked immunosorbent assay and derivation of tissue interstitial concentrations. *J Pharm Sci.* 2021;110(1):446-457.
557. Urva SR, Yang VC, Balthasar JP. Physiologically based pharmacokinetic model for T84.66: A monoclonal anti-CEA antibody. *J Pharm Sci.* 2010;99(3):1582-1600.
558. Sun Y, Cai H, Hu Z, et al. Balancing the affinity and pharmacokinetics of antibodies by modulating the size of charge patches on complementarity-determining regions. *J Pharm Sci.* 2020;109(12):3690-3696.
559. Kaur H. Characterization of glycosylation in monoclonal antibodies and its importance in therapeutic antibody development. *Crit Rev Biotechnol.* 2021;41(2):300-315.
560. Goloba M, Raghuraman R, Botros N, et al. Early life microcirculatory plasticity and blood pressure changes in low birth weight infants born to normotensive mothers: A cohort study. *Am J Hypertens.* 2019;32(6):570-578.
561. Datta-Mannan A, Croy JE, Schirtzinger L, Torgerson S, Breyer M, Wroblewski VJ. Aberrant bispecific antibody pharmacokinetics linked to liver sinusoidal endothelium clearance mechanism in cynomolgus monkeys. *mAbs.* 2016;8(5):969-982.
562. Yellepeddi VK, Joseph A, Nance E. Pharmacokinetics of nanotechnology-based formulations in pediatric populations. *Adv Drug Deliv Rev.* 2019;151-152:44-55.
563. Basu S, Lien YTK, Vozmediano V, et al. Physiologically based pharmacokinetic modeling of monoclonal antibodies in pediatric populations using PK-Sim. *Front Pharmacol.* 2020;11:868.
564. Chang HP, Kim SJ, Wu D, Shah K, Shah DK. Age-related changes in pediatric physiology: Quantitative analysis of organ weights and blood flows. *AAPS J.* 2021;23(3):50.

565. Chang H, Shah D, Funk R, Frymoyer A, Park K, Shakhnovich V. FDA-labelled dosing of IFX falls short of target trough concentrations for pediatric IBD: A population PBPK modeling approach. Paper presented at: Clin Pharmacol Ther 2021.

Appendix

Appendix A: Supplementary Material for Chapter 3

Derivation of the Degradation Rate of mAb-HER2 Complexes (K_{deg}^{Ag})

We denote the amount of mAb bound to HER2 on the cell membrane by A_{CM} and the amount bound to HER2 in the intracellular space by A_{IC}. The time-varying rate of mAb binding to HER2 is given by $v(t)$. The rate at which the mAb-HER2 complex on the cell membrane is internalized is denoted by K_{int}^{Ag}. A fraction (FR^{Ag}) of intracellular mAb-HER2 complex is recycled back to the cell membrane at a certain rate $\left(K_{exit}^{Ag}\right)$. The remaining fraction $(1 - FR^{Ag})$ is degraded. This process is described by the following differential equations:

$$\begin{aligned} \frac{dA_{CM}}{dt} &= v(t) - K_{int}^{Ag} \times A_{CM} + K_{exit}^{Ag} \times FR^{Ag} \times A_{IC} \\ \frac{dA_{IC}}{dt} &= K_{int}^{Ag} \times A_{CM} - K_{exit}^{Ag} \times FR^{Ag} \times A_{IC} - K_{exit}^{Ag} \times (1 - FR^{Ag}) \times A_{IC} \end{aligned} \tag{A1}$$

Let:

$$A_T \coloneqq A_{CM} + A_{IC} \tag{A2}$$

So that (A1) becomes:

$$\begin{aligned} \frac{dA_{CM}}{dt} &= v(t) - K_{int}^{Ag} \times A_{CM} + K_{exit}^{Ag} \times FR^{Ag} \times (A_T - A_{CM}) \\ \frac{dA_T}{dt} &= v(t) - K_{exit}^{Ag} \times (1 - FR^{Ag}) \times (A_T - A_{CM}) \end{aligned} \tag{A3}$$

Under the assumptions that K_{int}^{Ag} and K_{exit}^{Ag} are of the same order and that $FR^{Ag} \approx 1$, it follows that $K_{exit}^{Ag} \times (1 - FR^{Ag}) \ll K_{int}^{Ag}, K_{exit}^{Ag}$. To represent this difference in magnitude, we let $k_1 \coloneqq \epsilon \times K_{int}^{Ag}$, $k_2 \coloneqq \epsilon \times K_{exit}^{Ag} \times FR^{Ag}$ and $k = K_{exit}^{Ag} \times (1 - FR^{Ag})$, where ϵ is a small parameter that makes k_1 and k_2 are of the same order as k. Then, (A2) becomes

$$\epsilon \times \frac{dA_{CM}}{dt} = \epsilon \times v(t) - k_1 \times A_{CM} + k_2 \times (A_T - A_{CM}) \tag{A4}$$

$$\frac{dA_T}{dt} = v(t) - k \times (A_T - A_{CM})$$

The separation of timescales introduced by the small parameter ϵ allows us to make an approximation. Since $\epsilon \approx 0$ we can say (informally) that:

$$-k_1 \times A_{CM} + k_2 \times (A_T - A_{CM}) \approx 0 \quad \text{(A5)}$$

This step can be shown formally using a standard application of Tikhonov's theorem. Therefore, we obtain $A_{CM} \approx k_2 \times A_T/(k_1 + k_2)$and, from (A4), the following approximation holds over time:

$$\frac{dA_T}{dt} = v(t) - K_{deg}^{Ag} \times A_T$$

where:

$$K_{deg}^{Ag} \coloneqq k \times \frac{k_1}{k_1 + k_2} = K_{exit}^{Ag} \times (1 - FR^{Ag}) \times \frac{K_{int}^{Ag}}{K_{int}^{Ag} + K_{exit}^{Ag} \times FR^{Ag}}$$

is the rate of degradation of mAb-HER2 complexes.

A final numerical value of 0.0789 was calculated using the kinetic parameter values determined by Hendriks et al.[269,270]

Model Equations

In the following equations, the subscript i represents a specific organ tissue compartment being considered. For all organ tissue compartment equations except the lung and liver, subscript j refers to the lung. For the lung equations, subscript j refers to the plasma compartment concentration. The liver plasma space is described separately in equations 7 and 8. Table A1 below defines any equation terms that are undefined in the main body of the work.

Table A1 A listing and description of the previously undefined parameters used in the model equations. For all other parameter definitions, see Table 6 in the main body of the work.

Term	Units	Definition
PLQ_{Lung}	L/h	Total body plasma flow
$L_{LymphNode}$	L/h	Total body lymph flow
PLQ_i	L/h	Plasma flow into and out of each organ
L_i	L/h	Lymph flow into and out of each organ
C_{Plasma}	nM	Concentration of mAb in plasma space
$C_{LymphNode}$	nM	Concentration of mAb in lymphatic system
C_i^P	nM	Concentration of mAb in organ plasma space
C_i^{EBound}	nM	Concentration of mAb in endosomal space bound to FcRn
$C_i^{EUnbound}$	nM	Concentration of unbound mAb in endosomal space
C_i^{IS}	nM	Concentration of mAb in interstitial space
$C_i^{CMBound}$	nmol / L interstitial	Concentration of mAb bound to HER2 on the cell membrane
V_{Plasma}	L	Volume of plasma space
$V_{LypmhNode}$	L	Volume of lymphatic system components
V_i^P	L	Volume of organ plasma space
V_i^E	L	Volume of endosomal space
V_i^{IS}	L	Volume of interstitial space
C_{Plasma}^{ECD}	nM	Concentration of mAb-ECD complexes in plasma space
$C_{LymphNode}^{ECD}$	nM	Concentration of mAb-ECD complexes in lymphatic system
$C_i^{P,ECD}$	nM	Concentration of mAb-ECD complexes in organ plasma space
$C_i^{IS,ECD}$	nM	Concentration of mAb-ECD complexes in interstitial space

Blood Compartment: Plasma

Equation A6:

$$V_{Plasma} \times \frac{dC_{Plasma}}{dt}$$

$$= (PLQ_{Heart} - L_{Heart}) \times C_{Heart}^{P} + \left(PLQ_{Kidney} - L_{Kidney}\right) \times C_{Kidney}^{P}$$

$$+ (PLQ_{Muscle} - L_{Muscle}) \times C_{Muscle}^{P} + (PLQ_{Skin} - L_{Skin}) \times C_{Skin}^{P}$$

$$+ (PLQ_{Brain} - L_{Brain}) \times C_{Brain}^{P} + \left(PLQ_{Adipose} - L_{Adipose}\right) \times C_{Adipose}^{P}$$

$$+ \left(PLQ_{Thymus} - L_{Thymus}\right) \times C_{Thymus}^{P}$$

$$+ \left(PLQ_{Liver} - L_{Liver} + PLQ_{Stomach} - L_{Stomach} + PLQ_{Spleen} - L_{Spleen}\right.$$

$$\left. + PLQ_{Pancreas} - L_{Pancreas} + PLQ_{SInt} - L_{SInt} + PLQ_{LInt} - L_{LInt}\right) \times C_{Liver}^{P}$$

$$+ (PLQ_{Bone} - L_{Bone}) \times C_{Bone}^{P} + (PLQ_{Other} - L_{Other}) \times C_{Other}^{P}$$

$$+ L_{LymphNode} \times C_{LymphNode} - PLQ_{Lung} \times C_{Plasma}$$

$$- K_{on}^{ECD} \times (ECD - C_{Plasma}^{ECD}) \times C_{Plasma} \times V_{Plasma}$$

$$+ K_{off}^{ECD} \times C_{Plasma}^{ECD} \times V_{Plasma}$$

Equation A7:

$$V_{Plasma} \times \frac{dC_{Plasma}^{ECD}}{dt}$$

$$= (PLQ_{Heart} - L_{Heart}) \times C_{Heart}^{P,ECD} + \left(PLQ_{Kidney} - L_{Kidney}\right) \times C_{Kidney}^{P,ECD}$$

$$+ (PLQ_{Muscle} - L_{Muscle}) \times C_{Muscle}^{P,ECD} + (PLQ_{Skin} - L_{Skin}) \times C_{Skin}^{P,ECD}$$

$$+ (PLQ_{Brain} - L_{Brain}) \times C_{Brain}^{P,ECD} + \left(PLQ_{Adipose} - L_{Adipose}\right) \times C_{Adipose}^{P,ECD}$$

$$+ \left(PLQ_{Thymus} - L_{Thymus}\right) \times C_{Thymus}^{P,ECD}$$

$$+ \left(PLQ_{Liver} - L_{Liver} + PLQ_{Stomach} - L_{Stomach} + PLQ_{Spleen} - L_{Spleen}\right.$$

$$\left. + PLQ_{Pancreas} - L_{Pancreas} + PLQ_{SInt} - L_{SInt} + PLQ_{LInt} - L_{LInt}\right) \times C_{Liver}^{P,ECD}$$

$$+ (PLQ_{Bone} - L_{Bone}) \times C_{Bone}^{P,ECD} + (PLQ_{Other} - L_{Other}) \times C_{Other}^{P,ECD}$$

$$+ L_{LymphNode} \times C_{LymphNode}^{ECD} - PLQ_{Lung} \times C_{Plasma}^{ECD}$$

$$+ K_{on}^{ECD} \times (ECD - C_{Plasma}^{ECD}) \times C_{Plasma} \times V_{Plasma}$$

$$- K_{off}^{ECD} \times C_{Plasma}^{ECD} \times V_{Plasma} - K_{deg}^{ECD} \times C_{Plasma}^{ECD} \times V_{Plasma}$$

Lymph Node Compartment

Equation A8:

$$V_{LymphNode} \times \frac{dC_{LymphNode}}{dt}$$

$$= (1 - \sigma_{Heart}^{IS}) \times L_{Heart} \times C_{Heart}^{IS} + \left(1 - \sigma_{Kidney}^{IS}\right) \times L_{Kidney} \times C_{Kidney}^{IS}$$

$$+ (1 - \sigma_{Muscle}^{IS}) \times L_{Muscle} \times C_{Muscle}^{IS} + \left(1 - \sigma_{Skin}^{IS}\right) \times L_{Skin} \times C_{Skin}^{IS}$$

$$+ \left(1 - \sigma_{Brain}^{IS}\right) \times L_{Brain} \times C_{Brain}^{IS} + \left(1 - \sigma_{Adipose}^{IS}\right) \times L_{Adipose} \times C_{Adipose}^{IS}$$

$$+ \left(1 - \sigma_{Thymus}^{IS}\right) \times L_{Thymus} \times C_{Thymus}^{IS} + \left(1 - \sigma_{Liver}^{IS}\right) \times L_{Liver} \times C_{Liver}^{IS}$$

$$+ (1 - \sigma_{Stomach}^{IS}) \times L_{Stomach} \times C_{Stomach}^{IS}$$

$$+ \left(1 - \sigma_{Spleen}^{IS}\right) \times L_{Spleen} \times C_{Spleen}^{IS}$$

$$+ (1 - \sigma_{Pancreas}^{IS}) \times L_{Pancreas} \times C_{Pancreas}^{IS} + (1 - \sigma_{SInt}^{IS}) \times L_{SInt} \times C_{SInt}^{IS}$$

$$+ (1 - \sigma_{LInt}^{IS}) \times L_{LInt} \times C_{LInt}^{IS} + (1 - \sigma_{Bone}^{IS}) \times L_{Bone} \times C_{Bone}^{IS}$$

$$+ (1 - \sigma_{Other}^{IS}) \times L_{Other} \times C_{Other}^{IS} + \left(1 - \sigma_{Lung}^{IS}\right) \times L_{Lung} \times C_{Lung}^{IS}$$

$$- L_{LypmhNode} \times C_{LymphNode}$$

$$- K_{on}^{ECD} \times \left(ECD - C_{LymphNode}^{ECD}\right) \times C_{LymphNode} \times V_{LymphNode}$$

$$+ K_{off}^{ECD} \times C_{LymphNode}^{ECD} \times V_{LymphNode}$$

Equation A9:

$$V_{LymphNode} \times \frac{dC_{LymphNode}^{ECD}}{dt}$$

$$= (1 - \sigma_{Heart}^{IS}) \times L_{Heart} \times C_{Heart}^{IS,ECD} + (1 - \sigma_{Kidney}^{IS}) \times L_{Kidney} \times C_{Kidney}^{IS,ECD}$$

$$+ (1 - \sigma_{Muscle}^{IS}) \times L_{Muscle} \times C_{Muscle}^{IS,ECD} + (1 - \sigma_{Skin}^{IS}) \times L_{Skin} \times C_{Skin}^{IS,ECD}$$

$$+ (1 - \sigma_{Brain}^{IS}) \times L_{Brain} \times C_{Brain}^{IS,ECD} + (1 - \sigma_{Adipose}^{IS}) \times L_{Adipose} \times C_{Adipose}^{IS,ECD}$$

$$+ (1 - \sigma_{Thymus}^{IS}) \times L_{Thymus} \times C_{Thymus}^{IS,ECD} + (1 - \sigma_{Liver}^{IS}) \times L_{Liver} \times C_{Liver}^{IS,ECD}$$

$$+ (1 - \sigma_{Stomach}^{IS}) \times L_{Stomach} \times C_{Stomach}^{IS,ECD}$$

$$+ (1 - \sigma_{Spleen}^{IS}) \times L_{Spleen} \times C_{Spleen}^{IS,ECD}$$

$$+ (1 - \sigma_{Pancreas}^{IS}) \times L_{Pancreas} \times C_{Pancreas}^{IS,ECD} + (1 - \sigma_{SInt}^{IS}) \times L_{SInt} \times C_{SInt}^{IS,ECD}$$

$$+ (1 - \sigma_{LInt}^{IS}) \times L_{LInt} \times C_{LInt}^{IS,ECD} + (1 - \sigma_{Bone}^{IS}) \times L_{Bone} \times C_{Bone}^{IS,ECD}$$

$$+ (1 - \sigma_{Other}^{IS}) \times L_{Other} \times C_{Other}^{IS,ECD} + (1 - \sigma_{Lung}^{IS}) \times L_{Lung} \times C_{Lung}^{IS,ECD}$$

$$- L_{LypmhNode} \times C_{LymphNode}^{ECD}$$

$$+ K_{on}^{ECD} \times (ECD - C_{LymphNode}^{ECD}) \times C_{LymphNode} \times V_{LymphNode}$$

$$- K_{off}^{ECD} \times C_{LymphNode}^{ECD} \times V_{LymphNode} - K_{deg}^{ECD} \times C_{LymphNode}^{ECD} \times V_{LymphNode}$$

Tissue Compartment: Plasma Space

Equation A10:

$$V_i^P \times \frac{dC_i^P}{dt} = PLQ_i \times C_j^P - (PLQ_i - L_i) \times C_i^P - F2 \times (1 - \sigma_i^V) \times L_i \times C_i^P - CLup_i \times C_i^P$$
$$+ CLup_i \times FR \times C_i^{EBound} - K_{on}^{ECD} \times \left(ECD - C_i^{P,ECD}\right) \times C_i^P \times V_i^P$$
$$+ K_{off}^{ECD} \times C_i^{P,ECD} \times V_i^P$$

Equation A11:

$$V_i^P \times \frac{dC_i^{P,ECD}}{dt} = PLQ_i \times C_j^{P,ECD} - (PLQ_i - L_i) \times C_i^{P,ECD} - F2 \times (1 - \sigma_i^V) \times L_i \times C_i^{P,ECD}$$
$$+ K_{on}^{ECD} \times \left(ECD - C_i^{P,ECD}\right) \times C_i^P \times V_i^P - K_{off}^{ECD} \times C_i^{P,ECD} \times V_i^P$$

Equation A12:

$$V_{Liver}^P \times \frac{dC_{Liver}^P}{dt}$$
$$= PLQ_{Liver} \times C_{Lung}^P + (PLQ_{Stomach} - L_{Stomach}) \times C_{Stomach}^P$$
$$+ \left(PLQ_{Spleen} - L_{Spleen}\right) \times C_{Spleen}^P + (PLQ_{Pancreas} - L_{Pancreas}) \times C_{Pancreas}^P$$
$$+ (PLQ_{SInt} - L_{SInt}) \times C_{SInt}^P + (PLQ_{LInt} - L_{Lint}) \times C_{LInt}^P$$
$$- \left(PLQ_{Liver} - L_{Liver} + PLQ_{Stomach} - L_{Stomach} + PLQ_{Spleen} - L_{Spleen}\right.$$
$$\left. + PLQ_{Pancreas} - L_{Pancreas} + PLQ_{SInt} - L_{SInt} + PLQ_{LInt} - L_{LInt}\right) \times C_{Liver}^P$$
$$- F2 \times (1 - \sigma_{Liver}^V) \times L_{Liver} \times C_{Liver}^P - CLup_{Liver} \times C_{Liver}^P$$
$$+ CLup_{Liver} \times FR \times C_{Liver}^{EBound} - K_{on}^{ECD} \times \left(ECD - C_{Liver}^{P,ECD}\right) \times C_{Liver}^P \times V_{Liver}^P$$
$$+ K_{off}^{ECD} \times C_{Liver}^{P,ECD} \times V_{Liver}^P$$

Equation A13:

$$V_{Liver}^{P} \times \frac{dC_{Liver}^{P,ECD}}{dt}$$

$$= PLQ_{Liver} \times C_{Lung}^{P,ECD} + (PLQ_{Stomach} - L_{Stomach}) \times C_{Stomach}^{P,ECD}$$

$$+ \left(PLQ_{Spleen} - L_{Spleen}\right) \times C_{Spleen}^{P,ECD} + (PLQ_{Pancreas} - L_{Pancreas}) \times C_{Pancreas}^{P,ECD}$$

$$+ (PLQ_{SInt} - L_{SInt}) \times C_{SInt}^{P,ECD} + (PLQ_{LInt} - L_{Lint}) \times C_{LInt}^{P,ECD}$$

$$- \left(PLQ_{Liver} - L_{Liver} + PLQ_{Stomach} - L_{Stomach} + PLQ_{Spleen} - L_{Spleen}\right.$$

$$\left. + PLQ_{Pancreas} - L_{Pancreas} + PLQ_{SInt} - L_{SInt} + PLQ_{LInt} - L_{LInt}\right) \times C_{Liver}^{P,ECD}$$

$$- F2 \times (1 - \sigma_{Liver}^{V}) \times L_{Liver} \times C_{Liver}^{P,ECD}$$

$$+ K_{on}^{ECD} \times \left(ECD - C_{Liver}^{P,ECD}\right) \times C_{Liver}^{P} \times V_{Liver}^{P} - K_{off}^{ECD} \times C_{Liver}^{P,ECD} \times V_{Liver}^{P}$$

$$- K_{deg}^{ECD} \times C_{Liver}^{P,ECD} \times V_{Liver}^{P}$$

Tissue Compartment: Endosomal Space

Equation A14:

$$\frac{dC_i^{EUnbound}}{dt} = \frac{CLup_i}{V_i^E} \times \left(C_i^P + C_i^{IS}\right) - K_{on}^{FcRn} \times C_i^{EUnbound} \times FcRn_i + K_{off}^{FcRn} \times C_i^{EBound}$$

$$- K_{deg}^{FcRn} \times C_i^{EUnbound}$$

Equation A15:

$$\frac{dC_i^{EBound}}{dt} = K_{on}^{FcRn} \times C_i^{EUnbound} \times FcRn_i - K_{off}^{FcRn} \times C_i^{EBound} - \frac{CLup_i}{V_i^E} \times C_i^{EBound}$$

Equation A16

$$\frac{dFcRn_i}{dt} = K_{off}^{FcRn} \times C_i^{EBound} - K_{on}^{FcRn} \times C^{EUnbound} \times FcRn_i + \frac{CLup_i}{V_i^E} \times C_i^{EBound}$$

Tissue Compartment: Interstitial Space

Equation A17:

$$V_i^{IS} \times \frac{dC_i^{IS}}{dt} = F2 \times (1 - \sigma_i^V) \times L_i \times C_i^P - \left(1 - \sigma_i^{IS}\right) \times L_i \times C_i^{IS} - CLup_i \times C_i^{IS}$$
$$+ CLup_i \times (1 - FR) \times C_i^{EBound} - K_{on}^{Ag} \times C_i^{IS} \times \left(Ag - C_i^{CMBound}\right) \times V_i^{IS}$$
$$+ K_{off}^{Ag} \times C_i^{CMBound} \times V_i^{IS} - K_{on}^{ECD} \times \left(ECD - C_i^{IS,ECD}\right) \times C_i^{IS} \times V_i^{IS}$$
$$+ K_{off}^{ECD} \times C_i^{IS,ECD} \times V_i^{IS}$$

Equation A18:

$$V_i^{IS} \times \frac{dC_i^{IS,ECD}}{dt}$$
$$= F2 \times (1 - \sigma_i^V) \times L_i \times C_i^{P,ECD} - \left(1 - \sigma_i^{IS}\right) \times L_i \times C_i^{IS,ECD}$$
$$+ K_{on}^{ECD} \times \left(ECD - C_i^{IS,ECD}\right) \times C_i^{IS} \times V_i^{IS} - K_{off}^{ECD} \times C_i^{IS,ECD} \times V_i^{IS}$$
$$- K_{deg}^{ECD} \times C_i^{IS,ECD} \times V_i^{IS}$$

Tissue Compartment: Cell Membrane

Equation A19:

$$\frac{dC_i^{CMBound}}{dt} = K_{on}^{Ag} \times C_i^{IS} \times \left(Ag - C_i^{CMBound}\right) - K_{off}^{Ag} \times C_i^{CMBound} - K_{deg}^{Ag} \times C_i^{CMBound}$$

Miscellaneous Equations

Equation A20:

$$CLup_i = CLup \times V_i^E$$

Equation A21:

$$V_{Plasma}^{Total} = V_{Plasma} + \sum V_i^P$$

Global Sensitivity Analysis Method

We can describe the PBPK model by an ordinary differential equation parameterized by a vector $p = [p_1 \quad \cdots \quad p_n]$:

$$\frac{dx}{dt}(t) = f(x(t), p, t)$$
$$y(t, p_1, \cdots, p_n) = g(x(t))$$

where x is a vector of concentrations of mAb in all compartments, with y being the measured output – the concentration of mAb in plasma. Starting from zero initial conditions (representing the absence of mAb prior to administration), the concentration of mAb in the different compartments over time is given by the solution to this ODE. For the global sensitivity analysis, we seek to quantify the variance of the area under the curve, $A(p_1, \cdots, p_n) = \int_0^T y\, dt$, when the parameters $p_1, \cdots, p_n$ are sampled from a given distribution. To calculate this variance, we adopt the approaches of Sobol and Saltelli.[297] Without loss of generality, each of the parameters $p_1, \cdots, p_n$ is assumed to vary independently and have a uniform distribution over the interval $[0,1]$. Under these assumptions, the expected value A_0 of A is given by

$$A_0 = E[A] = \int_0^1 \cdots \int_0^1 A(p_1, \cdots, p_n) \prod_{i=1}^{n} dp_i$$

while the variance D of A is

$$D = E[A^2] - E^2[A] = \int_0^1 \cdots \int_0^1 A^2(p_1, \cdots, p_n) \prod_{i=1}^{n} dp_i - A_0^2$$

It is possible to also formulate an expression for the deviation between A, averaged over all parameters except p_j, and the expected value A_0:

$$A_j(p_j) = \int_0^1 \cdots \int_0^1 A(p_1, \cdots, p_n) \prod_{\substack{i=1 \\ i \neq j}}^{n} dp_i - A_0$$

for which $E[A_j] = 0$. For a given value of p_j, this function quantifies the deviation of A from the expected value A_0. The variance D_j of $A_j(p_j)$ over the distribution of p_j gives an absolute measure of the sensitivity of A with respect to variations solely in p_j. This variance is given by

$$D_j = \int_0^1 A_j^2(p_j)dp_j$$

To compare sensitivity with respect to the different parameters, one can define the relative sensitivity of A with respect to p_j, given by:

$$S_j = \frac{D_j}{D}$$

Beyond the sensitivity of A with respect to variation solely in p_j, it is instructive to quantify the relative sensitivity of A with respect to p_j varying together with the other parameters. A derivation similar to that above, given in Homma & Saltelli,[298] defines this *relative total sensitivity* with respect to p_j, denoted S_{T_j}, as

$$S_{T_j} = 1 - \frac{\overline{D}_j}{D}$$

where $\overline{D}_j$ quantifies the variance of A due to variations in all parameters save p_j.

Since there is no analytical expression for A due to the nonlinearity of the PBPK model, the integrals used to evaluate S_j and S_{T_j} were calculated using quasi-Monte Carlo integrals. To ensure that these integrals were evaluated over a suitably large range of points that covers the parameter space, a Sobol sequence was constructed to generate test points as described in Saltelli.[297]

The parameters were sampled from uniform distributions centered on mean values with domains spanning plus and minus one standard deviation. The means of these distributions, along with the coefficients of variation used to calculate the domains of the distributions are given in Table 7 in the main body of the work along with the result of the global sensitivity analysis.

Definitions:

The **first order global sensitivity** of an output with respect to a parameter assesses the normalized variance of the output when marginalized over all parameters except the parameter of interest.

The **total global sensitivity** of an output with respect to a parameter assesses the difference between the normalized variance of the output and its normalized variance when marginalized over the parameter of interest.

Reference Parameters

Table A2. Basic reference parameters for a Caucasian adult male

Parameter	Value
Height	1.77 m
Body Mass	73.00 kg
Body Surface Area	1.90 m^2
Cardiac Output	360.50 L/h
Total Plasma Flow	198.28 L/h
Total Blood Volume	5.67 L
Total Plasma Volume	3.12 L
Hematocrit	0.45

Table A3. Organ sizes and fluid flow rates for the reference male

Organ	Mass (kg)	Density (kg/L)	Plasma Flow (L/h)	Lymph Flow (L/h)[b]
Blood[a]	2.85	1.06	198.28	
Lymph	0.2621	1		0.4084
Heart	0.386	1.03	8.58	0.01716
Kidney	0.422	1.05	40.75	0.0815
Muscle	29.784	1.04	36.46	0.07292
Skin	3.468	1.1	10.72	0.02144
Brain	1.5172	1.03	25.74	0.05148
Adipose	17.26	0.916	10.71	0.02142
Thymus	0.0064	1	0.079	0.000158
Liver	2.36	1.05	13.94	0.02788
Stomach	0.206	1.05	2.14	0.00428
Spleen	0.2284	1.05	6.44	0.01288
Pancreas	0.1736	1.04	2.14	0.00428
S. Intestine	0.8628	1.04	21.45	0.0429
L. Intestine	0.4932	1.04	8.58	0.01716
Bone	7.018	1.3	4.28	0.00856
Other	5.09029	1	6.23	0.01246
Lung	0.612	1.05	198.28	0.0119

[a] Total blood mass includes the mass in circulation within organs

[b] Initial guess for total lymph flow was 0.2% of plasma flow

Table A4. Organ sub-compartment volumes for the reference male

Organ	Total Vol. (L)	Plasma Vol. (L)	Endosomal Vol. (L)	Interstitial Vol. (L)	Cell Vol. (L)
Blood[a]	2.69E+00				
Lymph	2.62E-01				
Heart	3.75E-01	1.44E-02	1.88E-03	5.36E-02	2.93E-01
Kidney	4.02E-01	2.20E-02	2.01E-03	6.03E-02	2.99E-01
Muscle	2.86E+01	6.30E-01	1.43E-01	3.72E+00	2.36E+01
Skin	3.15E+00	1.17E-01	1.57E-02	1.04E+00	1.88E+00
Brain	1.47E+00	3.24E-02	7.37E-03	2.65E-01	1.14E+00
Adipose	1.88E+01	2.07E-01	9.42E-02	3.20E+00	1.52E+01
Thymus	6.41E-03	3.53E-04	3.21E-05	1.09E-03	4.65E-03
Liver	2.25E+00	1.92E-01	1.12E-02	4.50E-01	1.44E+00
Stomach	1.96E-01	4.90E-03	9.81E-04	1.96E-02	1.67E-01
Spleen	2.18E-01	2.64E-02	1.09E-03	4.36E-02	1.25E-01
Pancreas	1.67E-01	9.15E-03	8.31E-04	2.89E-02	1.20E-01
S. Intestine	8.30E-01	1.33E-02	4.16E-03	1.45E-01	6.57E-01
L. Intestine	4.74E-01	7.56E-03	2.37E-03	8.25E-02	3.76E-01
Bone	5.40E+00	1.19E-01	2.70E-02	1.00E+00	4.15E+00
Other	5.09E+00	2.14E-01	2.55E-02	8.72E-01	3.80E+00
Lung	5.83E-01	3.21E-02	2.91E-03	1.75E-01	3.47E-01

[a] Total blood volume includes the volume in circulation within organs

Table A5. Basic reference parameters for a Caucasian adult female

Parameter	Value
Height	1.637 m
Body Mass	60 kg
Body Surface Area	1.66 m^2
Cardiac Output	328.6 L/h
Hematocrit	0.40

Table A6. Organ sizes and fluid flow rates for the reference female

Organ	Mass (kg)	Density (kg/L)	Plasma Flow (L/h)	Lymph Flow (L/h)[b]
Blood[a]	1.7835	1.06	197.15	
Lymph	0.2154	1		0.406
Heart	0.291	1.03	10.58	0.0212
Kidney	0.357	1.05	36.41	0.0728
Muscle	17.93	1.04	25.5	0.0510
Skin	2.423	1.1	10.6	0.0212
Brain	1.35	1.03	25.5	0.0510
Adipose	21.15	0.916	18.045	0.0361
Thymus	0.0053	1	0.094	0.0002
Liver	1.81	1.05	13.814	0.0276
Stomach	0.181	1.05	2.11	0.0042
Spleen	0.1874	1.05	6.46	0.0129
Pancreas	0.1446	1.04	2.056	0.0041
S. Intestine	0.7558	1.04	23.5	0.0470
L. Intestine	0.4502	1.04	10.616	0.0212
Bone	5.223	1.3	4.247	0.0085
Other	5.241	1	7.35	0.0147
Lung	0.502	1.05	197.15	0.0118

[a] Total blood mass includes the mass in circulation within organs

[b] Initial guess for total lymph flow was 0.2% of plasma flow

The volumes of the organ sub-compartments (plasma space, endosomal space, interstitial space and cellular space) were calculated for each organ based on the same fractions used for healthy males.

Tumour volume was 20 mL. Estimates for the vascular, interstitial and cellular volume fractions, the reflection coefficients, plasma flow and lymph flow of the tumour were the same as in the model by Glassman and Balthasar.[109] The endosomal volume fraction was 0.5% of tumour volume, consistent with the platform model.[135] Concentration of HER2 in the tumour was set to be 25-fold higher than in normal reference tissue according to the measurements by Olsen at al.[293]

Table A7. Tumour Parameters

Parameter	Value	Parameter	Value
Plasma Volume (L)	1.40E-03	Plasma Flow (L/h)	3.38E-02
Endosomal Volume (L)	1.66E-04	Lymph Flow (L/h)	6.78E-05
Interstitial Volume (L)	1.09E-02	Vascular Reflection [σ^V]	0.842
Cellular Volume (L)	7.70E-02	Lymph Reflection [σ^{IS}]	0.2
HER2 Conc. [Ag_{Tumour}](nM)	25		

Table A8. Reflection Coefficients

Organ	σ^V Estimate	σ^V Effective	σ^{IS} Estimate
Heart	0.95	0.83	0.2
Kidney	0.9	0.67	0.2
Muscle	0.95	0.83	0.2
Skin	0.95	0.83	0.2
Brain	0.99	0.97	0.2
Adipose	0.95	0.83	0.2
Thymus	0.9	0.67	0.2
Liver	0.85	0.50	0.2
Stomach	0.95	0.83	0.2
Spleen	0.85	0.50	0.2
Pancreas	0.9	0.67	0.2
S. Intestine	0.9	0.67	0.2
L. Intestine	0.95	0.83	0.2
Bone	0.85	0.50	0.2
Other	0.95	0.83	0.2
Lung	0.95	0.83	0.2

The initial values for the reflection coefficient, as well as the effective vascular reflection coefficients (σ^v) are given in Table A8. The fitted value for $F2$ was 3.35. Effective vascular reflection coefficients for each tissue were calculated as:[109]

$$\sigma_{Eff}^{V} = 1 - [F2 \times (1 - \sigma_{O}^{V})]$$

Appendix B: Supplementary Material for Chapter 6

Table B1 Data collected for derivation of the ontogeny profile for capillary density

Age	**Medium**	**Median Capillary Density ($1/mm^2$)**	**Median Capillary Density (1/mm)**
Dolezalova et al., 2002[528]			
2 years	Nail Fold		6.75
3 years	Nail Fold		6.80
4 years	Nail Fold		6.85
5 years	Nail Fold		6.90
6 years	Nail Fold		6.96
7 years	Nail Fold		7.01
8 years	Nail Fold		7.06
9 years	Nail Fold		7.11
10 years	Nail Fold		7.16
11 years	Nail Fold		7.21
12 years	Nail Fold		7.27
13 years	Nail Fold		7.32
14 years	Nail Fold		7.37
18 years	Nail Fold		7.58
25 years	Nail Fold		7.94
30 years	Nail Fold		8.20
Top et al., 2011[467]			
[0-7] days	Buccal Mucosa		8.1
[8-30] days	Buccal Mucosa		6.9
[1-6] months	Buccal Mucosa		7.3
[0.5-3] years	Buccal Mucosa		6.7
D'Souza et al., 2011[468]			

Preterm Neonate	Skin (toe)	36	
Term Neonate	Skin (toe)	29	
Schaefer et al., 2016[464]			
[0-1] years	Peritoneum	223	
[1-2] years	Peritoneum	89	
[2-7] years	Peritoneum	76	
[7-12] years	Peritoneum	35	
[12-18] years	Peritoneum	89	
[18-40] years	Peritoneum	106	

Method for Ontogeny Profile Generation:

The U-curve shape was obtained from Schaefer et al., 2016,[464] Figure 3 and the review by Ingegnoli et al.,[527] 2013, section "Capillaroscopy in Healthy Children" with acknowledgement of the animal studies mentioned in the main body of the manuscript.[533-535]

For this analysis, the mean adult is defined as a healthy male with an age of 30 years.

All ontogeny factors were calculated relatively to the adult or other previously established measurements in the workflow.

Ontogeny factors are rounded to the nearest tenth of a decimal to acknowledge the uncertainty around the measurements.

The latter part of the capillary density profile (2 years – 30 years) can be constructed using the linear regression from Dolezalova et al., 2002,[528] Figure 3.

Age	**Capillary Density** (Fraction of Adult)
2 – 6 years	0.8
6 – 12 years	0.9
12 – 18 years	1.0
Adult	1.0

The relative difference in capillary density between an infant at birth and a child at 2 years of age was calculated as the mean of the relative differences reported in Top et al., 2011[467] and Schaefer et al., 2016.[464]

Age	**Capillary Density** (Fraction of Adult)
Birth	1.3
2 – 6 years	0.8

A linear interpolation over time according to age was then applied between birth and age 2.

Age	**Capillary Density** (Fraction of Adult)
Birth	1.3
1 – 3 months	1.1
3 – 6 months	1.0
6 – 12 months	0.9
1 – 2 years	0.8
2 – 6 years	0.8

Finally, the relative capillary density in a preterm infant was calculated with reference to the capillary density at birth using the data reported by D'Souza et al., 2011,[468] Figure 1.

Age	**Capillary Density** (Fraction of Adult)
Preterm	1.6
Birth	1.3